37771

National Library of Canada / Bibliothèque nationale du Canada

CANADIAN THESES ON MICROFICHE / *THÈSES CANADIENNES SUR MICROFICHE*

NAME OF AUTHOR/*NOM DE L'AUTEUR* Mr. Taymour Dorry El-Kasabgy

TITLE OF THESIS/*TITRE DE LA THÈSE* A Study of the Mechanisms of Degradation During Reduction of Iron Ore Pellets

UNIVERSITY/*UNIVERSITÉ* McMaster

DEGREE FOR WHICH THESIS WAS PRESENTED/ *GRADE POUR LEQUEL CETTE THÈSE FUT PRÉSENTÉE* Ph.D.

YEAR THIS DEGREE CONFERRED/*ANNÉE D'OBTENTION DE CE DEGRÉ* 1978

NAME OF SUPERVISOR/*NOM DU DIRECTEUR DE THÈSE* Dr. W-K. Lu

Permission is hereby granted to the NATIONAL LIBRARY OF CANADA to microfilm this thesis and to lend or sell copies of the film.

The author reserves other publication rights, and neither the thesis nor extensive extracts from it may be printed or otherwise reproduced without the author's written permission.

L'autorisation est, par la présente, accordée à la BIBLIOTHÈQUE NATIONALE DU CANADA de microfilmer cette thèse et de prêter ou de vendre des exemplaires du film.

L'auteur se réserve les autres droits de publication; ni la thèse ni de longs extraits de celle-ci ne doivent être imprimés ou autrement reproduits sans l'autorisation écrite de l'auteur.

DATED/*DATÉ* June 9, 1978 SIGNED/*SIGNÉ* Taymour El-Kasabgy

PERMANENT ADDRESS/*RÉSIDENCE FIXÉ* Department of Metallurgy
McMaster University

A STUDY OF THE MECHANISMS OF DEGRADATION OF IRON ORE PELLETS DURING REDUCTION

by

T. ElKasabgy, B.Eng. (Hons.)

A Thesis

Submitted to the School of Graduate Studies

in Partial Fullfilment of the Requirements

for the Degree

Doctor of Philosophy

McMaster University

April, 1978

A STUDY OF THE MECHANISMS OF DEGRADATION OF IRON ORE PELLETS DURING REDUCTION

Doctor of Philosophy (1978)

McMaster University
Hamilton, Ontario

TITLE: A Study of the Mechanisms of Degradation of Iron Ore Pellets During Reduction

AUTHOR: Taymour Dorry ElKasabgy, B.Eng. (Cairo University)

SUPERVISOR: Professor W-K. Lu

NUMBER OF PAGES: xvi, 233

ABSTRACT

Minor impurities in iron ore pellets such as lime and alkali oxides or in the reducing gas (alkali metal vapors) may cause the pellets to degradate when reduced under conditions relevant to the operation of the iron blast furnace.

New techniques have been designed to clarify the mechanisms of iron whisker formation during metallization, since the relationship between their growth and abnormal swelling has been established. In the absence of a significant amount of impurities, it has been observed that the reduction of heterogeneous wustite incurs iron whisker growth.

Calcium oxide, as the main impurity with wustite, promotes iron whisker growth when it is unevenly distributed in the calcio-wustite. It is reasonably confirmed that nucleation and growth of iron occurs at sites higher in calcium oxide on the wustite surface. Magnesium oxide has no pronounced effect on the growth of the iron whiskers. In the present work, the effect of magnesium oxide has been surmounted when lime is also added. The influence of CaO and MgO in solid solutions on enhancing the kinetics of wustite metallization have been related to the extent of disturbing the wustite lattice structure.

Alkalis cycling inside the blast furnace affect the stability of the silica-rich gangue in iron ore. The mechanism and certain measures to control the degradation of commercial pellets subject to alkali attack have been investigated. The silica-rich gangue plays an important role in bearing with the destructive forces suffered by the iron oxide grains during reduction. When they are available during reduction of pellets, alkalis would flux the silica and react with ferrous oxide

to form low melting point primary liquid slags which cause the pellets to degradate long before metallization:

ACKNOWLEDGMENTS

The author is indebted to his supervisor Professor W-K. Lu for his continuing guidance, help and most of all his criticism during the course of this work. Helpful suggestions from the other two members of the supervisory committee, Professors W.W. Smeltzer and R.B. Anderson, are also gratefully appreciated.

The author extends his gratitude and thanks to the faculty, staff and fellow graduate students of the Department of Metallurgy and Materials Science, McMaster University, for many helpful discussions and aid. In particular, thanks are due to Professor J.S. Kirkaldy for his advice and encouragement.

The financial assistance of the National Research Council of Canada (in the form of a research grant to Professor Lu) is gratefully acknowledged. Thanks are also due to Ford Motor Company and Eveleth Mines for supplying the commercial iron ore concentrate and pellets. The author wishes to thank the laboratory staff at Dominion Foundries and Steel Limited for doing the chemical analyses for the iron ore concentrate and pellets.

Many thanks are given for the excellent typing of this thesis by Mrs. A. Neumayer.

Finally, the author commends his wife, Nagwa, for the efforts made in drawing some of the graphs and for all her moral support throughout the course of this work.

TABLE OF CONTENTS

LIST OF TABLES

LIST OF FIGURES

INTRODUCTION

The iron and steel industry has played an important role in the development of our industrial civilization. The iron blast furnace, which is considered to be the backbone of this industry, has been a means of producing metallic iron which continues to be a major building block of heavy industry.

The principal purpose of the iron blast furnace is to smelt iron oxide-bearing materials together with fluxes such as limestone and dolomite, using coke as fuel and as a source of reducing agents, to produce molten pig iron and liquid slag. The furnace is a tall refractory-lined steel shell having a circular cross section. It consists of four main parts: throat, stack, bosh and hearth. The solid raw materials are charged from the top to the furnace throat which is cylindrical. The stack, on the other hand, is slightly conical and its diameter widens as the charge descends. The furnace bosh is also conical; however, its diameter lessens downward, since it is the place where fusion takes place and the apparent volume of burden materials decreases. The hearth has a crucible shape, where the molten pig iron and slag are collected at the furnace bottom.

The iron blast furnace has its name because a blast of air is used to burn the coke at the bottom of the bosh zone to produce heat and carbon monoxide which is the main reducing agent in the furnace. The air is blasted from a number of nozzles-called "tuyeres" near the top of the

hearth. The blast furnace is a counter current heat and oxygen exchange reactor with solid charges descending and reducing gases ascending in the opposite direction.

The present day blast furnace has resulted from the slow and gradual development of the art and later the science of Ferrous Metallurgy. The best blast furnaces operating in the early 20th century were producing up to 500 tons per day, with a coke consumption of about one ton per ton of molten pig iron. Today, modern blast furnaces in Japan and the U.S. produce up to 11,000 tons per day, with a coke consumption of about 400 kgs. per ton of molten pig iron.

The production increase resulted not only from increasing the blast furnace size, but also from improving its productivity. A commonly used method of expressing the furnace productivity is to compute the net tons of iron produced per day per cubic meter of working volume, or NT/day/m^3 WV. The blast furnace productivity was about 0.71 (1910), 0.75 (1940), 2.15 (1963) and 2.8 (1974) NT/day/m^3 WV[1].

The above numbers show that about 25 years ago a revolution in iron-blast furnace technology began. It started with the use of the first large-scale commercial pelletizing plant for agglomerating iron ore concentrates. Pellets in the burden improve the permeability in the blast furnace and lower the slag volume. At the beginning, the total production of iron ore pellets was principally from pilot plant facilities and totalled thousands of tons per year; at the present time the world production is slightly in excess of 280 million tons per year[2].

The innovation has not been without problems and the specific effects of physical and metallurgical properties of iron ore pellets upon blast furnace performance has been controversial for quite some time.

This is conceivable, since there have been no suitable tests that could describe the behavior of iron ore pellets in the blast furnace related to pellet properties as well as reducing conditions.

Experience in recent years has shown that considerable difficulties have occasionally arisen during blast furnace operation, especially with iron ore pellets containing only small proportions of gangue. Causes for these difficulties have been granule disintegration in the temperature range around 500°C under weakly reducing conditions, excesssive volume increase during reduction as a result of iron whisker growth, and also the softening of the pellets due to formation of primary liquid slag at low temperature. The term "degradation of iron ore pellets during reduction" can be used as the criterion to cover all these adversities which affect the stability of the pellets inside the blast furnace.

The objective of this thesis is to study the phenomenon of degradation and investigate the possible mechanisms in an attempt to control the behavior of the iron ore pellets during reduction for better blast furnace performance and higher production rate.

This research program will be concerned with the iron oxide properties, the silica rich gangue phase, basic impurities (such as CaO, MgO and alkali oxides) and reactions between these constituents under various reduction conditions.

CHAPTER 1

LOW TEMPERATURE DEGRADATION

1.1 INTRODUCTION

During reduction of ordinary hematite pellets, they swell up to 20% their initial volume. This increase in volume is inevitable and is associated with the phase transformation from hematite to magnetite. It is defined as "normal swelling"[3].

However, depending on the composition of the pellets and their treatment during the production process, sometimes they tend to lose their coherent structure and break down at the temperature range of 500 - 600°C, under weakly reducing conditions[4,5]. Many authors suggested that internal strain arises due to anisotropic change in dimensions during reduction of hematite to magnetite and is responsible for such detrimental phenomenon[4 - 9]. In the literature this phenomenon is usually referred to as low temperature breakdown, or "LTB". It may occur to all kinds of iron ore compacts such as sinter and pellets.

1.2 VOLUMETRIC CHANGES DURING REDUCTION

The following volume changes during hematite to iron reduction in $CO - CO_2$ mixture at 1000°C were reported by Edstrom[10]:

Original Oxide: Hematite Fe_2O_3

Product Phase		Fe_3O_4	FeO_x	Fe
Apparent Volume	100	125	132	127
	100			148

Original Oxide: Magnetite Fe_3O_4		Fe
Apparent Volume	100	96

The change in volume during hematite to magnetite phase change stems from the frequently described changes in structure. This involves restructure of a hexagonal lattice of hematite to a cubic lattice of magnetite which necessarily results in some distortion of the structure. On the other hand, and because both magnetite and wustite lattices are cubic, a small change is expected during the second step of reduction. The final reduction step from wustite to iron is associated with shrinkage because the molar volume of iron is smaller than that of the iron oxides.

The explanation of the cause for structural disintegration during the conversion of hematite to magnetite lies in a particularly dense occupation of the (0001) plane of hematite or the (111) plane of magnetite with the large oxygen ions, which leads to straining of the lattice during the phase transformation[11]. Claudinon[12] studied the effect of transformation of the crystal structure and its relation to the micropores and suggested that phase transformation from hematite to magnetite will break the periodicity of the lattice structure and create very fine pores leading to an increase of the overall volume.

1.3 FACTORS AFFECTING "LTB"

The ability of the iron ore compacts (sinter or pellets) to withstand the strain associated with the hematite-magnetite phase change, depends on their grain structure, the amount and distribution of the gangue phase, and the reducing agent.

1.3.1 Grain Structure

Walker et al.[9] showed that porous hematite compact swelled more than 100% during reduction. Surprisingly, few iron whiskers were observed

when they examined the reduced specimens under SEM. According to them, the grain structure of hematite and the magnetite which was formed during reduction were significantly influenced by the temperature of the hematite to magnetite step. Stone and Daniell et al[6,7] also found that high purity hematite has a high tendency to swell and crack when it is free from gangue phase. On the other hand, Nabi[13], during his study on the reduction step from hematite to magnetite using high purity dense hematite pellets, found that the specimens he used swelled normally. The contradiction in these findings may be related to the difference in the rate of reduction in each case, which will be discussed in more detail in Chapter 9, Section 9.II.1.

1.3.2 Chemical Composition

The amount of hematite to magnetite in a sinter prior to reduction seems to affect the swelling index. Inazumi et al.[8] studied the relationship between the quantity of hematite and the swelling index during reduction at 550°C and found that the less hematite content, the stronger the sinter during reduction.

The addition of slag bonding materials enhances the reduction strength and prevents internal cracking. Addition of sufficient amount of silica lowered the swelling index and suppressed the tendency of high purity hematite to swell and crack; also, other materials such as calcium silicate or ferrites had a positive effect when they were added[6].

1.3.3 Reducing Media

The phenomenon of LTB is independent of the reducing media. Most of the tests were carried out with $CO-CO_2$ mixtures to simulate blast furnace conditions; however, with the use of H_2-H_2O mixtures the same effects were observed[6,7].

CHAPTER 2

DEGRADATION DUE TO IRON WHISKER GROWTH

2.1 INTRODUCTION

During the initial stages of reduction of hematite up to 20 - 30% reduction, all kinds of iron ore pellets swell normally. Beyond this point, good pellets undergo a gradual decrease in volume with increasing reduction. On the contrary, the pellets which exhibit abnormal swelling show a second dramatic expansion between 25 - 70% reduction.

Figure 2.1 shows the behavior of two kinds of pellets. The lower curve represents those pellets which swell normally, while the upper one shows the abnormal increase of volume associated with certain kinds of pellets.

Observations have shown that abnormal swelling is characterized by the growth of a network of fine filaments (it has also been described as wires, fibres and whiskers) of iron[14-28]. The abnormal swelling has been clearly related to the step of metallization, and the nontopochemical reduction pattern for individual iron oxide grains. Therefore, one can study the macroscopic phenomenon of abnormal swelling by investigating the condition of growing the iron whiskers during reduction of individual iron oxide particles.

2.2 METALLOGRAPHIC EXAMINATION

Formation of iron whiskers inside the pellets which swell abnormally during reduction was observed by several authors[14-20, 26, 27]. Comparing

the pictures taken by them using SEM, the similarity of physical shape of the iron filaments is striking. This finding strongly suggests that abnormal swelling is the result of nontopochemical reduction which is related to the step of nucleation and growth of metallic phase. The cause of promoting certain points on wustite as the nucleation sites or of inhibiting others must be present.

In most pelletizing operations, the original mineral is magnetite, which is oxidized to hematite during firing to gain strength. Watanabe and Yoshinaga[14] found that when hematite (in the form of plates) intergrows with large magnetite grains of Marcona pellets, abnormal swelling during reduction is caused. On the other hand, with induration temperature raised to 1300°C to eliminate such intergrowth by having more completion of the conversion to hematite, the abnormal swelling did not appear during the metallization of the pellets.

Vom Ende, Grebe[redacted]d Thomalla[17,18] investigated the abnormal swelling of lime added to pellets during reduction. Iron whiskers were found only in the case where pellets had fine hematite crystals intergrown with magnetite grains.

2.3 CHEMICAL COMPOSITION OF ORES

Increasing attention has been given to the effect of foreign materials such as fluxes or impurities on the formation of iron whiskers during the reduction of iron ore pellets inside the blast furnace. Many authors suggested basic oxides in the iron ore pellets are the causes of abnormal swelling during reduction[14-19, 21-31].

Kondo et al.[28] suggested that the content of sodium in the iron oxide lattice in the correct quantity (not the overall value for the whole pellet), is related to its effect on abnormal swelling. Vom Ende et al.[17,18]

and Lu[26] suggest that the necessary condition for forming iron whiskers is the uneven distribution of lime and sodium oxide throughout the iron oxide grains. Bleifuss[16] on the other hand, suggested that even distribution of lime will help the iron whiskers to grow. The addition of 2% MnO or MgO to the iron ore failed to cause whiskers to form during metallization. According to him, the difference in the effect on whisker growth is because of the variation in diffusivities of these metal ions in wustite.

The introduction of silica to high grade concentrates has been established as one of the practical ways to suppress abnormal swelling. Lu[26] suggested that the effects of silica and alumina include:

(1) increasing the slag volume to resist the force exerted by growing whiskers, and

(2) acting as a sink for basic oxides which cause abnormal swelling.

Basicity and the amount of slag play an important role in the formation of iron whiskers during reduction. Nishida et al.[30] claimed that the maximum swelling was found near 0.5 basicity. Kojima et al.[21] have shown that over the basicity range 0.5 to 0.7 the swelling was maximum while the quantity of slag was minimum.

2.4 CHEMICAL COMPOSITION OF REDUCING GAS

It has been generally agreed on by many workers that formation of iron whiskers did not take place when the reducing gas was pure hydrogen. Abnormal swelling occurs when we reduce the pellets by CO/N_2 or $CO/CO_2/N_2$ mixtures. Vom Ende et al.[17,18] concluded that the faster they pass through oxidation stages, the larger the abnormal swelling.

Lu[26] recognized that individual grains in the pellets react with a gas which varies in composition from point to point and changes in time

under the condition that the main gas stream has constant composition and flow rate. Lu[24], Granse[31] and Vom Ende et al.[18] found that iron whiskers grew mainly on the particles in the interior of the pellet.

Nicolle and Rist[27] found that a very small amount of sulphur-containing compound in the reducing gas would cause the formation of iron whiskers. They thought that sulphur was adsorbed at the wustite surface and favored the iron phase to form as whiskers.

Nicolle and Lu[32] found that zinc vapor had the same effect on the formation of iron whiskers during reduction. They also thought that zinc was adsorbed at the wustite surface and favored the nucleation and growth of the iron phase on certain sites leading to nontopochemical reaction and filamentary pattern.

Although many authors reported that abnormal swelling did not take place under usual experimental conditions when hydrogen was the reductant [18,26,27], Granden[33] found that introducing hydrogen into a fluidized bed of iron ore may cause nodular iron growth and sticking of the fluidized particles. When the reducing potential of the gas in the bed was raised by cutting down the amount of ore in the system under otherwise identical conditions, the tendency of nodular iron formation and de-fluidization diminished.

Prereduction to magnetite or wustite by keeping the pellets under either 10% CO, 90% CO_2 or 50% CO, 50% CO_2 gas mixtures for a sufficiently long time at high temperature was accepted as a good method for suppressing the whisker growth during metallization of wustite[23].

According to Lu[25], Linder and Thaning observed the effect of the pellet size and found that larger iron ore pellets swelled less. This may be due to the effect of thermal treatment where the interior

particles remain in the form of magnetite and wustite for a longer time.

2.5.a. TEMPERATURES OF INDURATION AND OXIDATION

Insufficient firing which leads to hematite/magnetite intergrowth and weak bonding, was established as one of the factors which would cause abnormal swelling. In cases where lime was the major impurity which caused whisker growth, the abnormal swelling decreased with the increase of temperature of induration[25]. On the other hand, when alkali metal oxides are the major impurities, the swelling increases by increasing the induration temperature[17,18,24].

2.5.b. TEMPERATURE OF REDUCTION

Fuwa et al.[15] made extensive studies on the effect of temperature of reduction and concluded that there is an intermediate reduction temperature to give whiskers.

Lu[25,26] suggested that at low reducing temperatures the solubility of impurities in iron oxide may be too low to be effective in causing the formation of iron whiskers. He emphasizes that the homogenization of calcium in iron oxide at higher temperatures eliminates the necessary condition for whisker formation.

2.6 GRAIN SIZE

Fuwa et al.[15] studied the effect of pelletizing feed size on the abnormal swelling of Marcona pellets. They found that the abnormal swelling increases as the feed size decreases.

Nicolle and Rist[27] investigated the grain size effect on the chemical reaction rate and diffusion of ferrous ions during reduction of wustite. They suggest that fine wustite powder would favor iron whiskers to form during reduction, while large particles would be reduced topochemically.

2.7 THEORETICAL STUDIES

For the past several years, formation of iron whiskers during reduction of iron oxides has been a subject of research. Several mechanisms were suggested; however, there are diversified opinions on the cause and conditions under which iron whiskers are formed.

Fuwa et al.[15] carried out the first comprehensive investigation on this subject. With Wagner[34], they had suggested several possible causes for the formation of iron whiskers. To a certain extent, the following theories are the results of refinement of these suggestions.

2.7.1 Bleifuss Theory

Bleifuss' theory[16] is based on the idea that whisker growth is the result of restricted growth of iron from wustite. He proposed that during reduction of calciferrous wustite which is a solid solution of FeO and CaO, a layer of lime precipitates out, which partially covers the surface and prevents the completion of the lateral growth of iron; therefore, the formation of iron whiskers is the logical consequence. In the reduction of calciferrous wustite, the enrichment of CaO near the surface is due to the oxygen removal by chemical reaction and the migration of iron away from the gas/solid interface. The large calcium ions diffuse relatively much slower. He stated that at the time when reduction proceeds to a depth of some 300 to 400 Å, the surface layer is theoretically mantled with a monolayer of wustite saturated with lime. As the removal of surficial oxygen continues, the iron-rich lime layer becomes a tangible reality and tends to form a more or less continuous surface layer on the particles. Nucleation of metallic iron on this surface layer is difficult and the number of points at which metallic iron can nucleate on the individual particles is severely limited. The mechanism proposed

by Bleifuss may be explained with Figure 2.2.

The general validity of Bleifuss' theory may be questioned for the following reasons:

(1) This theory predicted that iron ore pellets containing more lime and fired at higher temperature to give even distribution of CaO, would exhibit larger swelling due to the formation of iron whiskers. However, the opposite facts have been found experimentally to be true[18,29].

(2) This theory does not suggest directly any reason why iron whiskers do not form during reduction at low or very high reducing temperature.

(3) It does not explain the important fact that intergrowth of fine hematite crystals in magnetite seems to be one of the necessary conditions to form iron whiskers.

(4) It does not place any requirement explicitly on the properties of reducing gas for the formation of iron whiskers.

(5) The theory does not pay attention to the grain size effect on the formation of iron whiskers.

2.7.2 Vom Ende, Grebe and Thomalla Theory

Vom Ende et al.[18] proposed a theory on the formation of iron whiskers based on the idea that whisker growth is the result of preferential nucleation on certain sites where uneven distribution of CaO will help the spot containing more CaO to form iron nucleus.

It is certainly true that the calcium ion is bigger than the iron ion and would cause some distortion locally in the wustite lattice. Based on energetics, nucleation is a thermally activated process, and would be more easily carried out at these high energy spots due to strain. How-

ever, the chemical aspect of this situation indicates the opposite effect. CaO, the solute, would reduce the activity of the solvent, FeO (wustite); therefore, the thermodynamic driving force for chemical reaction and nucleation, involving the disappearance of iron oxide, will be reduced. Lime will reduce the driving force as well as the energy barrier to be overcome so it has two opposite effects. On the other hand, Vom Ende's theory did not explain the effect of reducing gas, reducing temperature and grain size on the formation of iron whiskers. This theory did not suggest any reason to expect that whisker growth must follow after the nucleation of iron, instead of topochemical pattern which is normal in wustite reduction.

2.7.3 Nicolle and Rist Theory

Nicolle and Rist[27] proposed a mechanism for iron whisker growth during wustite reduction based on Wagner's mechanism for the reduction of nonstoichiometric oxides and sulphides[34]. According to Wagner, the surface reaction between the reducing gas (CO or H_2) and wustite may be written as:

$$\begin{matrix} CO \\ H_2 \end{matrix} + O^{-2} + 2Fe^{+3} + \text{vacancy} = 2Fe^{+2} + \begin{matrix} CO_2 \\ H_2O \end{matrix}$$

The reaction involves transportation of oxygen from the wustite crystal lattice to the gas phase, migration of vacancies to the surface where they vanished and formation of two ferrous ions at the surface due to conversion of two ferric ions.

The result of surface reaction is the increase of Fe^{+2}/O^{-2} ratio. Gradients are formed causing the ferrous ions to diffuse inward and vacancies to diffuse outward, together with the associated positive charges. Therefore, the activity of iron will change with time, eventually exceeding the value of 1 (equilibrium with iron) and creating a supersaturation

region below the surface. The nucleation of iron like any activated process, needs a certain amount of supersaturation which is a function of the two rates of chemical reaction at the surface and diffusion of vacancies in wustite.

Nicolle and Rist defined a dimensionless parameter α, which is a function of the chemical rate constant K, the diffusion coefficient of vacancies in wustite D, and the initial radius of the wustite particle r_o (assuming it is spherical), as follows:

$$\alpha = \frac{K}{D} r_o$$

The idea was to identify the rate-controlling step according to the value of α. There are three cases for discussion represented in Figure 2.3 as follows:

(1) Under pure vacancy diffusion control (high values of α) the transport capacity of ferrous ions inward is negligibly small compared to the capacity of producing such ions at the surface. Many points at the surface reach the critical value for nucleation and there is no buildup of iron to feed them from inside; therefore, they grow at their periphery in plate shape until they form a topochemical layer of iron.

(2) Under pure chemical or gas transport control or any combination of controls not including vacancy diffusion (when vacancy diffusion is very fast compared to all the other mechanisms in series (small values of α)). The wustite particle acts as a reservoir for ferrous ions and the activity of iron grows slowly and remains uniform. Nucleation is thus delayed; once a nucleus forms it can grow from its root outward as whiskers since the

solid state diffusion is much faster than the removal of oxygen around its base.

(3) Under mixed control including vacancy diffusion (the diffusion has about the same velocity as the other mechanism in the series), the buildup of supersaturated region covers only a fraction of the grain volume, the activity of iron at the surface can reach the critical value at several points, and their outward growth is restricted since the amount of ferrous ions stored prior to nucleation is small compared to case (b). In such a case conical iron whiskers followed by a layer of iron are expected.

Nicolle and Rist discussed the effects of various parameters (such as the wustite particle size, impurities, reducing agent and condition), based on their influences on the value of α and suggested that presence of impurities such as CaO and alkali oxides promotes the iron whisker growth due to their effect in increasing the rate of diffusion.

Although Nicolle and Rist's theory gave strong suggestions about iron whisker growth, the theory did not explain why wustite heterogeneity is one of the factors to be considered for pronounced iron whisker growth. They also did not state that uneven distribution of impurities, such as CaO, in solid solution with wustite, is necessary for iron whisker formation during reduction of basic iron ore pellets.

2.7.4. Lu's Theory

Lu[25] summarized the favorable conditions for iron whisker growth during reduction of some commercial iron ore pellets. The following conditions were assumed:

(1) Porous iron ore pellets were used.

(2) The pellets contained significant amounts of basic oxides as impurities.

(3) The iron oxides in the pellets consisted of both hematite and magnetite with fine hematite crystals intergrown with the magnetite grains.

(4) The reductant is carbon monoxide.

Magnetite, a spinel crystal ~~structure,~~ would have relatively high solubility of lime in comparison with hematite. Therefore, the initial distribution of calcium oxide may be uniform in activity but not in concentration. During reduction to wustite, the distribution of lime in the wustite grains would be multiform due to the slow diffusion of calcium ions. Since wustite has a much higher solubility of lime[35], the newly formed wustite which was magnetite and contained more lime, will not reject any solute during reduction. Therefore, the uneven distribution of CaO will be preserved at least for some time.

The atmosphere around an iron ore particle in the interior of the pellet changes continuously with the reaction time. At a given location, the reduction potential of the gas increases as the oxidation state of the iron oxide decreases as demanded by thermodynamics. The equilibrium diagram for the system of lime-saturated wustite, CO/CO_2 and temperature is shown in Figure 2.4.

The presence of lime in the solid solution should make the thermodynamical activity of wustite less than one unit. Its chemical effett on reduction is to increase the value of CO/CO_2 ratio in equilibrium with iron and wustite. Therefore, wustite of different amounts of lime content will have different values of CO/CO_2 ratio for equilibrium and possibly for nucleation of metallic iron.

The mechanism of iron whisker formation proposed by Lu can be explained with the use of Figure 2.5. The grains of relatively pure and wustite-containing lime are located next to each other in the interior of the pellet. As soon as the local gas composition gives a value of CO/CO_2 ratio slightly above that in equilibrium with pure wustite (68/32 at 900°C), then the chemical reaction involving the stripping of oxygen from the solid surface to form CO_2 will take place as shown in Figure 2.4. The continuation of this reaction will have two effects:

(1) to counter balance the incoming flux of carbon monoxide from the main gas stream and to slow down the enrichment of CO in the gas phase near the wustite surface, and

(2) to increase the Fe/O ratio in the relatively pure wustite, especially for the region near the gas/solid interface.

After certain time of reaction, the supersaturation of ferrous ions in the wustite lattice becomes relatively unstable, therefore leading to the nucleation of metallic iron. The reduction of pure wustite will continue, hence, the enrichment of CO in the gaseous phase will be maintained at a low rate if it happens at all. At the same time, the wustite-containing lime does not participate significantly in any chemical reaction (Figure 2.5 (c))). In a later stage of reduction, the wustite-containing lime will eventually begin to be reduced due to the continuing supply of CO from the main gas stream and the removal of CO by diffusion in the gas phase (Figure 2.5 (d)). The presence of lime in wustite may speed the ferrous iron diffusion in the wustite-containing lime. With the presence of the metallic iron at the grain boundary next to its zone, and coupled with fast transformation of ferrous ions, growth as iron whiskers will result due to the presence of the oxygen ions (which are considered

immobile relative to ferrous ions).

Lu related the influence of the temperature of reduction to its effect on the distribution of lime prior to the appearance of metallic iron; however, the effects of temperature on the chemical reaction, diffusion and nucleation are not clearly stated in his theory.

This theory does not consider the influence of foreign ions such as Ca^{+2} and Na^{+1} on disturbing the wustite crystal lattice, which may help the places containing more lime to be metallized prior to the relatively clean wustite.

According to Lu's theory, high purity iron oxides will not form iron under any conditions of reduction; however, other workers in the field reported the growth of the iron whiskers when high purity iron oxides were used as specimens[15,27].

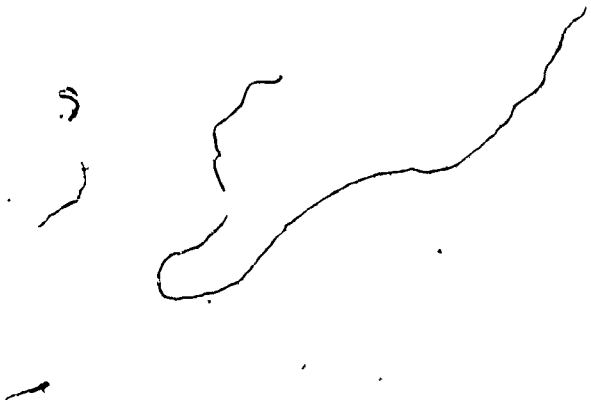

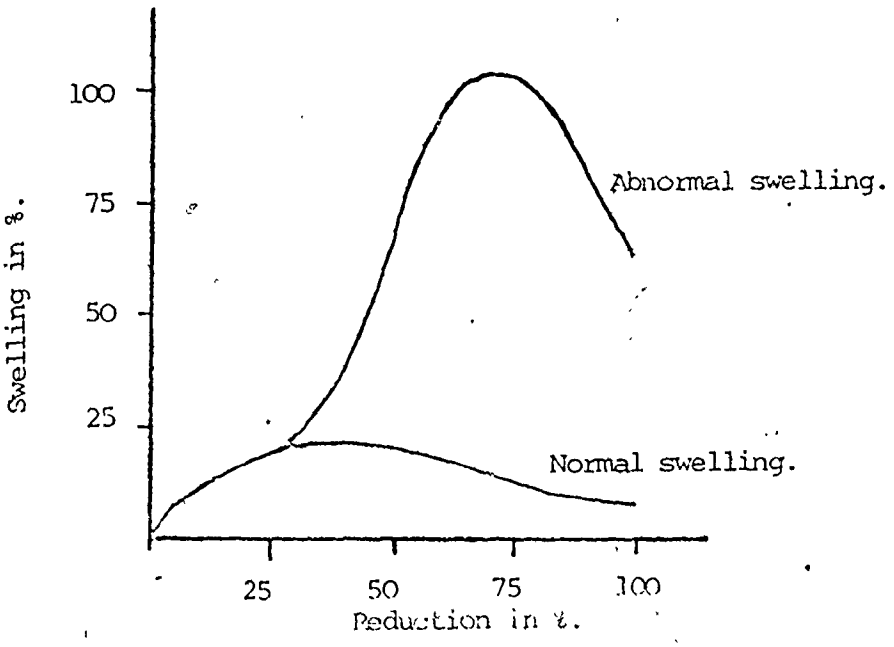

Figure 2.1 Swelling, reduction curves.[3]

INDURATION-OXIDATION

Calciferrous magnetite → Calciferrous hematite

$(Fe_{1-x}Ca_x)O \cdot Fe_2O_3 \longrightarrow (Fe,Ca)_2O_3$

Reduction at 900°C

1.	Calciferrous magnetite	$(Fe_{1-x}Ca_x)O\ Fe_2O_3$; $x = 0.02$
	↓	
2.	Calciferrous wustite	$(Fe_{1-x}Ca_x)O$; $x = 0.01$
	↓	
3.	Calciferrous wustite	$(Fe_{0.955}Ca_{0.005})_{1-y}O$
	↓	
4.	Iron-rich lime (surface layer)	$(Ca_{0.94}Fe_{0.06})_{1-y}O$
5.	Metallic iron filaments	Alpha-Fe

Figure 2.2 Bleifuss' representation of iron whisker growth.[16]

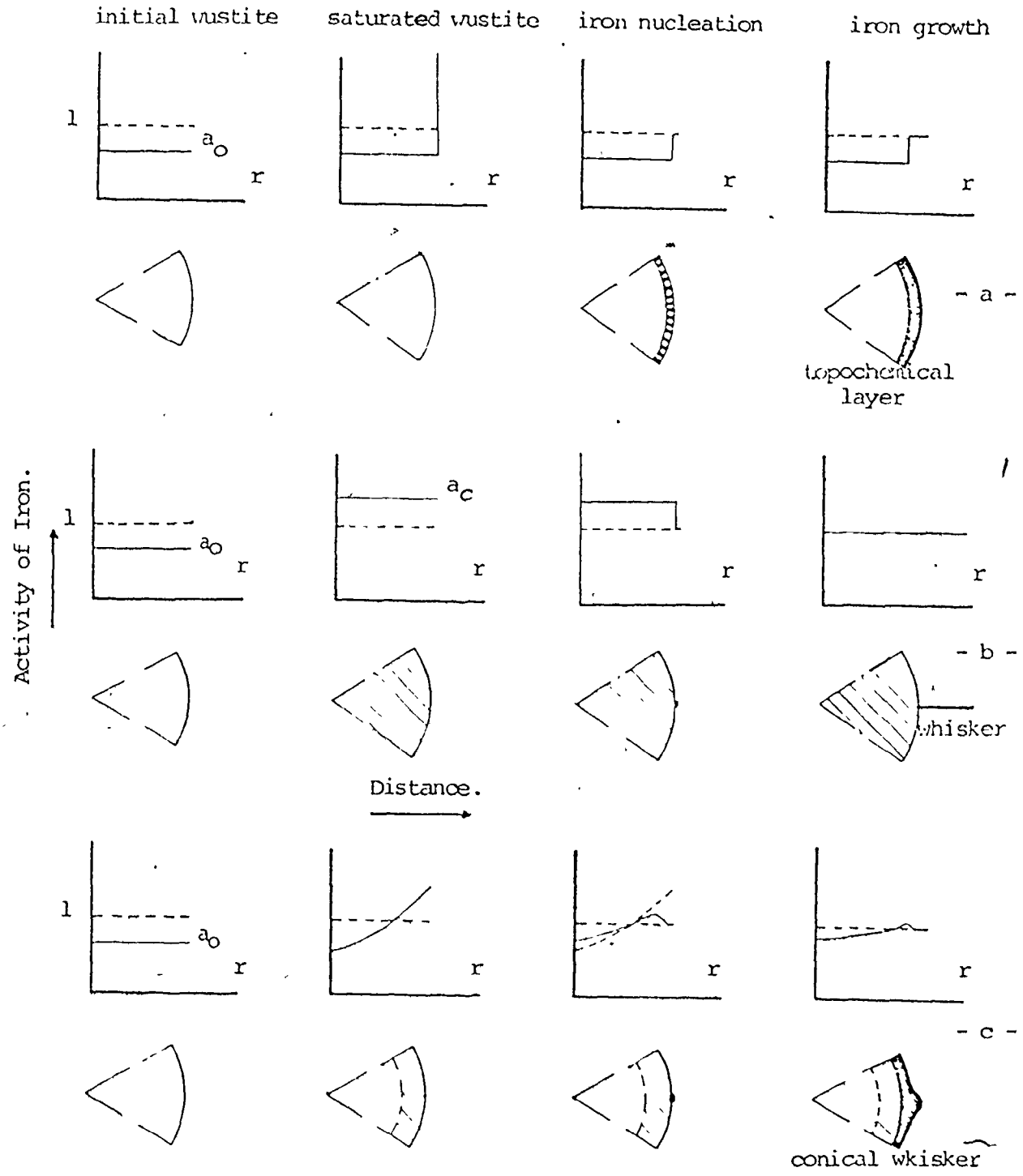

Figure 2.3 Nicolle and Rist representation of iron whisker growth.[27]

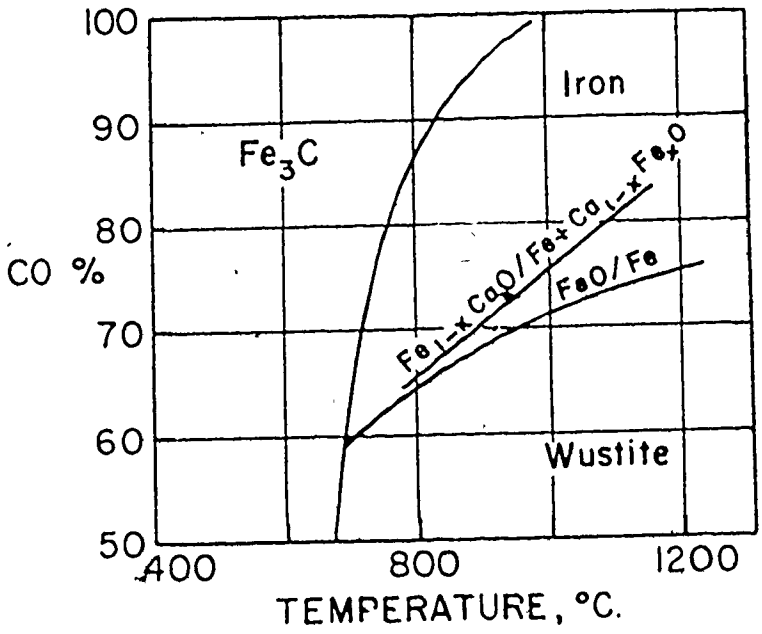

Figure 2.4 The equilibrium relations between lime-saturated wustite and CO/CO_2 mixtures.[36]

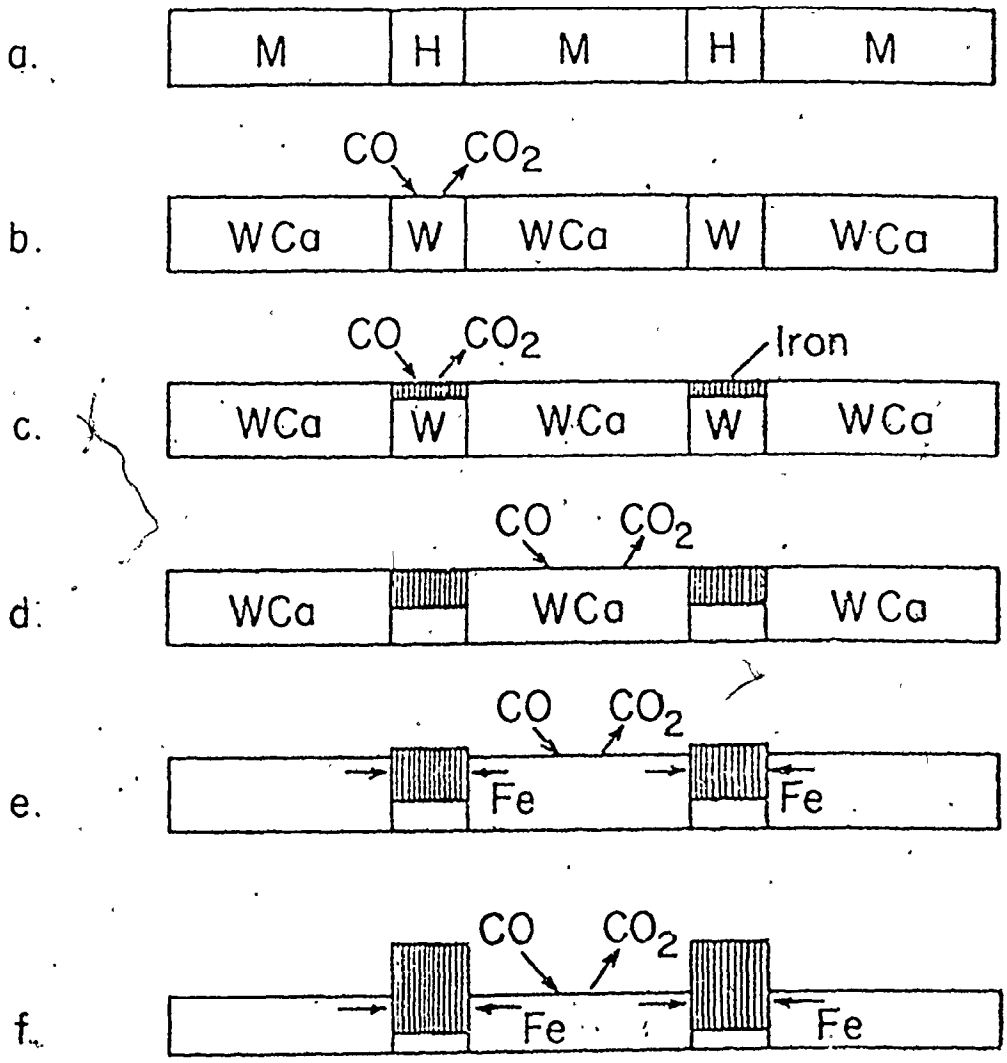

Figure 2.5 . Schematic presenation of steps in iron whisker growth, according to Lu.[25]

CHAPTER 3

DEGRADATION DUE TO SOFTENING

3.1 INTRODUCTION

The importance of the softening behavior of iron ores, sinters and pellets with respect to the iron blast furnace operation have been emphasized on several occasions. Several authors have already attempted to develop laboratory tests for softening which would yield representative and reproducible results; these tests will be discussed in the following chapter. Others studied the causes of this phenomenon[37,43], the influence of the nature of the gangue[45], the degree of reduction reached[39,43,46] and some of the physical properties of the pellets[43]. Unfortunately, the conclusions that have been drawn from these investigations are not always entirely consistent and numerous problems are still unsolved.

The phenomenon of softening of iron ores, sinters and pellets is not new. As early as 1945, Haword[37] obtained values ranging from 1568°C for an iron ore with 64.25% iron and 2.38% silica to 1238°C for an iron ore containing 33.75% iron, 12.64% silica and 16.52% lime. The values he obtained represent the temperature of complete melting of the ores he examined. However, this temperature merely defined the upper limit of a temperature range in which they softened. The plastic flow due to presence of sufficient amount of liquid phase which is defined as softening, may take place at a lower temperature level prior to complete

melting and fusion.

Softening of commercial iron ore pellets affects blast furnace operation in the following ways:

(1) The diminished porosity of the softened pellets will retard further reduction.

(2) The plastic flow of the softened pellets will increase the surface of contact between iron oxide and coke, thus aiding direct reduction and the transfer of sulphur from coke to reduced iron.

(3) Burden voids will be greatly reduced in regions of softening, with consequent uneven distribution of the ascending blast furnace gases across the stack or an excessive pressure drop through the burden bed.

(4) The presence of softening and "sticky" pellets together with hard coke may be conducive to arch formation and hanging in the stack.

Softening of iron ores, sinters and pellets may be divided into two categories, according to temperature:

(1) high temperature range over 1000°C

(2) low temperature range below 1000°C.

Softening of iron ores, sinters and pellets at high temperature has been a subject of numerous investigations[37-47]. On the other hand, formation of low melting point slags, as a result of the presence of minor impurities such as alkali oxides, sulphur and zinc oxide during reduction of the burden materials inside the blast furnace and their relation to swelling and softening mechanisms are not clear yet.

3.2 HIGH TEMPERATURE SOFTENING

Grieve[38] investigated the softening of iron ores at high tempera-

ture in air and during reduction under compressive stresses. He found that the softening temperatures and their range were related to the amount and composition of the gangue and to ferrous oxide content which reacts with silica and leads to fayalite formation and rapid softening. According to him, the harmful effects of softening may be minimized by increasing the indirect reduction of the ore in the stack of the blast furnace.

Lecomte et al.[39] at CNRM Laboratories carried out extensive studies on the softening of sinters, pellets and iron ores. They attempted to point out and explain the influence of:

(1) iron content

(2) basicity, and,

(3) initial degree of oxidation and degree of reduction.

The softening properties of sinters which were produced by steel companies affiliated with their laboratories varied over a wide range. They strongly believed that the results obtained are of general application. The main conclusions they reached may be summarized as follows:

(1) For unreduced sinters, the softening temperatures increase with the total iron content, the initial degree of oxidation, atoms O/atoms Fe and the basicity index CaO/SiO_2.

(2) As the reduction progresses the softening temperatures first diminish and reach a minimum at a reduction degree which increases with the gangue amount.

(3) Higher minima, softening temperatures of partly reduced sinters may be reached by:

(i) increasing the initial oxidation degree and,

(ii) increasing the basicity index CaO/SiO_2.

The effect of gangue constituents on the degradation of iron ore

pellets with particular reference to phase diagram $CaO-FeO_x$ and SiO_2, was investigated by Kortmann in W. Germany[40]. After firing pellets with different amounts and composition of gangue at high temperature (1300°C), he tested their swelling behavior and softening properties under load when reduced at 1000°C, with CO and N_2 mixtures. He linked the results of the swelling test with the ternary system of $CaO-FeO_x$ and SiO_2, and found that there was a critical swelling zone including all the pellets showing a volume increase of more than 20%. This zone lay in the region of low basicity, up to a value of 0.7 and covered a range of between 0 and 10 wt.% gangue within the pellets.

Kortmann claimed that formation of olivines and their penetration into the zone of weakness was associated with the destruction process which simultaneously took place with reduction and caused the pellets to swell. According to the phase diagram between FeO, CaO and SiO_2 (see Figure 6.11) one may challenge his claim, since the minimum temperature at which liquid olivine may appear is about 1100°C and he conducted his tests at only 1000°C. However, it is well known that small amounts of impurities which are unavoidable when commercial iron ores are used, may help in forming the liquid phase at lower temperature.

Sayama and Uedo[41] investigated the effect of forming liquid slag during reduction of ore pellets containing carbon in the range 1200 - 1300°C. They found that the amount of liquid phase increases by adding CaO up to a certain limit over which there was a retarding tendency. The observed results were found to be very sensitive to the temperature of reduction. They did not interpret their results according to the $CaO-FeO_x$ and SiO_2 phase diagram which will be included in Chapter 6.

The influence of hydrogen sulphide on the softening of iron ore

pellets was studied by Takahashi et al.[42]. They suggested that sulphur compounds seem to play a great role in forming liquid slags during reduction of the iron ore pellets at 1100°C using reductant gas mixture of CO and N_2 containing H_2S. On the other hand, the same effect was reported when pyrite was added before reduction[41]. Sulphur as an impurity also had a deteriorating effect on the strength of the iron ore pellets after firing. Cracks and fissures developed after firing and cooling of these pellets. According to Statnikov et al.[43] the formation of low melting point slags of complex silicate-containing sulphur between the hematite grains is synchronized with the thermal stresses leading to splitting and cracking across the grain boundaires and the formation of the fissures.

Magnesium oxide substituted for calcium oxide in self-fluxed pellets was employed by Nishida et al.[44]. They found that the melting down of the slag increased by increasing the MgO and decreasing CaO and SiO_2. Kawaguchi et al.[45] investigated the effect of dolomite on the rate of reduction at 1250°C. They found that dolomite enhanced the kinetics of reduction of the iron ore pellets.

3.3 LOW TEMPERATURE SOFTENING

It is well known that adding silica to high-grade iron ore concentrates is a practical way of suppressing the intrinsic tendency of certain ores to swell due to formation of iron whiskers during reduction, as discussed in Chapter 2.

Silica-rich gangue phase acts as a sink for basic oxides such as CaO, MgO and alkali oxides (Na_2O and K_2O). However, the stability of the silicate binders during reduction can be affected by these basic oxides and may be sensitive to the temperature as well as to the condition of

reduction.

Alkali oxides are known to circulate and accumulate inside the blast furnace and to build up to a level several orders of magnitude higher than that in the raw materials. During reduction in the upper parts of the stack ferrous iron is produced during the reduction of hematite to lower oxides (magnetite and wustite). If this reaction is synchronized with the presence of alkali compounds, due to circulation together with the silicate gangue phase, one may expect a glassy phase of alkali ferrous silicate to form. The melting point of this newly formed phase can be as low as about 700°C, which is the lowest melting point of the eutectic temperatures in the ternary system between K_2O (Na_2O), FeO_x and SiO_2 (see Figures 6.14 and 6.15).

The opinion was held that alkali oxides can cause iron whisker growth[14-16, 22,29,32] and many workers in the field suggested that degradation of iron ore pellets inside the blast furnace may be explained accordingly. On some occasions, laboratory tests showed acceptable swelling index and no iron whiskers for those samples representing pellets used during periods of furnace irregularities[48]. The difference can arise from the testing conditions. In the laboratories, pellets were reduced using clear reductant gases, while inside the blast furnace alkali vapors or minute particles (solids or liquids) of alkali compounds are mixed with the ascending blast furnace gas.

Degradation of commercial iron ore pellets due to alkali influence needs careful investigation. Unfortunately, in the literature, most of the experimental tests were carried out with specimens which were prepared by adding the alkalis prior to pelletizing and firing of high grades of iron ore or chemical reagent hematite.

Peart and George[49] tested their commercial pellets after impregnation in alkali carbonate solution, without firing. They reported swelling and cracking without iron whisker growth. Vom Ende and Grebe[50] suggested that alkalis may cause plastic deformation of partially reduced iron ore pellets prior to metallization. They thought that breaking of the tiny little bridges binding the iron oxide due to excessive swelling may lead to yielding under mechanical load and cause the pellets to degradate. However, the photographs they presented in another paper[17] which show sticking and sintering of the partially reduced pellets in a pattern difficult to attain without the help of some liquid phase, suggest that the pellets deformed due to the formation of liquid slags containing alkalis rather than solid state deformation which is unlikely to cause softening.

CHAPTER 4

TESTS FOR THE STRENGTH OF IRON ORE PELLETS ACCEPTED BY INDUSTRY

4.1 INTRODUCTION

Specifications on the chemical, physical and metallurgical properties of the iron blast furnace burden are steadily becoming more stringent. Tests have been designed for relative predetermination of pellet behavior where the effects of temperature, reduction gas composition and physical load in the blast furnace are considered.

World-wide, a variety of tests are employed; however, their results do not always predict blast furnace performance. It should be clearly understood that industrial tests are designed to demonstrate if certain burden materials are acceptable or not from an operational viewpoint. They are not intended to study the factors influencing their characters or to investigate how they act, why they behave in a certain way or what can be done to improve their behavior.

Kortmann and Burghardt[51] summarized these tests and divided them into categories according to the nature of each group of tests and their relation to the iron blast furnace. The tables presented in this chapter were taken from their paper.

4.2 TEST METHODS FOR MEASURING PELLET STRENGTH PRIOR TO REDUCTION

The crushing strength test is one of the oldest. It provides a measure of the behavior under mechanical load, prior to heating and reduction. It is possible to measure the crushing strength by breaking indi-

vidual pellets under compression load; sometimes it may be necessary to test as many as 200 pellets to get meaningful representative results. The uniformity of the crushing strength values can be regarded as an indication of the uniformity of the firing and induration processes.

Another method is to test the pellets under dynamic strength by tumbling the samples in a drum for a predetermined time. The tumble tests are described in Table 4.1. Here in Canada and the U.S., the crushing strength of commercial iron ore pellets is characterized by a parameter called the Q Index which is defined as the product of the weight fraction of + 1/4 inch (6.35 mm) before and after tumbling, according to the ASTM tumble test.

4.3 TEST METHODS FOR MEASURING PELLET DEGRADATION

The strength of iron ore pellets during reduction is measured by different tests which try to reveal the degradation properties during reduction and smelting of the burden materials inside the iron blast furnace.

The term "reduction strength" is usually implied to express these properties. However, it can bear different interpretations depending on the temperature of reduction, the rates of heating and removal of oxygen and the state the sample reaches after reduction. At the premetallization zone of the iron blast furnace, hematite pellets may disintegrate on conversion to magnetite as already shown in Chapter 1. Low temperature disintegration tests are designed to test this phenomenon. On the other hand, prevailing in the blast furnace stack other tests are employed to test the pellets during the early stages of metallization. At higher temperature levels, tests are designed to examine the softening and melting of parts of the burden constituents in conditions which are intended

to simulate the blast furnace bosh.

The strength of the pellets during reduction is also measured by testing the samples under compression load and in some cases the sample is prereduced before examination. These tests are more representative of the actual blast furnace operation; however, they are more expensive and it takes a longer time to prepare and carry out a test.

A more simple way to test the degradation is to measure the increase of the apparent volume of the pellets, or swelling after isothermal reduction at 900 - 1000°C. The swelling tests are widely used since they are simpler and take a shorter time than other tests. However, they are less representative of blast furnace practice.

4.3.1 Test Methods for Measuring Low Temperature Degradation

These tests are designed to test the reduction strength at low temperature, usually 500°C, during reduction, using weakly reducing gas mixtures. A source of mechanical load is needed to examine the pellets and to measure their ability to withstand low temperature degradation or breakdown (LTB).

Two groups of tests are shown in Table 4.2 The dynamic tests use rotation during isothermal reductions as a source for the mechanical stress, while the static tests do not employ any outside stresses on the sample during testing. However, the reduction strength is measured afterward by tumbling the partially reduced sample in a tumbler drum. The correlation between the dynamic tests and blast furnace operation at the prometallization zone is more expressive since it is almost impossible to test with any certainty the strength after partial reduction followed by cooling to room temperature.

4.3.2 Test Methods for Measuring High Temperature Degradation

For modern iron blast furnaces, the iron ore pellets may reach temperature levels higher than that of low temperature degradation before any extensive reduction has time to occur. It is of more immediate interest to test the strength of the pellets in the lower portion of the thermal and chemical reserve zones before direct reduction and melting start.

The reduction strength of the pellets at high temperatures of 900 - 1000°C is tested by reducing the pellets with gas mixtures of higher reducing power than those used to test the low temperature degradation.

The simplest way to measure the high temperature strength of the iron ore pellets is to determine their swelling index after isothermal reduction as shown in Table 4.3. The swelling test of iron ore pellets will be discussed in more detail in Chapter 7, Section 7.2. The test criterion for commercial acceptance is the maximum swelling value which must not exceed 20% increase of the initial pellet volume.

There are the high temperature degradation tests which are given in Table 4.4. The idea of the static tests is to reduce the sample. Sometimes this is done using programmed reducing gas mixtures with changing CO/CO_2 ratio toward higher values (Boric, France); or isothermally with constant flow of reduction gas mixtures (IRSID and Japanese steel mills); followed by tumbling or crushing at room temperature. Again, the main disadvantage of these tests arises from measuring the mechanical strength at room temperature.

The dynamic test for high temperature degradation was originally designed by Linder in 1958[52]; it is also included in Table 4.4. The object of this test is to determine the susceptibility of iron ore, sinter or pellets for the blast furnace process, which is simulated by

reducing the sample together with coke particles using programmed gas mixture which increases in CO/CO_2 ratio as the testing time and temperature increase up to 1000°C. The reduction strength is determined by tumbling the sample during reduction followed by screening and measuring the weight fraction of fines less than 1 mm and 3 mm.

The view was held that the Linder test does not provide sufficient information about the properties of the iron ore pellets during reduction (53). The fine materials tend to stick to the wall of the tube and form accretion during rotation. Thus, the measured fractions do not always reflect the true strength of the tested pellets.

4.3.3 Test Methods for Measuring Softening and Melting Down Behavior

In Chapter 3, softening was defined as the plastic flow of the iron ores, sinter or pellets, dur to formation of liquid phase (slag) during reduction. However, in the literature any plastic flow which occurs during reduction at high temperature under compression load, is usually called softening.

The test methods given in Table 4.5 summarize some industrial tests for softening and melting down behavior where the sample is prereduced prior to testing. In Table 4.6 the test methods for measuring the reduction behavior under load are given, where the sample is reduced with CO and N_2 gas mixture under compression load. The strength during reduction is determined according to the expansion and contraction of the sample or the gaseous pressure drop across the reduced bed at constant flow rate due to plastic deformation which diminishes the connected pores.

4.4 SUMMARY

In an endeavor to test the behavior of the iron ore pellets and to predict their performance in the blast furnace, many industrial tests are employed. They are presented in Tables 4.1 to 4.6. However, since there are many factors which must be considered, there is not a single standard test which determines pellet behavior and gives general acceptable results. On the other hand, the certainty of any test and how close it simulates the blast furnace process are emanated when complex tests are employed. In such cases the test takes a longer time and costs more money in terms of equipment and operating expenses.

Table 4.1 **Test Methods for Measuring the Tumbler Strength of Iron Ores, Pellets, and Sinter**

Test Method	ISO 3271 1975 (E)	ASTM	BISRA	BHP	JIS M 8712 1971	Micum	IRSID ½ and ¼ Micum
Apparatus	1000 mm ID 500 mm wide 2 liters 50 ± 5 mm	914 mm ID 457 mm wide 2 liters 50.8 ± 6.35 mm	ASTM drum (see column 2)	ASTM drum (see column 2)	ASTM drum 914 mm ID 457 mm wide 2 liters 50 ± 5 mm	1000 mm ID 1000 mm wide 4 liters 100 mm high	1000 mm ID, but 500 resp. 250 mm wide
Number of revolutions	200 @ 25 rpm	200 @ 25 rpm	200 @ 25 rpm	200 @ 25 rpm	200 @ 25 rpm	100 @ 25 rpm	100 @ 25 rpm
Kind of tested materials	Ores, pellets, sinter	Ores, pellets, sinter	Ores and pellets	Ores and agglomerates	Pellets and sinter	Ores, pellets, sinter	Ores, pellets, sinter
Weight of material (dry)	15 kg	11.3 kg	11.3 kg	Ores 22.7 kg Sinter and Pellets 11.3 kg	23 kg ± 0.23	50 kg	25 kg at ½ Micum 15 kg at ¼ Micum
Size of material	Pellets 6.3-40 mm Ores and sinter 10-40 mm Screened at 40/25/16/10 mm	Pellets 6.35-38.1 mm Ores and sinter 9.52-50.8 mm Screened at 50.8/19.1/12.7 and 9.57 mm	Pellets 6.35-38.1 mm Screened at 38.1/25.4/19.1/12.7-9.52 and 6.35 mm Ores 9.52-50.8 mm Screened at 50.8 38.1/25.4/19.1/12.7 and 9.52 mm	Pellets 6.35-38.1 mm Ores 6.35-76.2 mm Screened at 76.2/63.5/50.8/38.1/31.7/25.4/19.1/12.7/9.52 and 6.35 mm Sinter 6.35-50.8 mm of that 10% 25.4-50.8 mm 20% 19.1-25.4 mm 20% 12.7-19.1 mm 25% 9.52-12.7 mm 25% 6.35-9.52 mm	Pellets <5 mm Sinter 10-50 mm	10-25 mm	7-25 mm
Expression of results	a) Tumbler index T + Wt % + 6.3 mm b) Abrasion index A Wt % -0.5 mm	a) Tumbler index T + Wt % + 6.35 mm b) Abrasion index Wt % -0.595 mm	a) Tumbler index T + Wt % + 6.35 mm b) Abrasion index T Wt % -0.5 mm	a) Tumbler index T + Wt % + 6.35 mm b) Abrasion index T Wt % -0.5 mm	Pellets a) Wt % + 5 mm b) Wt % -1 mm Sinter a) Wt % +10 mm b) Wt % -5 mm	a) Tumbler index T + Wt % + 10 mm b) Abrasion index T Wt % -2.5 mm	Abrasion index ½ Micum I Wt% -5mm Abrasion index ¼ Micum = Wt% -3 mm

SMALL PRINT

Table 4.2 **Test Methods for Measuring the Low Temperature** Degradation

Test Method	Dynamic Test		Static Test	
	BISRA L T B Great Britain	Studiengesellschaft Othfresen Fed Rep of Germany	Numerous German Steel Mills	Japanese Steel Mills
Apparatus length diameter lifter revolutions	Rotating tube 200 mm 130 mm 4 10 rpm	Rotating tube 500 mm 150 mm 4 10 rpm	Thermobalance double wall reduction tube 83 ⌀ basket 75 ⌀	Thermobalance one wall reduction tube 75 ⌀
Sample preparation Weight of the sample Grain size	Drying at 105°C weighing 500 g 10-12 5 mm	Drying at 105°C weighing 500 g 10-12 5 mm ores and pellets 12 5-16 mm sinter	Drying at 105°C weighing 500 g 10-12 5 mm	Drying at 105°C weighing 500 g 20-25 mm or 10-15 mm or other
Reduction temperature	Isothermic 500°C (400/600)	Isothermic 500°C (400/600)	Isothermic 500°C (400/600)	500/550/600/700°C prevailing 500/550°C isothermic
Gas composition and quanity a) during heating b) during testing	N_2 20 % CO 20% CO_2 60% N_2 } 20 Nl/min	24% CO 16% CO_2 60% N_2 } 15 Nl/min	N_2, 20 Nl/min 20% CO 20% CO_2 60% N_2 } 20Nl/min Preheating in double wall retort N_2 to 350°C	N_2 or reduction gas 30% CO 70% N_2 or 26% CO 14% CO_2, 60% N_2 15 or 20 Nl/min Preheating in lower part of retort N_2 15 to 120 min
c) during cooling	To 350°C in arrested tube under N_2 inside the furnace, after that outside the furnace in closed tube	To 400°C in further rotating tube under N_2 after that outside the furnace in closed tube		
Reduction time a) during heating b) during testing c) during cooling	30-40 min 60 min to room temperature	30-40 min 60 min to room temperature	n d 60 min n d	30-120 min 30/60 min 15-120 min
Treatment of sample after reduction	Weighing, screening at 12 5 10 0, 6 3, 3 15, and 0 5 mm Chemical analysis Ferot, Fe++ before reduction	Weighing, screening at 12 5 10 0, 6 3, 3 15, and 0 5 mm Chemical analysis Ferot, Fe++ before reduction	Tumbling of the sample in a tumbler drum of 200 mm inside length, 130 mm ⌀ 2 lifters @20 mm 10 min 30 rpm, after that screening at 6 3, 3 15, and 0 5 mm	Tumbling of the sample in a tumbler drum of 200 mm inside length, 130 mm ⌀ partly 2 lifters 30 min 30 rpm after that screening at 10 5 3, and 1 mm
Test results and evaluation	a) Degree of reduction from loss of weight, paying regards to loss of ignition b) Bases of evaluation Wt % +6 3 mm Wt % +3 15 mm Wt % -0 5 mm	a) Degree of reduction from loss of weight paying regard to loss of ignition b) Bases of evaluation Wt % +6 3 mm Wt % +3 15 mm Wt % -0 5 mm	Bases of evaluation Wt % +6 3 mm Wt % +3 15 mm Wt % -0 5 mm	Bases of evaluation either Wt % - 3 mm and 1 mm or Wt % + 5 mm (+3 mm, +1 mm) or mean size

SMALL PRINT

Table 4.3 Test Methods for Measuring the Swelling of Pellets or Ores*

Test method	LKAB Sweden	CRM, Belgium	JIS Japan
Apparatus length diameter	Thermobalance pellet holder with 3 decks in double wall reduction tube 640 mm high, 57 ⌀	Vertical tube	Horizontal tube 50 ⌀ Reduction tube 360 mm length 30 mm ⌀ Boat of silica 70 mm length 20 mm width 5 mm depth
Sample preparation	Drying at 110°C weighing measuring of volume by mercury displ	Drying weighing measuring of volume by mercury displacement	120 min drying at 105°C ± 5°C measuring of volume by mercury displacement
Quantity/weight of the sample	18 pellets = 60 0 ± 0 1 g	60 g ± 2 g	2 = 3 individual pellets
Grain size of the sample	10-12 5 mm	10-20 mm for ores for pellets as received	-5 mm for pellets 10-15 mm for ores
Heating velocity	In about 15 min to 1000°C	n d	In 60 min to 900°C after that further 30 min at 900°C
Reduction temperature	1000°C ± 5°C	1000°C	900°C ± 10°C
Gas composition a) during heating b) during testing c) during cooling d) gas quantity	N_2 40% CO/60% N_2 preheating in double wall retort N_2 (20 min) 20 Nl/min	N_2 40% CO/60% N_2 preheating in spiral tube N_2 16 7 Nl/min	12 Nl/hr N_2 or Ar for 30 min 30 ± 1% CO/rest N_2, cleaned and dryed < 1% H_2 N_2 or Ar to room temperature 30 Nl/min
Reduction time	120 75 40 15 min	Several periods depending upon reducibility	60 min
Measuring of reduction course	Continuous weighing and measuring the remaining weight	Remaining weight	Remaining weight
Measuring of volume	Mercury displacement	Mercury displacement	Mercury displacement of each individual piece seperately to $V = \frac{W + w}{S} 1$
Test results and evaluation	Measuring of sample weight and sample volume, from that a) Swelling to $\frac{V_1 - V_0}{V_0} 100$ (in %) b) Degree of reduction to $O_{x_{loss}} 100$ (in %) $O_{x_{tot}}$ c) Reducibility to $RG_{60} = \frac{O_{x60}}{O_{x_{tot}}} 100$ (in %) Where V_0 = total volume of the sample prior to reduction V_1 = total volume of the sample after reduction, $O_{x_{loss}}$ = removed oxygen in g (measured by weighing) $O_{x_{tot}}$ = total oxygen of Fe and Mn oxides before reduction calculated from chemical analysis O_{x60} = removed oxygen after 60 min reduction in g	Measuring of sample weight and sample volume from that a) Swelling to $V_1 \cdot \frac{V_0}{V_0} 100$ (in %) b) Degree of reduction at the end of the test $Po - Pa$ 100 (in %) O Where Po weight of the sample prior to red PR weight of the sample after red c) graphic representation swelling vs degree of reduction	Measuring the volume of each individual piece seperately from that $Sw = \frac{V_2 - V_1}{V_1} 100$ (in %) report mean value with max and min values t Where V = volume in ml of sample W = weight in grams of the sample w = weight in grams of the balance weights S = spec gravity of Hg at the tested temp V_1 = volume prior to reduction (ml) V_2 = volume after reduction (ml) Sw = swelling index (in %)

*Besides the above described methods there are a lot of other methods, for example optical or photometrical, for measuring the volume increase

SMALL PRINT

Table 4.4 **Test Methods for Measuring the High Temperature** Degradation

Test Method	Linder Test (Dynamic)	IRSID Test (Static)	Japanese Steel Mills (Static)	Boris Furnace (Counterflow-Static-Reduction Method)
Apparatus length diameter lifter revolutions	Linder tube 200 mm 130 mm 30 rpm	Vertical tube, 70 ϕ	Thermobalance one wall reduction tube, 75 ϕ	Vertical tube, 4 m high 45 ϕ
Sample preparation Weight of the sample	Drying, weighing 500 g ores, pellets or sinter 200 g coke	Drying, weighing 500 g	Drying, weighing 500 g	Drying, weighing about 20 kg
Grain size	20-40 mm resp 30-40 mm	8-20 mm or closer fractions	Ores and sinter 20 ± 1 mm Pellets 12 ± 1 mm	Max 20 mm
Reduction temperature	20-1000° C with 350 resp 100° C/hr	20-950° C in 30 min, after that 15 min at 950°	900° C isothermic	Max 950° C
Gas composition and quantity a) during testing	Varying from . 30-32 5% CO 10-2% CO_2 59 5-65% N_2 0 5% H_2 15 Nl/min const	30% CO 15% CO_2 55% N_2 50 Nl/min	N_2 during heating after that 30% ± 1% CO 70% ± 1% N_2 15 Nl/min	Gas programs of CO, CO_2 H_2 N_2 if wanted under pressure up to 5 bar
b) during cooling	At first under N_2, after that in closed tube to room temperature		N_2	N_2 inside the tube water cooling outside the tube
Reduction time a) during heating b) during testing c) during cooling	5 hr	30 min 15 min	60 + 30 mm 180 min	From 0 5-10 hr in wide ranges
Treatment of sample after reduction	Sorting of coke Weighing, screening, chemical analysis Fetot, Fe++ Femet	Screening at 5 mm, weighing the material at 5mm and screening at 2 mm	a) Tumbling of the sample in a tumbler drum 20 mm inside length 130 mm ϕ 30 min rpm screening at 1 mm	a) Rist diagram b) Reduction curve c) Testing the reduction product on Volume, porosity, abrasion by tumbling and screening with a drum screen, microscopic evaluations, chemical analysis of different sections
Test results and evaluation	a) Degree of oxidation ref to formula $100\ (1 - \frac{\%\ Fe^{++}}{3\%\ Fe_{tot}} - \frac{\%\ Fe_{met}}{\%\ Fe_{tot}})$ b) disintegration Wt %-1 mm Wt % -3 mm	1) -2 mm is the product of reduction + 2 mm at first 500 sec, after that 1000 sec tumbling in a drum screen (2 mm # 150 mm ϕ 250 mm length 60 rpm) 2) -2 mm is the product of tumbling. Weighing all products, chemical analysis	b) Measuring the cold crushing strength	
Remarks				Similar to this procedure is the blast furnace simulator of Technical University Aachen, Fed. Rep. of Germany

SMALL PRINT

Table 4.5 **Test Methods for Measuring the Softening**

Test method	CRM, Belgium	DFB Apparatus, Studiengesellschaft, Othfresen, Fed. Rep. of Germany	Meltdown Test Japan
Apparatus	Steel crucible	Alumina crucible, alumina rod	Graphite crucible 110 mm high with holes in the bottom
length diameter	33 mm 30 mm		
Sample preparation	Prereduction to different red degrees	Prereduction to different red degrees after that grinding to -0.1 mm and pressing a cylinder of 18.4 ϕ and 16-25 mm high (40 000 N load)	Prereduction in reduction tube 70 ϕ at 900° C in 30% CO 70% N_2 for 1.45 hr 3 hr 4 hr Sinter 250 g 15-20 mm Ores 500 g 15-20 mm Pellets 500 g, 10-15 mm
Kind of sample	n.d.	Cylinder 18.4 ϕ x 16-25 mm.	120 g reduced material, 40 g of coke (10-15 mm size) as floor layer and top layer Total height about 90 mm
Grain size	1.4 - 2.0 mm		
Reduction temperature	Heating from 800° C with at first 5, falling to 0.5° C/min max temperature about 1400° C	Preheating with 3.75° C/min to 1350° C under N_2, load 10 N/Cm^2	Preheating under Ar and N_2 (about 1 Nl/min each) in 15 min from 900° C to 1100° C after that with 10° C/min to 1650° C
Gas composition a) during heating b) during testing c) during cooling	 N_2 N_2	 N_2 N_2 Air	Ar and N_2
Gas quantity		1.7 Nl/min	See above
Gas preheating Reduction time Mechanical load	— — 20 N/cm^2	— — 10 N/Cm^2	 See above
Measuring of reduction course	Step by step before softening test	Step by step before softening test	—
Test results and evaluation	Measuring of expansion and contraction related to temperature Bases of evaluation: T_1 = temperature at 3% contraction T_2 = temperature at 25% contraction plotting T_1 and T_2 over degree of reduction	Measuring of expansion and contraction related to temperature T_A = temperature at 0.6% contraction after max. expansion T_E = temperature at 20% contraction related to T_A plotting T_A and T_E over degree of reduction. Bases of evaluation T_A 30, T_A 60 T_A 80 Δt 30, Δt 60, Δt 80	Observing the dropping of molten material sampling at each rise of 50° C in the crucible temperature Contour picturing of molten material, crushing magnetic separation, chemical analysis on Fe FeO, CaO, SiO_2 Al_2O_3, MgO of nonmagnetic material

SMALL PRINT

Table 4.6 Test Methods for Measuring the Reduction Behavior under Load

Test method	Pressure Reduction - Softening Studiengesellschaft, Othfresen, Fed. Rep. of Germany	On-Load Test, Japan	Metallurgical Test Center Luleå, Sweden
Apparatus length diameter	Thermobalance 800 mm high 125 ø	Al_2O_3-reaction pipe 110 ø 1200 mm high, graphite container 70 ø width, graphite push rod	Graphite container and push rod perforated
Sample preparation	Drying, weighing	Drying, weighing	Prereduction at 1000° C to about 60% degree of reduction
Weight of the sample	1200 g	About 500 g (70 x 70 mm, constant volume)	1000 g
Grain size	10-12.5 mm (sample is embedded in alumina balls)	10 ± 1 mm	
Reduction temperature	1050° C (max 1100° C) isothermic	In 60 min from 200 to 600° C without load, from 60 to 260 min from 600° C to 1200° C, 10 N/cm² load, from 260 to 300 min from 1200° C to 1400° C, 10 N/cm² load	Preheating under N_2 to 1000° C, after that heating to 1350° C with 200° C/hr under 30% CO 70% N_2 load 5 N/Cm²
Gas composition a) during heating b) during testing c) during cooling	N_2 40% CO/60% N_2 (drying and cleaning by silica gel) Air	30% CO/70% N_2	See above
Gas quantity	83 Nl/min	20 Nl/min	See above
Gas preheating Reduction time Mechanical load	Wall of the tube 150 min or to 80% degree of reduction 5 N/Cm²	Alumina balls See above	See above
Measuring of reduction course	Balance with ± 1 g accuracy	Waste gas analysis	Waste gas analysis
Test results and evaluation	Measuring of a) Pressure drop of the reducing gas in mm W G b) Expansion and contraction of the sample c) Reducibility by oxygen removal-time curve Bases of evaluation a) Pressure at 80% degree of red (mm W G) b) Exp. or contr. at 80% degree of red (in %) c) Reducibility $\frac{(dR)}{(dt)}$ 40 (in %/min)	Measuring of a) Pressure drop b) Expansion and contraction c) Degree of reduction	Measuring of a) Pressure drop b) Expansion and contraction

SMALL PRINT

CHAPTER 5

THE CIRCULATION AND ACCUMULATION OF ALKALIS INSIDE THE BLAST FURNACE

5.1 INTRODUCTION

Alkalis are introduced into the blast furnace mainly in the form of complex silicates, as part of the iron ore sinter or pellets with the gangue phases, or combined with the coke ashes. They leave the furnace (except the portion absorbed by the refractory lining) with the slag and as suspended fine particles with the blast furnace gas.

For short duration, the total input of alkalis in the raw materials (iron oxide-bearing materials and coke) is normally not exactly matched by the total output in the slag and the top gas leaving the furnace. This means that the iron blast furnace has the capacity to accumulate and occasionally to drain alkalis from its system.

Samples taken from the working blast furnace and direct observations during relining of many furnaces have shown that the alkali content in the burden materials increases on their way downward toward the melting zone[54].

The circulation and accumulation of alkalis are sensitive to the total alkali input to the furnace. The higher the alkalis in the raw materials, the easier they circulate and accumulate and build up to dangerously high levels.

The adverse effects of alkalis are more pronounced when the

stability of the coke and/or the gangue phase of the iron oxide-bearing materials (sinter or pellets) is relatively low. The consequences are higher coke rate, poor quality of hot metal and deterioration of the refractory lining[55].

5.2 STABILITY OF ALKALI COMPOUNDS

The key to finding a measure of stability of various alkali compounds, under a given condition relevant to the commercial blast furnace, is to determine the partial pressure of alkali metals in equilibrium with these compounds. The lower the value of the partial pressure the more the particular compound is stable with respect to an atmosphere which does not contain alkalis initially.

It is conceivable that all kinds of combinations of temperature and reducing potential may prevail in certain locations in the blast furnace. However, in order to simplify the calculations the temperature and the gas composition will be assumed constant in each horizontal level in the furnace. The temperature distribution and the corresponding partial pressures of CO and CO_2 inside the blast furnace are taken from Kitaev et al. who measured their values using vertical probe[56] The standard free energy changes (ΔG°) of the various compounds will be determined according to the Ellingham diagram[57] or Janaf thermochemical tables[58], that means all chemicals (reactants and products) are at their standard states, as a function of temperature. Standard state of condensed phases are pure substances and for gases at one atmosphere partial pressure.

The starting point is to calculate the partial pressure of oxygen in the various levels inside the iron blast furnace, which is in equilibrium with the furnace gas at the same temperature, according to the

following reaction:

$$2CO + O_2 = 2CO_2 \qquad (1)$$

$$\Delta G^\circ_{(1)} = -135{,}000 - 20.71\ T \pm 2{,}000\ cal \qquad (61)$$

where T is the absolute temperature in degrees Kelvin.

The partial pressure of oxygen at different temperature levels in the blast furnace is given in Table 5.1.

Looking to Table 5.1 one can recognize that the reducing power of the blast furnace gases increases slowly up to a temperature of about 1200°K (or 900-1000°C) which is the temperature of the thermal reserve zone; then boosts to very high values in terms of (P_{CO}:P_{CO_2}) as the burden descends toward the tuyeres level.

5.2.1 Alkali Oxides

Alkali oxides are the least stable among the alkali compounds. They do not form molecular gases[58,59]; however, they decompose to form alkali vapors and molecular oxygen. The decomposition reaction may be written as:

$$4K_{(g)} + O_{2\,(g)} = 2K_2O_{(s)} \qquad (2a)$$

$$4Na_{(g)} + O_{2\,(g)} = 2Na_2O_{(s)} \qquad (2b)$$

Assuming the activity of alkali oxides equal to unity and using the partial pressure values of oxygen in Table 5.1, the equilibrium partial pressures of K and Na in equilibrium with the blast furnace gas are listed in Table 5.2

Table 5.2 demonstrates that alkali oxides are not stable inside the blast furnace since the equilibrium partial pressures of their vapors are much higher than any practical value expected to exist in the system.

5.2.2 Alkali Carbonates

Since the blast furnace gas contains CO, CO_2 and the alkali vapors, one may expect a reaction between these three components to form alkali carbonates. This reaction may be written as:

$$2K_{(g)} + 2CO_{2(g)} = K_2CO_3 + CO_{(g)} \quad (3a)$$

$$2Na_{(g)} + 2CO_{2(g)} = Na_2CO_3 + CO_{(g)} \quad (3b)$$

where K_2CO_3 and Na_2CO_3 can be in liquid or solid state depending on the temperature. The melting points of pure K_2CO_3 and Na_2CO_3 are 1174°K and 1123°K respectively.

Reactions (3a) and (3b) may take place in two steps as follows:

$$2K_{(g)} + CO_{2(g)} = K_2O + CO_{(g)} \quad (3aI)$$

$$K_2O + CO_2 = K_2CO_3 \quad (3aII)$$

when added $2K_{(g)} + 2CO_{2(g)} = K_2CO_3 + CO_{(g)}$ (3a)

where K_2O may be considered as the activated complex.

Following the same routine as before, the partial pressures of alkali metals in equilibrium with their carbonates and the blast furnace gas are calculated and listed in Table 5.3.

5.2.3 Alkali Cyanides

The formation of alkali cyanides is thermodynamically favorable in the lower region of the blast furnace where both the temperature and activities of carbon, nitrogen and alkali vapors are relatively high. The stoichiometric relation of this chemical reaction (taking place in the gas stream) may be written as:

$$K_{(g)} + 2CO_{(g)} + \tfrac{1}{2}N_{2(g)} = KCN_{(g,l)} + CO_{2(g)} \quad (4a)$$

$$Na_{(g)} + 2CO_{(g)} + \tfrac{1}{2}N_{2(g)} = NaCN_{(g,l)} + CO_{2(g)} \quad (4b)$$

The melting points of KCN and NaCN are relatively low; also, they boil at high temperatures. Therefore, they may exist in liquid state over a wide range of temperatures (895°K - 1898°K for KCN and 835°K - 1803°K for NaCN).

At very high temperatures (close to the tuyeres level), they may also form when alkali vapors come in contact with coke. The chemical reaction may be written as:

$$K_{(g)} + C_{(s)} + \tfrac{1}{2}N_{2(g)} = KCN_{(g,l)} \qquad (5a)$$

$$Na_{(g)} + C_{(s)} + \tfrac{1}{2}N_{2(g)} = NaCN_{(g,l)} \qquad (5b)$$

If $(P_{N_2})^{\frac{1}{2}}$ is approximated to a value of about 1.2 (in the temperature range of 1000°K to 1800°K inside the blast furnace), partial pressures of alkali metals with liquid alkali cyanides may be calculated according to Reactions (5a) and (5b) as listed in Table 5.5.

On the other hand, at lower temperature Reactions (4a) and (4b) may be used to calculate their values as shown in Table 5.4. The partial pressures of alkali cyanides over pure liquid cyanides are given in Table 5.6 which is calculated based on the following reaction:

$$KCN_{(L)} = KCN_{(g)} \qquad (6a)$$

$$NaCN_{(L)} = NaCN_{(g)} \qquad (6b)$$

At high temperature levels (over 1400°K) the equilibrium partial pressures of alkali metals and alkali cyanide vapors are very close to each other as one can see from Tables 5.5 and 5.6. On the other hand Table 5.4 demonstrates that cyanides are less stable than carbonates at temperatures less than 1400°K (Table 5.3). For example, the equilibrium partial pressure of K vapor over $KCN_{(L)}$ is 6.17×10^{-2} atm.

while it is 1.07×10^{-4} atm. over $K_2CO_{3(L)}$ at 1200°K. This conclusion is clearly seen in Figure 5.1 which will be discussed later.

5.2.4 Alkali Silicates

Alkali silicates may originate in the raw material or form in the blast furnace when alkali vapors or minute droplets of alkali carbonates and cyanides come in contact with the silica in the burden or the coke ash. Silicates are the most stable of all the alkali compounds.

Alkali silicates may be decomposed at high temperature zones in the bosh and the hearth. The decomposition reactions may happen in two ways:

(1) When liquid slag (containing alkali silicates) comes in contact with carbon in coke or in liquid metal. The reaction in this case may be written as follows:

$$K_2SiO_{3(slag)} + 3C = 2K_{(g)} + Si_{(hot\ metal)} + 3CO_{(g)} \quad (7a)$$

$$Na_2SiO_{3(slag)} + 3C = 2Na_{(g)} + Si_{(hot\ metal)} + 3CO_{(g)} \quad (7b)$$

Reactions (7a) and (7b) may be written in two steps as follows:

$$K_2SiO_{3(slag)} + C = 2K_{(g)} + SiO_{2(slag)} + CO_{(g)} \quad (7aI)$$

$$Na_2SiO_{3(slag)} + C = 2Na_{(g)} + SiO_{2(slag)} + CO_{(g)} \quad (7bI)$$

$$SiO_{2(slag)} + 2C = Si_{(hot\ metal)} + 2CO \quad (7aII)$$

(2) When carbon reacts with the coke ash which contains alkali silicates. The reaction may be written as:

$$K_2SiO_{3(ash)} + 2C = 2K_{(g)} + SiO_{(g)} + 2CO_{(g)} \quad (8a)$$

$$Na_2SiO_{3(ash)} + 2C = 2Na_{(g)} + SiO_{(g)} + 2CO_{(g)} \quad (8b)$$

Reactions (8a) and (8b) may take place in two steps as follows:

$$K_2SiO_{3(ash)} + C = 2K_{(g)} + SiO_{2(ash)} + CO \quad (8aI)$$

$$SiO_{2(ash)} + C = SiO_{(g)} + CO \quad (8aII)$$

$$K_2SiO_{3(ash)} + 2C = 2K_{(g)} + SiO_{(g)} + 2CO \quad (8a)$$

The formation of alkali silicates at lower temperature levels in the blast furnace stack, as the result of reactions between the silica (in ore and coke) together with the alkalis in the gas stream (as vapors or droplets of carbonates and cyanides) may be represented as follows:

$$2K_{(g)} + SiO_{2(charge)} + CO_{2(g)} = K_2SiO_{3(charge)} + CO_{(g)} \quad (9a)$$

$$2Na_{(g)} + SiO_{2(charge)} + CO_{2(g)} = Na_2SiO_{3(charge)} + CO_{(g)} \quad (9b)$$

$$2KCN_{(g,l)} + SiO_{2(charge)} + 3CO_{2(g)} = K_2SiO_{3(charge)} + 5CO_{(g)} + N_{2(g)} \quad (10a)$$

$$2NaCN_{(g,l)} + SiO_{2(charge)} + 3CO_{2(g)} = Na_2SiO_{3(charge)} + 5CO_{(g)} + N_{2(g)} \quad (10b)$$

$$K_2CO_{3(l,g)} + SiO_{2(charge)} = K_2SiO_{3(charge)} + CO_{2(g)} \quad (11a)$$

$$Na_2CO_{3(l,g)} + SiO_{2(charge)} = Na_2SiO_{3(charge)} + CO_{2(g)} \quad (11b)$$

The stability of alkali silicates, measured in terms of the partial pressures of alkali vapors can be calculated according to the partial pressure of O_2 in the system. Two cases may be considered. At low temperature levels (below 1600°K) the partial pressure of O_2 will be calculated in equilibrium with the blast furnace gas (from Table 1). At high temperature levels (above 1600°K) the partial

pressure of O_2 will be calculated based on Reaction (12) and assuming that the partial pressure of CO is almost constant with a value of about 0.4 atm.

The two reactions to be considered are (13a) and (13b). They were used to calculate the partial pressures of alkali metals inside the blast furnace in equilibrium with their silicates, as shown in Table 5.7 taking conservative estimated values of $a_{K_2SiO_2}/a_{SiO_2}$ or $a_{Na_2SiO_2}/a_{SiO_2}$ as 10^{-2} and 10^{-3}.

$$C_{(s)} + O_{2\,(g)} = 2CO_{(g)} \qquad (12)$$

$$\Delta G°_{(12)} = -53{,}400 - 41.9T \qquad \pm 1{,}000 \text{ cal}^{(59)}$$

$$4K_{(g)} + 2SiO_{2\,(charge)} + O_{2\,(g)} = 2K_2SiO_{3\,(charge)} \qquad (13a)$$

$$4Na_{(g)} + 2SiO_{2\,(charge)} + O_{2\,(g)} = 2Na_2SiO_{3\,(charge)} \qquad (13b)$$

$\Delta G°$ = $-300{,}700 + 64.4T$ (337°K - 1049°K)

(13a) = $-376{,}400 + 136.6T$ (1049°K - 1250°K)

= $-351{,}600 + 116.6T$ (1250°K -)

$\Delta G°$ = $-308{,}000 + 62.0T$ (371°K - 1187°K)

(13b) = $-400{,}500 + 139.9T$ (1187°K - 1361°K)

= $-376{,}300 + 122.1T$ (1361°K - 1986°K)

(The accuracy of measuring the standard free energy of formation for the alkali silicate is rather poor. It may have an error of more than ± 10,000 cal/mole[59].)

The stabilities of various alkali compounds are represented graphically in Figure 5.1 which shows that:

(1) Silicates are the most stable alkali compounds inside the

blast furnace, and

(2) Alkali carbonates are more stable than cyanides up to a temperature of about 1400°K; then liquid cyanides become more stable than liquid alkali carbonates.

Also, it is important to point out again that the partial pressures of alkali metals and their cyanides vapors are very close in value at temperatures above 1400°K as shown in Tables 5.5 and 5.6.

5.3 THE CIRCULATION OF ALKALIS INSIDE THE BLAST FURNACE

At the blast furnace bosh and hearth, formation of alkali vapors is thermodynamically favored. The alkalis originated in the raw materials (mainly in silicate form) or formed due to condensation of alkali vapors at low temperature levels in the furnace stack (Reactions 3 - 5 and 9 - 11) may be reduced again (Reactions 7 and 8) due to the high temperature and the absence of alkali vapors in the coming gas.

According to Figure 5.1, above the tuyeres level alkali cyanides and carbonates are unlikely to survive; also the alkali silicates may be reduced to form alkali vapors with the blast furnace gases with partial pressures as high as 10^{-2} atm. The simultaneous formation of silicon carbide or the passage of silicon into the molten pig iron (Reaction (7aII)) or the formation of silicon monoxide (Reaction (8aII)), wherever conditions are locally suitable, could cause considerable change in the driving force as well as the reaction path to result in an increase in the vapor pressure of the alkalis as metals. Another important factor is the activity of alkali silicates in the slag which is sensitive to its basicity. The more the basic oxides in the final slag (CaO and MgO) the higher the probability the alkali silicate to be gasified.

With the concentrations of alkalis actually found in the tapped slag (about 0.6 wt.% K_2CO_3 and 0.2 wt.% Na_2CO_3 for normal slag), the formation of alkali vapors would proceed in the hottest zone where the gas is essentially alkali-free. However, the fast ascending gases may have little chance to come into equilibrium with respect to the reacting condensed phases. Much lower values for the partial pressures for alkali metals and cyanides of the order of 10^{-3} to 10^{-5} atm. in the bosh may be more realistic for studying their influence on the burden material and coke.

The conversion of alkali vapors to carbonates and cyanides (Reactions 3, 4 and 5) as suspended droplets in the gas stream is thermodynamically favorable at low temperatures (see Figure 5.1). However, the kinetic aspects may lead to the presence of alkalis as vapors or suspended droplets (carbonates and cyanides) together in the gas stream at temperature range of 1200°K to 1400°K.

In the upper parts of the blast furnace stack where the temperature is low and the reducing power of the gas is weak (Table 5.1) the movement of the alkalis is in the opposite direction, i.e. from the ascending gas stream toward the condensed phases which move downward by riding on the burden materials and coke. In the presence of available silica, alkali cyanides and carbonates will be converted to alkali silicates (Reactions 9 and 10) which may be gasified again when they arrive to the high temperature zones. The counter-current flows of gas and solids and reactions (gasification and condensation of alkali-containing species) are the segments of the cycling of alkalis in the blast furnace.

5.4 ALKALIS CYCLING AND THE BLAST FURNACE OPERATION

The cycling and build up of alkalis inside the blast furnace may

lead to operational problems, including the formation of scaffolds and a decrease of permeability in the stack and bosh. The phenomenon can be eliminated by using raw materials and coke free from alkalis, but this is economically impractical.

5.4.1 Alkalis and the Furnace Permeability

It is generally accepted that charging fine materials hinders the blast furnace process and lowers the permeability of the solid column in its stack. This problem becomes more pronounced with a blast furnace with a higher level of alkalis. The Spanish blast furnace operators found that better blast furnace performance and lining life could be obtained when the burden materials were sized to remove all the fines before charging to the furnace[60].

When there are fines with the charge together with a high level of alkalis cycling, it is highly probable that they agglomerate, using the alkali droplets (carbonates or cyanides) as binding phase, and lower the permeability of the solid column in certain regions of the stack, leading to scaffold formation.

5.4.2 The Extent of Alkalis Cycling

In essence a practical solution to the alkalis cycling in the blast furnace, many workers in the field directed their attention to the slag[49,60,61], since it is easier to drain the accumulated alkalis from the furnace with the slag, rather than to withdraw them as suspended particles with the gases leaving the furnace top.

The extent of alkalis cycling can be controlled through the slag in two ways:

(1) When the slag volume is increased the activity of the alkali silicates will decrease; hence, the gasification processes

occur with more difficulty.

(2) The basicity of the slag has the opposite effect, where more basic oxides (CaO and MgO) in the slag result in increasing the activity of the alkali silicates and enhance the gasification process.

Based on plant data Ashton et al.[61,62] reported two empirical relations which related the alkali output to the slag and the hot metal chemistry through its basicity as follows:

$$(K_2O)_{slag}\ wt\% = 1.44\ (\frac{B}{A})^{-7.47} \qquad (14)$$

$$(K_2O)_{slag}\ wt\% = 0.08 + 1.18\frac{[Mn]_{slag}\ wt\%}{[Mn]_{hot\ metal}\ wt\%} \qquad (15)$$

where B = Σ basic oxides wt%

A = Σ acid oxides wt%

Equation (14) is a straightforward relation between the slag basicity and the alkali output. On the other hand, Equation (15) may be explained according to the influence of the basic oxides on both the alkalis and manganese. Alkali and manganese silicates are the weaker partners in the slag compared to calcium and magnesium silicates. This means that their activities may be affected by the basicity in a similar manner, since the slag is the link between the two kinds of reactions between the alkalis in the gas phase, the silica in the slag and manganese in hot metal. These reactions can be represented as follows:

$$2K_{(g)} + SiO_{2(slag)} + \tfrac{1}{2}O_{2(g)} = K_2SiO_{3(slag)} \qquad (16)$$

$$[Mn]_{hot\ metal} + SiO_{2(slag)} + \tfrac{1}{2}O_{2(g)} = MnSiO_{3(slag)} \qquad (17)$$

Therefore $\frac{(K_2SiO_3)_{slag}}{(p_K)^2_{gas}} \propto \frac{(MnSiO_3)_{slag}}{[Mn]_{hot\ metal}}$

To keep the partial pressure of K vapor constant then:

$$(K_2SiO_3)_{slag} \propto \frac{(MnSiO_3)_{slag}}{[Mn]_{hot\ metal}}$$

or

$$(K_2O)_{slag} \propto \frac{(Mn)_{slag}}{[Mn]_{hot\ metal}}$$

Based on reactions (7a) and (7b) it is thermodynamically obvious that the alkalis taken with the final slag is also a function of [Si] in the hot metal and the temperature of the hot metal (which reflects the temperature inside the blast furnace in the hot zone). The alkali content of the slag increases as the hot metal silicon decreases and its temperature decreases.

Lowering the slag basicity sounds like a practical solution for draining the accumulated alkalis in the blast furnace. However, especially with those furnaces operating with relatively lower slag/hot metal ratio, the sulfur content of the hot metal may go up with lowering the slag basicity and the hot metal temperature. To overcome this problem and to satisfy the steelmakers' requirements, the hot metal which has higher sulfur content than the accepted standards has to be desulfurized outside the blast furnace in the ladle or the torpedo car. External desulfurization is a well-known practice nowadays, especially here in Canada[63].

5.4.3 Calcium Chloride as a Cleaner

Calcium chloride was used as a cleaner, based on experience that the alkali content in the slag was increased after a few hours of steadily charging $CaCl_2$[64]. However, Ashton et al.[62] reported that no substantial improvement in alkali removal in the two tests they carried out at Dofasco were discovered. They suggested that the alkali input was too

low for accumulation to occur; hence, the effect of $CaCl_2$ could not be observed.

The sudden increase in alkali removal could mean a cut-down in accumulation. However, the mechanism of the removal action is still unknown. Lu[65] suggested that $CaCl_2$ may evaporate to form $CaCl_2$ vapor inside the blast furnace and attack the scaffold's binding phase (which contains mainly alkali carbonates and cyanides). This may weaken the structure of the scaffold and lead to its collapse. The period of high alkalis in slags may be the results of higher alkalis in the scaffold which just arrived at the furnace bottom. According to his suggestion $CaCl_2$ may be helpful when the furnace is really deeply in trouble.

Table 5.1 The partial pressures of CO_2, CO and O_2 at different temperature levels in the blast furnace.

Partial Pressure Atm.	Temperature °K					
	600	800	1000	1200	1400	1600
P_{CO_2}	0.242	0.218	0.198	0.186	0.032	0.006
P_{CO}	0.518	0.536	0.554	0.570	0.686	0.732
P_{O_2}	2.4×10^{-39}	1.04×10^{-27}	9.07×10^{-21}	3.78×10^{-16}	1.02×10^{-14}	1.78×10^{-13}
$P_{CO}:P_{CO_2}$	2.14	2.46	2.80	3.06	21.43	122.00

Total pressure is 2 atm.

Table 5.2 The partial pressures of alkali metals in equilibrium with their oxides and the blast furnace gas.

Partial Pressure Atm.	Temperature °K					
	600	800	1000	1200	1400	1600
P_{O_2}	2.4×10^{-39}	1.04×10^{-27}	9.07×10^{-21}	3.78×10^{-16}	1.02×10^{-14}	1.78×10^{-13}
P_K	7.04×10^{3}	4.50×10^{2}	112	86.9	39.8	126
P_{Na}	262	60.8	22.2	13.5	49.5	321

The error in measuring $\Delta G°$ is ± 10,000 cal according to Richardson and Jeffes[59].

Table 5.3 The partial pressures of alkali metals in equilibrium with their carbonates and the blast furnace gas.

Partial Pressure Atm.	Temperature °K					
	600	800	1000	1200	1400	1600
P_{CO_2}	0.242	0.218	0.198	0.186	0.032	0.006
P_{CO}	0.518	0.536	0.554	0.570	0.686	0.732
P_K	1.88×10^{-16}	2.82×10^{-10}	3.37×10^{-7}	1.07×10^{-4}	3.90×10^{-2}	4.17
P_{Na}	7.05×10^{-16}	6.24×10^{-10}	5.40×10^{-7}	4.70×10^{-5}	2.11×10^{-2}	2.59

The errors in measuring $\Delta G°$ are ± 13,000 cal for Na_2CO_3 and more than that for K_2CO_3 according to Richardson and Jeffes[59].

Table 5.4 The partial pressures of alkali metals in equilibrium with their cyanides and the blast furnace gas.

Temp.°K	Reaction (4a)		Reaction (4b)	
	K_p	P_K atm.	K_p	P_{Na} atm.
900	1.92×10^{5}	2.97×10^{-6}	1.92×10^{4}	2.97×10^{-5}
1000	5.28×10^{3}	1.02×10^{-4}	6.82×10^{2}	6.94×10^{-4}
1200	7.72	6.17×10^{-2}	4.06	0.117
1400	5.87×10^{-2}	0.962	3.19×10^{-2}	1.778

The error in $\Delta G°$ for the alkali cyanides is ± 5,000 cal/mole[59].

Table 5.5 The partial pressures of alkali metals in equilibrium with their cyanides and coke.

Temp.°K	Reaction (5a)		Reaction (5b)	
	K_p	P_K atm.	K_p	P_{Na} atm.
1400	33.65	2.48×10^{-2}	18.24	4.54×10^{-2}
1600	5.408	0.154	3.027	0.275
1800	1.330	0.626	0.771	1.089

Table 5.6 The partial pressures of alkali cyanide vapors in contact with pure alkali cyanide liquids.

Partial Pressure Atm.	Temperature °K					
	900	1000	1200	1400	1600	1800
P_{KCN}	1.08×10^{-5}	1.05×10^{-4}	3.01×10^{-3}	3.16×10^{-2}	0.178	0.668
P_{NaCN}	2.37×10^{-5}	2.16×10^{-4}	5.60×10^{-3}	5.38×10^{-2}	0.282	0.986

Table 5.7 The partial pressures of alkali metals in equilibrium with their silicates inside the blast furnace.

		In equilibrium with blast furnace gas				In equilibrium with coke			
Temperature °K		1000	1200	1400	1600	1600	1700	1800	1900
P_{O_2} (atm.)		9.07×10^{-21}	3.73×10^{-16}	1.02×10^{-14}	1.78×10^{-13}	4.23×10^{-18}	1.14×10^{-17}	2.74×10^{-17}	6.00×10^{-17}
$P_{K(g)}$ atm.	$\lambda = 0.010$	1.25×10^{-9}	6.60×10^{-7}	1.43×10^{-5}	3.61×10^{-4}	5.17×10^{-3}	2.05×10^{-2}	7.00×10^{-2}	0.21
	$\lambda = 0.001$	3.75×10^{-10}	7.80×10^{-8}	4.29×10^{-6}	1.08×10^{-4}	1.64×10^{-3}	6.50×10^{-3}	2.20×10^{-2}	6.60×10^{-2}
$P_{Na(g)}$ atm.	$\lambda = 0.010$	3.70×10^{-10}	1.83×10^{-8}	3.03×10^{-6}	3.22×10^{-4}	1.46×10^{-3}	6.49×10^{-3}	2.45×10^{-2}	8.04×10^{-2}
	$\lambda = 0.010$	5.10×10^{-11}	5.47×10^{-9}	9.09×10^{-7}	9.22×10^{-5}	4.62×10^{-4}	2.05×10^{-3}	8.69×10^{-3}	2.54×10^{-2}

$$\lambda = \frac{a_{K_2SiO_3}}{a_{SiO_2}} \text{ or } \frac{a_{Na_2SiO_3}}{a_{SiO_2}}$$

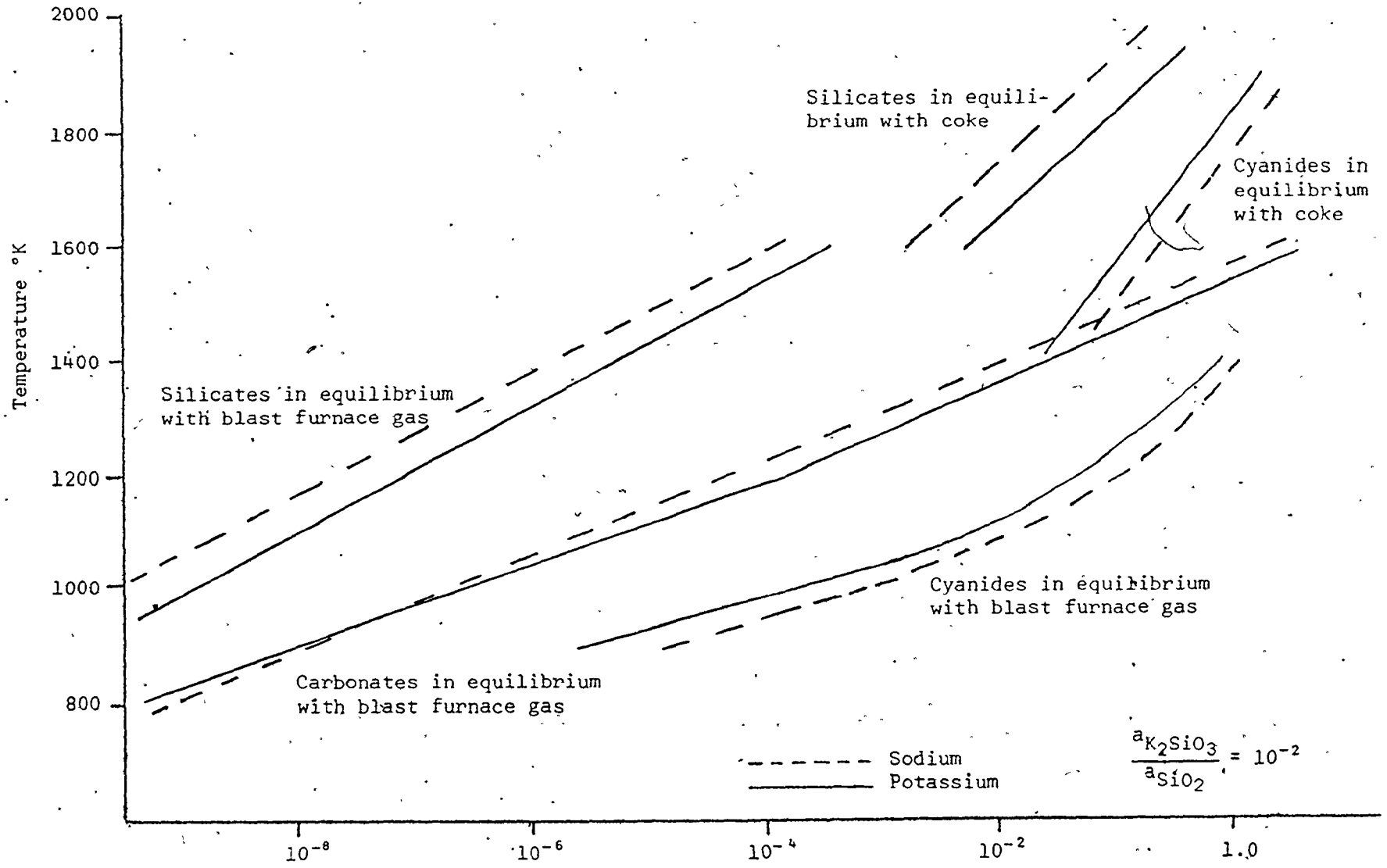

Figure 5.1 Stability of alkalis in the blast furnace.

CHAPTER 6

FORMATION OF LIQUID PHASES

DURING INDURATION AND REDUCTION OF IRON ORE PELLETS

6.1 INTRODUCTION

In the making of satisfactory pellets, it is necessary first to produce good green balls which have the following characteristics:

(1) proper size

(2) uniformity of size

(3) physical strength and resiliency

(4) resistance to thermal shock.

The second step is to indurate the pellets at high temperature to gain sufficient structural strength to withstand without significant breakage, the normal handling between the pellet furnace and the blast furnace skip. During firing and induration in air at high temperatures, magnetite concentrates are bound, as grain growth accompanies the oxidation to hematite. Grain bridges are formed, particles are enlarged and recrystallization takes place. High local temperatures help in forming liquid slag which reinforces the oxide network and produces a coherent pellet structure after cooling. Accordingly, formation of liquid slag of a limited amount during firing and induration is desirable if not necessary to make strong iron ore pellets.

Formation of liquid slags and their relation to the softening and degradation of the pellets during reduction inside the blast furnace were

recognized by many workers in the field, as cited in Chapter 3.

The phase diagrams between iron oxides and the gangue constituents will be accounted in order to inquire about the conditions under which the liquid slag is likely to appear during firing and induration in air or during reduction inside the blast furnace. One should keep in mind that the information gathered from the equilibrium phase diagram represents the ideal conditions where only a limited number of compounds are present. Therefore, the calculated amounts of liquid phase based on the phase diagrams represent the upper limit of that formed inside the pellets in reality.

6.2 APPEARANCE OF LIQUID PHASES DURING FIRING AND INDURATION

For hematite ores with no impurities, one cannot expect liquid phase to emerge at temperatures lower than the melting point of magnetite (1588°C) whereas hematite decomposes to give magnetite in air at about 1380°C. The sintering and binding of the iron oxide particles and the formation of the bridges between them depend predominantly on surface and solid state diffusion. Hematite bridges are merely the binding phase knotting the particles together when iron ore pellets are made of high purity magnetite concentrates.

Considering the case when silica is the only impurity presented with the iron ore and according to the phase diagram $Fe_2O_3 \cdot FeO - SiO_2$ in air shown in Figure 6.1, the first liquid may appear at 1455°C which is too high to be reached during firing and induration of the iron ore pellets. However, silica in commercial pellets comes in the form of complex silicate which may contain ferrous iron and small amounts of minor impurities such as CaO, Al_2O_3, MgO and MnO. Addition of bentonite as binding phase, to the green balls, may act as a source of these minor

impurities. One may expect the melting point of the gangue phase to be lower than 1455°C.

6.2.1 Systems of Fe_2O_3 - CaO - SiO_2

For self-fluxed pellets, lime or limestone is added before firing. According to the binary diagram between CaO and Fe_2O_3 shown in Figure 6.2, the formation of liquid as a result of dissolution of CaO in Fe_2O_3 may take place above 1205°C which is the eutectic temperature in the binary system. It is well known that raising the temperature of induration and firing of self-fluxed pellets helps in suppressing their tendency to swell during reduction. It may be suggested that those pellets indurated at high temperatures above 1200°C had the opportunity to form stable calcium silicates during firing and to minimize if not to eliminate the free lime which causes abnormal swelling and iron whisker growth during metallization, as shown in Chapter 2.

The phase diagram for the ternary system of Fe_2O_3 - CaO - SiO_2 shown in Figure 6.3 surmises the states when both CaO and SiO_2 are present during induration at high temperatures. Depending on the $CaO:SiO_2$ ratio in the pellet, liquid phases may appear at a temperature of about 1200°C at four different locations in the diagram:

(1) at 1204°C with $CaO:SiO_2$ = 1:2, liquid slag composed of 72 wt.% CaO + SiO_2 and 28 wt.% hematite

(2) at 1214°C with $CaO:SiO_2$ = 1:0.78, liquid slag composed of 61.5 wt.% CaO + SiO_2 and 38.5 wt.% hematite

(3) at 1192°C with $CaO:SiO_2$ = 1:0.27, liquid slag composed of 33 wt.% CaO + SiO_2 and 67 wt.% hematite

(4) at 1205°C with $CaO:SiO_2$ = ∞, liquid slag phase composed of 20 wt.% CaO and 80 wt.% hematite (see Figure 6.2).

6.2.2 Systems of Fe_2O_3 - MgO and Fe_2O_3 - MgO - SiO_2 - CaO

Magnesium oxide alone or in a mixture of CaO - MgO "burned dolomite" was recognized as a good substitute for lime in self-fluxed pellets. MgO as an impurity within the iron ore pellets did not cause abnormal swelling like that originated by CaO[16,27].

The binary diagram between Fe_2O_3 and MgO (Figure 6.4) shows that it is difficult to form liquid slag if MgO is the only impurity present, and, the only way for MgO to incorporate in solid solution with hematite is by surface and solid state diffusion.

MgO is a refractory material with a very high melting point. Adding MgO will not help in lowering the melting point of the gangue phase during induration and firing. Figure 6.5 represents the system between Fe_2O_3, MgO, CaO and SiO_2 which shows that the minimum temperature to form liquid slag between these oxides is about 1300°C.

6.2.3 Systems of Fe_2O_3 - SiO_2 - Alkali Oxides

The pseudobinary diagram between $K_2O \cdot 6SiO_2$ and $K_2O \cdot Fe_2O_3 \cdot 6SiO_2$ is shown in Figure 6.6 which indicates eutectic temperature at about 750°C with liquid phase composed of 13 wt.% Fe_2O_3 and 87 wt.% SiO_2 + K_2O. This slag phase is able to dissolve more hematite to raise its content to about 25 wt.% when the induration temperature reaches 1100°C. Figure 6.7 shows the corresponding ternary diagram for Fe_2O_3 - SiO_2 - Na_2O, which shows that liquid silicate may form at about 830°C. This liquid contains about 13 wt.% hematite and as the firing temperature reaches 1000°C the hematite content in the liquid silicate increases to 28 wt.%.

For acid pellets, alkali oxides ameliorate the formation of liquid slag during induration and firing, as shown in Figures 6.6 and 6.7; which enhances the sintering process leading to strong and dense pellets after

cooling. These pellets may show better crushing index when tested at room temperature; however, their ability to withstand dynamic stresses drops sharply when the same test is carried out at temperatures higher than the melting point of the alkali glass phase bonding the iron oxide particles.

6.3 FORMATION OF LIQUID SLAG DURING REDUCTION

During reduction of the iron ore pellets inside the blast furnace, the gangue phase is accountable for the strength and resistance to degradation before the appearance of a dense layer of iron to reinforce the pellet structure. Formation of liquid slag as a result of the reaction between the gangue constituents and the ferrous iron during heating and reduction induces critical circumstances; the consequence is lower resistance to swelling and softening.

For high purity hematite pellets, formation of liquid slag may be neglected since the melting point of wustite FeO is about 1380°C. The problem the pellets may face is low temperature breakdown during the reduction from hematite to magnetite at the upper parts of the blast furnace stack, as already mentioned in Chapter 1.

The binary diagram between FeO and SiO_2 is shown in Figure 6.8 which indicates eutectic point at 82 wt.% FeO at temperature of 1180°C. During reduction of acid pellets and considering that silica is the only impurity present, the first liquid phase may form at 1180°C. The amount of liquid fayalite extends up to 20.8 wt.% of the pellets with 5 wt.% silica. The presence of liquid fayalite may not be as dangerous as liquid calciowustite, which may form also at temperatures close to 1200°C, since the viscosity of the calciowustite is much lower than that of the iron silicates (fayalite). Therefore, addition of CaO (lime)

can be very harmful as far as high temperature softening is concerned.

6.3.1 Systems of FeO - CaO - SiO_2

Considering the binary system between FeO - CaO, the presence of CaO in solid solution with wustite (FeO) may not lead to liquid formation at a temperature lower than 1300°C when its amount is less than about 5 wt.% of the pellet, as shown in Figure 6.9. This statement may be misleading because CaO may not completely dissolve in the wustite phase, it may be present as calcium ferrites which melt at about 1200°C (Figure 6.2).

Figure 6.11 represents the ternary system FeO - CaO - SiO_2 in equilibrium with metallic iron. According to this diagram, liquid olivine may form during reduction at a temperature of 1093°C. The composition of liquid olivine is FeO 47 wt.%, CaO 18 wt.% and SiO_2 38 wt.%. With commercial iron ore pellets which varied in basicity between 0 to 18/38 ≈ 0.40, the temperature where liquid slag may emerge decreases from about 1180°C at point A (the eutectic temperature in Figure 6.8) to about 1100°C at Point B near the eutectic temperature in the ternary system where liquid olivine forms. On the other hand, when the CaO:SiO_2 ratio exceeds 0.4 behind point B, the melting temperature (when the tie line crosses the liquidus surface) climbs to higher temperature levels with an increase in the basicity of the pellets.

6.3.2 Systems of FeO - MgO - SiO_2 - CaO

The binary system between FeO and MgO has not been studied in detail, but the equilibrium diagram is believed to be as shown in Figure 6.10, where MgO is completely soluble in FeO.

The ternary system FeO - MgO - SiO_2 is given in Figure 6.12. It suggests that iron ore pellets with MgO and SiO_2 as the main gangue

constituents have a poor chance to form liquid slag. The more MgO added the higher the temperature is for forming liquid phase. Liquid olivine which may appear at 1093°C (Figure 6.11) does not form below 1350°C when MgO participates as part of the gangue phase, as shown in Figure 6.13. According to these diagrams MgO seems to be very useful in raising the temperature for softening when added alone or in a mixture of MgO - CaO (burned dolomite) to the commercial iron ore pellets.

6.3.3 Systems of $FeO - SiO_2$ - Alkali Oxides

It is well known that alkalis are undesirable impurities in the blast furnace; among other things they impair the stability of the gangue phase of the commercial iron ore pellets. Their possible influence in forming low melting point slags can be seen in Figures 6.14 and 6.15. Eutectic compounds rich in silica and ferrous iron oxide may form during reduction at temperatures as low as about 750°C in the presence of significant amounts of alkali oxides.

The ternary system $FeO - SiO_2 - K_2O$ was chosen as an example to calculate the extent of liquid slag formation during reduction. The procedure of the calculation is as follows.

(1) It is assumed that during reduction silica reacts first with the potassium oxide to form liquid potassium silicate, which in the latter stage dissolves some ferrous oxide to reach the equilibrium composition according to the phase diagram in Figure 6.14.

(2) The computed results are given in Figures 6.16, 6.17 and 6.18. The ratio of liquid slag phase (potassium iron silicate) to the sum of the silica and potassium oxide content (PLF) is plotted against the ratio of potassium oxide to silica (RK).

A family of curves for various temperatures is given in Figure 6.16. The sudden drop of the amount of liquid silicate present at 700°C when RK reaches about 0.3 is attributed to the intermediate compound ($FeO \cdot 5SiO_2 \cdot K_2O$) which has a melting point of about 900°C. PLF increases with elevating the temperature of reduction and the ratio of potassium oxide to silica in the pellet RK; however, when RK exceeds about 0.4 PLF lessens owing to the movement of the liquidus isotherms from the fayalite to wustite zone in Figure 6.14, where the liquid phase has a lower tendency to dissolve FeO.

(3) The amount of liquid slag formed at 900°C during reduction inside the iron ore pellets with silica as the main gangue constituents is plotted as a function of the silica content. A family of curves which represents pellets with different amounts of silica and potassium oxide is given in Figure 6.17.

The objective in preparation of Figure 6.17 is to illustrate the extent and the quantity of liquid slag which is expected to form during reduction. The curves shown in this figure demonstrate that the liquid alkali iron silicates are sensitive to both the silica and alkali contents of the iron ore pellets.

(4) Acid pellets with the same amount of potassium oxide seem to have a better chance to resist alkali attack and liquid formation when they contain more silica or silicate gangue phase, as shown in Figure 6.18. The silica-rich gangue phase may have a dual effect on the degradation properties of these pellets. Besides its effect on liquid slag formation in the presence of alklai oxides, the remaining binding bridges (which are formed

by adequate firing) are roughly proportional to the silica content of the pellets. These bridges would be responsible for absorbing the stresses which cause the pellets to degradate during reduction.

Figure 6.18 is given to show the combined effect of silica on the liquid slag formation and the binding phase. The degradation parametef (DP), which is defined as the ratio of the amount of liquid alkali iron silicate to the silica content, is plotted against the silica content and a family of curves are given for various amounts of potassium oxide with the pellets.

According to Figure 6.18, the degradation parameter decreases substantially when the silica content of the acid iron ore pellets is increased.

6.3.4 Systems of SiO_2 - CaO(MgO) - Alkali Oxides

The systems SiO_2 - CaO - K_2O are given in Figure 6.19. According to these diagrams, eutectic compounds may form at a temperature of about 900°C which is higher than the eutectic temperature in the SiO_2 - FeO - K_2O ternary system ($\sim$ 700°C), shown in Figure 6.14. However, 900°C may not be high enough to suggest a substantial improvement in the degradation caused by liquid slag formation when alkalis attack iron ore pellets containing CaO and SiO_2 as the main gangue constituents.

Figure 6.20 shows the SiO_2 - MgO - K_2O systems which also suggest that MgO, as part of the gangue phase with the SiO_2, has a positive effect in elevating the temperature where liquid slag may be formed during reduction of basic iron ore pellets which contain MgO. Ilmoni et al[66] studied the influence of dolomite addition on the temperature of initial melting of the gangue phase of acid pellets subject to alkali attack.

They reported that in the presence of potassium oxide, the initial melting temperature of the acid gangue phase was increased by adding dolomite to the mixture.

Natural olivine (which is magnesium iron silicat) was claimed by Ellenbaum et al.[67] as an additive which may improve pellet behavior in the blast furnace with high alkali cycling. They did not support their claim with experimental results. However, they claimed that plant experiments showed a drop in alkalis and improvement in gas flow inside the blast furnace when granules of olivine were charged with the burden materials.

The beneficial effects of olivine are not yet established. However, the following explanation may be given to show its influence on blast furnace practice.

Natural olivine contains MgO (40 - 52 wt.%), SiO_2 (35 - 45 wt.%) and FeO (6.5 - 10 wt.%). It is high in MgO; therefore it should be difficult to melt down compared to acid gangue phase, even in the presence of alkali oxides. When it is charged with the burden as granules it may improve the permeability of the blast furnace stack by remaining in solid state. Of course, the extent of its effect depends on the method of charging it to the blast furnace. On the other hand, if it is added to the pellets (prior to pelletizing and firing) the resultant gangue phase may also have the above-mentioned benefits.

All the phase diagrams presented in this chapter were taken from reference (68).

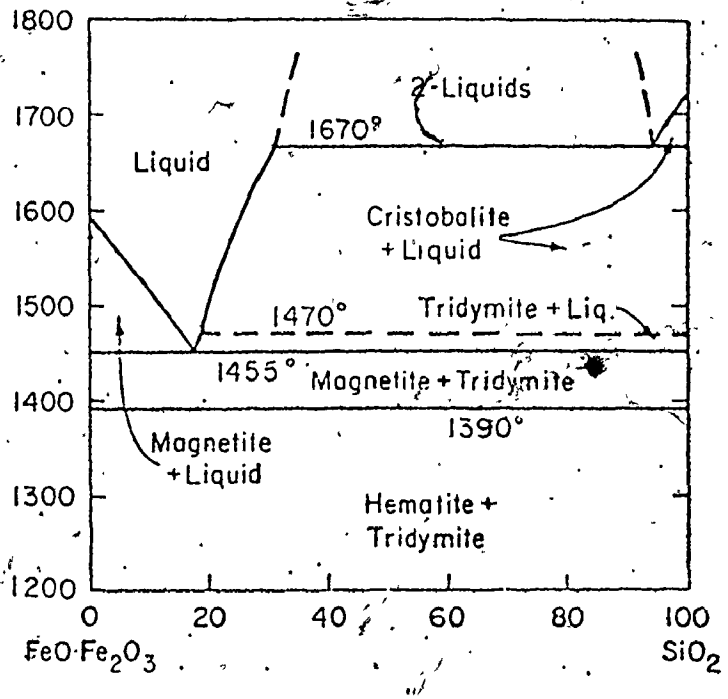

Figure 6.1 System $FeO \cdot Fe_2O_3$-SiO_2 in air; isobaric.

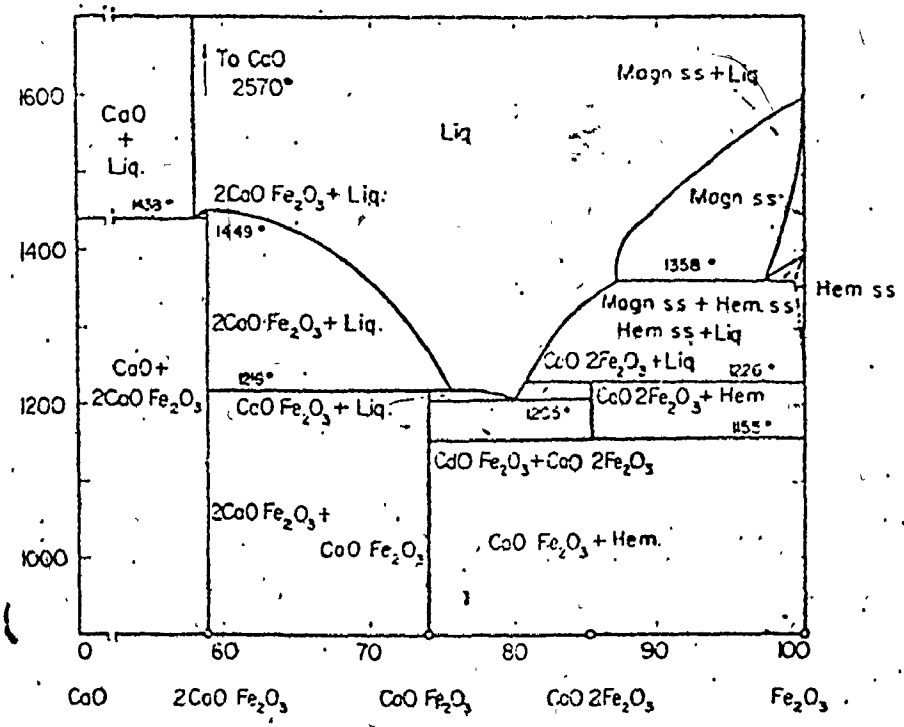

Figure 6.2 System CaO-Fe_2O_3 in air. Hem = hematite, Magn = magnetite, ss = solid solution. Curve A-A in triangular diagram shows compositionof liquids at liquidus temperatures.

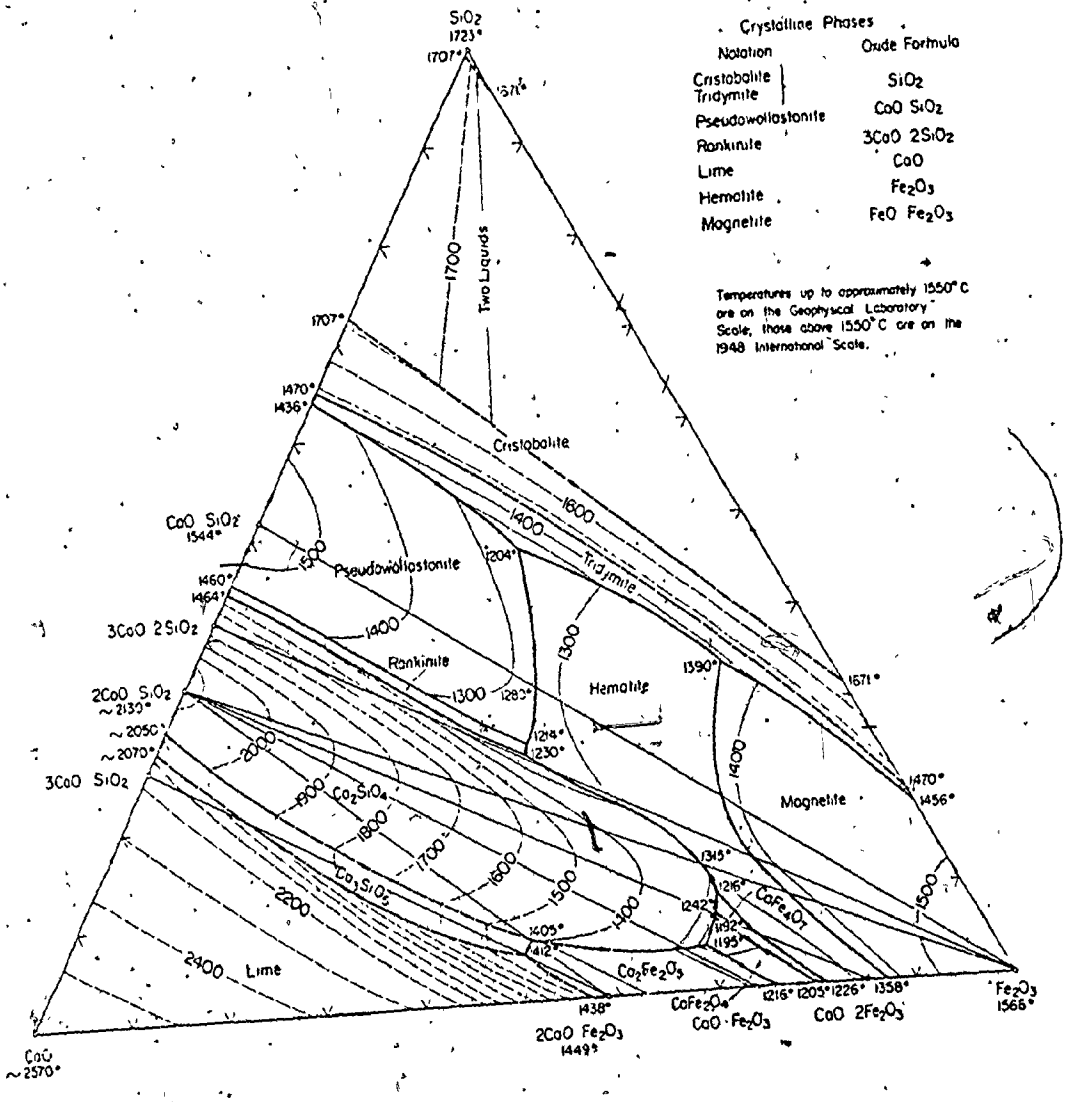

Figure 6.3 System CaO-"Fe_2O_3"-SiO_2; composite; (condensed phases in equilibrium with air)

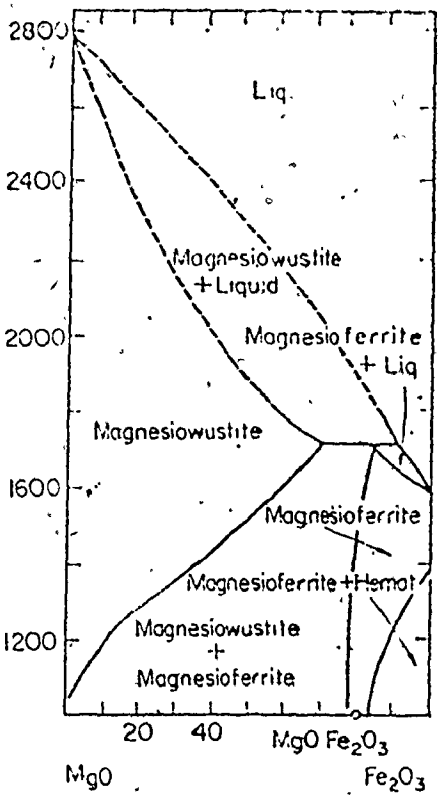

Figure 6.4 System $MgO-Fe_2O_3$ in air.

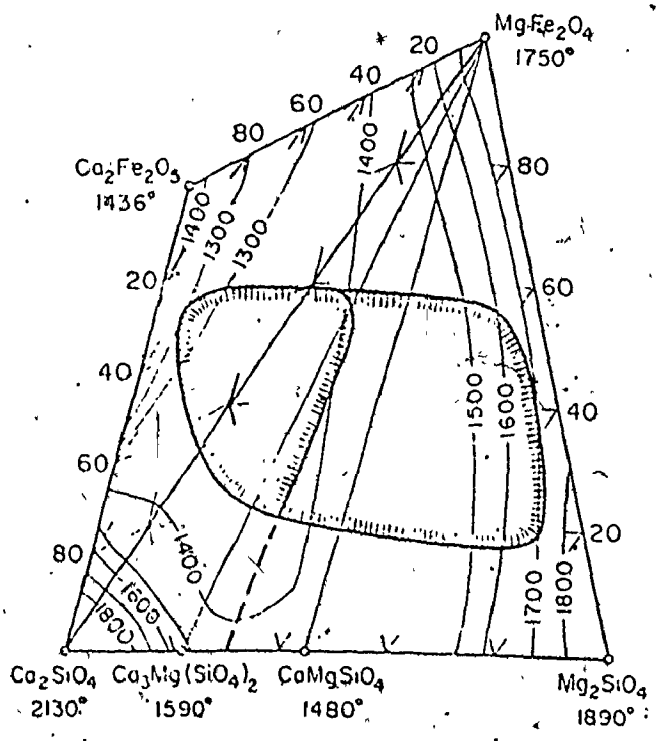

Figure 6.5 System $Ca_2Fe_2O_5-Ca_2SiO_4-MgFe_2O_4-Mg_2SiO_4$, melting isotherms.

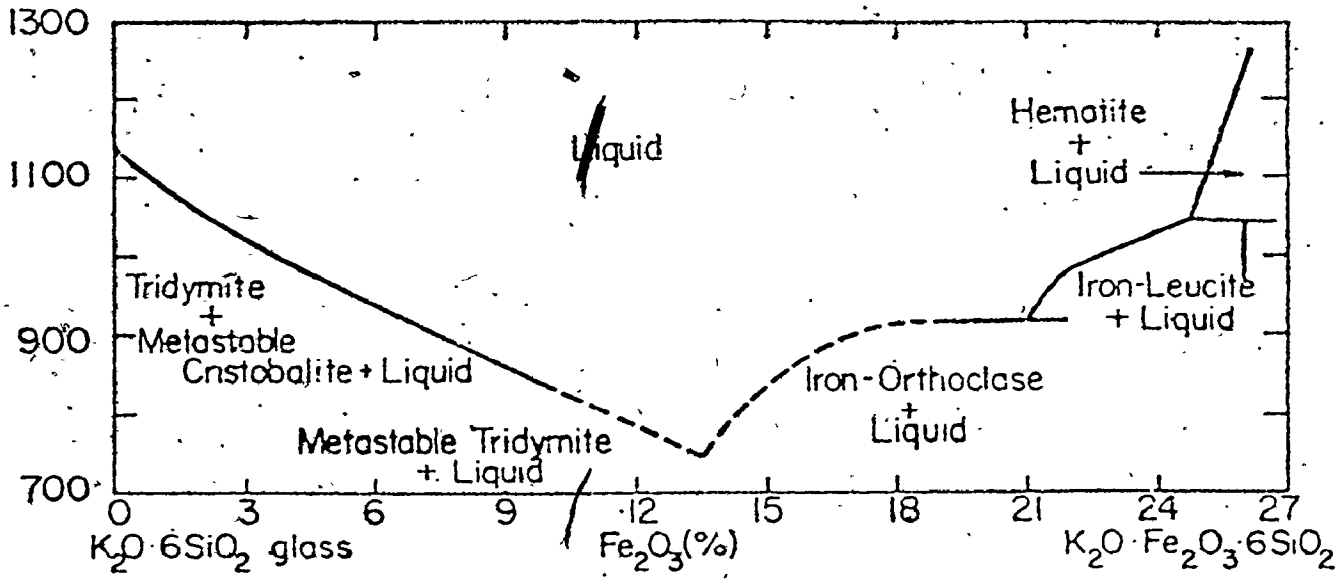

Figure 6.6 System $K_2O \cdot 6SiO_2$-$K_2O \cdot Fe_2O_3 \cdot 6SiO_2$, pseudo-binary. Liquidus temperatures along line X-$K_2O \cdot Fe_2O_3 \cdot 6SiO_2$ of system K_2O-Fe_2O_3-SiO_2.

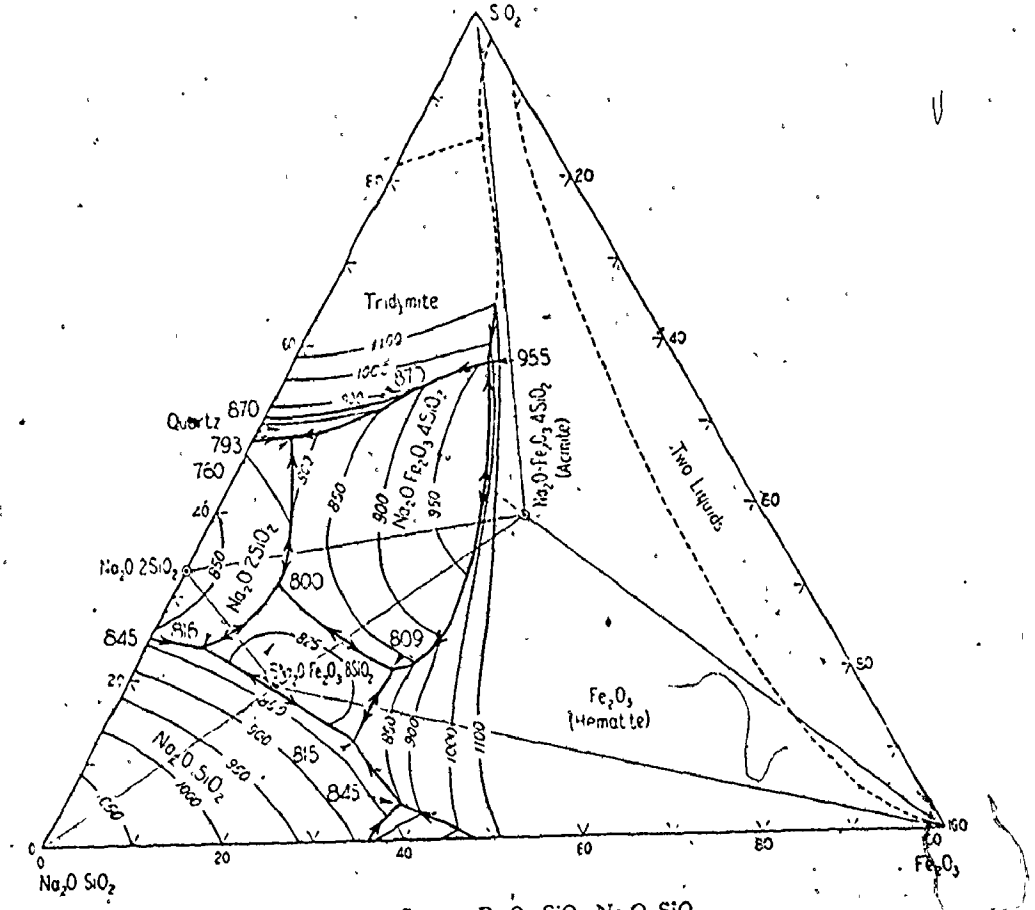

–System Fe_2O_3–SiO_2–$Na_2O \cdot SiO_2$.

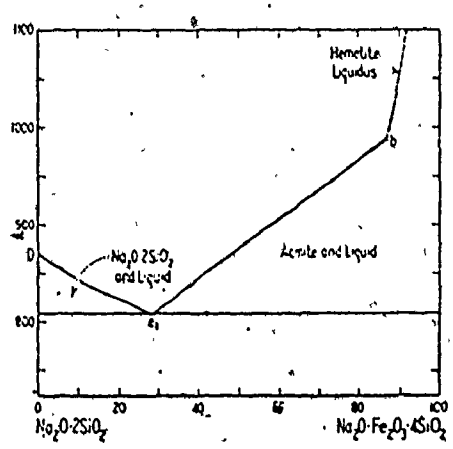

–Join $Na_2O \cdot 2SiO_2$–$Na_2O \cdot Fe_2O_3 \cdot 4SiO_2$ (acmite) of system Na_2O–Fe_2O_3–SiO_2.

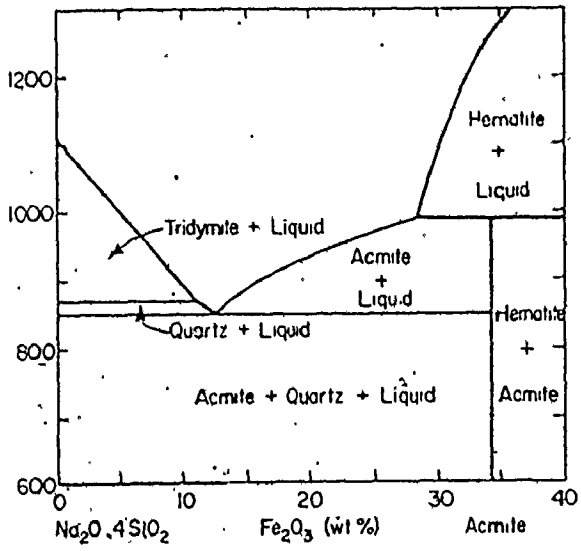

–Section $Na_2O \cdot 4SiO_2$–$Na_2O \cdot Fe_2O_3 \cdot 4SiO_2$ of system Na_2O–Fe_2O_3–SiO_2.

Figure 6.7 Systems of Fe_2O_3–SiO_2–Na_2O.

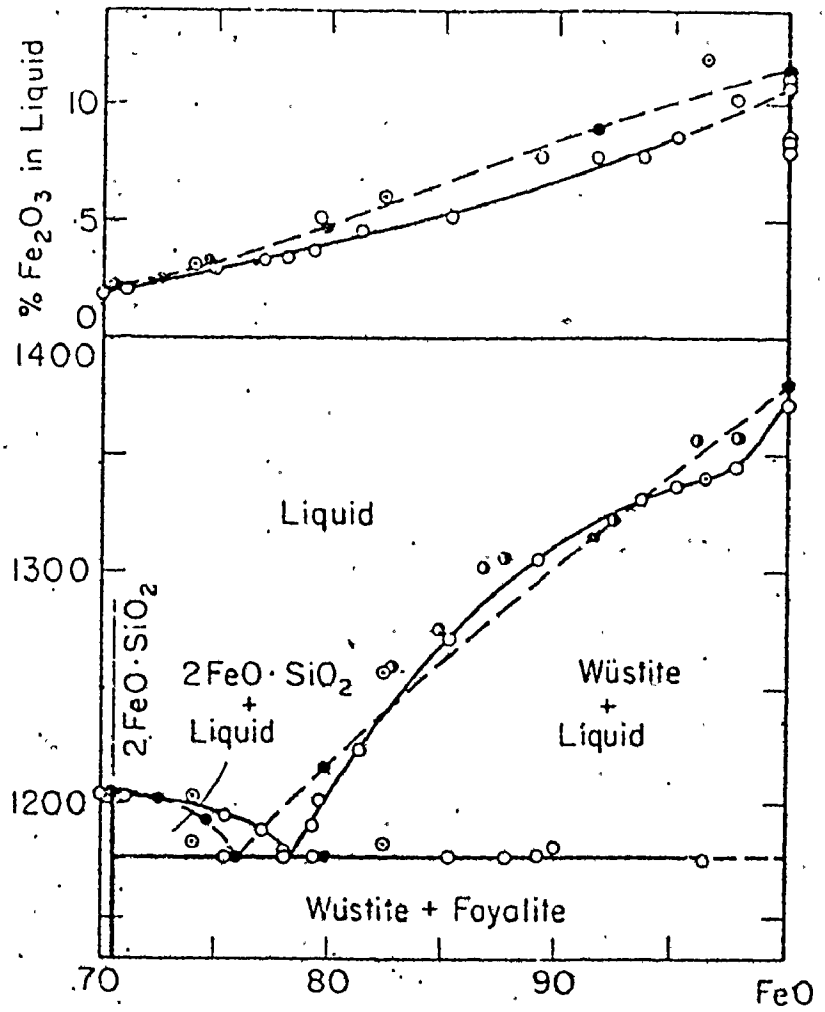

Figure 6.8 System $2FeO \cdot SiO_2$-FeO.

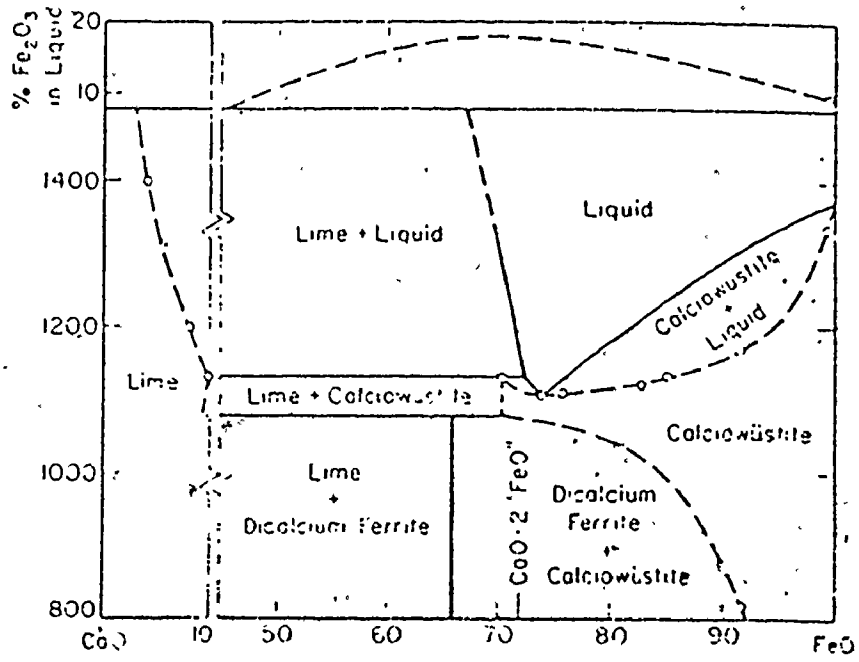

Figure 6.9 System CaO-FeO. Circles - estimated limits of solid solution.

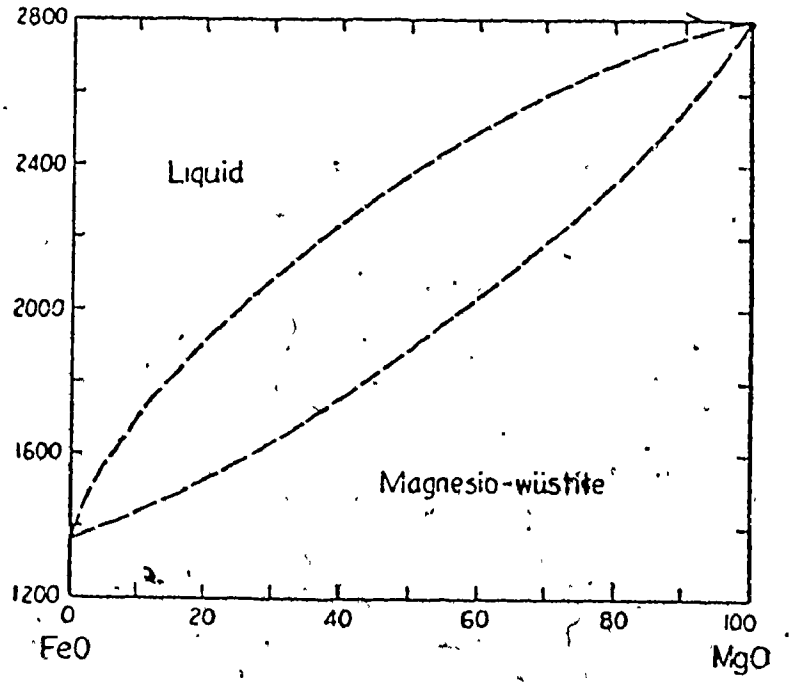

Figure 6.10 System FeO-MgO; this system has not been studied in detail, but the equilibrium diagram is believed to be as shown above if the incongruent melting of FeO is neglected.

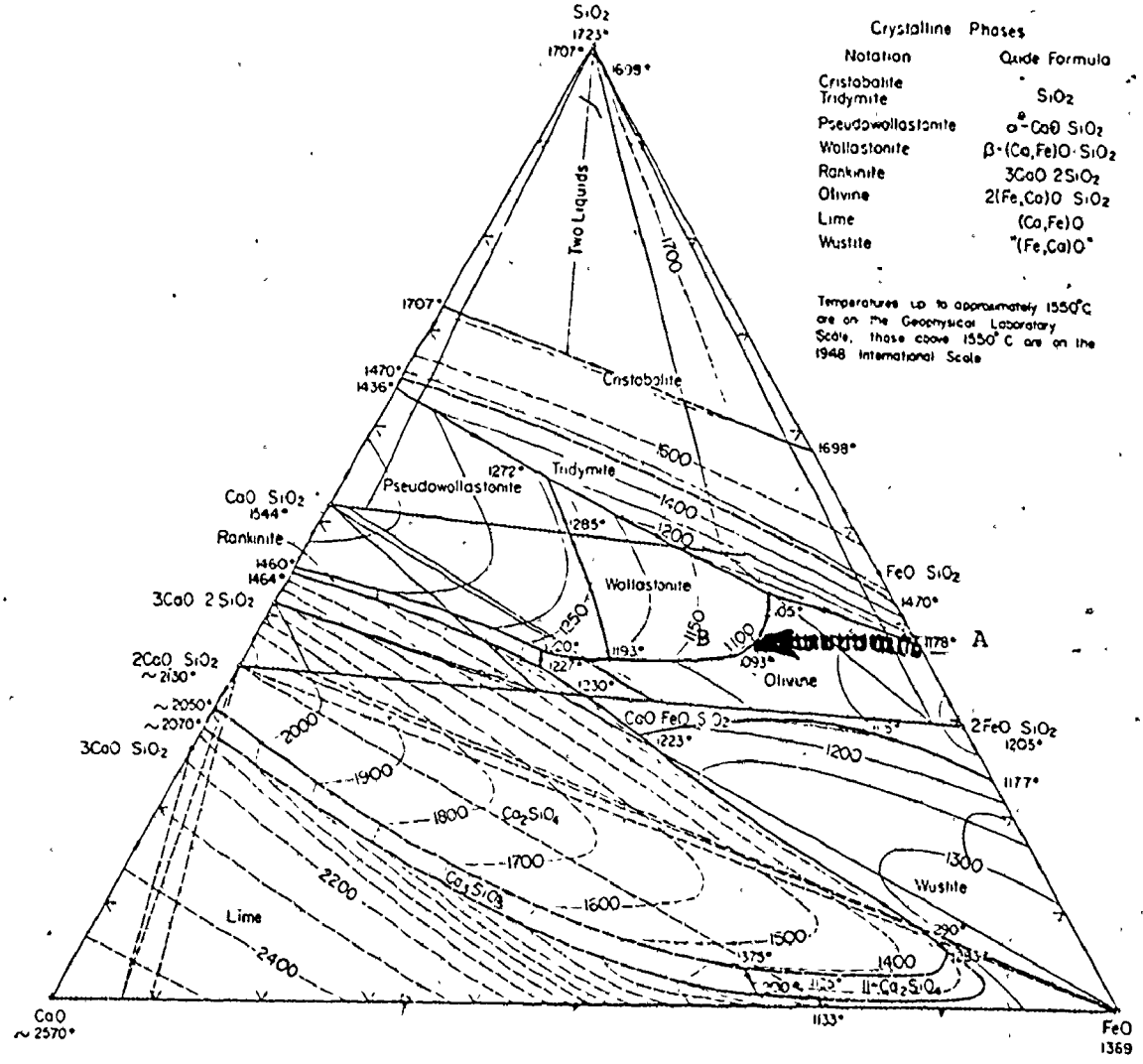

Figure 6.11. System of CaO– FeO– SiO_2 (in equilibrium with Fe).

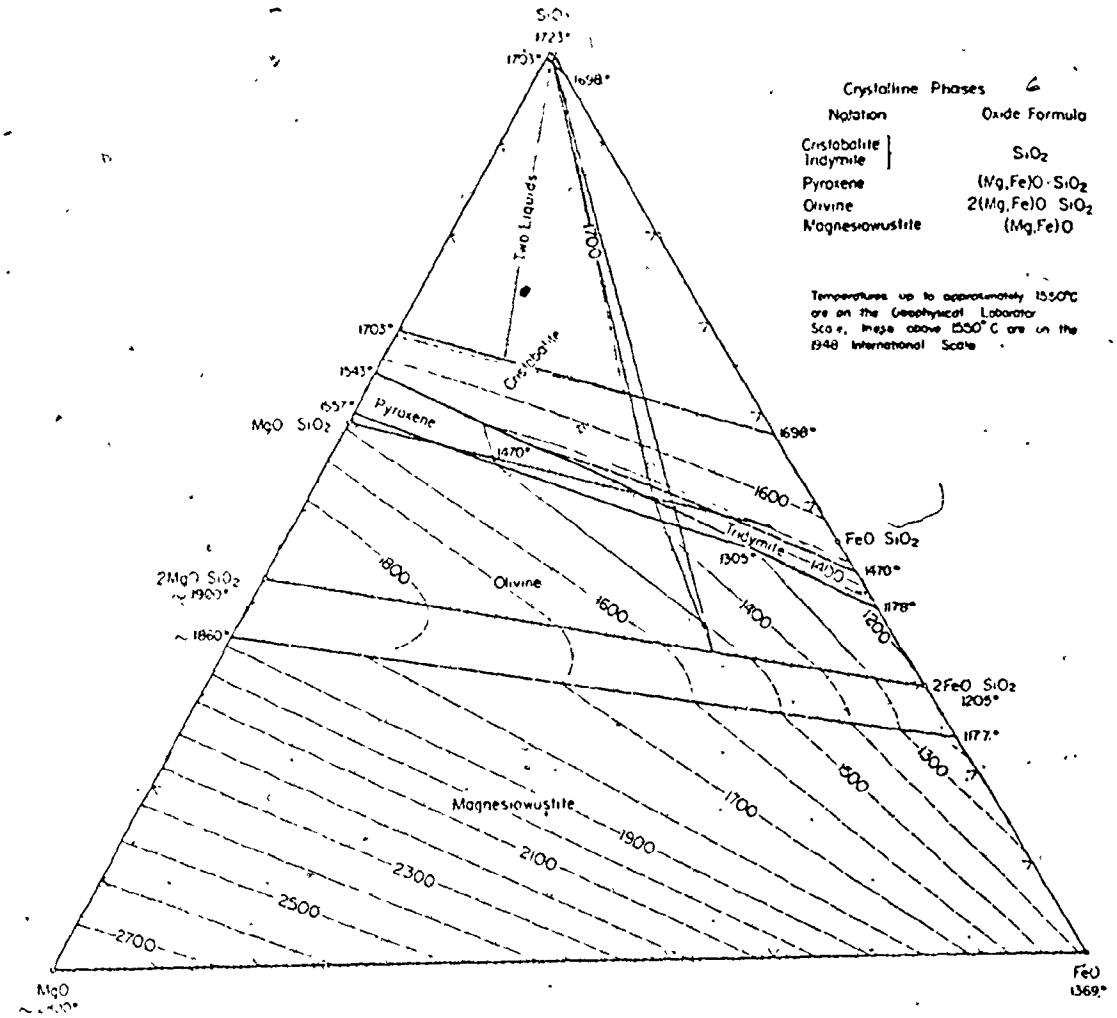

Figure 6.12. System of MgO- FeO- SiO_2 (in equilibrium with Fe).

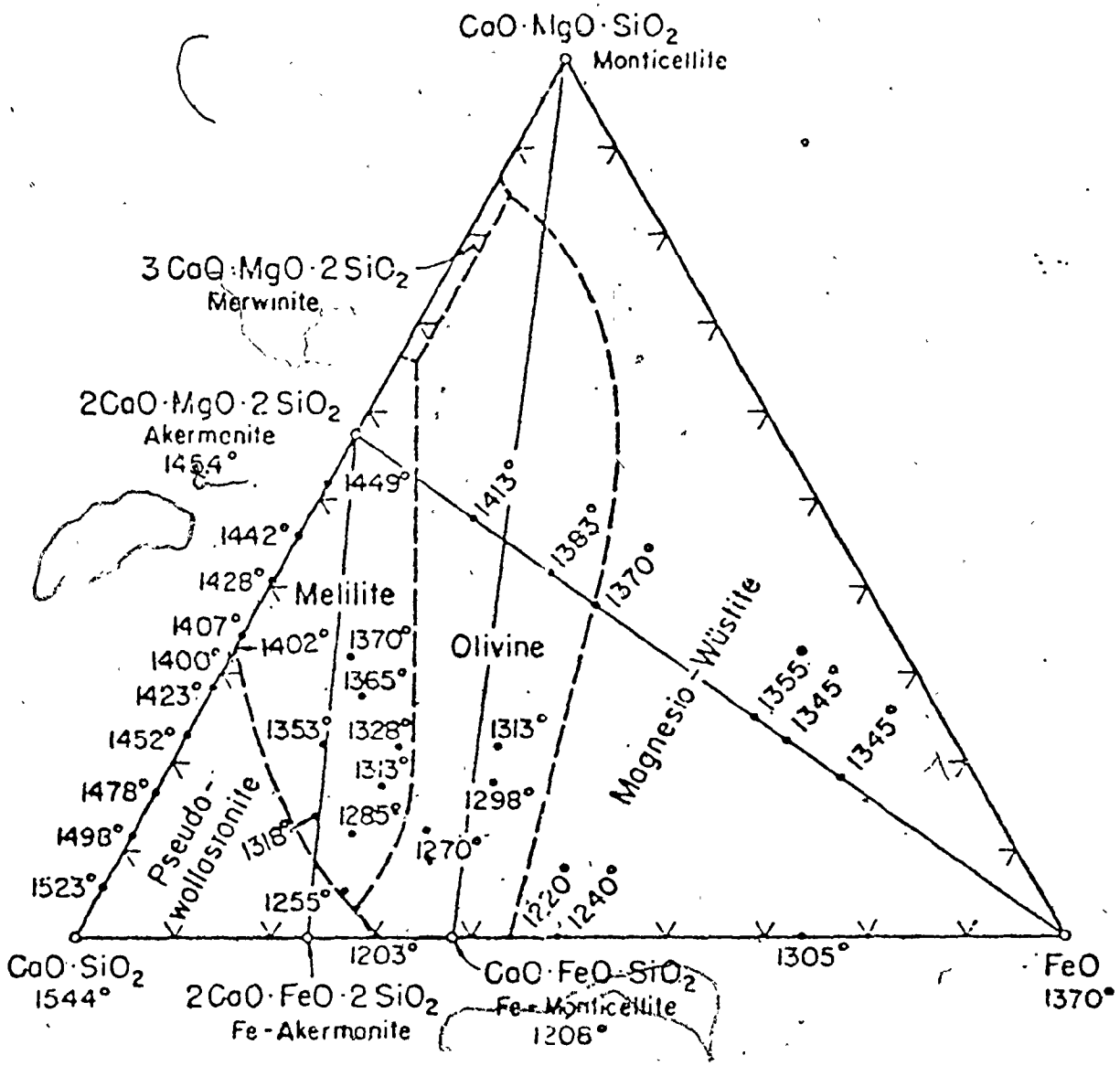

Figure 6.13 System $CaO \cdot SiO_2$-$CaO \cdot MgO \cdot SiO_2$(monticellite)-FeO.

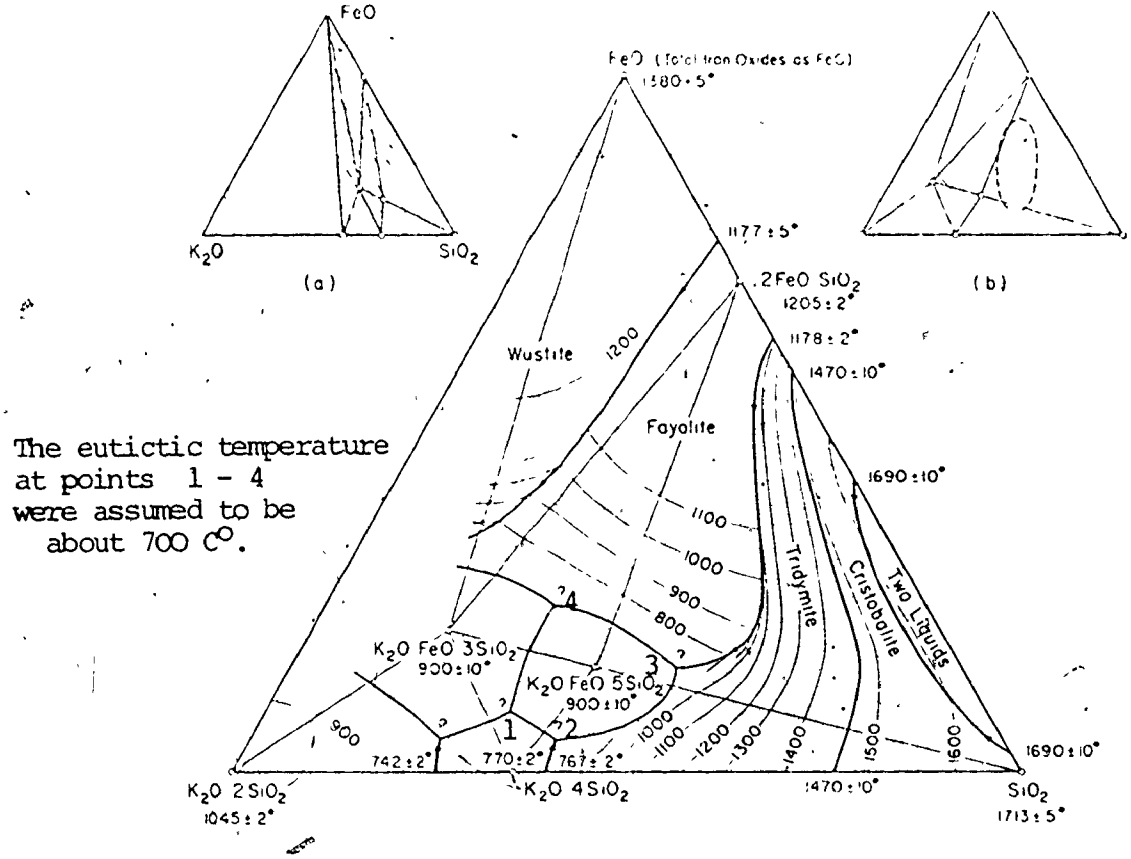

The eutictic temperature at points 1 - 4 were assumed to be about 700 C°.

Figure 6.14 System of K_2O-SiO_2-FeO (in equilibrium with Fe).

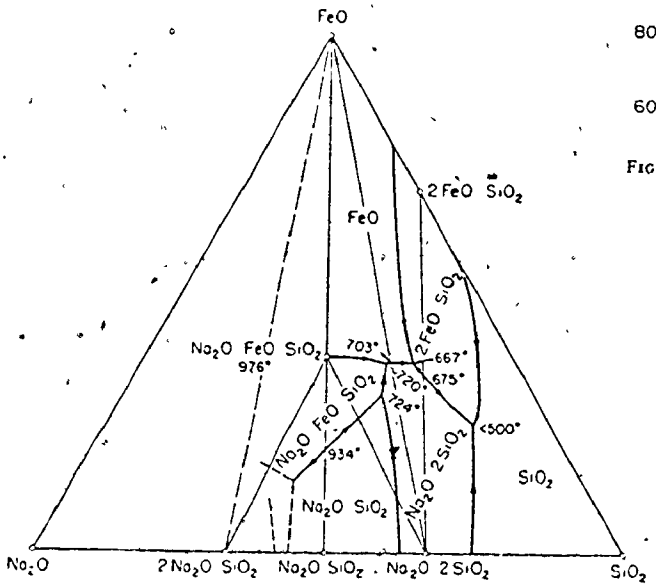

—System Na_2O–FeO–SiO_2.

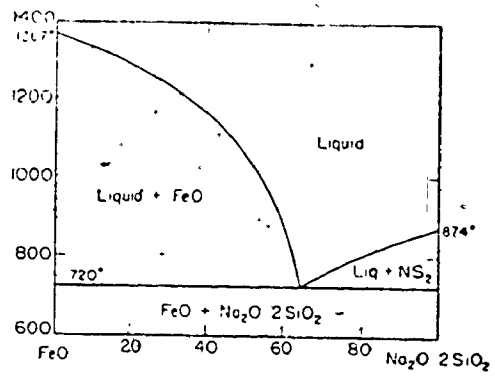

Fig 489.—System Na_2O $2SiO_2$–FeO (true binary); N = Na_2O, S = SiO_2.

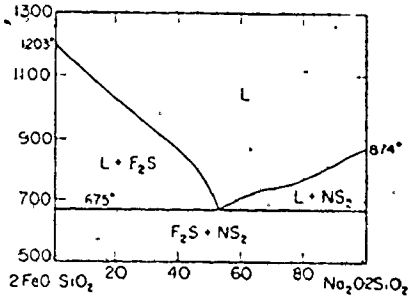

—System Na-O $2SiO_2$–2FeO·SiO_2 (true binary); F = FeO, N = Na_2O, S = SiO_2, L = liquid

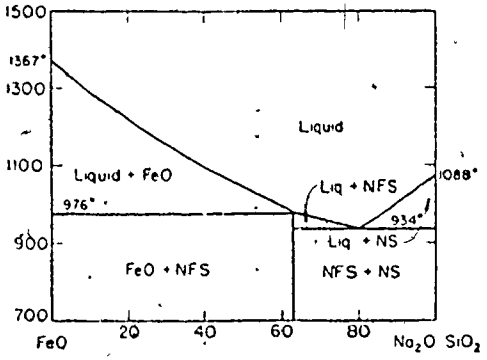

—System $Na_2O·SiO_2$–FeO (true binary); N = Na_2O, F = FeO, S = SiO_2.

Figure 6.15. Systems of Na_2O- SiO_2- FeO (in equilibrium with Fe).

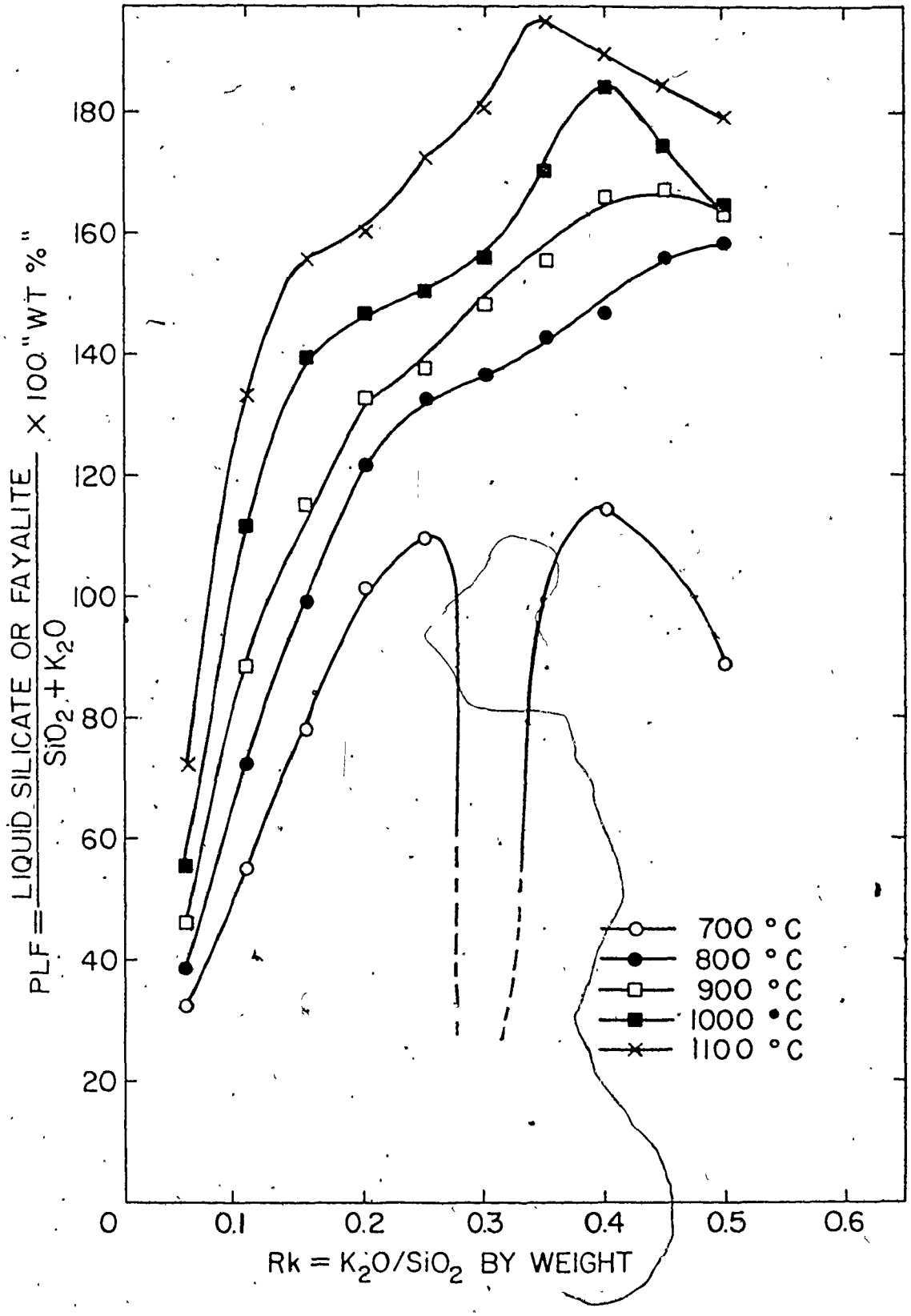

Figure 6.16 Formation of liquid slag during reduction.

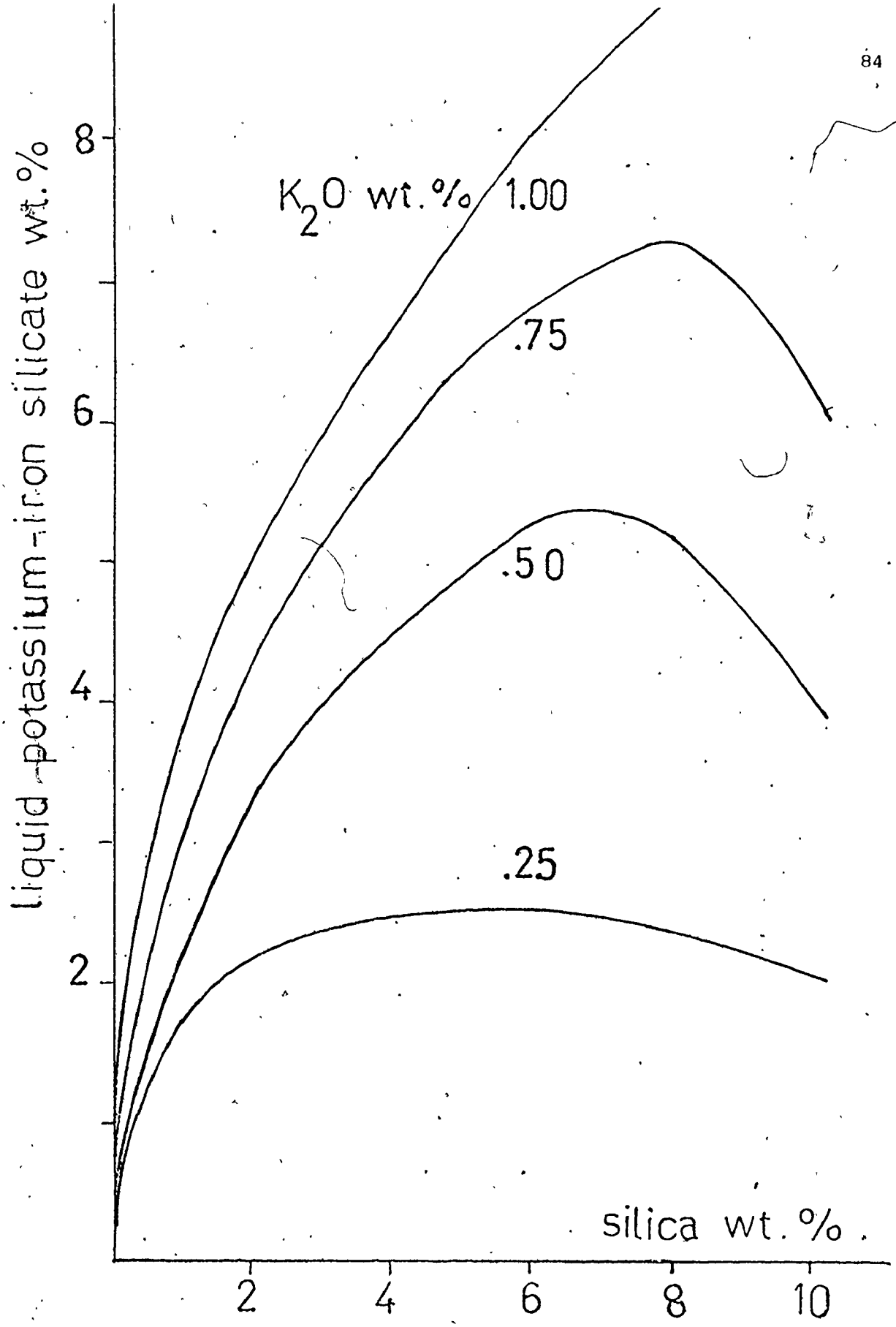

Figure 6.17 Effect of silica on the liquid slag.

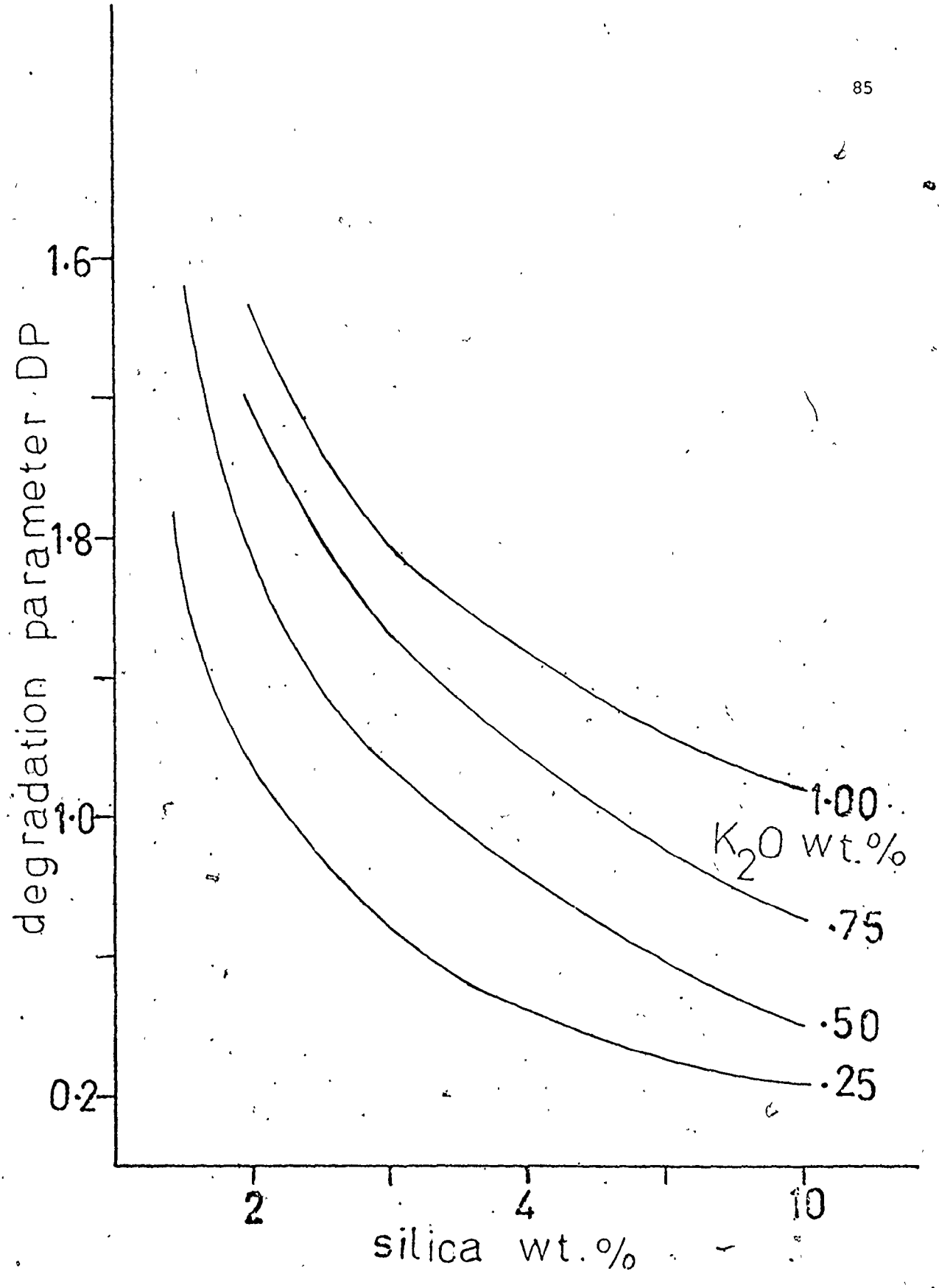

Figure 6.18 Effect of silica content on the degradation of acid pellet.

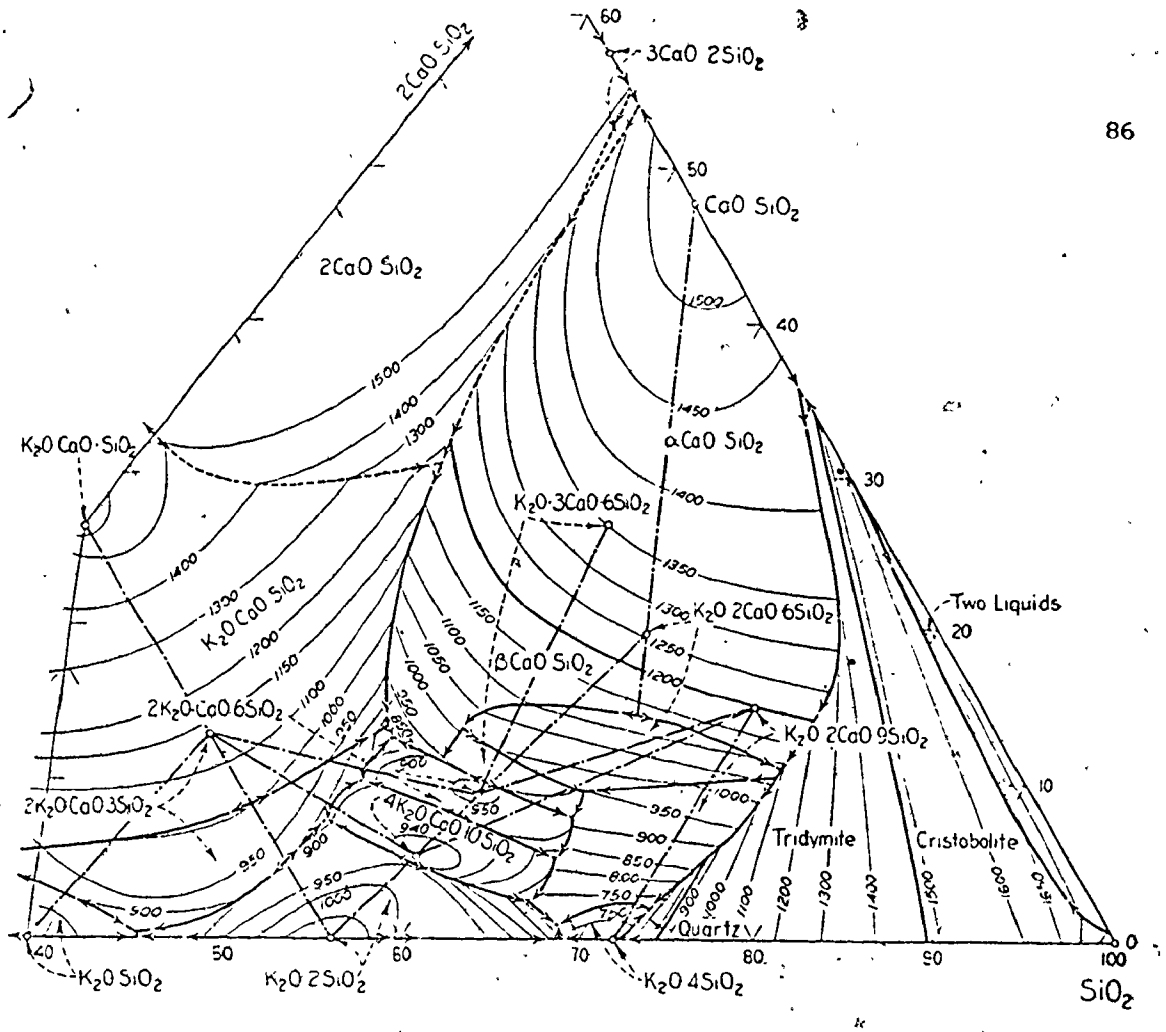

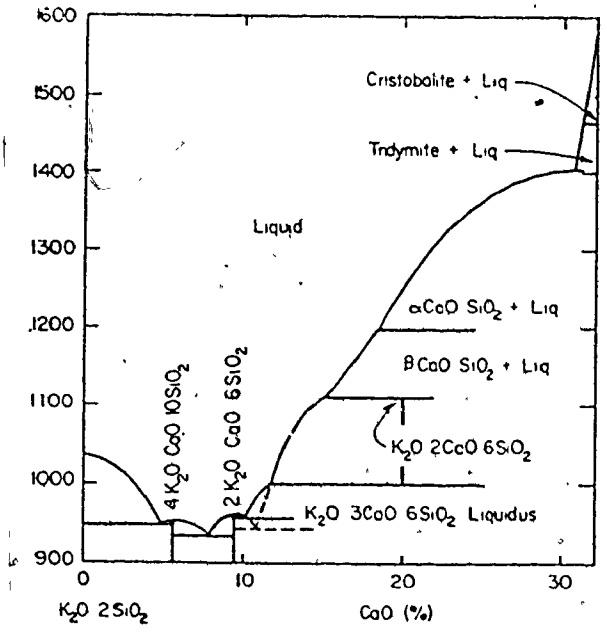

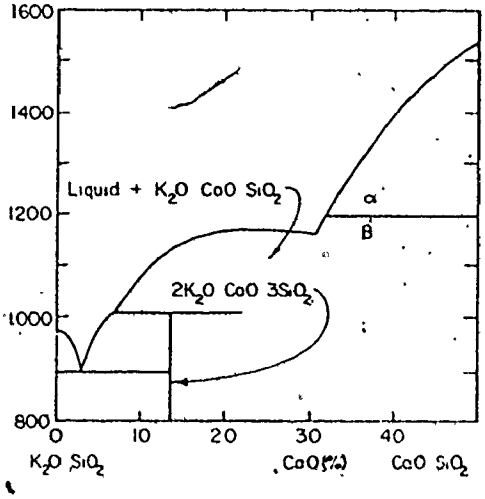

Figure 6.19. Systems of $CaO-SiO_2-K_2O$.

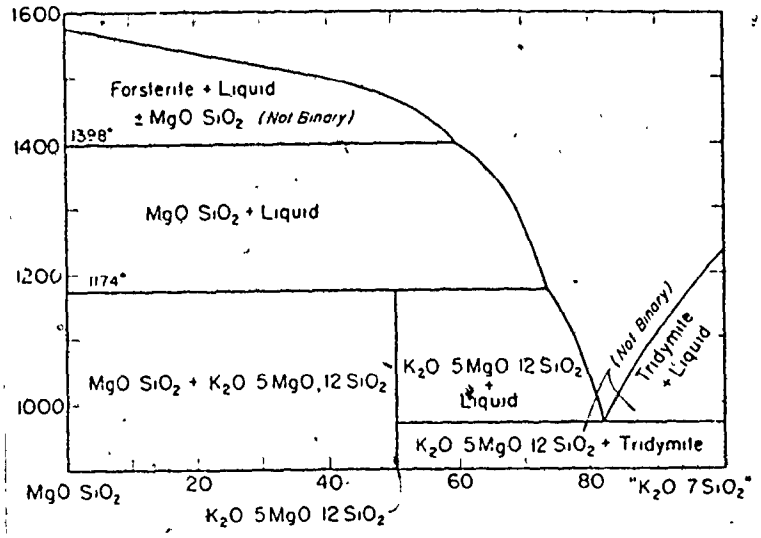

System $MgO \cdot SiO_2$–$K_2O \cdot 5\,MgO \cdot 12SiO_2$; partially binary; "$K_2O \cdot 7SiO_2$" not a compound.

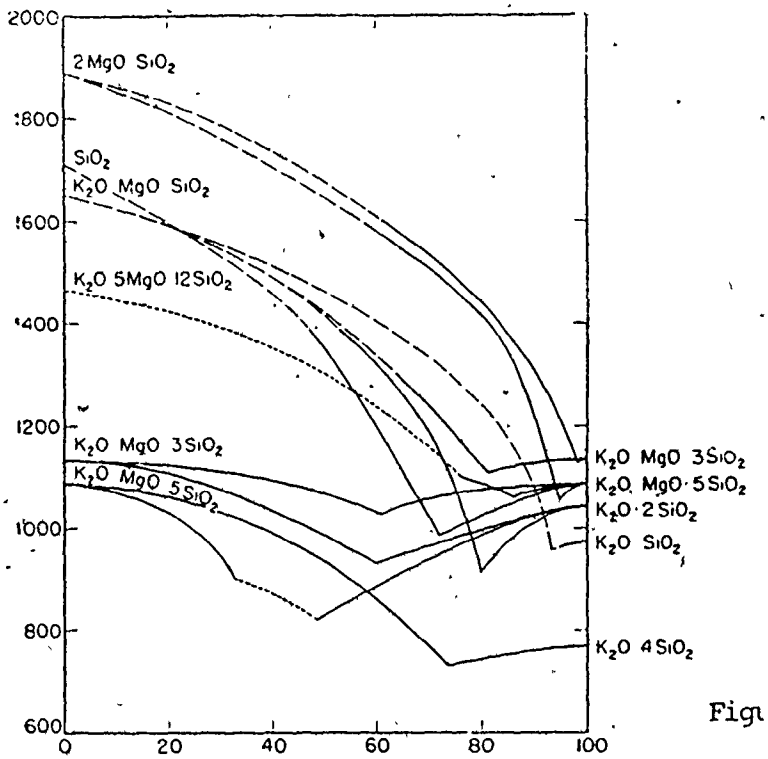

Figu

—System K_2O–MgO–SiO_2; various binary sub-systems; the two dotted lines indicate non-binary (ternary) equilibrium for those portions.

Figure 6.20 Systems of MgO-SiO_2-K_2O.

CHAPTER 7

EXPERIMENTAL WORK

7.1 THE STRATEGY OF EXPERIMENTAL DESIGN

Degradation of iron ore pellets could happen during reduction, due to the physical or chemical changes in the iron oxide or the gangue phases. The effects of reduction conditions and the presence of certain kinds of impurities and their influences on the characteristics of the reaction products, could cause the individual ore pellet to lose its coherent structure and easily swell and break up.

As shown in Chapter 2 a well-known cause for some pellets to swell abnormally during reduction is the formation of iron whiskers. The mechanism of their growth is not clearly understood and more systematic study is needed in this area. It is intended that the present work will contribute to the effort aimed at this goal.

Degradation may also happen when alkalis attack the gangue phase. The creation of primary liquid slag (rich in silica and alkali oxides) at relatively low temperature on the reduction behavior of commercial iron ore pellets will be considered in the present work.

The optical microscope, the scanning electron microscope (SEM), and the electron probe microanalyzer were employed to investigate the morphology of iron and the formation and movement of the slag phase.

7.1.1 Experiments to Study Iron Whisker Growth

In the formation of iron whiskers, they grow during the last step of reduction, i.e., from wustite to iron or metallization. In order to assess the characteristics of the wustite specimens, it is desirable to start with wustite rather than hematite or magnetite specimens.

The wustite samples should be prepared under controlled conditions to give certain chemical as well as physical properties. The apparatus for reduction experiments was designed for good control of temperature, flow rate and composition of reaction gas mixtures and reaction time. It was also used in preparing the iron oxide samples from high purity iron.

The first part of the investigation was to prepare wustite specimens of known grain size by oxidizing high purity iron. The parameters to be varied during reduction experiments were:

(1) the oxidizing/reducing power of CO, CO_2 and N_2 gaseous mixtures prior to and/or during metallization of wustite, and,

(2) the temperature of reduction.

The second part was to investigate the influence of CaO and/or MgO on the morphology and kinetics of metallization. These oxides are good fluxes in iron blast furnace practice and are being used for making basic pellets. The presence of CaO has been reported to promote the tendency of the filamentary growth of iron. Even though MgO is similar to CaO chemically, its effect on suppressing iron whisker growth is known to be pronounced. The combined effect of CaO and MgO on the non-topochemical reduction and on iron whisker growth will be studied.

A new technique was employed to study the effect of CaO and MgO on the growth of the iron phase. Wustite specimens in the form of plates

were covered with a thin film of Fe, Ca or Mg by vapor deposition through screens to give regular patterns. Ca and Mg films were converted to CaO and MgO by low temperature oxidation prior to the reduction experiments.

7.1.2 Experiments to Test Commercial Iron Ore Pellets

The objective was to simulate blast furnace reducing conditions to understand the extent and the mechanism of degradation of commercial iron ore pellets inside the furnace. The adverse effects of alkalis on the behavior of the commercial pellets during reduction was investigated with the use of iron ore pellets with silica as the main gangue constituent. The sole effect of alkali oxides was also studied using silica-free pellets as specimens.

Swelling was chosen to mark degradation of the pellets. A simple device was designed where the apparent volume of the pellets was determined based on mercury displacement before and after each reduction experiment.

Alkali oxides were introduced in three different ways:

(1) as part of the gangue phase: representing iron ore of high alkali content.

(2) as alkali carbonate near the surface of the pellets: representing pellets with precipitated alkali compounds on their outer shell as a result of condensing the alkali vapors in the upper parts of the furnace stack.

(3) as alkali vapors mixed with reducing gas mixtures: representing the conditions of reduction by blast furnace gas which is loaded with alkali vapors.

7.2 SWELLING TEST FOR IRON ORE PELLETS

Different ways for determining the swelling of the iron ores, sinters and pellets had been proposed in the literature[9,10,22,23,69,70]. These methods differ by the weight of the sample, the reduction procedures and the method of determination of degree of swelling.

In general, it is essential to plot the swelling as a function of the degree of reduction. The relationship between the swelling index and the reduction time is much less important. Besides isothermal reduction, even with the use of programmed gases, it is not intended to simulate the flow rate nor composition-time relationships in the blast furnace.

7.2.1 Definition of Swelling and Degree of Reduction

Most of the workers in the field agree on defining swelling and degree of reduction by the following formulae:

$$\text{Swelling, \%} = \frac{\text{Volume after reduction} - \text{Volume before reduction}}{\text{Volume before reduction}} \times 100$$

$$\text{Degree of Reduction, \%} = \frac{\text{Oxygen removed during reduction}}{\text{Oxygen in iron oxide before reduction}} \times 100$$

7.2.2 Measurements for the Apparent Volume

The apparent volumes of the samples have been determined using different methods. In some cases it was done by measuring the dimensions of the specimens of regular shape before and after reduction[9,10]. The dilatometric method was used by Bleifuss to measure the linear expansion or contraction of the pellet during reaction[69]. The above-mentioned ways of measuring the apparent volume of a specimen have two main disadvantages:

(1) they are very sensitive to the specimen shape which may change during reaction, and,

(2) they have poor accuracy since the error in determining the apparent volume is proportional to the square of the diameter of the specimens and the error in their measurements.

Vidal et al.[70] designed a device which used mercury displacement to measure the apparent volume of their samples. The idea was to immerse the pellets in mercury which overflows from a glass container. The apparent volume was determined by measuring the volume of the overflowing mercury, which was used because it has high surface tension and it does not penetrate the small pores. They claim that the scattering of their results was within ± 2% absolute.

The overflow-volumenometer they designed might have an adequate accuracy; however, it has two disadvantages:

(1) a safety hazard may arise from mercury escape. It is undesirable to move mercury from one container to another, especially if it has to be done twice, before and after reduction experiment, and

(2) it is sensitive to vibrations and also takes a lot of time and care to prepare the device for measuring the volume of the pellets.

7.2.3 The Mercury Volumenometer

A new mercury volumenometer was designed, here at McMaster University, to measure the apparent volume of any solid specimen. It is good for specimens of a size between 0.7 - 2.4 cm and a volume up to about 8.0 cc.

Figure 7.1 shows a photograph taken of this mercury volumenometer together with a sketch representing the two main parts of its assembly. Also, it uses mercury displacement in measuring the apparent volume of

the specimen. However, the measurement is done without moving the mercury outside the volumenometer and with adequate accuracy.

The following procedures may be employed to determine the apparent volume of a specimen.

(1) The glass container is first filled with about 25 cc mercury.

(2) The first reading, R1, may be taken by lowering the volumetric column all the way inside the glass container where the mercury is forced into its graduated tube to occupy a certain volume. It is not important to have a precise height of mercury in the device since the apparent volume of the specimen is calculated by measuring the volume of the displaced mercury.

(3) Then, the specimen is placed inside the glass container. The second step is repeated again, with the specimen immersed in the mercury and a second reading, R2, is taken.

(4) After removing the specimen from the device, the second step may be done again to make sure no mercury has been absorbed or escaped with the specimen.

(5) The volume of the displaced mercury - which is equivalent to the apparent volume of the specimen - is determined by subtracting R1 from R2.

The volumetric column is graduated in cc's and tenth fractions. With the help of an eye magnifier the second decimal digit in the measurement is determined. The accuracy of this device was checked, using steel ball bearings with precise diameters; it was found that the error in determining the apparent volume is less than $\pm$ 0.015 cc (see Appendix B).

7.2.4 Using the Mercury Volumenometer to Measure the Volume of the Pellets

The mercury volumenometer described in the last section was used to determine the apparent volume of the iron ore pellets. In most cases a single pellet was measured at one time; however, depending on the size and shape of the pellets, up to six pellets can be measured together. It is understandable that the surface of the pellets is not perfectly smooth; they may have cavities and hairline cracks. The pellets were examined with the naked eye; those with defects on their surfaces were rejected and were not used as specimens for the reduction experiments. According to the mechanical balance equation between the pressure and the surface forces[71], and taking the contact angle between the mercury and the pellet as 140°[72], the smallest diameter of a cavity to be penetrated by mercury was calculated. It was in the range of 10 - 12 microns if one took the total pressure during measurement in the range of 1 - 1.2 atm. (assuming the height of the mercury column over the pellet was less than 15 cm which is equivalent to about 0.2 atm. pressure).

7.2.5 Determining the Swelling Index

The swelling index of the iron ore pellets was calculated using the formula defined in Section 7.2.1. Considerable care was exercised in measuring the apparent volume of the pellets using the mercury volumenometer before and after reduction. On some occasions, and due to the effect of alkali oxides, cracks and fissures were developed during reduction. The apparent volumes of the reduced specimens measured by the mercury volumenometer did not include that of the fissures with width larger than 10 - 12 microns. Accordingly, the calculated swelling

index is smaller than that including the fissures by a value "f", which can be defined as:

$$f = \frac{\text{Volume of the fissures}}{\text{Initial volume of the specimen}} \times 100$$

Unfortunately, it is difficult to measure the volume of these fissures and cracks; hence, the results will be presented without adding the correction value "f" to the calculated swelling index. This value "f" is a function of the amount and distribution of alkali oxides in the silicate gangue phase within the iron ore pellets.

7.2.6 Measuring the Degree of Reduction

The degree of reduction of the partially reduced pellets was calculated using the formula defined in Section 7.2.1. The weight of oxygen in the iron oxide before reduction was calculated based on the chemical analysis of the commercial pellets and iron ore concentrate. It was assumed that for the commercial pellets and those made in the laboratory from iron ore concentrate and fired in air at temperatures of 1100°C or higher, hematite is the only iron oxide present after firing. The error in calculating the degree of reduction based on this assumption was checked. It was less than 1% (in the relevant range of 25 to 50% reduction) if it is assumed that the iron oxide within the pellets was composed of 90% hematite and 10% magnetite instead of 100% hematite. Of course it is unlikely to have more than 1 to 2% ferrous iron oxide after firing the pellets in air at high temperature and for a long period of two hours[73].

The weight of the oxygen removed from the pellets during reduction was measured by weighing the dry pellets before and after each reduction test. For the iron ore pellets impregnated with alkali carbonated with-

out firing, the loss in weight was assumed to occur due to iron oxide reduction and calcination of the alkali carbonate. Hence, the weight of CO_2 evolved during the reduction experiment was subtracted before calculating the degree of reduction reached.

7.3 THE EXPERIMENTAL DESIGN

The experimental apparatus was designed to serve three purposes:

(1) to control the flow rates of the reaction gases and to adjust their composition in terms of $CO:CO_2$ ratio,

(2) to have a reaction zone of accurate temperature level and heating or cooling rate, and,

(3) to determine the reaction time with high accuracy.

7.3.1 Apparatus Assembly

Figure 7.2 shows a schematic representation of the apparatus assembly. It consists mainly of a Marshall resistance-heated tubular furnace F, which has three zone windings to adjust the temperature profile. A horizontal quartz tube F1, which was moved easily in and out of the furnace for controlling the temperature was used to carry the specimen and its holder. The quartz reaction tube was 4 cm inner diameter and about 100 cm long. The components of the reaction gas mixtures CO, CO_2 and N_2 were supplied by separate cylinders A, B and C, respectively. They were purified prior to mixing together, by passing through glass wool in the glass container D. All three gases were first passed through silica gel granules to remove the water vapor. N_2 and CO were also passed through drierite ($CaSO_4$), soda lime and ascarite for CO_2 removal. N_2 was passed over hot zirconium flakes at about 700°C to remove O_2.

The gas flow rates could be adjusted using the three micro needle valves, A1, B1 and C1, together with three manometers A3, B3 and C3 which

were calibrated (prior to carrying out the experiments) using the three soap bubble flow meters A5, B5 and C5.

For some experiments potassium vapor was introduced to the reduction gas mixture, by passing it over molten potassium carbonate. An inner mild steel tube of 3.4 cm inner diameter was used to protect the reaction tube from attack by potassium vapor.

7.3.2 Reaction Gas Mixtures

As mentioned in the last section, the reaction gas mixtures were made up by mixing CO, CO_2 and N_2; see Table 7.1. For all the experiments carried out, the flow rate of N_2 was 300 cc (STP)/min., while that of CO and CO_2 was 200 cc (STP)/min. (except GRH).

The error in measuring the flow rates of the reaction gases was calculated based on the accuracy of determining the time taken by a soap bubble to scan the soap bubble meter with constant speed. The error in determining the flow rates of CO and CO_2 are given in Table 7.2, while that of N_2 was ± 10 cc (STP)/min., when it flowed at a rate of 300 cc (STP)/min.

For the experiments carried out to investigate the influence of potassium vapor on the reduction of commercial iron ore pellets, the reduction gas mixture was passed first over molten potassium carbonate in a platinum crucible placed upstream with respect to the location of the pellet, as shown in Figure 7.3. The partial pressure of K vapor was calculated in an indirect way, by weighing the crucible containing the potassium carbonate before and after reduction, and assuming the rate of its gasification was constant during the experiment. Table 7.3 is given to show the potassium contents in the reducing gases.

7.3.3 Heating and Cooling of the Specimens

The temperature of the reaction zone around the specimen holder was adjusted prior to each experiment. The specimen could be moved to the predetermined location of known temperature as shown in Figure 7.2. Also, it was checked during the experiments from time to time with the thermocouple, F3. The error in determining the reaction zone temperature was calculated to be less than ± 5°C for temperatures up to 1100°C.

The standard temperature of reduction was 900°C. The heating and cooling (under flowing N_2) curves of the specimens from room temperature to reach 900°C, and from it to 100°C, are given in Figure 7.4. It was found that about 6 minutes was needed to each 900°C after the quartz tube was moved from the cool end of the furnace (with specimens essentially at room temperature) to the middle of the furnace. After the predetermined reaction time the quartz tube was taken out again to the original position. About 20 minutes was needed to cool the specimen to about 100°C without switching the furnace off. With the use of the mild steel tube inside the quartz tube these two times (for heating and cooling) were about 9 minutes and 30 minutes, respectively.

7.4 EXPERIMENTAL PROCEDURES

The experimental procedures were the same for oxidation or reduction experiments. The specimens were heated under N_2 (reaction gas GN, Table 7.1), to reach the desired reaction temperature. They were usually left in position for 2 - 3 minutes to insure that the isothermal reaction temperature was reached before introducing the reaction gas mixture. The reaction time was counted from the moment of introduction of the reaction gas to the furnace. At the end of each experiment the reaction

gas was switched off and the specimen was left under N_2 (reaction gas GN in Table 7.1) after moving the quartz tube to the cool end without switching the furnace off.

A platinum boat (2.5 x 5 cm and 1.3 cm high) was used to hold the specimens during reaction. For the experiments carried out to test the swelling characteristics of the commercial iron ore pellets, they were placed on top of ceramic of platinum boats (1 x 10 cm and 1 cm high).

The reduction time of the pellets was in general one hour at 900°C with reducing gas GRS (Table 7.1). The pellets were weighed and their volume was determined using the mercury volumenometer before and after each reduction experiment to calculate the swelling index and the degree of reduction as described in Sections 7.2.5 and 7.2.6.

7.5 METALLOGRAPHIC EXAMINATION

Metallographic examinations were carried out with the use of the optical microscope, the scanning electron microscope (SEM) and the electron probe microanalyzer. The morphology of the iron phase formed during reduction was examined by using the SEM. The photographs taken by the SEM camera are labelled E, followed by the photograph number, e.g., E6.

The optical microscope used in examining the specmens was the Universal Camera Microscope MeF made by Reichert in Vienna, Austria. The specimens were impregnated in Epofix epoxy resin under vacuum, before sectioning and polishing. The photographs taken will be labelled O, followed by the photograph number, e.g., O1.

Qualitative chemical analysis in microscope scale was carried out using the X-ray unit attached to the SEM (Cambridge Stereoscan Mark IIA) or the electron probe microanalyzer (Camera Microprobe MS64)

manufactured by Acton Laboratories, Inc.

7.6 MATERIALS USED IN THE EXPERIMENTS

The following materials were used in the present work:

(1) high purity iron,

(2) chemical reagent grade compounds,

(3) commercial iron ore concentrate and pellets, and,

(4) high purity gases.

7.6.1 High Purity Iron

Two kinds of high purity iron were used. Iron fragments were cut by lathe from electrolytic iron block and iron foils of about 0.01 mm were prepared by rolling clean sheets of ARMCO iron. Both were cleaned after cutting or rolling, with diluted hydrochloric acid followed by acetone.

The electrolytic iron was supplied by Colt Industries Canada Ltd. and the ARMCO iron by Armco Steel Corp., in the U.S.A. The chemical analysis of these samples used (according to the companies' certified listing) are given in Table 7.4.

7.6.2 Chemical Reagent Grade Compounds

The chemical reagent hematite was supplied by Alfa U.S. with a purity of 99.9% Fe_2O_3. Its chemical analysis according to the company's catalogue is given in Table 7.5.

The other chemical reagents used as additives are given in Table 7.6. Silica of about 99% SiO_2 and free from iron oxides was also used in investigating the kinetics of alkali silicate formation.

7.6.3 Commercial Iron Ore Concentrate and Pellets

Magnetite iron ore concentrates and fired pellets from the same iron ore deposit were supplied by a U.S. steel company. The chemical

analysis of these are given in Table 7.7.

7.6.4 High Purity Gases

The gases were supplied in separate gas containers, by Canadian Liquid Air Ltd. The purity of these gases according to the company catalogue is as follows:

(1) Nitrogen: 99.5 - 99.8% N_2 with 2000 - 5000 ppm O_2 and 128 ppm H_2O

(2) Carbon Dioxide: 99.9% CO_2 with less than 0.1% $N_2 + O_2$ and 125 ppm H_2O

(3) Carbon Monoxide: 99.97% CO "Research" with:

H_2	less than	10 ppm
H_2O	less than	5 ppm
N_2	less than	100 ppm
O_2	less than	25 ppm

and total hydrocarbons less than 150 ppm

7.7 SPECIMEN PREPARATION

7.7.1 Iron Oxides of High Purity

Samples of iron oxides and wustite plates (5 x 5 mm and 100 - 200 microns thickness) were prepared from high purity electrolytic iron and ARMCO iron foils. They were oxidized under controlled conditions in an atmosphere of CO, CO_2 and N_2. Wustite fine powder (less than 53 microns) was also prepared by reducing the chemical reagent grade hematite at 900°C. The conditions of preparing these specimens are given in Table 7.8 together with the photographs showing the phases present in the specimens.

The iron oxides prepared at 900, 1000 and 1060°C using reaction gas mixture GW (see Table 7.1) was found to be composed of wustite only.

The specimens prepared at 1000°C using reaction gas GMW which is close to wustite/magnetite equilibrium curve (see Figure 7.5) was found to be a mixture of magnetite, wustite and a few iron spots. The reason for this mixture could be the decomposition of wustite during cooling to result in magnetite and metallic iron.

Powders were made after grinding and screening of the prepared specimens W_E and M_E. Two kinds of powders were used as specimens. The first powder represented particles of sizes between 150 - 180 microns. They were washed with acetone to remove the fine dust. The second powder represented those particles of less than 53 microns. For the sake of simplicity, they will be referred to as coarse and fine powders in the rest of this work.

7.7.2 Wustite Powders Doped with CaO and/or MgO

Fine wustite powders doped with CaO and/or MgO are listed in Table 7.9. CaO and/or MgO were introduced in the following ways:

(1) by mixing wustite powder (prepared from reagent hematite) with CaO and/or MgO flours. For example, W-C5 and W-M2 are powders of 5 wt.% CaO and 2 wt.% MgO, respectively.

(2) by melting reagent hematite with CaO and/or MgO in an iron crucible (in air) at 1400°C, followed by treatment at 900°C for 4 hours with reaction gas in equilibrium with wustite (GW in Table 7.2). Chemical analysis showed that the prepared powders WSC1.8 contained 1.8 wt.% CaO while WSM1.7 contained 1.7 wt.% MgO in solid solution with wustite.

(3) by mixing the powders of solid solutions prepared in (2) with MgO or CaO. For example, WSC1.8-M1 refers to the mixture of solid solution WSC1.8 with 1 wt.% MgO.

7.7.3 Wustite Plates Coated with Fe, CaO or MgO

Wustite plates were coated with thin films (200 - 300 angstroms) of Fe, Ca or Mg using vapor deposition technique described in Appendix A. The Ca or Mg films were converted to CaO or MgO by low temperature oxidation at 300°C for about 15 minutes under flow of reaction gas GW (Table 7.1). Copper grids with openings of different sizes were placed on the plate during evaporation and deposition to result in making thin films of regular patterns.

7.7.4 Iron Oxide Pellets

Four kinds of pellets were used as specimens for the swelling tests:

(1) commercial iron ore pellets,

(2) laboratory pellets made of iron ore concentrate,

(3) laboratory pellets made of reagent hematite, and,

(4) laboratory briquettes made of iron ore concentrate after removing the silica.

7.7.4.a Commercial Iron Ore Pellets

The commercial iron ore pellets and three of the modified forms were used as specimens for the swelling tests. They are:

(1) As-received fired pellets (their chemical analysis is given in Table 7.7): the density is in the range of 3.6 to 3.8 gm/cc. The individual pellets accepted as specimens were free from surface defects which could be seen with the naked eye. Each of them had a weight in the range 3.0 - 4.5 gms.

(2) Magnetite and wustite pellets: prepared by reducing the commercial pellets at 900°C with reaction gases in equilibrium with magnetite and wustite as shown in Table 7.10.

(3) Restructured pellets: having the same chemical composition as the as-received commercial pellets but differing in structure. They were prepared by re-oxidizing the wustite pellets in air at 800°C for 4 hours.

Some of the above-mentioned pellets were impregnated with an aqueous solution of alkali carbonates under vacuum, followed by drying at about 150°C. The distribution of the alkali throughout the body of the pellets was not the same in all cases. For as-received pellets (which contain relatively much fewer open pores since they were fired in air at temperatures of 1200 - 1300°C), alkali carbonates in the dried pellets concentrated near the surface of the pellets. For the other kinds of pellets, the distribution of alkali was much more uniform throughout the pellets.

7.7.4.b Laboratory Pellets Made of Iron Ore Concentrate

Two kinds of pellets (with and without alkali carbonate additions) were made of iron ore concentrate (its chemical composition is given in Table 7.7) and fired for two hours in air at 1100, 1200 and 1300°C, respectively. A Chromel-Alumele thermocouple was used to check the error in measuring these temperatures which was found to be in the range of ± 5, 10 and 15°C, respectively.

For the alkali doped pellets, predetermined amounts of alkali carbonates were mixed thoroughly with the dry iron ore concentrate in a ball mill for 3 - 4 hours. All the green balls were made in a laboratory pelletizing device with a rotating tire of 40 cm inner diameter and 10 cm width. They were dryed at room temperature followed by heating in air at 150°C before induration and firing. Table 7.11 shows some of the characteristics of iron ore pellets made in the laboratory.

7.7.4.c Laboratory Pellets Made of Reagent Hematite

High purity hematite pellets (chemical analysis is given in Table 7.5) were rolled by hand and fired in air at 1200°C for 2 hours. The density of these specimens is in the range of 4.3 - 4.5 gm/cc.

7.7.4.d Laboratory Briquettes Made of Iron Ore Concentrate After Removing the Silica

Commercial iron ore concentrate (chemical composition is given in Table 7.7) which contains 4.57 wt.% SiO_2 was washed with warm concentrated hydrofloric acid followed by distilled water, to remove silica in the gangue. The treated iron ore was then dried and fired in air at 1200°C for about 24 hours to remove the fluoric acid and to decompose the ferrous and ferric fluorides. Chemical analysis showed that the treated iron ore concentrate had only 0.025 wt.% SiO_2.

Briquettes of the treated and fired iron ore concentrate (Table 7.11) were made by pressing its fine powder at room temperature in a tungsten carbide [illegible]ess of 0.92 cm inner diameter, under a load of about 5.5 tons using a laboratory hand press. The briquettes were fired and indurated at 1200°C and 1300°C for 2 hours and some of them were doped with alkali by mixing the treated powder with a predetermined amount of alkali carbonate before making the briquettes and firing.

CHAPTER 8

EXPERIMENTAL RESULTS

8.I EXPERIMENTAL RESULTS WITH IRON OXIDES

The experimental results using high purity iron oxides and wustite plates (free from CaO, MgO and alkali oxides which are known to cause iron whisker growth) are given in Figures 8.4 - 8.19 and 8.21. The results of the wustite powders doped with CaO and/or MgO are given in Figures 8.22 - 8.29. Also, wustite plates coated with CaO or MgO films on their surfaces and the reduced specimens are shown in Figures 8.31 - 8.37.

8.I.1 Reduction of high purity iron oxides

As already mentioned in Section 7.7.1 of Chapter 7, high purity iron oxide powders and wustite plates were prepared by oxidizing electrolitic iron chips and ARMCO iron foils. Two kinds of iron oxide powders were prepared from these high purity irons labelled as W_E and M_E. Optical microscope examination (up to a magnification of about x1100) showed that wustite specimen W_E appears to be a single phase, while specimen M_E which is essentially decomposed wustite is a mixture of magnetite, wustite and a few tiny iron specks, as shown in Figure 8.1.

Figure 8.2 shows the appearance of the wustite plates used as specimens. They had an almost flat and regular surface, each of the iron plates resulted in two dense layers of wustite splitting at the center. Some of the plates formed wustite whiskers during oxidation

(most of them appeared near the plates' corners); they were rejected and were not used for reduction experiments.

The reduction experiments were carried out under controlled conditions as already described in Sections 7.3 and 7.4 of Chapter 7. The metallization could be recognized by the naked eye as a result of color change due to iron formation. Using SEM the morphology of the metallized specimens was examined to determine the extent of the outward growth of the iron phase.

8.I.1.1 Iron oxide powders

From each iron oxide specimen (W_E and $\bar{M}_E$) two kinds of powders were prepared and used for reduction experiments, i.e. fine powders (particle size less than 53 microns) and coarse powders (particle size 150 - 180 microns).

During reduction and metallization the powders were contained in short cylindrical crucibles (about 3 mm I.D. and 5 mm height) made from an alumina tube in the upright position. The composition of the incoming gas mixture in each case was maintained constant during the course of reduction. The actual gaseous environment, individual particles exposed, was not only changing with time but also dependent on where it resided in the crucible. The particles, which were near or on the surface of the packing, would contact a gaseous phase of the bulk composition, with very little change with time. On the other hand, interior particles would contact a changing atmosphere adjusted by simultaneous mass transfer and chemical reaction processes. Therefore, in each reduction test, the morphology of the reduced particles under both conditions were examinated with SEM.

The powders were reduced at different temperatures, using various

reducing gases (different in $CO:CO_2$ ratio). The appearance of the reduced powders near or on the surface of the powder packing are shown in Figures 8.4 - 8.11.

It was difficult to quantitize the SEM observations. However, for the purpose of discussion, a systematic comparison, even qualitative, is desirable. Figures 8.4 - 8.7 illustrate the temperature dependence while Figures 8.8 - 8.11 show the effect of varying the reducing power of the reducing gas mixtures on the tendency of iron whisker growth, after partial reduction and metallization.

The difference in appearance after reduction of the surface and interior particles is shown in Figures 8.12 - 8.14. In all the experiments carried out in this work the extent of iron whisker formation was more pronounced in the first case (surface particles).

8.I.1.2 Treatment and reduction of high purity iron oxide powders

Iron oxide powders were reduced after treatment for homogenization, or decomposition, or oxidation to magnetite and the results are given in Figures 8.15 - 8.17.

For specimen M_E, Figure 8.15 shows the effect of high temperature homogenization on suppressing the tendency of iron whisker growth during metallization of wustite. On the other hand, Figure 8.16 illustrates the influence of wustite decomposition on W_E in promoting iron whisker growth.

Figure 8.17(a) shows two kinds of partially oxidized W_E powders. They are different in the distribution of magnetite phase near the external surface of these powders. The microphotograph 034 in Figure

8.17(a) shows that the magnetite layer is topochemical and continuous. On the other hand, for the interior particles, microphotograph 035 shows that only part of the surface of these particles are covered by magnetite phase. The difference may be due to the fact that the interior particle experienced much weaker oxidizing gas. In Figure 8.17(b), it is clear that under the usual reducing conditions, specimens as that shown in photograph 034 would not result in significant iron whisker growth but 035 would.

8.I.1.3 Reduction of wustite plates

Wustite plates were coated with a thin film of iron (about 200 Å), using the vapor deposition technique through a screen of 12 x 12 μm openings (Appendix A). After deposition there were three zones on the surface to be considered. They were the coated iron which was not covered by the screen, the uncoated which was covered by the rim of the screen, and the region with iron films of 12 x 12 μm and regularly spaced. The appearance of one of the wustite plates after iron deposition, is shown in Figure 8.18.

The plates with iron films deposited were reduced at 700°C and 900°C followed by SEM examination. Figure 8.19 shows the appearance of the metallized surfaces after reduction. Short but definite outward growth of iron originated for 12 x 12 μm iron films can be noticed when the reduction temperature was 700°C, while the morphology of the other two zones (with continuous iron film and the uncoated region) was almost the same and a sponge layer of iron with fine pores was seen after reduction at 700°C. The appearance of the three zones couldn't be differentiated and a dense layer of iron was observed on the surface of the plates after reduction at 900°C.

8.I.2 Reduction of iron oxides doped with CaO and/or MgO

CaO and/or MgO were introduced to wustite specimens prior to metallization, in different ways. Powders of wustite or their solid solutions (with CaO or MgO) were mixed with MgO and/or CaO to make fine powder specimens (Table 7.8 and 7.9). The wustite-CaO solid solution (WSC 1.8) was examined under optical microscope (magnification x1100) and appeared to be one phase as shown in Figure 8.20; so was the wustite-magnesia solid solution. Wustite plates with a thin film of CaO or MgO on their surfaces were prepared by depositing metal vapors through a screen, followed by low temperature oxidation to CaO and MgO.

The wustite-CaO, wustite-MgO and wustite-CaO-MgO specimens were reduced most of the time at 900°C; however, reduction was also carried out at 750°C and 1100°C in some cases. In all these experiments, the reducing gas used was GRS($CO:CO_2$ = 4:1). The reduction times for the powder specimens was 30 minutes and for the wustite plates 1 and 2 hours.

After reduction the metallization could be noticed due to color change resulting from iron formation. Also, the apparent volume of the specimens was noticed and found to increase after reduction due to iron whisker growth.

In all the experiments carried out at 1100°C the reduced wustite particles seemed to be sintered together, even in the cases where iron whiskers were observed under SEM and the increase in the specimen's apparent volume could not be noticed.

8.I.2.1 Wustite powders without CaO or MgO addition

As the reference for all experiments using doped wustite powders, specimens of wustite powder W_H (Table 7.8), which were prepared from high purity hematite, were reduced and are shown in Figure 8.21. Few

iron whiskers were observed when the powder was reduced at 900°C; however, the experiments carried out at 750°C, 900°C and 1100°C and the apparent volume of the specimen did not change to a noticeable extent due to reduction.

8.I.2.2 Mixtures of powders with CaO or MgO

Figure 8.22 shows the effect of the amount of lime particles present when the specimens were reduced at 900°C. The same effect as well as the temperature dependence of iron morphology, are shown in Figure 8.23. The extent of iron whisker growth increases with the amount of CaO in the powder mixture at 900°C. When the reduction was carried out at 750°C, CaO did not cause any noticeable change in the appearance of the reduced powder, similar to microphotograph E44 (Figure 8.21).

Wustite powder mixed with 2 Wt% MgO was reduced at 750°C, 900°C and 1100°C and no evidence of iron whisker formation could be seen when the specimens were examined using SEM after reduction.

8.I.2.3 Solid solutions containing CaO or MgO

Figure 8.24 shows the appearance of wustite-CaO solid solution (powder WSC 1.8) after reduction at 750°C, 900°C and 1100°C. Iron whiskers were formed at 750°C and 900°C but not at 1100°C, and the extent of iron whisker growth lessened with increasing the temperature of reduction.

When wustite-MgO solid solution (powder SEM 1.7) was reduced at 750°C, 900°C and 1100°C iron whiskers were not seen after reduction. Figure 8.25 shows the appearance of the wustite-CaO or MgO solid solution powders after reduction at 900°C for comparison.

8.I.2.4 Mixture of powders with CaO and MgO

Wustite powder W_{II} was mechanically mixed with CaO and MgO with

different CaO/MgO ratios (Table 7.9). Figure 8.26 shows the appearance of powder mix (2% CaO and 2% MgO) after reduction at 900°C and 1100°C. The extent of iron whisker growth was comparable to the case when the wustite powder was mixed with 2% CaO only. Also, the apparent volume of the specimen was increased noticeably due to iron whisker growth after reducation at 900°C. When CaO/MgO ratio was decreased to 1/10 with powder (W-C 0.5 - M5) which was also reduced at 900°C, iron whiskers were formed and seen under the SEM, similar to those shown in microphotograph E59 in Figure 8.37.

8.I.2.5 Solid solutions mixed with CaO or MgO

In all three experiments carried out at 900°C, iron whiskers formed during reduction as shown in Figure 8.27.

8.I.2.6 Reduction of treated powders

Two kinds of specimen (one mixture and one solid solution) were treated at 750°C and 900°C using reaction gas GW ($CO:CO_2$ = 1:1, Table 7.2), prior to reduction to examine the changes of the effects of calcia on iron whisker growth.

Figure 8.28 shows that 2% CaO in the mixture which was treated for 30 minutes then reduced at the same temperature, did not cause any noticeable changes (see picture E44, Figure 8.21). It should be noted that wustite has negligible solubility of lime at 750°C. When the treatment temperature was raised to 900°C, for 10 minutes, heavy iron whisker formation was observed.

The opposite results were observed with wustite-CaO solid solution (WSC 1.8). Figure 8.29 demonstrates that an increase of treatment time at 900°C reduced the tendency of whisker formation.

8.I.2.7 Wustite plates coated with CaO or MgO

A. Wustite plates coated with CaO

The appearance of the wustite surface, after deposition of the Ca film, is shown in Figure 8.30. There were three zones to be considered: continuously coated zone, uncoated zone and the zone with regularly spaced 30 x 30 μm films. As already described in Section 7.7.6 of Chapter 7, the Ca film was oxidized to CaO at low temperature prior to reduction at 900°C for 1 hour.

The morphology of iron in the three zones are shown in Figures 8.31 - 8.33. CaO enhances the rate of reduction and a porous iron layer was formed from the wustite surface covered with a CaO film.

The influence of CaO as a promoter for outward growth of iron is shown in Figures 8.34 - 8.36. Wustite plate was coated with regularly spaced 12 μm diameter CaO films. It was treated at 900° for about 5 minutes using gas GW($CO:CO_2$ = 1:1) to allow CaO to dissolve in wustite prior to reduction at 750°C. Figure 8.34 shows the appearance of zone 3 before and after reduction, also Figure 8.35 shows that the iron grew outward from the surface and Figure 8.36 confirms that the bright spots in picture E75 (Figure 8.35) are iron, not CaO.

B. Wustite plates coated with MgO

Following the same experimental procedures, MgO coated wustite plates were prepared and reduced at 900°C for 1 hour. The morphology of the three zones on the plates' surface could not be differentiated after reduction. Therefore, the reducing time was extended to 2 hours. Two specimens (one coated with MgO, the second was not) were reduced; their appearances are shown in Figure 8.37. A noticeable increase of iron layer as a result of MgO coating could be seen but not as porous

and not as thick compared to CaO coating (Figure 8.31).

8.I.3 Summary of results with iron oxides

The reduction of some high purity iron oxides could produce iron whiskers under certain conditions. One may conclude that contrary to some current theories, the presence of certain impurities (e.g. CaO, alkali oxides) is not the necessary condition for iron whisker growth during reduction.

From the results presented in Section 8.I.1, it is clear that heterogeneity in the specimens at the moment metallization begins, promotes the formation of iron whiskers.

Lime, to a much lesser extent for magnesia, in the specimen, influences the kinetics of iron oxide reduction and the morphology of the iron phase. CaO enhances the rate of reduction, partly due to the more porous iron layer. It appears that when the distribution of CaO in the wustite is less uniform the stronger the tendency for iron whisker growth during reduction from places containing more CaO on the wustite surface.

8.II EXPERIMENTAL RESULTS WITH COMMERCIAL AND LABORATORY IRON ORE PELLETS

Swelling tests were carried out using commercial iron ore/pellets and laboratory pellets made of the same iron ore concentrate which has silica as the main gangue (Table 7.7). The reduction experiments were designed to investigate the influence of alkalis on the behavior of these pellets under conditions close to those of the iron blast furnace with a high level of alkali cycling.

The experimental results with "as received commercial pellets"

and those made in the laboratory (with and without alkali addition (Table 7.11)) will be presented in four groups based on the method of introducing the alkalis. The reference for each case, is alkali free pellets. Also, high purity hematite pellets and silica free briquettes (Table 7.12) were tested to study the sole effect of alkalis. The results are given in Tables 8.1 - 8.5 and Figures 8.38 - 8.46; also some typical pictorial presentations are included in Figures 8.47 - 8.55. In all cases, except with silica free briquettes, alkalis cause the pellets to swell as a result of forming micro and macro cracks which were initiated long before metallization.

Most of the experients were carried out under the same standard reduction conditions, where the pellets were reduced for one hour at 900°C using reducing gas GRS ($CO:CO_2$ = 4:1).

8.II.1 Commercial pellets without additives

The experimental results with as received commercial pellets are given in Figure 8.38. Each test was carried out using three pellets which were reduced together. The maximum observed swelling (about 18%) was reached after one hour. Therefore, the standard reduction time for the swelling tests was chosen to be one hour.

It was noticed that for as received commercial pellets and laboratory pellets made of commercial iron ore concentrate and fired at normal firing temperatures of 1200 and 1300°C (Figure 8.43), the swelling index was less than 20% for those pellets without alkali additives.

8.II.2 Alkali impregnated pellets

Before reduction, as received commercial pellets, partially reduced commercial pellets to either magnetite or wustite and laboratory pellets made from either commercial concentrate or high purity hematite,

were impregnated in aqueous solution of alkali carbonates. The results of reduction experiments are given below.

It is obvious from Figures 8.39 and 8.40 that introducing alkalis to commercial iron ore pellets increases both the reducibility and swelling when they were reduced at 900 or 700°C. The experimental results presented in Figure 8.41 suggested that under usual experimental conditions the swelling approached it maximum value long before metallization when the pellets were transferred from hematite to magnetite.

The results in Table 8.1 shows that the swelling index of the commercial pellets is sensitive to pellet structure and the distribution of alkali carbonate. Modified commercial pellets showed a weaker tendency to swell.

The experiments carried out using high purity hematite pellets (see Table 8.3) indicate no evidence that alkalis alone (in the absence of silica) have a significate effect on the swelling and reducibility. These hematite pellets were fired at 1200°C for 2 hours and had a density of about 4.5 gms/cc. Hematite pellets lower in density (about 3.5 gms/cc, and fired for only 30 minutes at 1200°C) were reduced using the standard reducing conditions. They swell more than 30%. The swelling index was determined based on the measurements of dimensions, before and after standard reduction. In this case, the pellets lost their coherent structure after standard reduction.

8.II.3 Laboratory pellets and briquettes doped with alkali oxides

The results of the standard swelling tests with laboratory pellets made of commercial iron ore concentrate are given in Table 8.3 and Figures 8.42 - 8.44. Also, the reduction of silica free briquettes (Table 7.12) are listed in Table 8.4 together with the SEM photographs which

were taken after reduction.

For laboratory pellets without alkalis the extent of swelling and reducibility decreases with elevating the firing and induration temperature while the opposite effect is noticed for those doped with alkali oxides as in Figures 8.42 and 8.43. Also, Figure 8.44 shows that under the same conditions the swelling and reducibility increase with increasing the alkali content of the pellets.

The influence of the cooling rate (which may give an indication of how much stress was left in the pellets after firing and cooling) on the behavior of the alkali doped pellets are listed in Table 8.3.

Three rates of cooling were chosen:

(1) Fast cooling rate: The pellets were taken outside the tubular furnace (after induration at 1200°C) to room temperature. A cracking noise could be heard and microcracks were visible on the pellet surface.

(2) Standard cooling rate: This is the standard cooling rate in the preparation of all the pellets and briquettes in the present work:

(a) The pellets were moved after firing from the hot zone of the furnace to a location near the end of the tube at temperatures of about 700 to 800°C and left there for 30 to 35 minutes.

(b) Then, they were taken further to the end at about 200 - 250°C for another 30 to 35 minutes before being removed to cool at room temperature.

(3) Slow cooling rate: The pellets were cooled slowly in the temperature range 1200 to 1000°C by lowering the furnace temeprature 50°C every 30 minutes, then with the power off they were left in position to cool slowly overnight to reach room temperature.

The swelling and reducibility of the pellets seems to be sensitive to the way they were cooled from the firing and induration to room temperature.

The results presented in Table 8.4 show the effect of alkalis on the reduction behavior of silica free briquettes. It seems from these experiments and SEM observations (Figures 8.47 and 8.48) that alkalis promote iron whisker growth and abnormal swelling when the briquettes are fired and indurated at temperatures of 1200 and 1300°C. The extent of iron whisker growth and abnormal swelling increases by elevating the firing temperature to 1300°C.

8.II.4 Commercial pellets reduced with potassium containing gases

In this series of experiments alkalis were not introduced to the commercial pellets before reduction. The potassium vapor was introduced at the moment the reduction was initiated. The experimental results using reducing gas mixtures containing K vapor (Table 7.3) are given in Table 8.5 and Figures 8.45 and 8.46.

Figure 8.45 shows the results of swelling tests carried out at 900°C using reducing gas GK9H ($CO:CO_2$ = 1:0, $p_K \simeq 10^{-3}$ atm.). The introduction of potassium vapor did not drastically increase either the swelling nor the reducibility. For the sake of comparison, "as received commercial pellets" were reduced for one hour using the same reducing gas, but without potassium vapor and the results are included in Figure 8.45.

The experimental results in Figure 8.46 show the effect of varying the partial pressure of potassium in the standard reducing gas (Table 7.3). The swelling index and reducibility in this case increased with the increase of the potassium vapor pressure in the gas stream.

The experimental results in Table 8.5 show the reduction experiments using reducing gas GK9 ($CO:CO_2$ = 4:1, $p_K \simeq 2.5 \times 10^{-5}$ atm.) with pre-reduced commercial pellets (Table 7.10). Pre-reduction with alkali free gases seems to moderate the adverse effect of alkalis during further reduction.

8.II.5 Effect of cooling on swelling and cracking

The following experiments were carried out to investigate the effect of cooling of the specimens after standard reduction on the swelling and cracking. The question to be answered is: are these cracks formed during reduction or during the subsequent cooling?

(1) Six "as received" and six potassium carbonate impregnated pellets were reduced and cooled in two ways:

(a) Ordinary cooling (as described in Section 7.4)

(b) Slow cooling where the specimens were left to cool under flowing N_2 with the power on, from 900°C to 500°C. The furnace temperature was decreased by 50°C every 30 minutes. When the temperature reached 500°C, the power was switched off and the specimens were left in position to cool slowly (overnight) to room temperature.

Figure 8.49 shows that for both kinds (i.e. as received and potassium carbonate impregnated pellets) the difference in the appearance of the reduced specimens due to changing the cooling procedures, if there is any, is not noticeable.

(2) Alkali carbonate impregnated pellet (2.14 wt% K_2O, before reduction) was photographed during the course of standard reduction and cooling as shown in Figure 8.50. The cracks were much more visible during heating or cooling because of the change in temperature of the

edges taking place before the rest.

Based on the visual observations, we are convinced that alkalis cause swelling and cracking during the early stage of reduction. The adverse effects are not affected by the subsequent cooling of reduced specimens.

8.II.6 Chemical analysis of the pellets and briquettes containing alkalis

Wet chemical analysis of the laboratory pellets (Table 8.6), briquettes (Table 8.7), alkali impregnated pellets (Table 8.8) and commercial pellets which were reduced with potassium-containing reducing gas (Table 8.9) were carried out by the technqiue of atomic absorption.

Various cautious steps were taken to improve the accuracy of the results of the chemical analysis. The standard solutions were made from the same K_2CO_3 and Na_2CO_3 chemical reagents used as additives and high purity hematite was added to make them close to the tested solutions in iron content. The accuracy of the results, based on the error in the machine counts for Na or K in the range used in determining the alkali content of the tested specimens, was in the range ± 2% of the total counts.

According to Tables 8.6 and 8.8 the presence of silica stabilized the alkali in the commercial pellets during firing or reduction. The results in Table 8.9 also show that the pellets absorbed potassium and retained it after they were reduced with potassium-containing reducing gases. On the other hand, with silica free briquettes (Table 8.7) the alkali content diminished during firing and showed further decrease during reduction.

8.II.7 Microscopic examination of partially reduced commercial pellets

Three commercial pellets were examined after standard reduction using optical microscope and SEM, which was also employed in making distribution maps for K, Si and Fe of partially reduced potassium carbonate impregnated pellet (1.32 wt% K_2O before reduction); the results are given in Figures 8.51 - 8.55. The degree of reduction was 29.8% (as received pellet), 37.5% (potassium carbonate impregnated pellet) and 39.5% (as received pellet which was reduced with standard reducing gas with about 5.8×10^{-3} atm. potassium vapor.

As shown in Figure 8.51 "as received" pellets showed non-topochemical pattern in the sectioned specimens. On the other hand, potassium carbonate impregnated pellets had a highly metallized zone near their surface as shown in Figure 8.52 which was followed by a zone where the iron oxide grains are much smaller in size and with rounded edges, probably due to slag attack.

Two areas were chosen for K, Si and Fe mapping. Area (A) at the pellet surface where one of the cracks was initiated and area (B) in the interior close to its end. As shown in Figure 8.53 the distribution of K and Si strongly suggests the co-existence of silicon and potassium by forming slag which was seen in the few pockets surrounded by metallic iron but not connected network between the grains as shown in Figure 8.54 (area (B)). The difference between the distributions in Figures 8.53 and 8.54 certainly reflects the distribution of the slag phase in the two chosen areas.

The metallization was more pronounced when the pellets were reduced with standard gas containing potassium vapor as shown in Figure 8.55;

also, it was not concentrated near the surface zone as in the case when the pellets were impregnated with potassium carbonate prior to standard reduction.

8.II.8 Formation and movement of alkali silicate slag

Mixtures of SiO_2 and K_2CO_3 powders (with different SiO_2:K_2CO_3 ratios) of about 0.5 grams in each case were heated to 900°C in about 10 minutes; once the temperature was reached they were allowed to cool in the furnace to room temperature in about 30 minutes. The heating and cooling were carried out under flowing N_2. The extent of calcination of the K_2CO_3 was calculated based on the weight loss due to CO_2 evolution. The results of these experiments together with another series with typical mixtures but blended with 0.5 grams of wustite powder WH (Table 7.8) each, are given in Figure 8.56. The dissociation of K_2CO_3 which would then react with silica seems to increase with increasing the silica content of the mixture and by addition of wustite. On the other hand, in the absence of SiO_2 the calcination process in the presence of wustite powder, under the same experimental conditions, was relatively slow. Only about 5% conversion occurred after heating K_2CO_3 and wustite mixture for one hour at 900°C.

In order to study the penetration or the movement of liquid carbonate and slag in pellets, the following experiments were carried out using "as received" commercial pellets.

(1) A pellet was left immersed in molten potassium carbonate, under flowing N_2 gas for one hour.

(2) A cylindrical specimen of about one gram (cut from "as received" pellet) was placed on top of about 0.1 grams of potassium carbonate, in the upright position. The specimen was then heated and reduced following

standard reduction procedures.

The two specimens were examined using the electron probe microanalyzer (with electron beam of about 30 μm diameter) and the distribution of K, Si and Fe were plotted as shown in Figures 8.57 and 8.58.

During heating, the penetration of potassium carbonate was rather difficult, as shown in Figure 8.57. Near the surface the silica was moved inward with the potassium to a distance of about 200 μm (region AB). Beyond this region where silica was depreciated there is another region BC of about 900 μm where Si and K appeared to be in phase. Further inward, the penetration of potassium nearly stopped and large peaks of Si representing the gangue phase was observed in the pellet's interior. The reproducibility of these results was checked in three different locations which showed the same profiles for K, Si and Fe.

During reduction, when wustite was available for slagmaking the movement of the potassium was relatively easier and all the K_2CO_3 was taken up by the specimen as shown in Figure 8.58, which indicated that the distributions of K and Si were almost identical in profile and uniformly dispersed throughout the specimen's body from the bottom to the top. No peaks of Si could be observed, which gave indication that almost all the gangue phase reacted with potassium carbonate to form alkali-iron silicate slag. It seemed that the liquid slag movement occurred against gravity due to the capillary force.

8.II.9 The effect of alkali vapors on the furnace tube

As already described in Section 7.3.2 an inner mild steel tube was used to protect the quartz tube of the furnace from potassium vapor attack. The preliminary experiments using reducing gases containing potassium vapors were carried out without this protection. As shown

in Figure 8.59, the potassium vapor attacked the furnace tube which was broken after carrying out two experiments using the standard reducing gas at 900°C and 1100°C.

8.II.10 Summary of the experimental results with commercial and laboratory pellets

During reduction the silica rich gangue plays a positive role in holding the iron oxide grains together, and in bearing the stresses which would cause the pellets to degradate. The experiments carried out to test commercial acid iron ore pellets show that the introduction of alkalis causes the pellets to swell and crack long before metallization; also they improve the reducibility of the pellets, partly due to enhancing the gaseous diffusion.

Under the experimental conditions used in the present work, when alkalis were introduced as metallic vapors mixed with the reducing gas, they have a more pronounced effect compared to the other two cases, i.e. when they were added before pelletizing and firing, and when the pellets were soaked with alkaline carbonate solutions prior to reduction.

It seems that the stresses arising during hematite to magnetite phase transformation, together with the residual stresses developed during rapid cooling after induration and firing, are the driving forces for swelling and cracking. During reduction of the pellet, alkali oxides react with the silica rich gangue and ferrous iron oxide to form low melting point slag which moves between the iron oxide grains due to capillarity forces and causes the disintegration and breaking of the grains.

With silica removed from industrial iron ore concentrate, alkalis cause abnormal swelling and iron whisker growth in partially reduced

briquettes which were indurated at 1200°C. The extent of iron whisker growth increases by elevating the firing temperature to 1300°C.

CHAPTER 9

DISCUSSIONS

9.I MORPHOLOGY CHANGES ASSOCIATED WITH METALLIZATION OF WUSTITE

Since the research into the explanation of the mechanisms involving iron whisker formation which hitherto have been carried out, has been concerned almost exclusively with the reduction behavior of hematite or magnetite specimens, emphasis has been laid within the framework of the present work on considerations of the last step of reduction from wustite to iron. In this section, attempts will be made to interpret the results of the present work, taking into consideration previous work in the field. The practical consequences arising out of the experiments will be briefly mentioned.

9.I.1 Influence of wustite properties and reduction conditions

The first point to discuss is the wustite properties and their influence on the iron whisker growth. It is well known that the presence of impurities such as CaO, Na_2O and K_2O may cause iron whisker growth[14-19,21-31]. As already cited in Chapter 2, some workers in the field suggested that the presence of these impurities is a necessary condition while others claimed that high purity iron oxide specimens may form iron whiskers during reduction[15,27].

The experimental results summarized in Figures 8.4 and 8.17 suggest that iron whisker formation is possible, even if the specimens are free from CaO, Na_2O or K_2O. However, the extent of iron whisker forma-

tion depends on the properties of the specimens and the reduction conditions.

At the moment of metallization the characteristic of wustite that was originated from specimen W_E (single phase wustite) may be different from that converted from M_E (a mixture of magnetite, wustite and a few iron specks), see Figure 8.1. The presence of magnetite and iron specks in specimen M_E is likely to be the result of wustite decomposition[74]. At the commencement of reduction, the wustite surface of the two specimens W_E and M_E may have a different degree of heterogeneity. During the early stage of reduction, prior to metallization, the disappearance of magnetite and even the iron specks under certain conditions is thermodynamically favorable. The iron specks which survive would become growth centers for the iron phase. One may suggest that presence of those iron specks in specimen M_E and the decomposed wustite (Figure 8.16) is necessary for iron whisker formation. However, the experimental results in Figure 8.17 show that without the iron specks iron whiskers were formed from partially oxidized wustite particles. On the other hand, the result given in Figure 8.15 shows that the tendency of iron whisker formation could be suppressed when the specimen was treated to make homogeneous wustite prior to metallization.

We agree with Nicolle and Rist (see Section 2.7.3. of Chapter 2) concerning the need of ferrous iron supersaturation in wustite for the nucleation and growth of the iron whiskers. The required supersaturation of ferrous iron in wustite for nucleation decreases with elevating the reduction temperature[75], while diffusion of iron ions increases. Therefore, we may come to a conclusion that for homogeneous wustite particles there must be a temperature where the tendency of iron whisker

growth reaches a maximum before it drops again with raising the reduction temperature. The results of this work show that this temperature is about 900°C which is in agreement with previous works[15-17,26,27].

9.I.1.1 Influence of wustite properties.

Since the mechanisms of iron whisker growth previously proposed in the literature (see Section 2.7 of Chapter 2) cannot adequately explain the fact that heterogeneous wustite reduction does result in significant iron whisker formation, a mechanism will be proposed here to consider this case.

During the early stage of reduction of heterogeneous iron oxide particles which are composed of wustite and magnetite crystals next to each other (Figure 9.1.A) introducing the reducing gas, which is capable of producing iron, the first reaction is to reduce the magnetite to wustite. A thin layer of wustite may form from the surface of the magnetite at this stage (Figure 9.1.B).

Before metallization, the reduction process may take place at the wustite/gas and wustite/magnetite interfaces and may be represented by the following defect equations[76]:

(1) At the wustite/gas interface:

$$CO_{(g)} + O_O^X + V_{Fe}'' + 2h^{\cdot} = CO_{2(g)}$$

(2) At the magnetite/wustite interface:

$$Fe_3O_4 = 3Fe_{Fe}^X + 4O_O^X + V_{Fe}'' + 2h^{\cdot}$$

where: Fe_{Fe}^X - an iron ion in wustite lattice site

O_O^X - an oxygen ion in wustite lattice site

V_{Fe}'' - vacancy of iron in wustite

$h^{\cdot}$ - positive hole

The concentrations of the vacancies and positive holes at the two reaction surfaces may be assumed constant (but not equal), since one is governed by the bulk gas composition (which is assumed to be independent of time) and the second by the thermodynamic equilibrium between magnetite and wustite. At any time there will be a concentration gradient between the two interfaces. However, the diffusion path varies, therefore the concentration gradient which may be represented in terms of (Fe^{x}_{Fe}/O^{x}_{O}) is relatively gradual in the original wustite (A) and rather steep in the freshly reduced magnetite (B) as shown in Figure 9.1.C.

Nucleation of iron needs certain level of supersaturation which would be relatively more difficult to reach at the surface closer to magnetite because it acts as a sink for iron and a source of vacancies. It may be assumed that nucleation of iron takes place only after magnetite has been consumed or receded from the gas/wustite interface beyond certain distance with negligible effect on the surface region (Figure 9.1.D).

It would be reasonable to assume that the specific reaction rate on gas/wustite interface is uniform, except the very initial moment. The region (A) is likely to have relatively higher supersaturation of iron close to the surface. However, its surface is energetically less active than region (B) which has more vacancies and other defects due to newly phase transformation. In arguing about where are the more probable spots for iron nuclei to appear, there will not be a clear-cut conclusion, because the surface region in (A) has larger driving force and that in (B) has lower energy barrier. The frequency of nucleation depends on both factors.

For the growth of iron nucleus there are advantages and disadvan-

tages in both (A) and (B) regions. In (A) the supersaturation is higher but distributed in a larger region below the surface and longer diffusion distance to result in slower delivery. It is just the opposite in region (B). In the absence of a clear-cut argument and in review of the fact that heterogeneity does cause large iron whiskers, we propose that the site for nucleation and growth might be close to the boundary between magnetite and wustite (or A & B) in the original specimen (Figure 9.1.E). It might take the best of both regions.

The experimental results in Figures 8.18 and 8.19 with 12 x 12 μm regularly spaced iron films on the wustite surface, support the idea that early nucleation of few sites on the surface is needed to cause iron whisker formation. However, we cannot assume that supersaturation has no influence on the growth. Within a short distance of the iron films supersaturation would be difficult to build up; therefore the outward growth would be less pronounced and mature height would be short as in microphotograph E44 of Figure 8.19.

The effect of "easier diffusion paths"[77,78] in the heterogeneous wustite may also aid the outward growth during reduction of heterogeneous wustite at lower temperatures of 600-750°C where the iron whisker growth is much more pronounced.

9.I.1.2 Influence of particle size and reduction conditions

The experimental results summarized in Figures 8.4 and 8.11 agree with Fuwa[15] and Nicolle and Rist[27] that the tendency of the iron whisker growth is inversely proportional to the wustite particle size.

The influence of the temperature of reduction on iron whisker formation during reduction of homogeneous wustite has been discussed. In the case of heterogeneous specimen M_E raising the reduction temperature

lowers the tendency as shown in Figure 8.6 due to its effect on increasing the nucleation frequency and lowering the supersaturation level of iron in wustite before metallization.

The experimental results summarized in Figure 8.8 - 8.11 show that the tendency of iron whisker formation increases with increasing the reducing potential of the reducing gas. We may suggest that the supersaturation level is a function of the amount of ferrous ions which has been produced at the gas/wustite interface up to the time under consideration. On the other hand, the defects in the newly formed wustite are being eliminated. Powerful reducing gas may be able to build sufficient supersaturation before significant homogenization of wustite. The difference in appearance between the surface and interior particles after reduction as given in Figures 8.12 - 8.14 may be attributed to the influence of gradual increase of the reducing potential of the reducing gas and its consequence on homogenizing the wustite prior to metallization.

On the practical implications which may be drawn from the experimental work discussed here, we suggest that insufficient firing in air of magnetite iron ore pellets and the formation of hematite as needles in the original magnetite, which is known as "Widmanstutten Structure", may cause, among other things, degradation due to iron whisker growth if the heterogeneity of the iron oxide particles remains during metallization of wustite.

9.I.2 Influence of carbon deposition

Among the reducing gas mixtures used in this work, on two occasions the deposition of carbon according to the following reaction[79]

$$2CO = CO_2 + C \qquad \Delta G^\circ = -40800 + 41.7T$$

are thermodynamically possible. They are:

(1) at 600°C using reducing gas GRS ($CO:CO_2$ = 4:1)

(2) at 900°C using reducing gas GRH ($CO:CO_2$ = 1:0)

The whiskers formed during reduction in those cases were examined with the X-ray unit attached to the SEM and found to be iron, not carbon. Nevertheless, to rule out the possibility of carbon deposition which is known to cause swelling of the burden materials[80]. Most of the experiments were carried out using the standard reducing gas GRS ($CO:CO_2$ = 4:1, Table 7.1) which was not in favor of CO decomposition and carbon formation above about 750°C (Figure 7.5).

9.I.3 Wustite whiskers appearing during oxidation of iron

On a few occasions wustite whiskers were seen on the wustite plates (Figure 8.3). They usually grew near the corners of the ARMCO iron foils during oxidation. The formation of these whiskers could be the result of stress concentration on certain sites on the iron surface prior to oxidation which provide high energy spots for early nucleation and growth of the wustite whiskers[81].

9.II INFLUENCE OF BASIC OXIDES ON IRON WHISKER GROWTH

Having defined the conditions of iron whisker growth regarding the wustite properties and reducing conditions, we now come to consider how the basic oxides affect the morphology of iron. As cited in Section 7.7.2 of Chapter 7, the wustite specimens were doped with CaO, MgO or both, in different ways, to investigate the effect of these impurities and their distribution in wustite on iron whisker formation.

9.II.1 Effect of CaO

On account of the effect of CaO, the results with wustite-CaO mechanically mixed powders (Figures 8.22, 8.23 and 8.28), suggest

that CaO may promote the iron whisker growth when it has the opportunity to be included in the wustite lattice structure before metallization begins. Since the solubility of CaO is very small at 750°C (Figure 6.9) there is no noticeable change of iron morphology due to the presence of CaO in the mixture. However, when the specimen was treated at 900°C, to dissolve some of the CaO in wustite prior to metallization, iron whiskers were formed with reduction at 750°C. One may conclude that it is not the total amount of CaO with the specimen which affects iron whisker growth, but the portion included with the wustite as solid solution. Therefore, the second step was to reduce calcio-wustite specimens. The influence of CaO distribution on promoting or suppressing the iron whisker growth can be seen in Figures 8.24 and 8.29. Homogenization of CaO in calcio-wustite either by elevating the reduction temperature (Figure 8.24) or by thermal treatment prior to metallization (Figure 8.29) suppresses the tendency of iron whisker growth.

The experimental results with CaO-doped wustite powders could be brought into harmony with those of the other workers in the field who suggested that non-uniform distribution of CaO in wustite is necessary to iron whisker growth[18,25]. As already mentioned in Chapter 2, the explanation of the iron whisker formation due to CaO is not clear even between those who agree on considering non-uniform distribution of CaO as the necessary condition.

Lu's[25] argument was based on the influence of CaO on lowering the activity of wustite in certain sites of the surface so that they become less reactive compared to the relatively clean sites (see Figure 2.5), while Grebe et al[18] suggested that CaO enhances the nucleation of iron due to its effect on lowering the energy barrier for nucleation;

therefore, they claimed that nucleation and growth of iron start from sites of higher CaO content.

In the question of the influence on iron whisker formation due to presence of CaO as the main impurity in wustite, attempts were made by this author to employ an electron probe microanalyzer for making Ca mapping before and after reduction, but discontinued for two reasons:

(1) The electron microprobe here at McMaster, has a take-off angle of about 15° and a minimum electron beam of about 1 μm in diameter. With specimens of less than 2 wt% CaO the background noise was relatively high on one hand, and the Ca mapping itself was extremely difficult to make around the whisker base (about 2 μm in diameter) due to the limitation on the beam size, on the other hand. The results were inconclusive[82].

(2) Even if Ca mapping were reliable[17,18,40] one cannot tell the exact location, on the wustite surface, where nucleation and growth of iron takes place, by making Ca mapping before and after reduction.

To overcome these difficulties wustite plates were coated with thin regularly spaced CaO films and used as specimens for reduction tests. Unfortumately, the smallest grid opening which were used in depositing the CaO films was 12 μm in diameter. The results in Figures 8.34 - 8.36 clearly show that the CaO coated areas are highly metallized and the iron phase grows outward from the original wustite surface. The mapping of iron shown in Figure 8.36 reasonably confirms that they are iron, not CaO. One may suggest that if the size of the CaO films are smaller, the outward growth of iron would be more pronounced.

Based on the above discussion it is reasonable to suggest that the

sites on the surface higher in CaO content are easier to nucleate and grow to form the iron whiskers. The present work supports the mechanism of the iron whisker growth proposed by Grebe et al[18], rather than that by Lu[25].

It is conceivable that presence of CaO in calcio-wustite, distorted the lattice structure due to the difference in size between Ca^{+2} and Fe^{+2} (the ionic size of Ca^{+2} is 0.99 A°, while that of Fe^{+2} is 0.74 A°only[83]). Such distortion would result in increased diffusion rate due to its effect on increasing the wustite lattice parameters[84,85]. It certainly conforms with Wagner's[34] original theory and that of Nicolle and Rist[27] that faster rate of diffusion favors iron whisker formation.

It is this author's opinion that a mechanism of iron whisker formation due to non-uniform distribution of CaO in calcio-wustite may be proposed and summarized as follows:

(1) Iron nucleates first at the sites higher in CaO on the surface. It means that the effect of lower energy barrier outweighs that of lower thermodyanmic driving force.

(2) Ca^{+2} ions have a tendency to diffuse away from the iron nucleation sites according to its concentration gradient. Two processes may be assumed to cause the outward growth of iron:

(a) Considering Ca^{+2} diffusivity is relatively slow, we may agree with Bleifuss[16] that a second phase of calcium-rich wustite will form and prevent the radial growth, leading ultimately to iron whisker formation. However, with the instruments used, no positive evidence of the presence of this second phase has been identified under optical microscope or SEM. Indeed, the discussion of Section

9.I.1 shows that iron whiskers may form even with wustite free from CaO. Therefore, formation of this second phase cannot be justified as a necessary condition for iron whisker growth.

(b) Considering Ca^{+2} diffusivity to be close to that of Fe^{+2}, the flow of Ca^{+2} away from the growth centers of iron must be matched by an opposite flow of Fe^{+2} to keep the electrical neutrality of the region. The compounded effects would cause a very large flux of iron to rush to the newly formed iron nuclei. As Wagner[34] suggested, the relatively large oxygen ions next to the iron nucleus may act as a barrier and slow down the radial spreading of iron. Hence, the only way to conserve the sudden incoming flow of iron is to erect an iron whisker in the free space outside the wustite surface.

9.II.2 Effect of MgO

The experimental results with MgO-doped wustite specimens are in agreement with the literature; no iron whiskers were observed, as expected[16,26,27]. The explanation offered regarding the size of Mg^{+2} ion, which is smaller than Fe^{+2} (the size of Mg^{+2} is 0.60 A° while that of Fe^{+2} is 0.74 A°[83]) and the complete solubility of MgO in wustite (Figure 6.10) may be adopted here to suggest that MgO is easier to distribute uniformly within the wustite lattice. Also, even if it is not uniformly distributed, its effect on changing the wustite lattice parameters is much less pronounced compared to that of CaO. Therefore, MgO is not expected to cause iron whisker growth.

9.II.3 The combined effects of CaO and MgO

Since both lime and magnesia are good fluxes for iron blast furnace slags, and available in the commonly used raw material dolomite, the combined effects of CaO and MgO on the morphology of iron is investigated in this work. If magnesia moderates the potential risk of lime for iron whisker formation, burned dolomite may be used instead of lime in the manufacture of basic pellets. However, the experimental results given in Figures 8.26 and 8.27 with the use of wustite specimens doped with CaO and MgO suggest that in all the cases studied in this work, CaO promotes the iron whisker growth even if MgO is added in relatively large amounts.

On the practical implications which may be drawn from the experimental work presented here, we may suggest that it is not advisable to charge cold bond iron ore pellets to the blast furnace which either contain or produce lime during reduction. On the other hand, addition of burned dolomite may not solve the problem of abnormal swelling due to iron whisker growth when CaO is free to dissolve in wustite during reduction. It appears that firing the pellets at high temperatures of 1200-1300°C for sufficient time is desirable to slag the free CaO; also to eliminate the heterogeneity in the iron oxide grains which may arise due to insufficient oxidation of magnetite. Excess amount of lime, beyond what silica is capable to combine with in pellets, will cause the formation of lime ferrite during firing and its decomposition during reduction; therefore it should be avoided.

9.II.4 Influence of basic oxides on the rate of reduction

As already discussed in the previous section, CaO may cause iron whisker growth and swelling of some basic iron ore pellets during reduc-

tion. The relationship between enlarging the voids between the iron oxide grains and the overall increase in reduction rate could be related to the enhancement of gaseous diffusion throughout the pellet.

Aside from the influence of CaO on iron whisker growth, the experimental results of this work relate the proportional effect of impurities such as CaO and MgO on the rate of reaction to their influence on the porosity of the iron appearing during metallization of wustite plates.

The experimental results shown in Figures 8.32 - 8.36 and 8.39 support the idea that both CaO and MgO promote the metallization of iron[86,87]. However, CaO seems to have much more pronounced effect, due to its influence on forming porous iron layer during reduction. The suggestion by Kohl and Engell[88] that high purity iron oxides lead to the formation of spongey iron, while impure wustite leads to a relatively pore-free iron layer, cannot be readily accepted.

Summarizing the discussions on the influence of wustite properties and the effects of impurities such as CaO and MgO, we may conclude that nucleation of iron and its growth are sensitive to the degree of the surface heterogeneity during metallization. The morphology change of iron due to the presence of CaO and MgO varies. CaO has much more pronounced effect in comparison with MgO, since Ca^{+2} is bigger than Mg^{+2} which is closer to Fe^{+2} in size. Homogenized, the calcio-wustite does not result in iron whisker formation during reduction.

9.III THE COMBINED EFFECTS OF SILICA-RICH GANGUE AND ALKALI OXIDES ON THE BEHAVIOR OF COMMERCIAL IRON ORE PELLETS

The research into the explanation of the degradation of iron ore pellets by abnormal swelling due to alkali oxides has been extensively

documented. Emphasis has been laid within the framework of the present work on the consideration of the silica-rich gangue and the interaction between iron oxides, the gangue phase and alkali oxides under conditions relevant to the iron blast furnace operation.

The primary consideration was to simulate basic features of blast furnace reducing conditions to understand the mechanism of degradation of commercial iron ore pellets due to alkali cycling. Alkalis were introduced to pellets in three different ways:

(1) before pelletizing and firing (representing an ore high in alkali content)

(2) as alkali carbonate crystals near the surface of the pellets (representing the condition when fine particles or droplets of alkali compounds are precipitated on the pellet's outer shell as a result of condensation of the alkali vapors in the upper parts of the blast furnace stack)

(3) as metallic vapors in the reducing gas as in the commercial blast furnace.

In all the cases studied (except with silica-free briquettes), alkali oxides caused the commercial pellets to swell and to crack long before metallization. The observed swelling and crack formation were checked and found to occur during the course of reduction and not during the subsequent cooling of the partially reduced pellets (Figure 8.50).

9.III.1 The influence of the gangue phase

Commercial iron pellets were fired at temperatures between 1200° and 1300°C. The pellets owe their strength to the formation of iron oxide and gangue bridges. Bridge formation via the iron oxide phase predominates if small proportions of the gangue are present or the

firing temperature is not high enough. The experimental results with commercial pellets (Figure 8.38) and those made in the laboratory (without alkali additives) from industrial concentrate and fired at 1100° to 1300°C (Figures 8.42 and 8.43), strongly suggest that in the presence of the silica-rich gangue, firing temperatures of 1200° and 1300°C for sufficient times are necessary. It seems that the silicate bridges between the iron oxide grains could bear the stresses which would cause the pellets to degradate. On the other hand, with high purity hematite pellet the swelling and the tendency to granular disintegration are very sensitive to the pellet density. Dense hematite pellets of about 4.5 gms/cc swell normally (16.5% after standard reduction test) while pellets of the same kind but with lower density of about 3.5 gms/cc swelled more than 30% and lost their coherent structure after standard reduction.

It seems that in the absence of the gangue phase, and under usual standard conditions pellets of relatively open structure degradate during the early stage of reduction when the hematite bridges break down during phase transformation to magnetite. The pellet's density is related to pore structure. Lower density would result in fewer and weaker bridges. Therefore, one may expect the number of these bridges which remain intact after reduction to be very small (if any) in light specimens in comparison with very dense hematite pellets.

9.III.2 Effect of alkali cycling in the blast furnace on the behavior of iron ore pellets

Having defined the initial position regarding the effects of firing the commercial pellets and the influence of the gangue bridges, we now come to consider how the alkali cycling affects the reduction and degradation behaviors of the pellets. Both the iron oxide phase and also the

silica-rich gangue can, of course, be affected by alkalis. The possible factors as regards the iron oxide phase are discussed in Chapter 2, where non-uniform distribution of alkali ions which are included in the wustite lattice, were quoted as being mainly responsible for iron whisker growth. From experiments in this work, the degradation due to the attack of alkali oxides on gangue phase and iron oxide were investigated.

9.III.2.1 Effect of alkali oxides

The influence of alkalis on the behavior of high purity hematite pellets and silica-free briquettes will be discussed first before considering the combined effects of silica and alkali oxides on the degradation and reduction behavior of commercial iron ore pellets.

The experimental results listed in Tables 8.2 and 8.4, using high purity hematite pellets which were impregnated with alkali carbonate prior to reduction, and silica-free briquettes which were doped with alkali oxides and fired at 1200° and 1300°C, showed that high temperature induration is needed for the alkalis to promote the iron whisker growth. The extent of swelling increased when the firing temperature was raised to 1300°C. The effect of high temperature induration here is the opposite compared to the case when lime causes iron whisker formation[25]. Based on Edström's work on the formation and stability of calcium ferrites[36,89], it is generally accepted that high temperature induration of basic iron ore pellets is likely to bond the lime with the gangue as calcium silicate and not as calcium ferrite, hence suppresses the tendency of iron whisker formation and abnormal swelling during reduction. It seems that the opposite effect is due with alkali oxides. From the chemical analysis of alkali doped silica-free briquettes (Table 8.7) one may suggest that the decrease of the alkali content after reduction is

the result of decomposition of alkali ferrites which are formed during firing and induration in air. It is the author's own opinion that the difference between lime and alkali oxides may arise from the difference in stability between calcium ferrites and alkali ferrites. We may suggest that the decomposition of the alkali ferrite during the early stage of reduction may allow them to incorporate with the wustite in irregular patterns and cause iron whisker growth.

9.III.2.2 Effect of alkalis on the degradation of commercial pellets

For "as received" pellets and laboratory pellets made of commercial iron ore concentrate in the presence of alkalis under conditions investigated in the present work the growth of iron whiskers is clearly not the cause of swelling and cracking observed here. Therefore, no further discussion on this subject can be justified. The swelling and cracking observed were due to the formation of low melting point alkali-rich slag which was verified by SEM x-ray mapping (Figures 8.53 and 8.54) and microprobe analysis (Figures 8.57 and 8.58).

The experimental results shown in Figures 8.39 - 8.41, 8.43, 8.44 and 8.46 and in Table 8.1 and 8.5, suggest that two necessary conditions are required to give large swelling and macrocracks, i.e. (1) alkalis, and (2) hematite to magnetite phase transformation. As already mentioned in Section 6.3.3 of Chapter 6, alkalis drastically reduced the melting point of the silica-ferrous iron oxide system to about 700°C and to flux the silica-rich bonds formed during firing and induration.

In the first stage of reduction from hematite to magnetite the pellets are always weakened by the breaking of the hematite bonds and exhibit "normal" swelling as shown in Figure 8.38. In the presence of

alkalis a chemical reaction between alkali oxides, silica and ferrous iron oxide causes the formation of alkali iron silicate in liquid form; of course, its amount is a function of the temprature and the amount of alkalis present (Figure 6.16). However, even though this reaction will result in breaking the silica-rich bonds and the formation of liquid slag, a driving force is needed to cause the iron oxide grains to split; hence, the pellet to swell and crack.

The residual stresses from firing and cooling are always there to help the pellets to crack and degradate (Table 8.3). The stresses arising during hematite to magnetite reduction may also be conisderable; however, the results listed in Table 8.1 with restructured pellets (which were pre-reduced and re-oxidized back to hematite at low temperature prior to impregnation and reduction (Section 7.7.4.a of Chapter 7)), show that hematite to magnetite transformation seems to have little effect when the stresses were released and alkalis were more uniformly distributed in the pellets.

During the drying of green wares in the ceramic industry[90], differential shrinkage rates due to uneven distribution of moisture near the surface is well known to cause cracks. The case under investigation in the present work is the reverse. The alkali-rich slag melt forms unevenly near the surface, during the early stage of reduction. The movement of this liquid slag due to capillarity force (Figure 8.58) causes the iron oxide grains near the surface to split; hence, starts tiny cracks which propagate during the course of reduction. It is the result of local agglomeration of the iron oxide grains together with tiny droplets of liquid slags which also weaken the pellet structure and flux the silica-rich bonds. The uneven distribution of liquid slag

at reduction temperature can be understood in the following way. With impregnated commercial pellets, the tiny crystals of alkali carbonates were unevenly distributed near the surface of the pellets where ferrous oxide became available first. When impregnation was done after pre-reduction to release the stress and to open the pores, the distribution of alkalis and ferrous iron oxide were both relatively uniform throughout the pellets, macrocracks and big swelling would not be observed under these conditions (Table 8.1).

When alkalis were added before pelletization, they helped the sintering process to occur during induration and firing of the green pellets and resulted in denser pellets (Table 7.11). Formation of liquid slag during firing in air was responsible for helping the sintering process as already discussed in Section 6.2.3 of Chapter 6. However, the presence of alkali-rich glass bonds between the iron oxide grains drastically reduced the pellet strength at reduction temperature. The stresses which initiate cracking may be due to the fact that reduction starts on the pellet surface.

With alkali-containing gas, ferrous oxide and alkalis are formed simultaneously at the gas/solid interface creating favorable conditions for crack formation, the extent of swelling is therefore increased with the partial pressure of alkali (Figure 8.46). The results in Figure 8.45 (with the use of higher reducing power gas mixture) and also those in Table 8.5 (with modified pre-reduced pellets), may be explained based on the fact that in both cases most of the stresses were released prior to slagging; therefore the pellets did not show high swelling index; however, the results in Table 8.9 show that after reduction the pellets retained the alkalis they absorbed during reduction.

The experiments carried out in this work suggest that testing the pellets in the laboratory causes swelling and cracking which is in agreement with George and Peart[49]. However, the important question is whether it happens inside the iron blast furnace. If alkali contents are high in the ore, which is of ordinary composition, at the moment when ferrous oxide becomes available, cracking and swelling are expected. The minimization of alkali content in the ore is always desirable.

In the case that alkalis come to the pellets from the blast furnace gas in the form of condensed carbonates and cyanides or in vapor state, the situation would be different from that mentioned above. It is very reasonable to suggest that the conversion of hematite to magnetite for locations near the pellets' surface would be completed before the introduction of alkalis to the same area by blast furnace gas. Swelling and cracking are not expected to cause serious problems if the pellets are reduced without applying compression load. However, plastic deformation is reported to occur when alkalis are introduced to the pellets during reduction under load[50]. Judging from the large fraction of materials in pellets which are in liquid state at 900°C when alkalis are high (Figure 6.17); also, the appearance of the partially reduced pellets which stuck and sintered as a result of alkalis and compression load[17] one may suggest that the real problem is softening.

Formation of molten alkali iron silica slags at relatively low temperature (Figure 6.14 and 6.15) would be the beginning of the problems inside the blast furnace, once a layer of burden materials start to soften. Accumulation of higher levels of alkalis is expected due to their cycling between the softened layer and the tuyere level. Slowly but gradually, higher vapor pressure zone will be widened leading to

further condensation of alkalis and widening of the softening zone. The consequences are lower stack permeability, hangs and scaffold formation and higher coke rate and lower productivity.

9.III.2.3 Effect of alkalis on the reducibility of commercial pellets

The results given in Figures 8.39, 8.40, 8.42, 8.44 and 8.46 and the microscopic examination given in Figures 8.51, 8.52 and 8.55 show that alkalis increase the rate of reduction and metallization of the commercial iron ore pellets.

Aside from the influence of alkalis on swelling and crack formation which enhance the mass transfer of the reducing gas between the iron oxide grains, it has been suggested that alkali oxides help the nucleation and growth of iron when they incorporate with wustite[86,87]. With Gransden and Sheasby[91] and observations in the present work (Figures 8.51 8.52 and 8.55), we may suggest that the internal nucleation and growth of iron with as received pellets is attributed to the presence of a thin layer of gangue on the iron oxide grains. The introduction of alkalis which flux the gangue and clean the grains' surface to result in more advanced metallization of iron and much less internal nucleation.

9.III.3 Comments on iron ore pellets and the cycling of alkalis in the blast furnace

The trend in the last decade here in North America is emphasizing on higher iron oxides to silica ratios in the commercial iron ore pellets. There is increasing demand for pellets made of "super concentrates" with as little as 2 wt.% silica or even less. The resultant decreased slag volume makes further economies in the iron blast furnace operation. Tests by The Steel Company of Canada, Limited (STELCO) and the U.S. Bureau of Mines had shown that the blast furnace can be operated with slag volumes

as low as 120 to 150 kgs. slag/ton of hot metal[92]. However, the trend of using those pellets is accompanied with accumulation of higher levels of alkalis inside the blast furnace, which in some cases causes operation problems as already discussed in Chapter 5.

On account of the gangue phase, the iron ore pellets with more acid gangue are expected to be more resistable to degradation when attacked with the same amount of alkali oxides as shown in Figure 6.18. Also, as already discussed in Section 6.3.4 of Chapter 6, additives such as dolomite or olivine may be used to increase the pellets' resistance to alkali attack. However, more investigations are needed in this area.

In this work, typical North American iron ore pellets and concentrates were tested. They behave normally when reduced without alkalis which were introduced to the pellets in different ways relevant to the iron blast furnace operation and found to cause them to degradate due to the formation of alkali iron silicate slags at low temperatures of about 700°C. The conclusion we reach is that the adverse effects of alkalis on the commercial iron ore pellets are unlikely to occur due to swelling caused either by iron whisker growth or macrocracks. Alkalis react with the silica-rich bonding phase and ferrous iron oxide to form liquid slag and weaken the pellets mechanically; therefore they become unstable and are likely to deform and soften during reduction inside the blast furnace.

The best strategy is to maintain a low level of alkali cycling in the blast furnace. The total alkali input with the charge should be as low as possible. From practical experience[93] it was found that the alkali input and the amount of alkalis leaving with the slag should be watched, where it is unlikely to accumulate alkalis when more than about 70% of the alkali input leaves with the slag. The remaining amount is

assumed to leave as suspended fine particles with the blast furnace gas except the small portion absorbed by the furnace lining.

As far as the iron ore pellets are concerned, we suggest that if sufficient amount of iron is formed prior to introducing alkalis to the pellets, they may have a better chance to bear with the mechanical stresses after fluxing the gangue bonds once they reach the high temperature level where the blast furnace gas is loaded with alkalis. Reducing gas injection into the furnace stack may sound like a practical way of solving the problem. However, this recommendation deserves further study to see its economic feasibility.

9.III.4 Stabilization of silica in the gangue

In iron ore pellets where silica and ferrous oxide are always available and the cycling of alkalis is difficult to avoid in commercial blast furnace, without drastic changes the problem of softening of partially reduced burden hardly has a solution.

One way to reduce the amount of low melting point slag formation is to stabilize the silica in the gangue during induration and firing of the green pellets, i.e., by forming magnesium silicate which is a refractory material. With calcium oxide the situation is much more complicated. Calcium silicate is more stable but calcium ferrite would cause serious problems during reduction, as discussed earlier. Two Japanese steel companies (Nippon Steel Company and Kobe Steel Ltd.) and one European iron ore company (LKAB in Sweden) have reported that they have made CaO-MgO fluxed iron ore pellets which can retain their strength at high temperatures even when they are exposed to alkali-containing gases[66,94,95,96]. Based on what we learned in the present work, one can imagine that the contact between solid reactants and firing condi-

tions must be extremely important for the purpose of stabilizing the silica.

SUMMARY AND CONCLUSIONS

The aim of this work is to study the mechanisms of degradation of iron ore pellets and to suggest possible solutions to improve their behavior for better blast furnace operation. This research program has been concerned with the iron oxides, the silica-rich gangue and their interaction with minor impurities such as CaO, MgO and alkali oxides under conditions relevant to the iron blast furnace.

The starting materials were chemically pure iron, hematite, calcium oxide, magnesium oxide, silica, sodium and potassium carbonates. Swelling and reduction tests were also carried out using commercial iron ore concentrate and commercial pellets with silica as the main gangue constituent. The experimental apparatus was designed to give accurate control of temperature, flow rate and composition (in terms of $CO:CO_2$ ratio) of the reaction gas mixtures. A new technique was designed whereby wustite plates were coated with calcium oxide or magnesium oxide films by evaporation and deposition of calcium or magnesium metals followed by low temperature oxidation and reduction. The effects of these oxides on wustite reduction could be positively assessed.

In an attempt to understand the influence of alkali cycling on the commercial acid pellets, commercial and laboratory pellets with and without the silica-rich gangue were tested and alkali oxides were introduced in different ways relevant to the situations in the iron blast furnace. The apparent volume of the pellets was measured before and after reduc-

tion to determine their swelling index using a newly designed mercury volumenometer of high accuracy. Metallographic studies with optical and scanning electron microscope (SEM) were carried out to investigate the effects the characteristics of wustite and the influence of CaO and MgO on the morphology of iron in the reduced specimens. Microprobe analyzer was also used in examining the partially reduced iron ore pellets and in studying the distribution and movement of the alkali containing slags.

From the results obtained in this work the following conclusions, concerning the kinetics of reduction and mechanisms of degradation of iron ore pellets can be reached.

(1) Contrary to some current theories, heterogeneous wustite may result in iron whiskers during reduction even if it is free from impurities. The wustite heterogeneity could be due to insufficient firing of the magnetite green pellets or the non-uniform distribution of impurities which are known to cause iron whisker growth such as CaO and alkali oxides.

(2) Concerning the mechanism of iron whisker growth due to the presence of lime as the major impurity with the iron oxide specimen, it is reasonably confirmed that:

   (a) It is not the total amount of CaO with the specimen which affects iron whisker growth, but the portion included in solid solution (calcio-wustite).

   (b) During reduction of calcio wustite, the nucleation and growth of iron starts from sites higher in CaO content, which supports the mechanism of iron whisker growth proposed by Grebe et al.[18] rather than that by Lu[25].

(3) Both lime and magnesia enhance the wustite metallization; however, CaO seems to have much more pronounced effect due to its influence in changing the morphology of iron. Magnesia does not cause iron whisker growth; this may be due to the difficulty of maintaining its concentration gradient in wustite under the present experimental conditions.

(4) With typical acid iron ore pellets produced in North America, the silica-rich bonding bridges formed during high temperature induration and firing at 1200°C - 1300°C for sufficient time, plays a positive role in bearing with the stresses causing the pellets to degradate during reduction inside the blast furnace. When alkalis are introduced, they flux these bonds and form low melting point slag at reduction temperature as low as 700°C. The formation of this low melting point slag, rather than the iron whisker growth, seems to be the actual cause of the operation problems arising as the result of pellet degradation inside the blast furnace with a high level of alkali cycling.

It follows that a simple solution is not likely to solve all the problems which may occur during reduction of the iron ore pellets inside the blast furnace. However, the process can be optimized by the right choice of additives which form stable gangue. The stability of the gangue phase may be judged based on phase diagrams which indicate its stability and resistance to alkali attack increases when higher MgO-containing gangue is formed. Of course, the firing and induration condition are also important. In general it is important to indurate the green pellets in air at 1200°C - 1300°C for sufficient time to oxidize

all the magnetite and to remove the heterogeneity in the iron oxide. High temperature induration is also needed to develop the gangue bonds which bear with the destructive forces suffered by the iron oxide grains during reduction.

APPENDIX A

THE VAPOR DEPOSITION TECHNIQUE

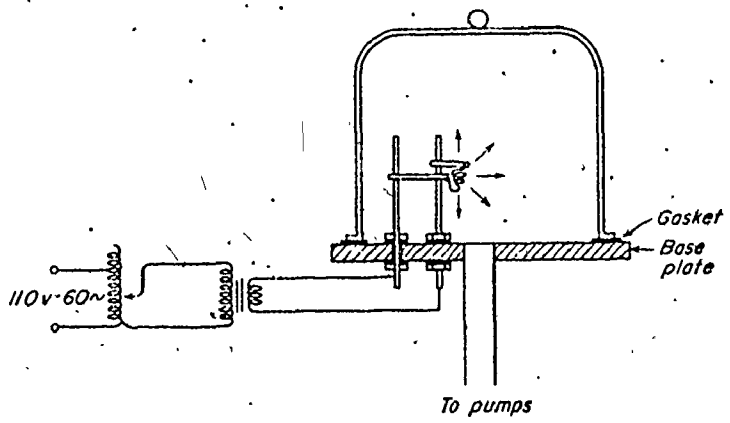

Figure A.1 Schematic diagram of the apparatus used in evaporation and deposition[97].

The wustite plates were coated with substances like Fe, Ca or Mg using the vapor deposition technique used for electron microscope specimen preparation. An automatically controlled vacuum evaporator unit VE-10, made by Varian Vacuum Division Company was used, a schematic representation of which is shown in Figure A.1.

The substance to be evaporated was carried in a conical spiral shaped tungsten filament which was heated by passing electrical current under vacuum of 10^{-4} - 10^{-5} mmHg. The thickness of the film deposited on the wustite surface could be calculated by weighing the substance prior to carrying out the evaporation and deposition and measuring the normal distance from the vapor source (the tungsten filament) and the wustite surface, e.g.:

M gms is the weight of the evaporated substance

r cm is the normal distance between the wustite surface and the tungsten filament

From the mass balance, the mass of deposited film per unit area of the wustite surface w is:

$$w = \frac{m}{4\pi r^2} \qquad (A.1)$$

Assuming the evaporation is equal in all directions, the thickness of the deposited film may be determined based on Equation (A.1) as follows:

$$t = \frac{m}{4\pi\zeta r^2} \qquad (A.2)$$

where t is the film thickness in cm.

ζ is the density of the deposited substance

Unfortunately, the vapor is not usually radiated with spherical symmetry; the error in determining the thickness using formula (A.2) may be as high as ± 50% [9]. However, it provides a useful estimate on occasions.

APPENDIX B

ACCURACY OF MEASURING THE APPARENT VOLUME USING THE MERCURY VOLUMENOMETER

The accuracy of measuring the apparent volume was checked using chromium coated steel bearing balls of precise diameters (supplied by Canadian Bearing Company). The balls used had different sizes and their diameters were in the range 0.3125 inches - 0.7500 inches (0.7938 cm. - 1.9050 cm.) and with a tolerance of 5×10^{-4} inches (12.70×10^{-4} cm) according to the company's catalogues. Some of these measurements were checked by using a micrometer and were found to agree with the company specifications.

The volumes of the balls were calculated based on their precise diameters. The differences between the calculated apparent volumes and those measured using the mercury volumenometer are given in Figure B.1, which indicates that the error in measuring the apparent volumes of the balls (up to about 8 cc) was less than 0.015 cc.

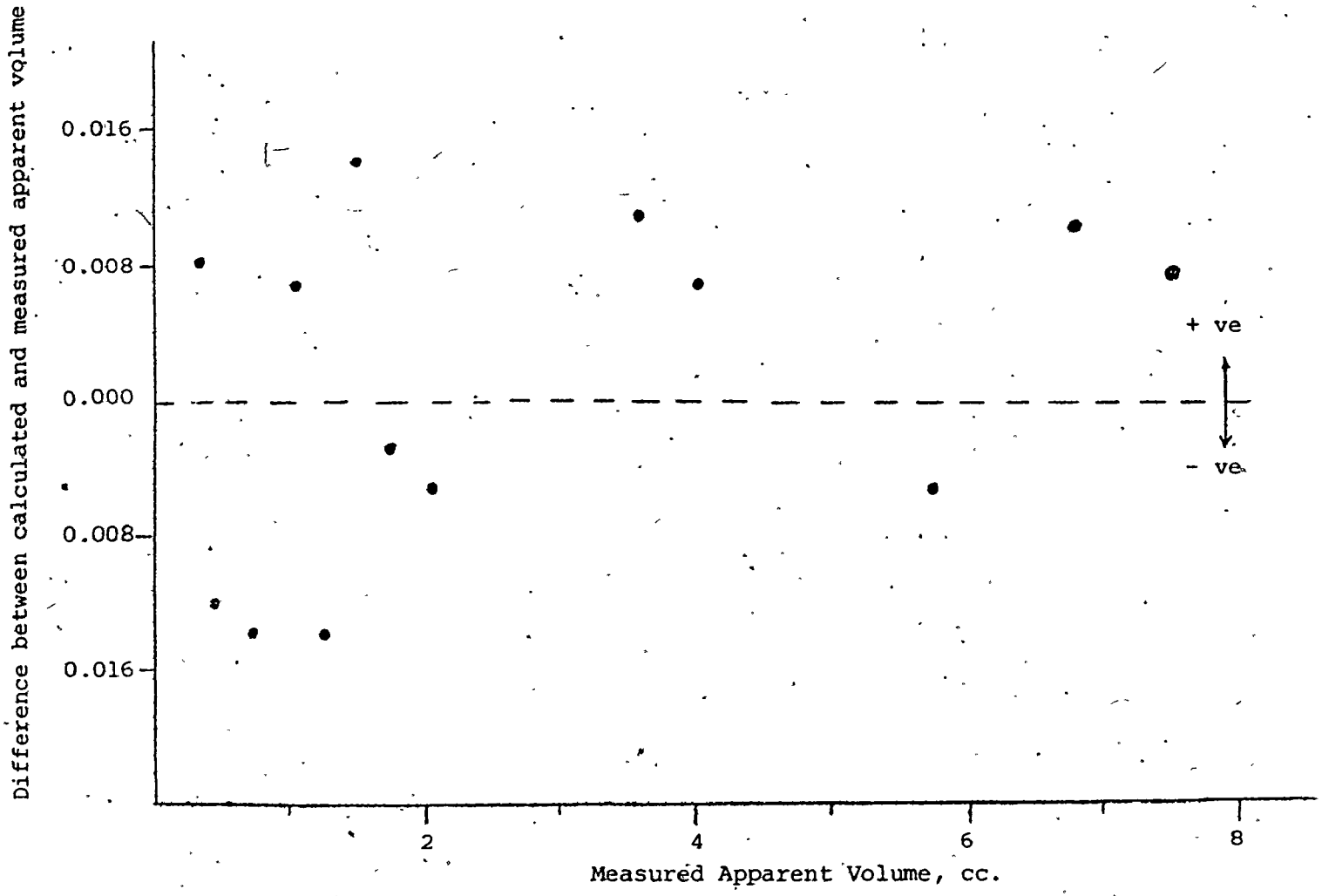

Figure B.1 Errors in measuring the apparent volume using the mercury volumenometer.

REFERENCES

1. Bouman, R.W., Lecture #1, Intensive Course on Blast Furnace Iron-making, McMaster University, June 1977.
2. English, A., and Frans, R.D., Proc. 2nd Int. Symp. on Agglomeration, AIME, 1 (1977) p.3.
3. Chang, M.C., Vilanty, J., and Kestner, D.W., 26th Ironmaking Conf., AIME, December 1967.
4. Grebe, K., Stahl u. Eisen, 88 (1968) p. 1098.
5. Grebe, K., Keddeinis, H., Int. Iron & Steel Cong., Düsseldorf, 1 (1974), p.1.1.29.
6. Edwards, H.B., Stone, H.E.N., and Daniell, B.L., J.I.S.I. 207 (1969) p.1565.
7. Surtees, N., Stone, H.E., and Daniell, B.L., J.I.S.I. 208 (1970) p.665.
8. Inazumi, T., Nagano, K., and Kojima, K., Proc. I.C.S.T.I.S., Trans. I.S.I.J. 11 (1971) p.56.
9. Walker, R.D., Ford, N.S., and Carpenter, D.L., Trans. I.S.I.J. 11 (1971) p.473.
10. Edstrom, J.O., J.I.S.I., 1975 (1953) p.289.
11. Bleifuss, R.L., Proc. I.C.S.T.I.S., Trans. I.S.I.J., 11 (1971) p.51.
12. Claudinon, J., Heizmann, J.J., and Baro, R., Memo. Scn. Rev. Metal., LXIV, #5, (1967) p.424.
13. Nabi, G., Ph.D. Thesis, McMaster University, November 1970.
14. Watanabe, S. and Yoshinaga, M., Tetsu-to-Hagane, 583 (1965), Brutcher Trans. HB#8496.
15. Fuwa, T. and Ban-Yo, S., Trans. I.S.I.J., 9 (1968) p.137.

16. Bleifuss, R.L., Trans. Soc. Min. Eng., AIME, 247 (1970) p.225.

17. vom Ende, H., Grebe, K., and Thomalla, S., Stahl u. Eisen, 90, (1970) p.667.

18. vom Ende, H., Grebe, K., and Thomalla, S., Stahl u. Eisen, 91, (1971) p.815.

19. Thaning, G., Jernkont. Ann., 155 (1971) p.47.

20. Kojuma, K., Nagano, K., Inazumi, T., and Koyama, K., Tetsu-to-Hagane, 56, #4 (1970), Lecture #20.

21. Kojuma, K., Nagano, K., Kishi, T., and Koyama, K., Tetsu-to-Hagane, 57 (1971), Lecture #15.

22. Lu, W-K., Scand. J. Metal., 2 (1973) p.65.

23. Lu, W-K., Scand. J. Metal., 2 (1973) p.169.

24. Lu, W-K., Scand. J. Metal., 2 (1973) p.273.

25. Lu, W-K., Scand. J. Metal., 3 (1974) p.49.

26. Lu, W-K., Proc. Ironmaking of AIME, 33 (1974) p.61.

27. Nicolle, R. and Rist, A., C.A.P.L.-M.R.P., and I.R.S.I.D. Meeting, Middlesborough, July 11th, 1973.

28. Kondo, S., Sasaki, M., Nakazawa, T., and Ito, K., Tetsu-to-Hagane, 57, #4 (1971), Lecture #14.

29. Lindberg, R., Report #R36/71, 1971, Ferrous Metallurgy Division, Royal Institute of Technology, Stockholm, Sweden.

30. Nishida, R., Horzumi, H., and Kanamota, N., Tetsu-to-Hagane, 56, (1970), #4, Lecture #12.

31. Granse, L., Proc. Internat. Conf. on Science & Tech. of Iron & Steel, Tokyo, Part 1 (1971) p.45.

32. Nicolle, R., and Lu, W-K., unpublished work.

33. Gransden, J.F., Ph.D. Thesis, University of Western Ontario, London, Ontario (1973).

34. Wagner, C., J. Metal, February 1952, p.214.

35. Civilli, V., and Burdese, A., Int. Symp. on Reactivity of Solids, 2 (1952) p.867.

36. Edstrom, J.O., Jernk. Ann., 140 (1956) p.101.

37. Haword, J.J., Blast Furnace and Steel Plant, 33 (1945) p.971.

38. Grieve, A., J.I.S.A., September 1953, p.1.

39. Lecomte, P., Vidal, R., Poos, A., and Decker, A., C.N.R.M., 21, December 1969, p.21.

40. Kortmann, H., Ph.D. Thesis, Faculty of Mining, Foundary and Mechanical Engineering of the Technical University of Clousthal, W. Germany (1973).

41. Sayama, S., and Uedo, Y., Trans. I.S.I.J., 14 (1974) p.357.

42. Takahashi, R., Ohmori, Y., and Takahashi, A., Tetsu-to-Hagane, 62, #9 (1967) p.5.

43. Statnikov, B. Sh., Avdonina, M.P., Bratchikov, S.G., and Tveritina, L.A., Stal. in English, 3 (1975), p.209.

44. Nishida, N., Shigemi, A., Ono, K., and Yonagychi, K., Tetsu-to-Hagane, 62, #9 (1976) p.1.

45. Kawaguchi, F., Takenaka, Y., and Fujita, K., Tetsu-to-Hagane, 62, (1976) p.51.

46. Ludwig, V., Bogdandy, L.V., and Schulz, Stahl & Eisen, 84 (1964) p.1561.

47. Förster, V.E. Schierloh, U., and Schmulling, W., Stahl u. Eisen, 89, (1969) p.1473.

48. Results of swelling tests received from Ford Motor Co., Michigan, U.S.A., June 1975.

49. George, D.W.R., and Peart, J.A., Proc. of Symp. "Alkalis in the Blast Furnace, McMaster University, Edited by Standish, N., and Lu, W-K., (1973) p.4-1.

50. vom Ende, H., Grebe, K., Speith, K.G., Proc. AIME 29 (1970) p.351.

51. Kortmann, H.A., Burghardt, O.P., Proc. 2nd Int. Symp. on Agglomeration, AIME, 1 (1977) p.219.

52. Linder, R., J.I.S.I., 189 (1958) p.233.

53. Hassler, B., CIM Conf., Quebec City, August 1973.

54. "Blast Furnace Theory and Practice", Strassburger, J.,H., Editor-in-Chief, Gordon and Breach publishers, New York, 2 (1969), Chapter XII.

55. Peart, J.A., and Standish, N., Proc. of Symp., "Alkalies in Blast Furnaces", McMaster University, Edited by Standish, N., and Lu, W-K., (1973) p.1-1.

56. Kitaev, B.I., Darochenko, J.G.D., and Soutshkov, V.D., Metalurgizdat (1957).

57. McGannon, H.E., Editor, "The Making, Shaping and Treating of Steel", 8th Edition (1964), p.32.

58. Janaff Thermochemical Table, 2nd Edition, Stull, D.R., and Prophet, H., U.S. Government Printing Office, Washington, D.C. (1971).

59. Richardson, F.D., Jeffes, J.H.E., J.I.S.I., 163 (1949) p.397.

60. Frores, F., Ballano, J., Lavandera, J., Cahue, M., and Viguri, M., Proc. Iron and Steel of AIME Meeting, St. Louis, U.S., 25 (1976) p.334.

61. Ashton, J.D., Gladysz, C.V., Holditch, J.E.R., and Walker, G.H., J. Metal, 26, #4 (1974) p.47.

62. Ashton, J.D., Galdysz, C.V., Walker, G.H., and Holditch, J.E.R., Proc. of Symp., "Alkalis in Blast Furnaces", McMaster University, Edited by Standish, N., and Lu, W-K., (1973) p.4-1.

63. External Desulphurization of Hot Metal, Proc. of Symp., McMaster University, Edited by W-K. Lu (1975).

64. Willems, J., Heynert, G. Quade, G., and Zischkale, W., Stahl u. Eisen, 84 (1964) p.57.

65. Lu, W-K. Proc. of Symp., "Alkalis in Blast Furnaces", McMaster University, Edited by Standish, N., and Lu, W-K., (1973) p.2-1.

66. Ilmoni, P.A., and Bjorkvall, B., Proc. 2nd Int. Symp. on Aggomeration, AIME, 2 (1977), p.784.

67. Ellenbaum, F.H., Hinsdale, I., and Ciesco, G., U.S. Patent #3, 966, 456, June 1976.

68. "Phase Diagrams for Ceramists" Edited by The American Ceramic Socity (1964) and (1969) supplement.

69. Bleifuss, R.L., Proc. I.C.S.T.I.S., and, Trans. I.S.I.J., 11 (1971) p.52.

70. Vidal, R., Ponghis, N., and Poos, A., Metal. C.N.R.M., #10, March 1967, p.3.

71. "The Surface Chemistry of Solids", Gregg, S.J., Chapmann & Hall Ltd., London (1965), p.284.

72. Ritter, H.L., and Drake, L.C., Industrial Engineering Chemical Analysis, 17 (1945) p.782.

73. Iron and Steelmaking Conf., edited by I.S.I.J., 1 (1972) p.264.

74. Fisher, V.W.A., and Hoffmann, A., Archiv das Eisenhüttenwesen, Feb. (1958) p.107.

75. Vellet, P.P., and Raccah, P., Mem. Scien. res. Rev. Metal LXIII #1 (1965). p.1.

76. "Nonstoichiometry, Diffusion and Electrical Conductivity in Binary Metal Oxides", Kofstad, P., Wiley-Interscience (1972) p.6.

77. Perrow, J.M., Smeltzer, W.W., and Embury, J.D., Acta Metal. 16 (1968) p.1209.

78. Khoi, N.N., Smeltzer, W.W., and Embury, J.D., J. of Elec. Soc. 122 (1975) p.1495.

79. "Physical Chemistry of Iron and Steel Manufacture", Bodwarth, C., London (1963) p.130 and 306.

80. Tenennbaum, M., Joseph, T.L., Proc. of AIME, Chicago, Oct. (1939) p.106.

81. Embury, J.D., private communications.

82. Brown, L.M. Professor, Cambridge University, U.K., private communication.

83. "Handbook of Chemistry and Physics", College Edition, 48 Edition (1967), F143.

84. Aubry, J., Brethet, A., Duchene, R., Etienne, H., Evrard, O., Jeannot, F., Cleitzer, C., Offray, C., and Perret, P., Ann. Chim. t.5 (1970) p.299.

85. Allen, W.C., and Snow, R.B., J. Amer. Ceram. Soc., 38 (1955) p.264.

86. Khalafalla, S.E., and Weston, P.L., Trans. Soc. AIME 239 (1967) p. 1494.

87. Piepenbrock R., Koch, K., and Tromel, G., Arch. Eisenhüttenwesen 47 (1976) p.141.

88. Kohl, H.K., Engell, H.J., Arch. Eisenhüttenwesen 34 (1963) p.411.

89. Edstrom, J.D., Jerk. Ann., 142 (1955) p.401.

90. Elements of Ceramics, Second Edition, Horton, F.H., Published by Reading Massachusetts, Ltd., p.14.

91. Gransden, J.F., and Sheasby, J.S., Can. Metal. Quart. 13 (1974) p.849.

92. Steward, J.L., and George, D.W.R., Can. Min. and Metal. Bull., June (1966) p.757.

93. Peart, J.A., Lecture #18 and its discussions "Intensive Course on Blast Furnace Ironmaking", McMaster University, June 1977.

94. Lu, W-K., private communication.

95. Saeki, O., Taguchi, K., Nishida, I., Fujita, I., Onoda, M., and Tachiya, O., Proc. 2nd. Int. Sym. on Agglomeration of AIME 2 (1975) p.803.

96. Ilmoni, P.A., and Bjorkvall, B., Proc. Ironmaking 36 (1977), p.366.

97. "Introduction to Electron Microscopy", Hall, C.H., McGraw Hill Book Co., (1966) p.279.

Table 7.1 Reaction Gas Mixtures

Reaction Gas	Flow Rate cc(STP)/min. N_2	CO	CO	$CO:CO_2$	Remarks*
GN	300	-	-	-	
GM	300	20	180	1:9	In equilibrium with magnetite at 900°C
GMW	300	40	160	1:4	Close to magnetite/wustite equil. curve at 1000°C
GW	300	100	100	1:1	In equilibrium with wustite over about 570°C
GRL	300	140	60	7:3	
GRS	300	160	40	4:1	The standard reducing gas
GRH	300	150	-	1:0	

*See Figure 7.5

Table 7.2 Errors in Measuring the Flow Rates of CO and CO_2

Flow Rate cc(STP)/min.	20	40	60	80	100	120	140	160	180	200
Error* cc(STP)/min.	0.04	0.16	0.36	0.64	1.00	1.44	1.96	2.56	3.24	4.00

* Based on an error of ± 0.01 min. in measuring scanning time of soap bubble

Table 7.3 Reaction Gas Mixtures Containing K Vapor

Original Gas Mixture	GRS (the standard gas mixture)			GRH
Temperature of K_2CO_3 Gasification (°C)	900	1000	1100	900
K Vapor (atm.)	2.5×10^{-5}	4.4×10^{-4}	5.8×10^{-3}	1.01×10^{-3}
Name of Gas Mixture	GK9	GK10	GK11	GK9H

Table 7.4 Chemical Analysis of the High Purity Iron

Starting Materials	Chemical Elements, wt.%									
	Fe	C	O	N_2	P	S	Zn	Mn	Si	Ni
Electrolytic Iron	99.88	.005	.033	.0008	.002	.005	-	.001	.006	.03
Armco Iron	99.85	.003	.001	.002	.003	.002	0.001	.020	.002	.02
	Cr	Cu	Co	V	W	Sn	Pb	An	Mo	Al
Electrolytic Iron	.001	.001	.003	.004	.01	.002	-	-	.001	.01
Armco Iron	.006	.078	.003	.003	-	.001	.0008	.001	.003	-

Table 7.5 Chemical Analysis of the Hematite Powder

	Fe_2O_3	SiO_2	CaO	MgO	Na_2SO_4	Al_2O_3	Mn	Cu
wt.%	99.9	.02-.04	.01-.02	.004-.01	.015-.02	.01-.02	.07-.08	.002-.005

Table 7.6 Chemical Reagent Grade Compound

Chemical Reagent	Supplied by	Lot #	Catalog #
Calcium Oxide	Fisher Scientific, U.S.A.	760366	C-117
Magnesium Oxide	Fisher Scientific, U.S.A.	-	M-51
Potassium Carbonate	Fisher Scientific, U.S.A.	-	P-271
Sodium Carbonate "Analar"	BDH Ltd., Poole, England	47301	-

Table 7.7 Chemical Analysis of the Commercial Iron Ore Concentrate and Pellets

	Fe	SiO_2	CaO	MgO	Al_2O_3	K_2O	Na_2O	MnO
Iron Ore Concentrate	67.35	4.57	0.21	0.34	0.31	0.015	0.018	0.12
Iron Ore Pellets	66.50	4.63	0.21	0.33	0.37	0.014	0.021	0.16

Table 7.8 Iron Oxide Specimens of High Purity

Sample	Origin	Gas*	Temp. °C	Time (Hrs)	Phases Present	Photo
W_H	Reagent Hematite	GW	900	4	Wustite	
W_E	Electrolytic Iron	GW	1060	25	Wustite	01
M_E	Electrolytic Iron	GMW	1000	20	Magnetite, Wustite & Iron Spots	02
Wustite Plates	ARMCO Iron	GW	1000	22-25	Wustite	E3, E4

* From Table 7.1

Table 7.9 Wustite Powders Doped with CaO and/or MgO

Powder	CaO wt.%		MgO wt.%	
	Mixed	Solid Solution	Mixed	Solid Solution
W-C2	2.0	-	-	-
W-C5	5.0	-	-	-
W-M2	-	-	2.0	-
W-C2-M2	2.0	-	2.0	-
W-C0.5-M5	0.5	-	5.0	-
W-C5-M0.5	5.0	-	0.5	-
WSC1.8	-	1.8	-	-
WSM1.7	-	-	-	1.7
WSC1.8-M1	-	1.8	1.0	-
WSC1.8-M10	-	1.8	10.0	-
WSM1.7-C0.5	0.5	-	-	1.7

Table 7.10 The Preparation of Magnetite and Wustite Pellets

Pellets	Reduction Conditions			Swelling %	Degree of Reduction %
	Gas*	Temp. °C	Time (Hrs)		
Magnetite Pellets	GM	900	4	8.35	7.43
Wustite Pellets	GW	900	6	11.00	26.70

* From Table 7.1

Table 7.11 Some Characteristics of Laboratory Pellets Made From Commercial Iron Ore Concentrate

Firing Temperature °C	Density of Pellets gms/cc		
	-	0.58 wt.% Na_2O	0.68 wt.% K_2O
1100	3.4	3.7	3.6
1200	3.6	4.1	4.0
1300	3.9	4.3	4.4

Laboratory Pellets Doped with Alkali Oxides and Fired at 1200°C

Alkali added in wt.%	Na_2O			K_2O		
	0.058	0.174	0.348	0.068	0.204	0.408
Density of Pellets gms/cc	3.8	3.8	4.0	3.7	3.9	4.0

Table 7.12 Density of Laboratory Briquettes Free From Silica

Alkali added wt.%	Density gms/cc	
	Fired at 1200°C	Fired at 1300°C
-	4.5	-
0.58 Na_2O	4.7	4.8
0.68 K_2O	4.7	4.9

Table 8.1 Standard reduction of impregnated modified commercial pellets.

Pellet specimens prepared from commercial pellets	Impregnation after pre-reduction to magnetite		Impregnation after pre-reduction to wustite		Impregnation after pre-reduction and oxidation back to hematite	
K_2O wt%	1.04	1.05	1.05	1.01	1.08	1.00
Accumulative Reduction %	36.7	34.2	57.2	38.6	34.1	32.9
Accumulative Swelling %	17.5	16.9	16.2	17.2	17.1	15.5
N_2O wt%	0.91	0.86	0.94	0.90	0.86	0.96
Accumulative Reduction %	36.9	36.0	40.2	39.7	31.9	33.5
Accumulative Swelling %	16.0	16.0	19.1	18.7	14.0	16.6

Table 8.2 Standard reduction of impregnated high purity hematite pellets.

Alkali wt%	-	Na_2O		K_2O	
		0.88	1.87	0.94	1.94
Reduction %	23.7	25.4	27.7	26.5	25.9
Swelling %	16.5	13.6	16.5	14.9	17.8

Table 8.3 Standard reduction of laboratory pellets with 0.68 wt% K_2O and fired at 1200°C followed by cooling with different rates.

Cooling rate	Fast		Standard*	Slow	
Reduction %	45.9	43.7	43.7	33.5	34.0
Swelling %	39.5	3.61	34.0	20.6	23.0

* From Figures 8.7 and 8.8

Table 8.4 Standard reduction of silica free briquettes. The swelling was determined based on the briquette dimensions before and after reduction. The SEM photographs are given in Figures 8.49 and 8.50.

Firing Temp.	1200°C			1300°C	
wt% of alkali added	-	0.68 K_2O	0.58 Na_2O	0.68 K_2O	0.58 Na_2O
Reduction %	37.2	48.8	43.5	61.5	57.9
Swelling %	26.6	38.8	56.6	13.8	17.2
SEM photos	E79	E80	E81	E82	E83

Table 8.5 Reduction of commercial pellets with reducing gas GK9 ($CO:CO_2$ = 4:1, $p_K = 2.5 \times 10^{-5}$ atm.)

Commercial pellets	As Received	Pre-reduced to	
		Magnetite	Wustite
Accumulative Reduction %	34.1	38.5	40.4
Accumulative Swelling %	50.3	22.4	24.2

Table 8.6 Chemical analysis of commercial laboratory pellets, fired at 1200°C, before and after standard reduction. The amount of alkali was calculated based on the weight before reduction in all cases.

	K_2O wt%			Na_2O wt%		
Before firing	0.680	0.408	0.204	0.068	0.580	0.174
Before reduction	0.688	0.391	0.212	0.072	0.591	0.162
After reduction	0.670	0.412	0.216	0.058	0.585	0.179

Table 8.7 Chemical analysis of silica free briquettes fired at 1200°C and 1300°C, before and after standard reduction. The amount of alkali was calculated based on the weight before reduction in all cases.

Firing temperature	1200°C		1300°C	
Kind of alkali	K_2O wt%	Na_2O wt%	K_2O wt%	Na_2O wt%
Before firing	0.680	0.580	0.680	0.580
Before reduction	0.522	0.434	0.453	0.361
After reduction	0.451	0.362	0.246	0.211

Table 8.8 Chemical analysis of impregnated alkali commercial pellets after standard reduction. The amount of alkali was calculated based on the weight before reduction in all cases.

	K_2O wt%	
Before reduction	0.681	1.182
After reduction	0.669	1.090

Table 8.9 Chemical analysis after reduction at 900°C for one hour of as received commercial pellets with reducing gases containing potassium vapor.

Reduction Conditions			K_2O wt%
Gas	$CO:CO_2$	p_K atm.	
GK9H	1:0	1.1×10^{-3}	0.941
GK11	4:1	5.8×10^{-3}	1.030

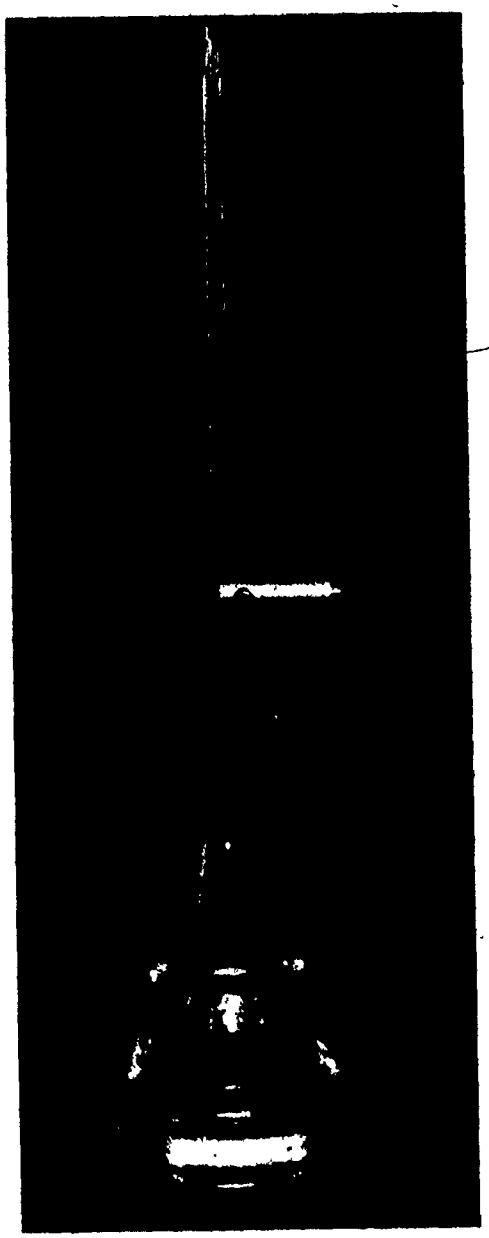

1 glass container
2 volumetric column
3 eye magnifier
4 conical flask

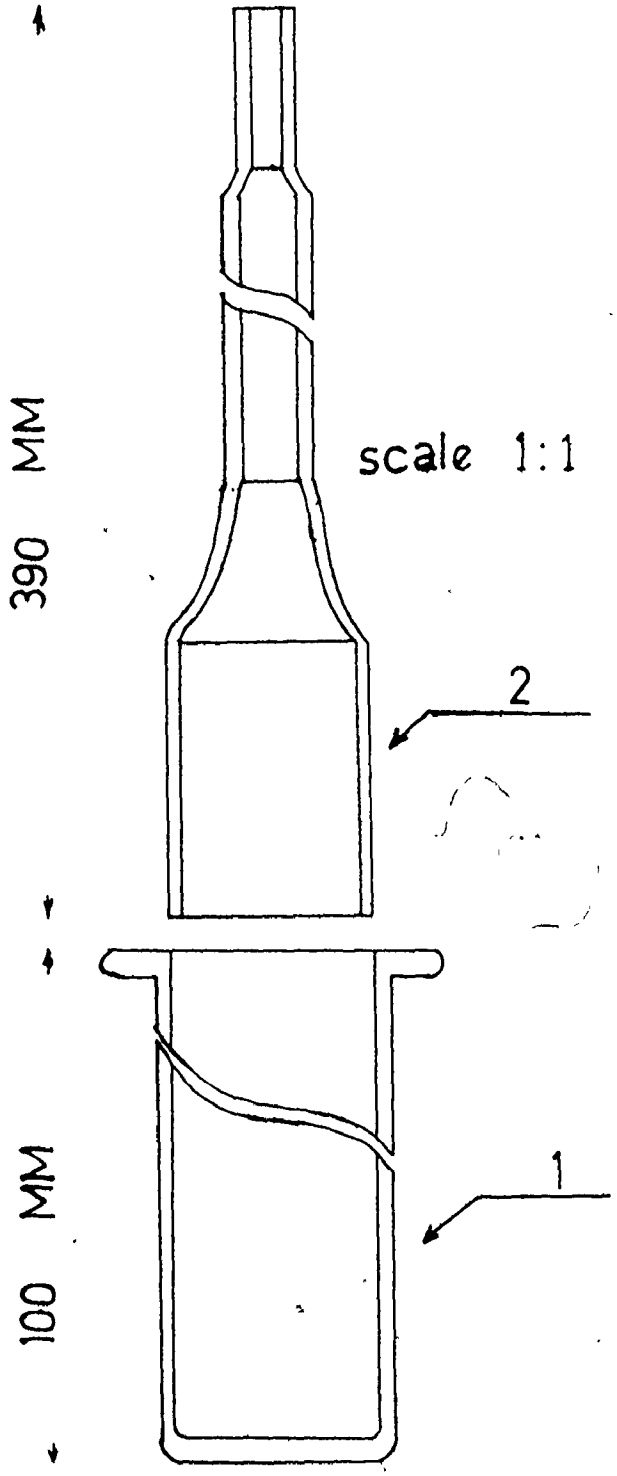

Figure 7.1. The mercury volumenometer.

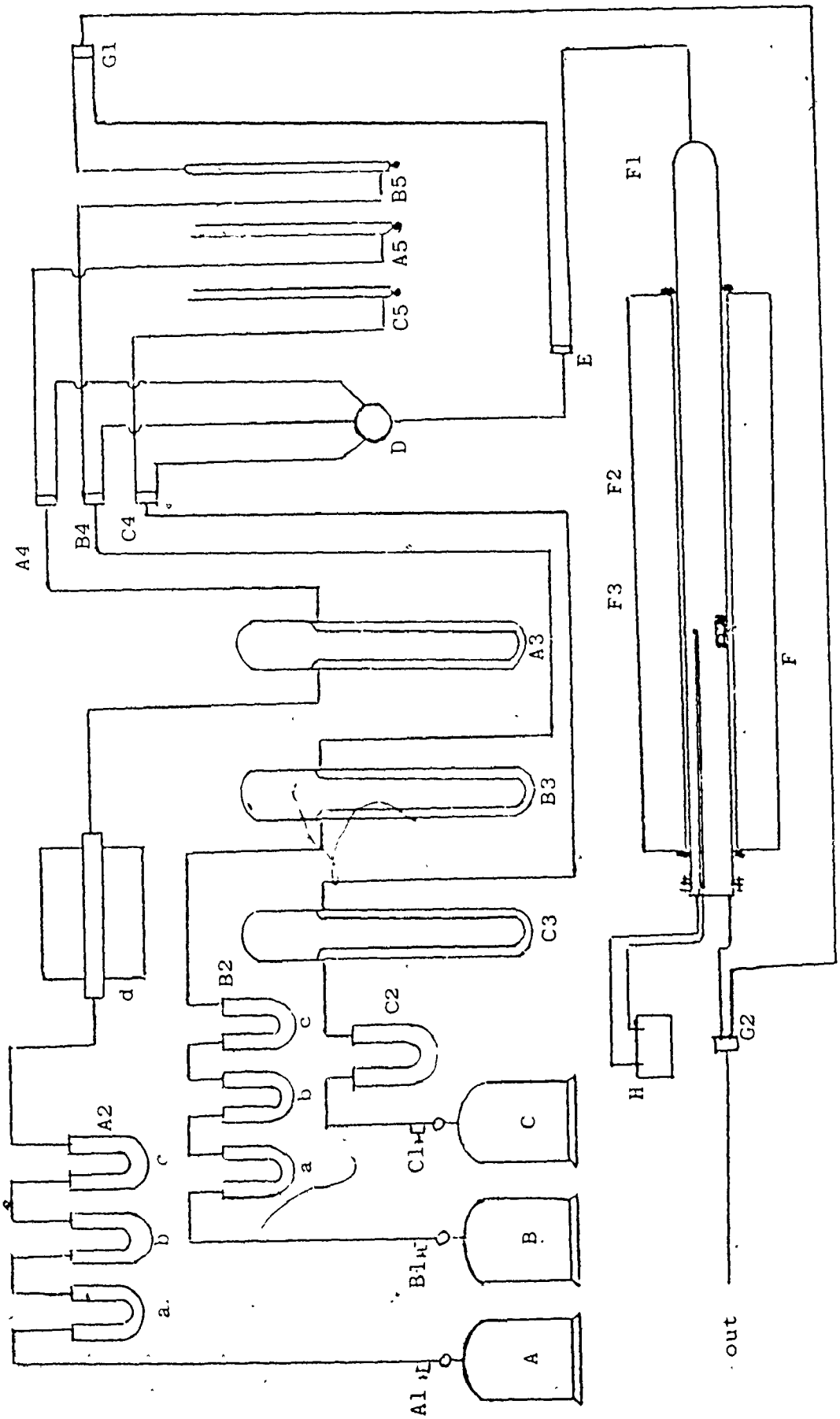

Figure 7.2 Schematic diagram of the experimental apparatus.

Assembly Parts of the Experimental Apparatus

A: Nitrogen gas container

A_1: Micro-needle valve

A_2: Nitrogen purification system:

a. U tube contains silica gel

b. U tube contains drierite ($CaSO_4$) + soda lime

c. U tube contains ascarite

d. Tube furnace contains zirconium flakes at 700°C

A_3: Manometer to measure nitrogen flow

B: Carbon monoxide gas container

B_1: Micro-needle valve

B_2: Carbon monoxide purification system:

a. U tube contains silica gel

b. U tube contains drierite ($CaSO_4$) + soda lime

c. U tube contains ascarite

B_3: Manometer to measure carbon monoxide flow

C: Carbon dioxide gas container

C_1: Micro-needle valve

C_2: U tube contains silica gel

C_3: Manometer to measure carbon dioxide

A_4, B_4, C_4, E, G_1 and G_1 are two-way valves

A_5, B_5 and C_5 are soap bubble flow measuring tubes

D: Gas mixture contains glass wool

F: Three zone tube funrace

F_1: Quartz tube (4 cm inside diameter and 100 cm long)

F_2: Specimen holder

F_3: Thermocouple

H: Potentiometer

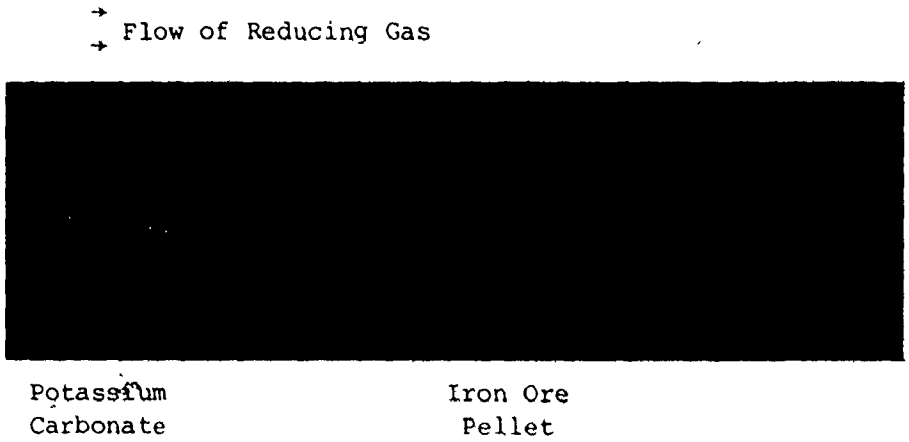

Figure 7.3 Gasification of potassium carbonate.

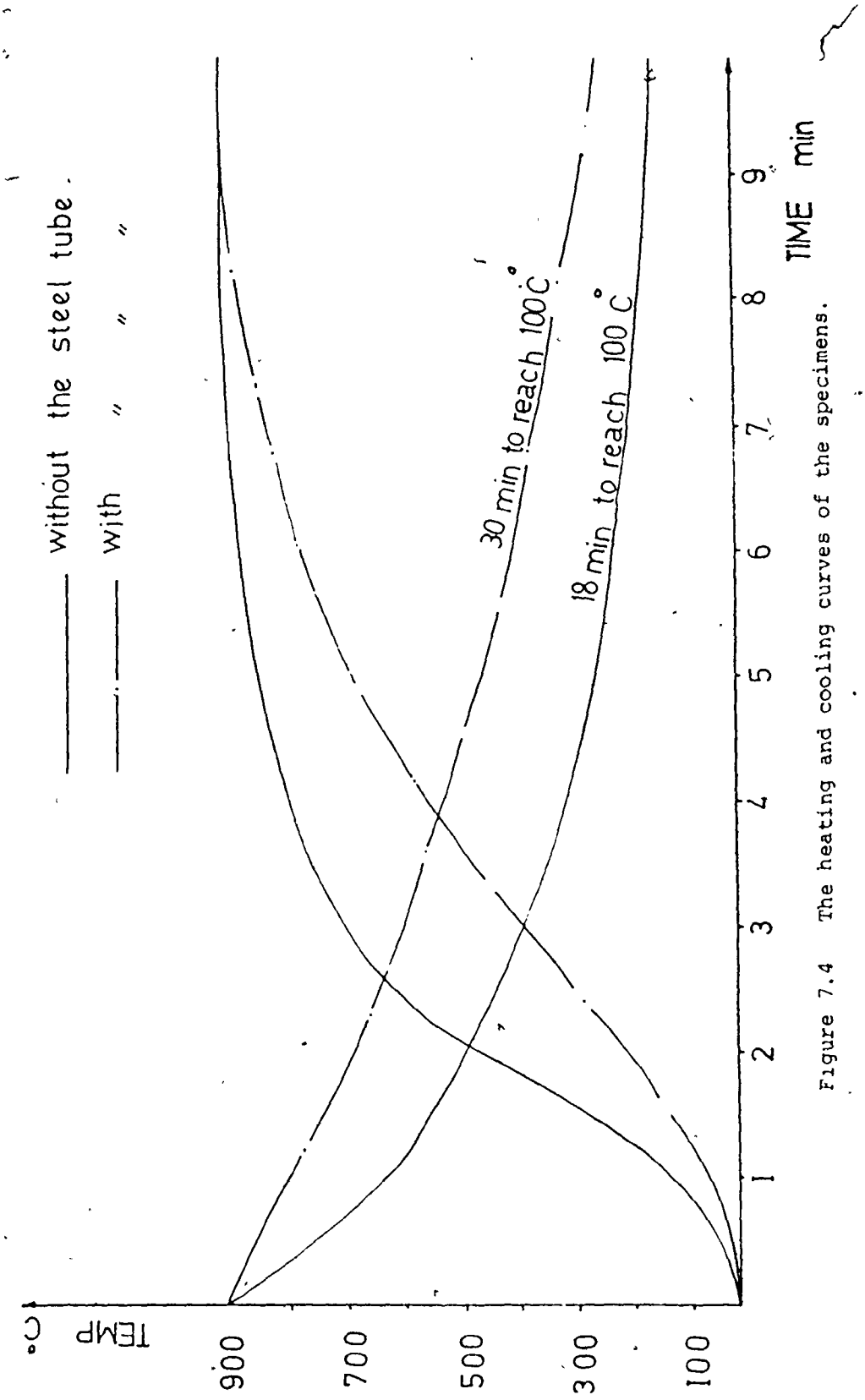

Figure 7.4 The heating and cooling curves of the specimens.

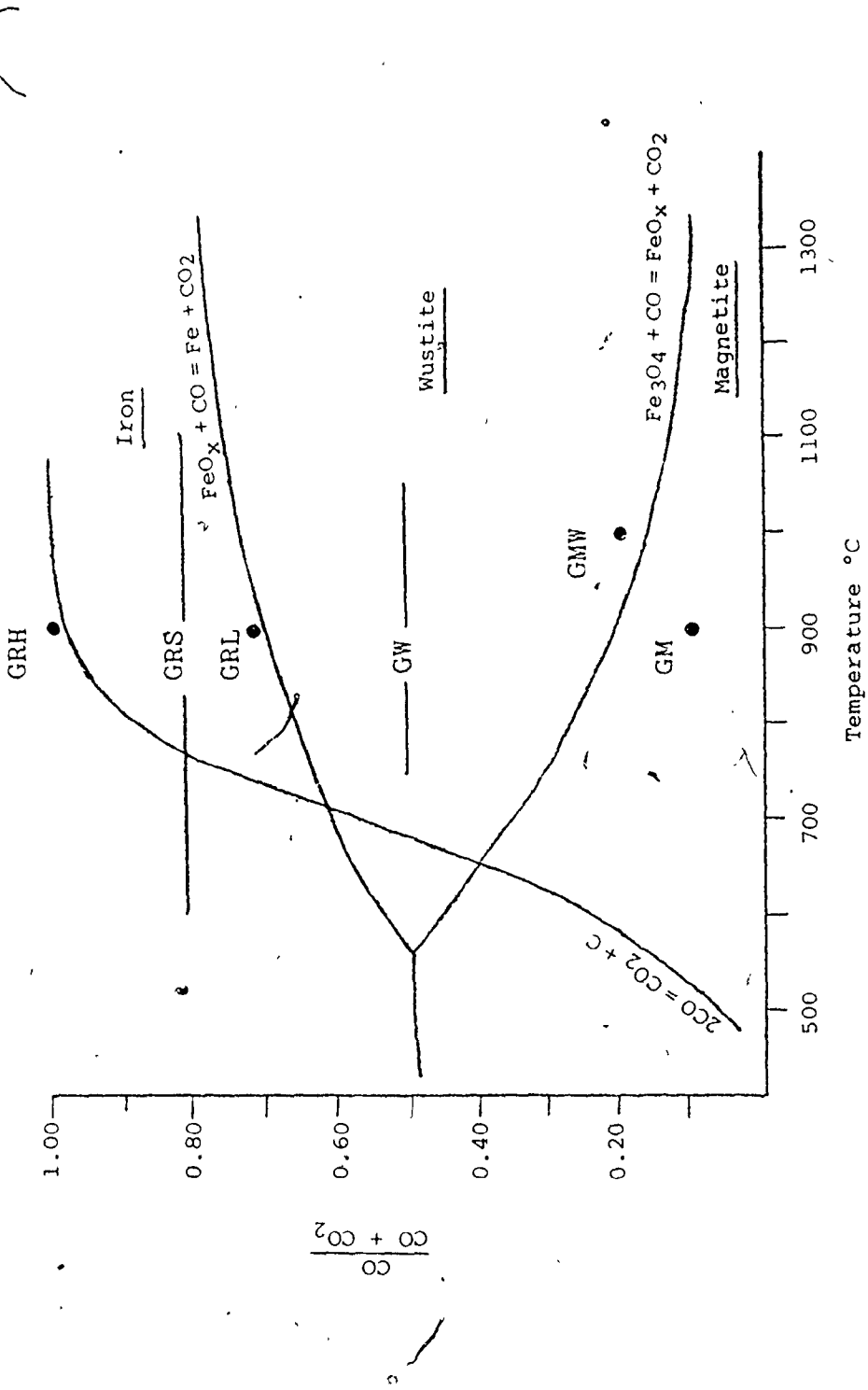

Figure 7.5 The equilibrium relation in the system iron, carbon and oxygen together with the reaction gases and the corresponding temperature range of those used in this work.

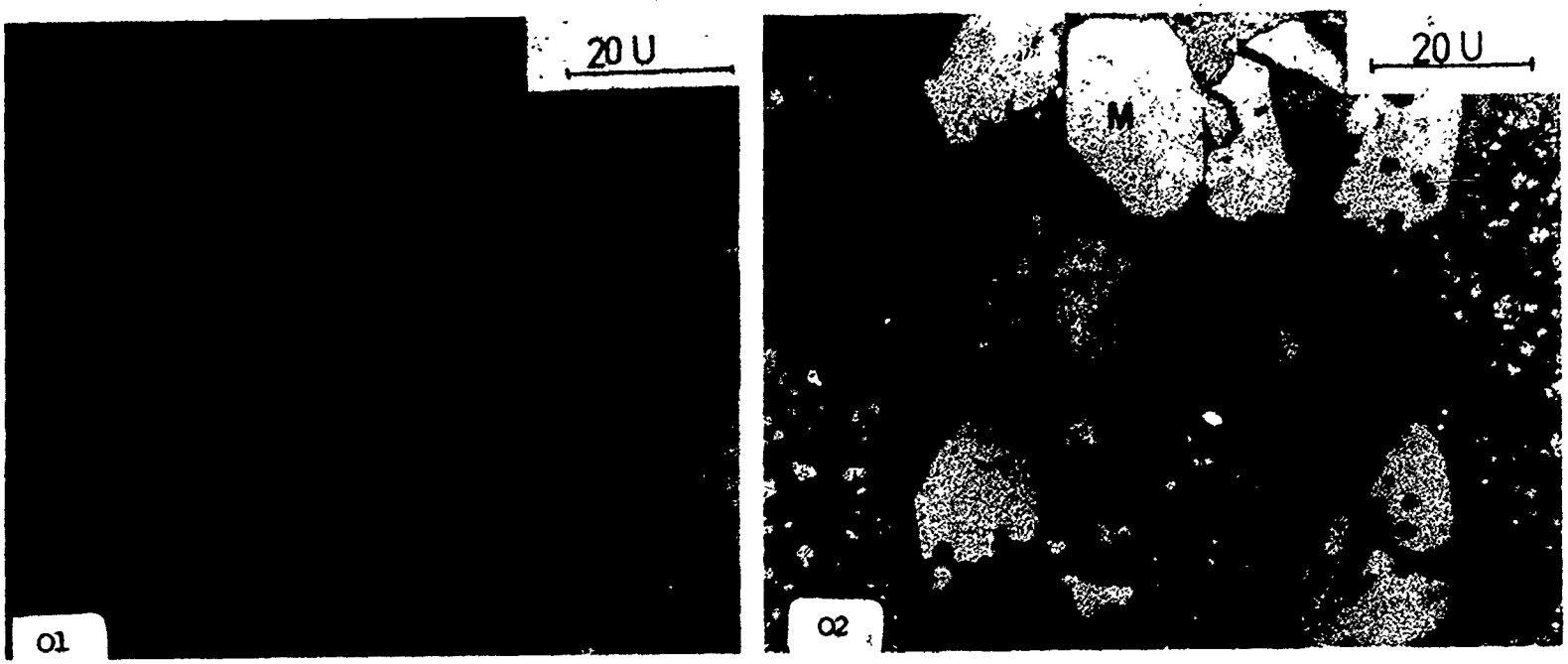

Specimen W_E

Specimen M_E

M Magne ite
W Wustite
Fe Iron

Figure 8.1 Appearance of the high purity iron oxide specimens.

Surface View

Cross Section
View

Figure 8.2 Appearance of the high purity wustite plates used as specimens.

Figure 8.3 Appearance of the wustite whiskers on the plates after oxidation. (The plates which had wustite whiskers were not used as specimens.)

750°C 910°C 1030°C

Figure 8.4 Appearance of Specimen W_E (fine powder) after reduction at different temperatures for 30 minutes, gas GRS ($CO:CO_2$ = 4:1).

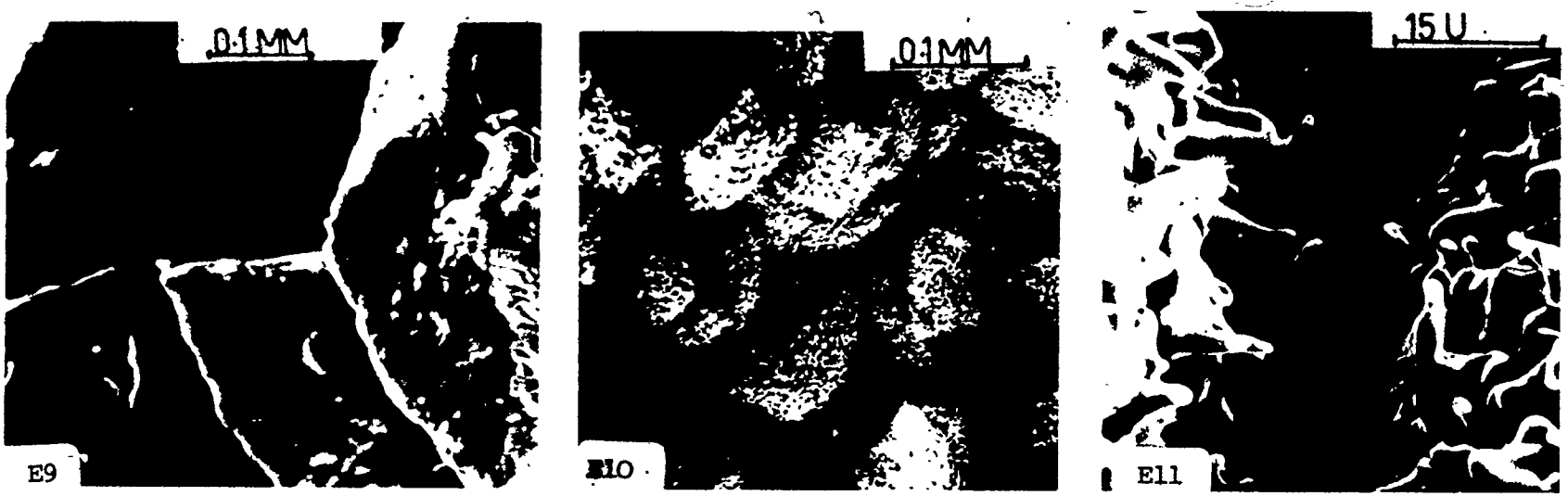

Figure 8.5 Appearance of Specimen W_E (coarse powder) after reduction at different temperatures for 30 minutes, gas GRS ($CO:CO_2$ = 4:1). The appearance of the reduced powder at 1030°C is similar to E9.

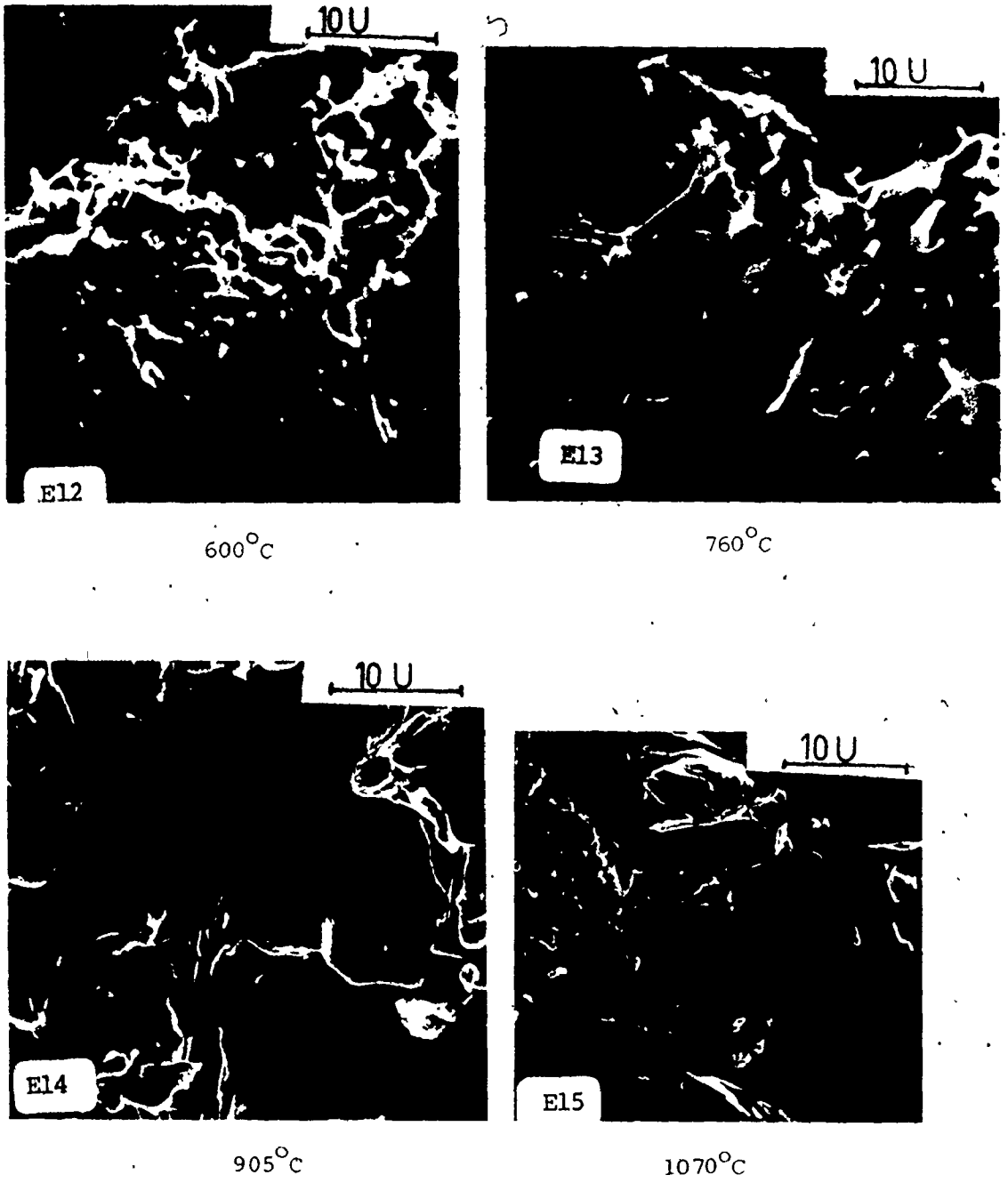

Figure 8.6 Appearance of Specimen M_E (fine powder) after reduction at different temperatures for 30 minutes (except E15 for 10 minutes), gas GRS ($CO:CO_2$ = 4:1).

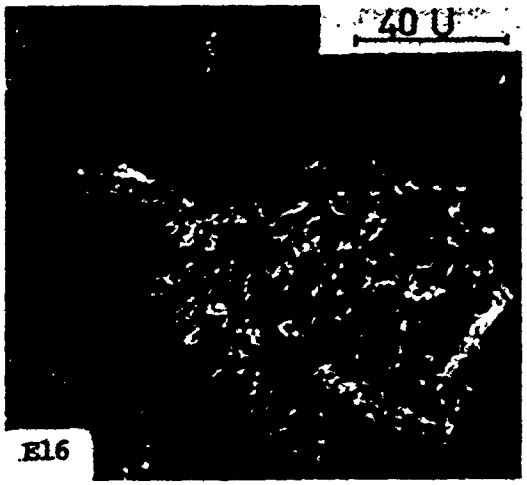

760°C 30 min

905°C 30 min

1070°C 10 min

Figure 8.7 Appearance of Specimen M_E (coarse powder) after reduction at different temperatures using gas GRS ($CO:CO_3$ = 4:1).

GRL ($CO:CO_2$ = 7:3)

GRS ($CO:CO_2$ = 4:1)

GRH ($CO:CO_2$ = 1:0)

Figure 8.8 Appearance of Specimen W_E (fine powder) after reduction using gases of different $CO:CO_2$ ratios for 30 minutes at 905°C.

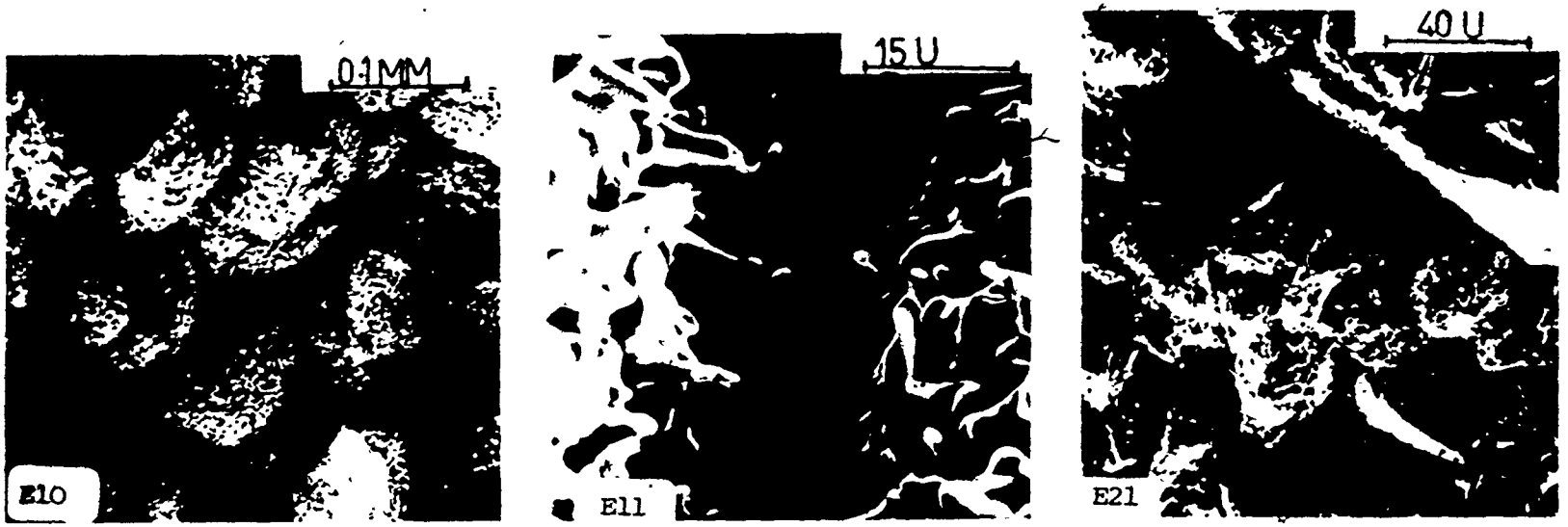

GRS ($CO:CO_2$ = 4:1)

GRS ($CO:CO_2$ = 4:1)

GRH ($CO:CO_2$ = 1:0)

Figure 8.9 Appearance of Specimen W_E (coarse powder) after reduction using gases of different $CO:CO_2$ ratios for 30 minutes at 910°C. No iron whiskers were observed when reduced using gas GRL ($CO:CO_2$ = 7:3).

GRL($CO:CO_2$ = 7:3) GRS($CO:CO_2$ = 4:1) GRH($CO:CO_2$ = 1:0)

Figure 8.10 Appearance of Specimen M_F (fine powder) after reduction using gases of different $CO:CO_2$ ratios for 30 minutes at 905°C.

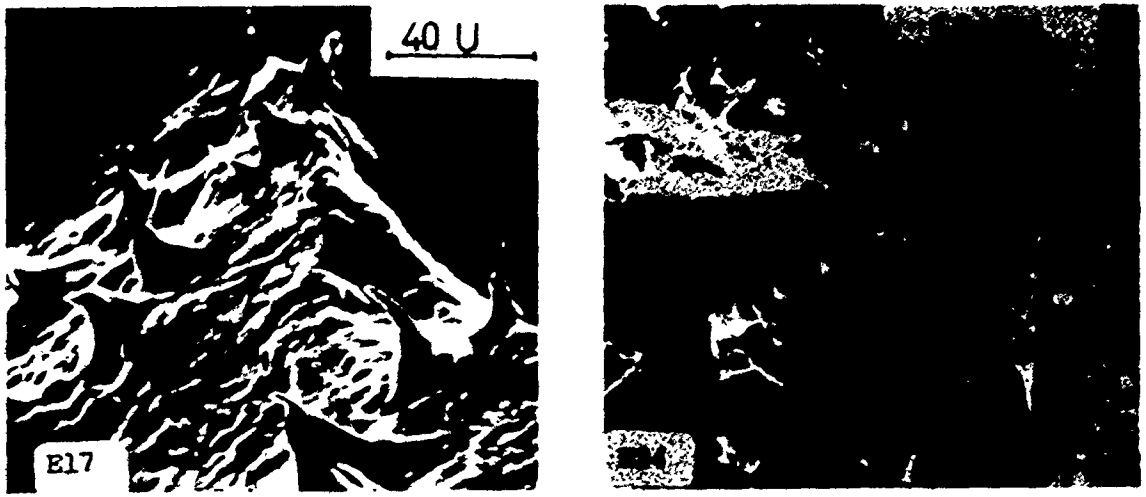

GRS ($CO:CO_2$ = 4:1)

GRH ($CO:CO_2$ = 1:0)

Figure 8.11 Appearance of Specimen M_E (coarse powder) after reduction using gases of different $CO:CO_2$ ratios for 30 minutes at 905°C.

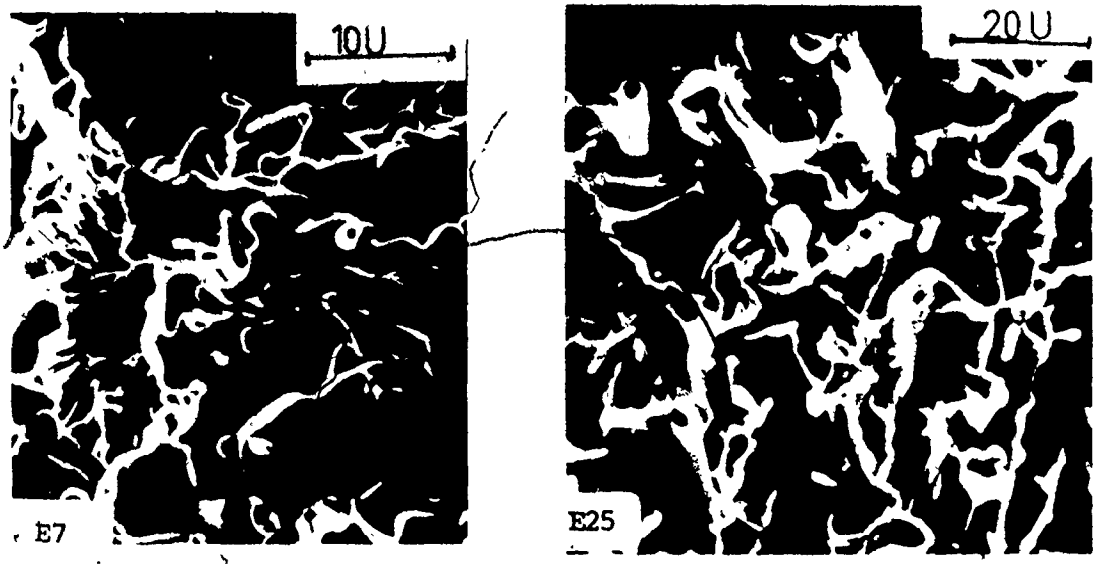

910°C 910°C

Specimen W_E

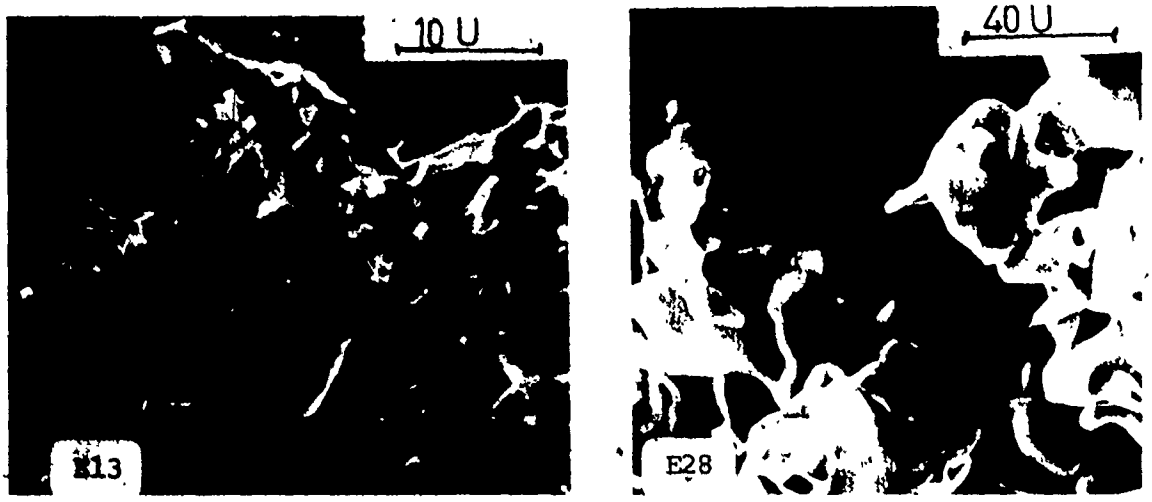

760°C 760°C

Specimen M_E

Surface View Interior View

Figure 8.12 Appearance of the reduced specimens for both surface and interior portions of fine powders of M_E and W_E for 30 minutes with gas GRS ($CO:CO_2$ = 4:1) at two temperatures.

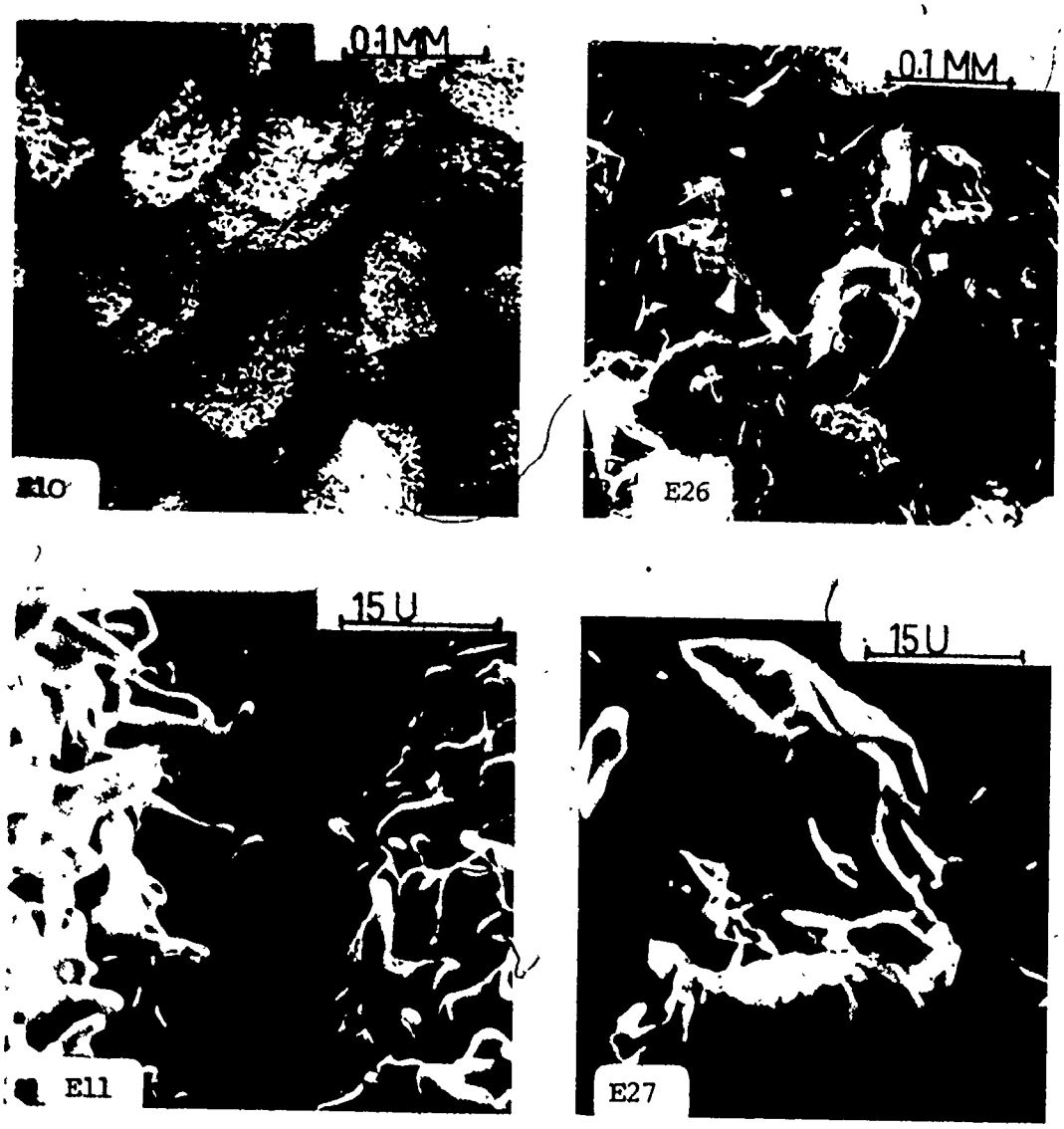

Surface View

Interior View

Figure 8.13 Appearance of the reduced coarse W_E powders for 30 minutes with gas GRS ($CO:CO_2$ = 4:1) at 910°C.

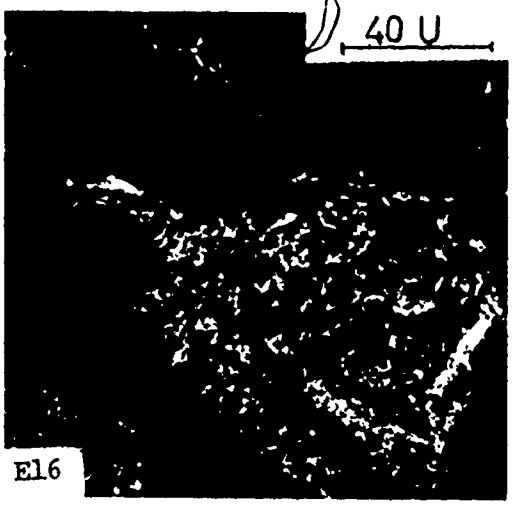

760°C

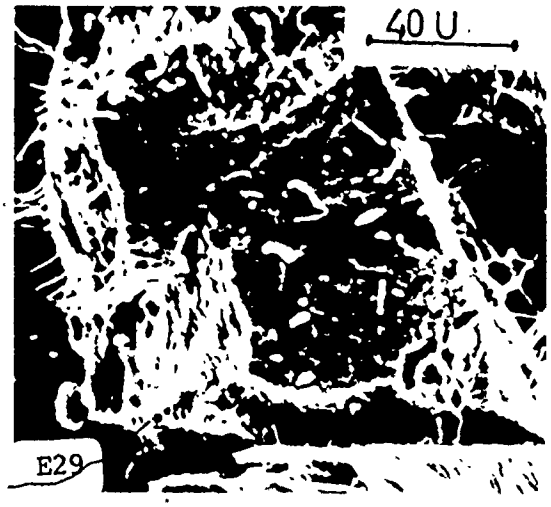

760°C

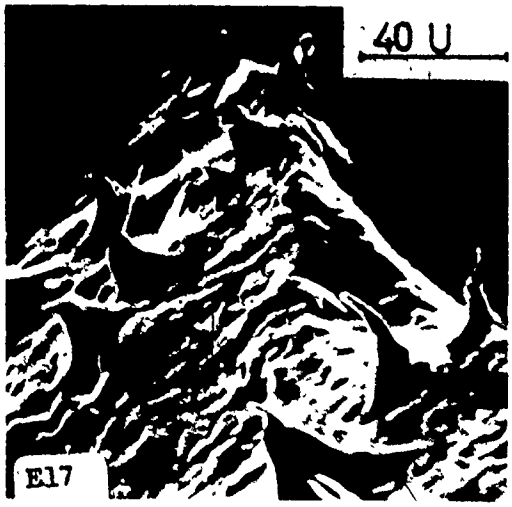

905°C

Surface View

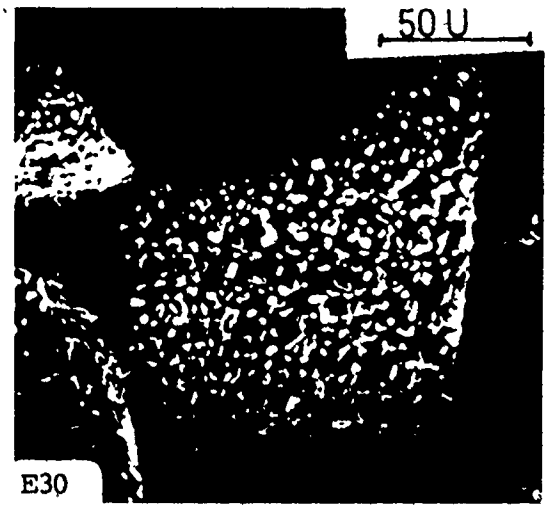

905°C

Interior View

Figure 8.14 Appearance of the reduced coarse M_E powders for 30 minutes with gas GRS ($CO:CO_2$ = 4:1).

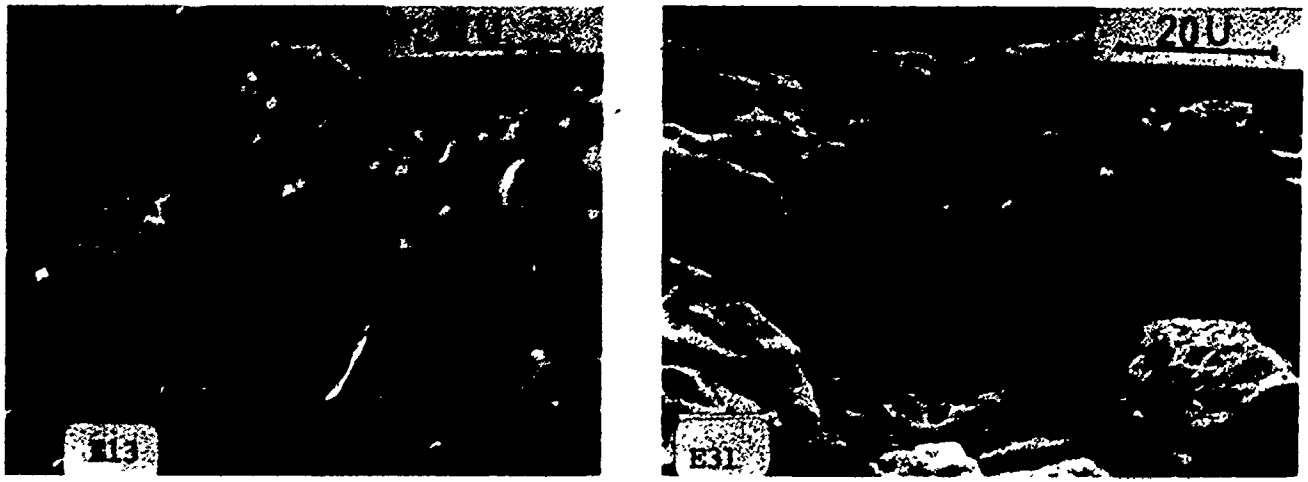

(a) No treatment

(b) Treated at 1050°C for 35 min. with gas GW ($CO:CO_2$ = 1:1)

Figure 8.15 Effect of treatment for homogenization of fine M_E powder on suppressing the iron whisker growth. Specimens were reduced by gas GRS ($CO:CO_2$ = 4:1) for 30 minutes at 760°C for (a) and 750°C for (b).

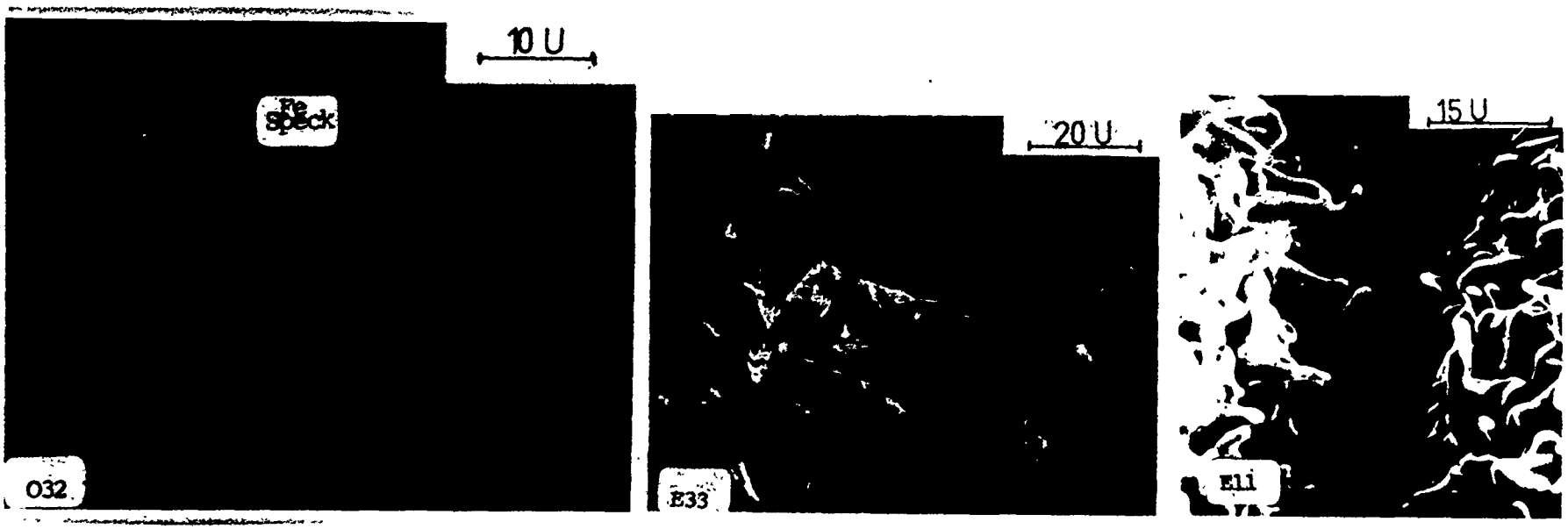

After treatment for decomposition for 21.5 hours at 510°C with purified N_2

Treated and reduced at 900°C

Reduced without treatment at 910°C

Figure 8.16 Effect of treatment for decomposition of coarse W_E powders on promoting iron whisker growth. The reducing conditions were gas GRS ($CO:CO_2$ = 4:1) for 30 minutes at the above stated temperatures.

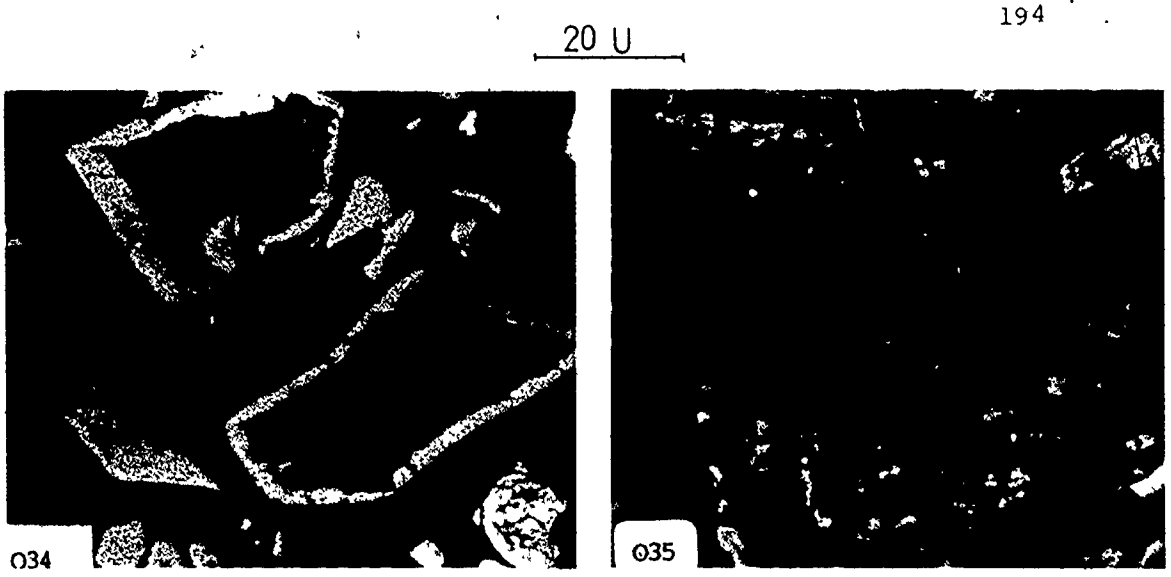

(a) Oxidized for 5 min. in gas GM($CO:CO_2$ = 9:1)

light phase: magnetite
dark phase: wustite

Surface View

Interior View

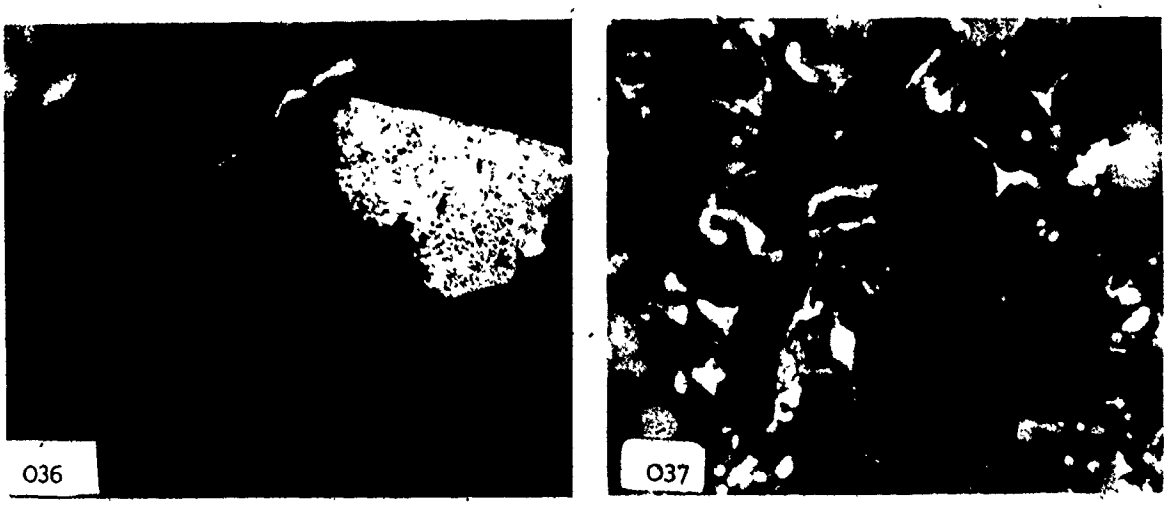

(b) Reduced for 30 min. in gas GRS($CO:CO_2$ = 4:1)

Surface View

Interior View
Iron whiskers are visible

Figure 8.17 Appearance of W_E specimens (a) partially oxidized and (b) partially oxidized and metallized at 900°C.

Grid screen openings

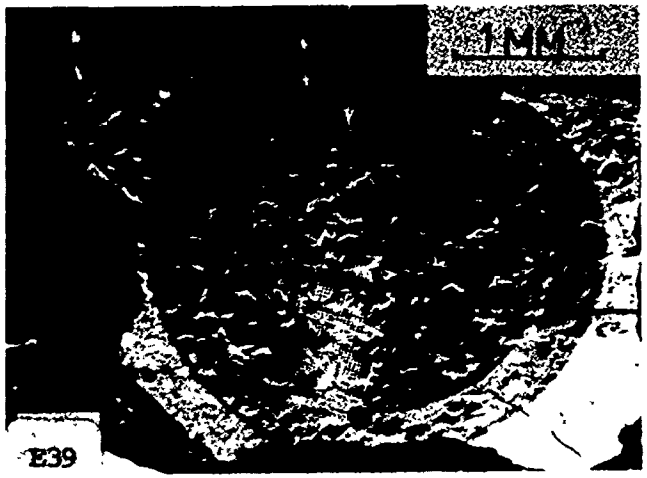

Zone with regularly spaced 12 x 12 μm iron films

Fe coated zone

Uncoated zone

Figure 8.18 Appearance of the wustite plate with Fe films deposited.

(a) Outward iron growth from the 12 x 12 μm iron film (the bright and sharp image is not iron)

(b) Sponge iron, similar for both uncoated or completely coated zones

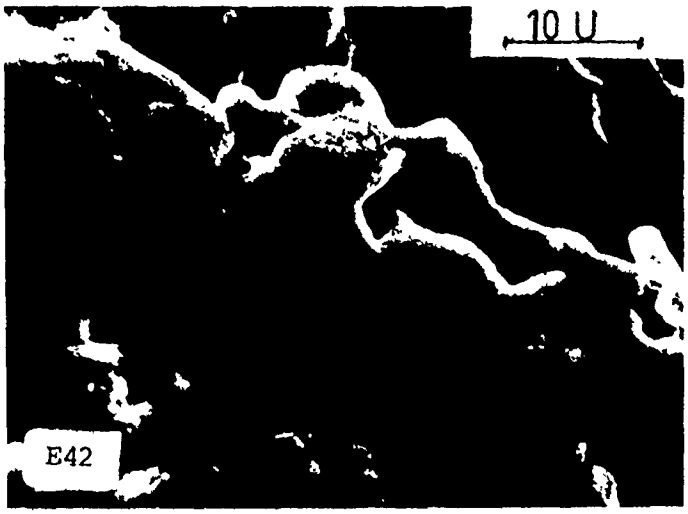

(c) Dense iron layer, similar for all three zones

Figure 8.19 Appearance of the metallized specimens with iron vapor deposition, using reducing gas GRS ($CO:CO_2$ = 4:1) and reaction time of one hour. The reduction temperatures were (a) 700°C, (b) 700°C and (c) 900°C.

Figure 8.20 Section of powder specimens of wustite-lime solid solution (WSC 1.8).

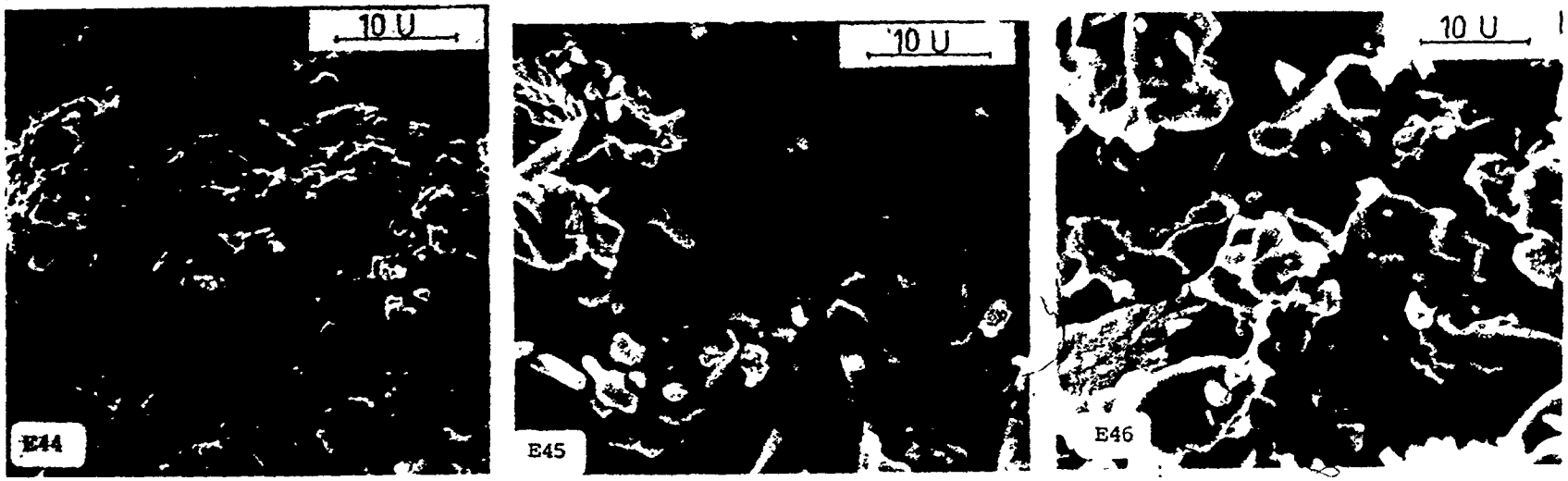

Reduction Temperature 750°C 900°C 1100°C

Figure 8.21 Appearance of reduced wustite powders, W_H which were prepared from hematite of high purity. Specimens were reduced by gas GRS ($CO:CO_2$ = 4:1) for one hour at various temperatures.

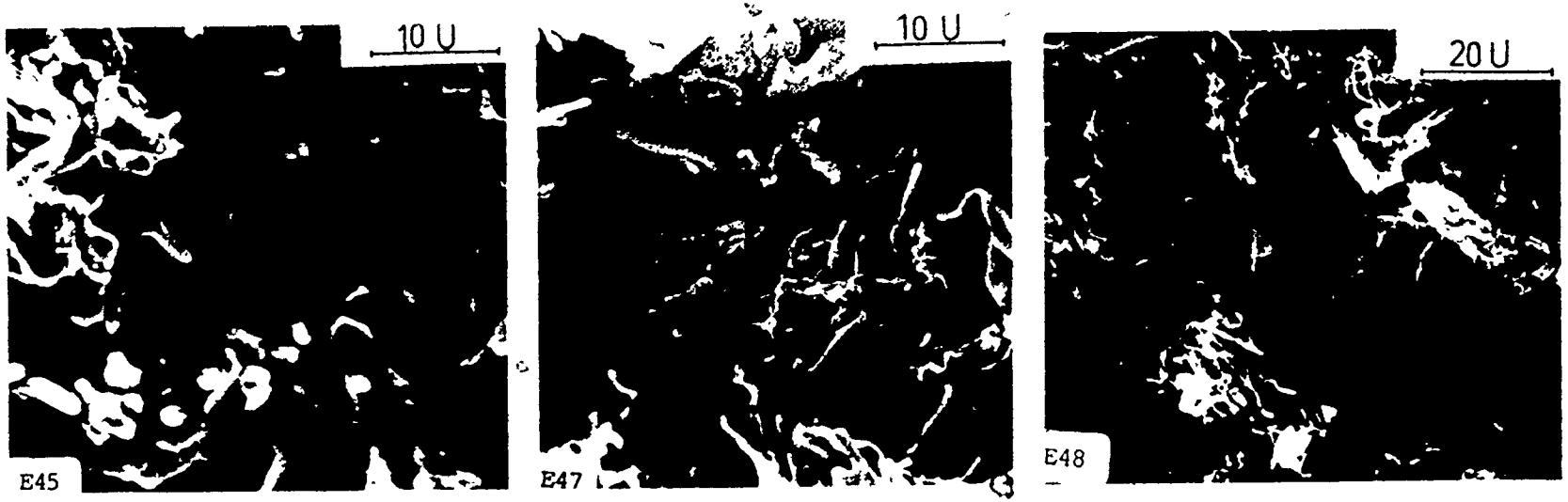

No lime added | 2% CaO | 5% CaO

Figure 8.22 Appearance of the reduced wustite powders W_H in the presence of lime particles under standard reducing conditions (900°C). The mixture of wustite and lime powders was not pre-treated before reduction.

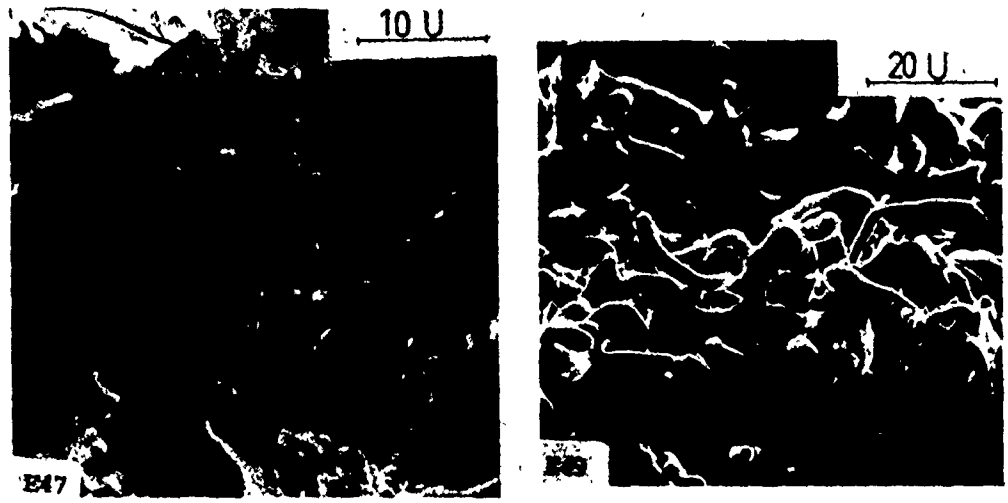

900°C 2% CaO 1100°C

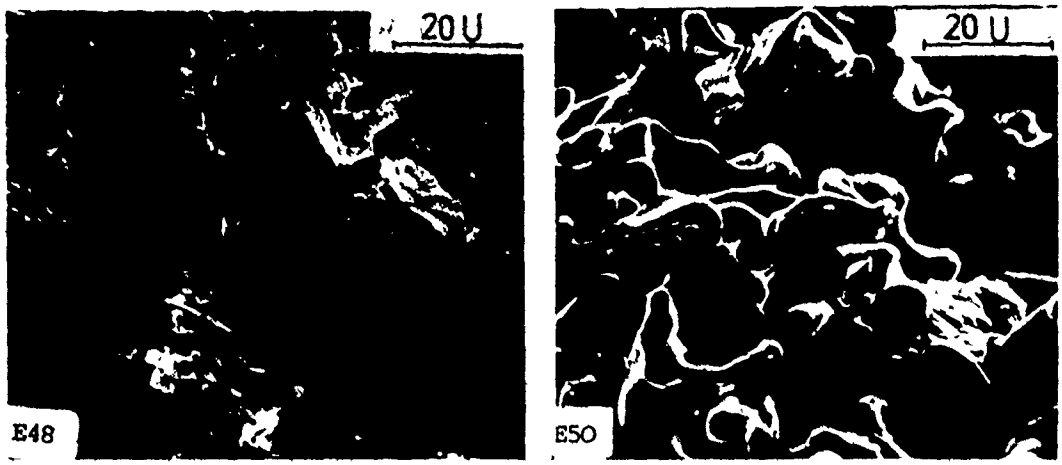

900°C 5% CaO 1100°C

Figure 8.23 Appearance of wüstite powders mixed with CaO, after reduction.

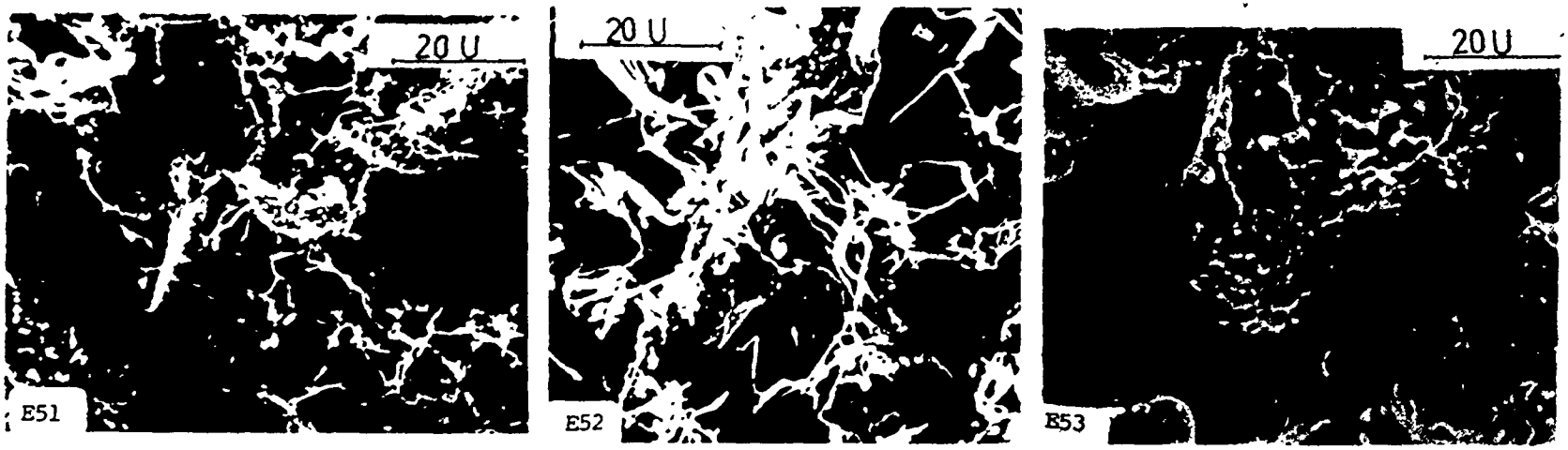

750°C 900°C 1100°C

Figure 8.24 Appearance of solid solution calcium wustite (1.8% a^{+}) after reduction by standard reducing gas for one hour but at different temperatures.

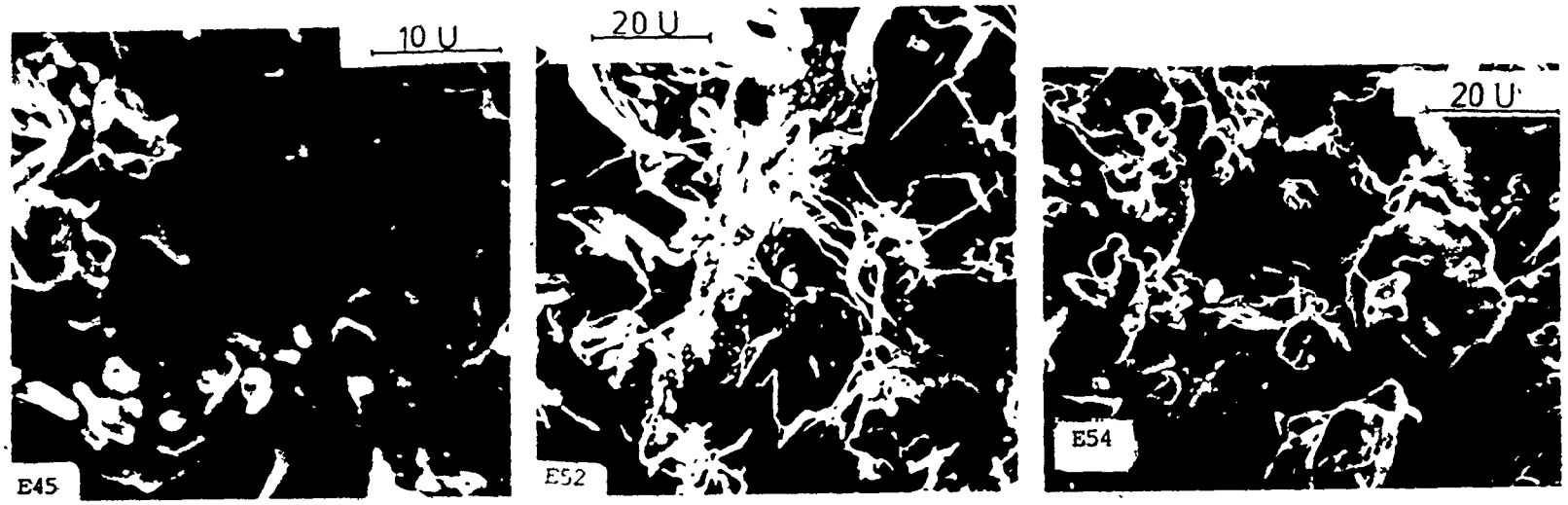

Figure 8.25 Appearance of powder specimens of solid solutions with CaO or MgO after reduction under standard conditions (900°C).

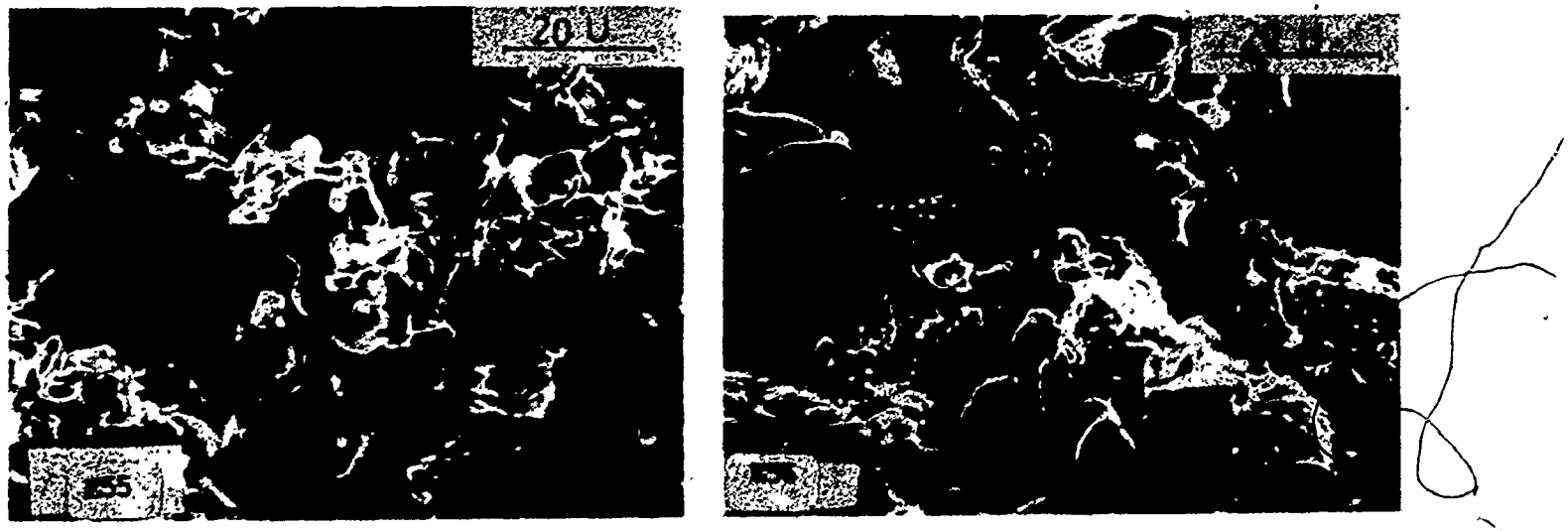

Reduction Temperature

900°C

1100°C

Figure 8.26 Appearance of powder specimens which are a mixture of 2% CaO and 2% MgO after reduction with standard reducing gas for one hour at different temperatures. The appearance after reduction at 750°C of the same powder mix is similar to E44 in Figure 8.23. The appearance after reduction at 900°C of powder mix (5% CaO and 0.5% MgO) is similar to E49 in Figure 8.25.

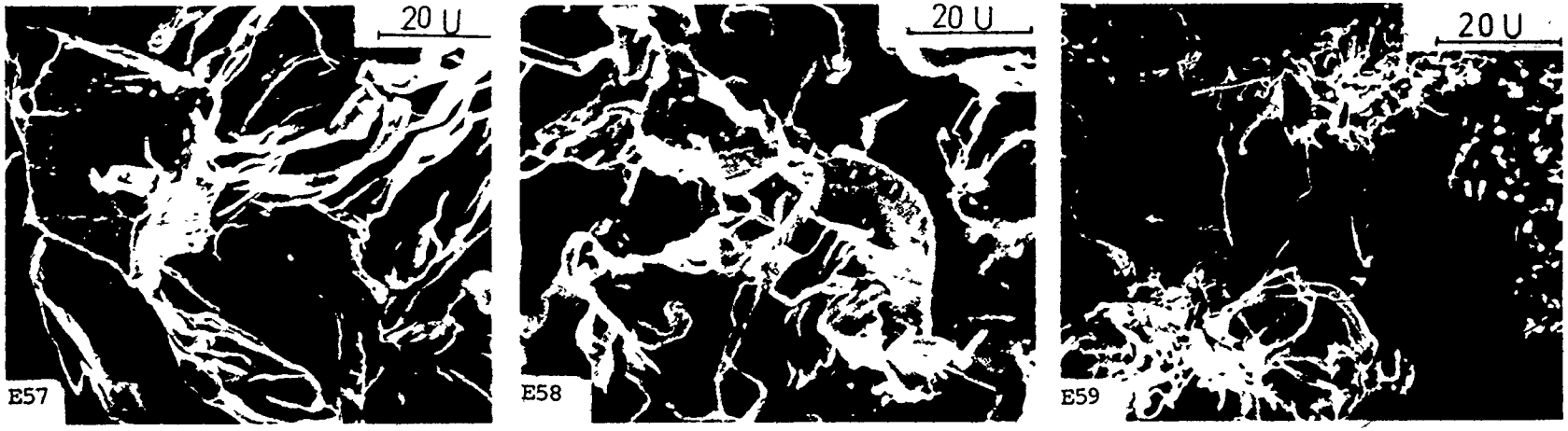

Calcium wustite (1.8% CaO) and 1% Magnesia

Calcium wustite (1.8% CaO) and 10% Magnesia

Magnesium wustite (1.7% MgO) and 0.5% Calcia

Figure 8.27 Appearance of reduced specimens which are mixtures of combinations of solid solutions and basic oxides.

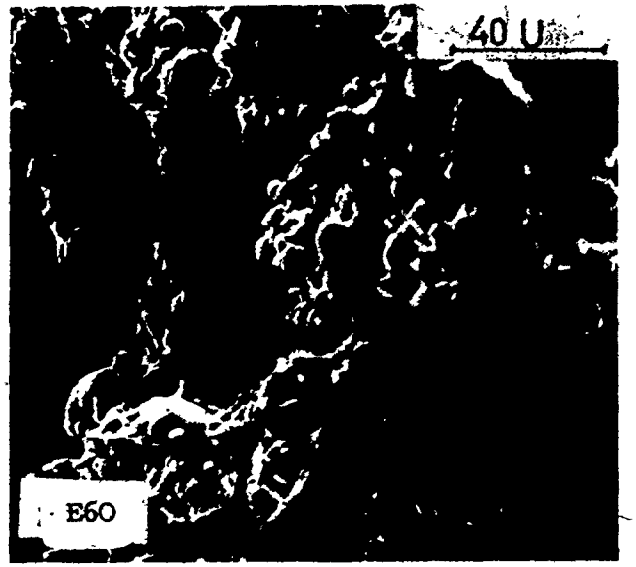

(a) Treated for 30 min. at 750°C

(b) Treated for 10 min. at 900°C

Figure 8.28 Appearance of mixture of powder W_H and 2% CaO after reduction at 750°C with gas GRS ($CO:CO_2$ = 4:1) for one hour. The thermal treatment of specimens before reduction was (a) 750°C for 30 minutes and (b) 900°C for 10 minutes. Extending the time of treatment at 750°C up to 400 minutes, the appearance of these reduced specimens are similar to E60.

No treatment before reduction

Treated at 900°C for 40 min. before reduction

Treated at 900°C for 250 min. before reduction

Figure 8.29 Appearance of calcium wustite (1.8% CaO) powders after these stated treatments and reduction at 900°C under standard reducing conditions.

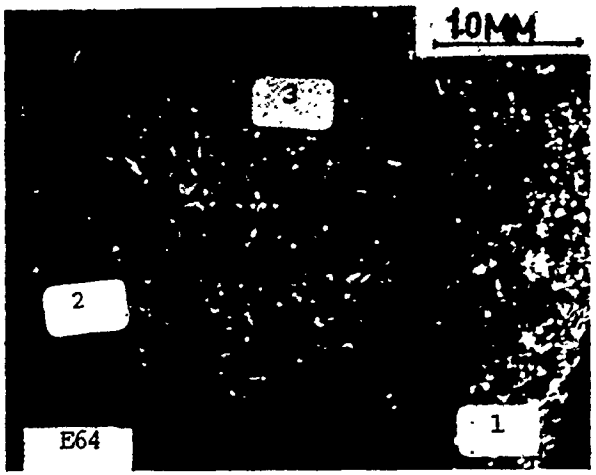

(a) There are three zones on the surface: (1) completely covered, (2) uncoated, under the rim, (3) 30 x 30 films of Ca

(b) Enlarged view of zone 3

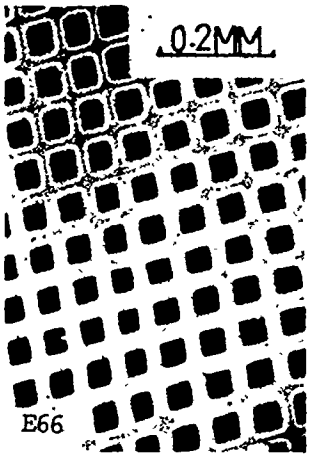

(c) The screen with 30 x 30 μm openings

Figure 8.30 Appearance of the wustite plate after Ca deposition.

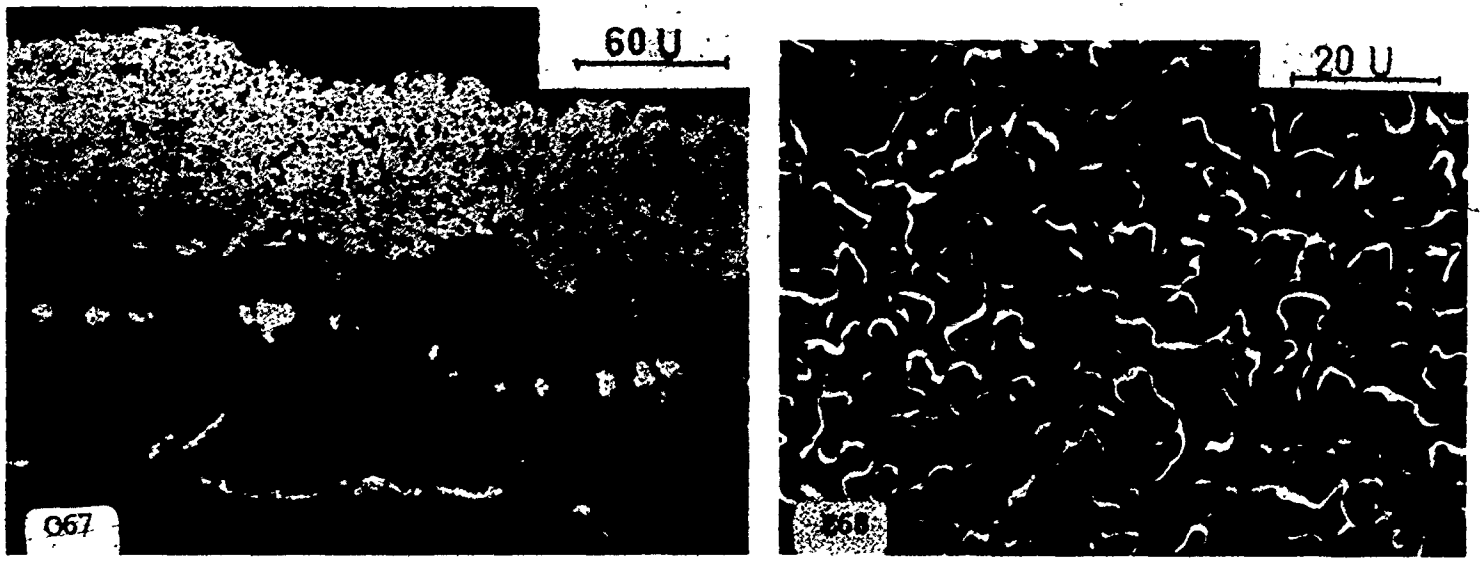

(a) Cross section of partially reduced specimen

(b) Surface morphology after reduction

Figure 8.31 Appearance of CaO-coated specimen (Zone 1 in Figure 8.33 (a)) after reduction for 1 hour at 900°C.

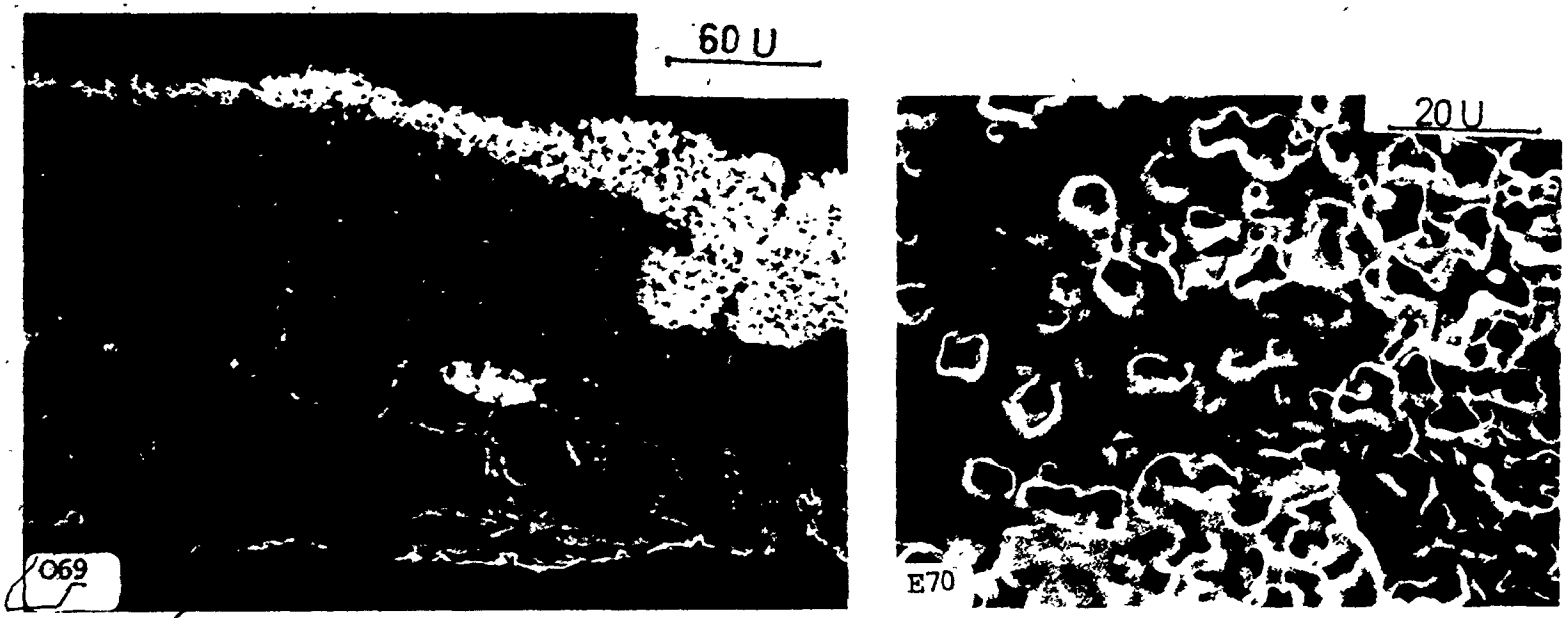

Figure 8.32 Comparison of the morphology of zone 1 (completely covered) and zone 2 (uncovered by CaO) after reduction at 900°C; (a) cross section of the plate and (b) surface.

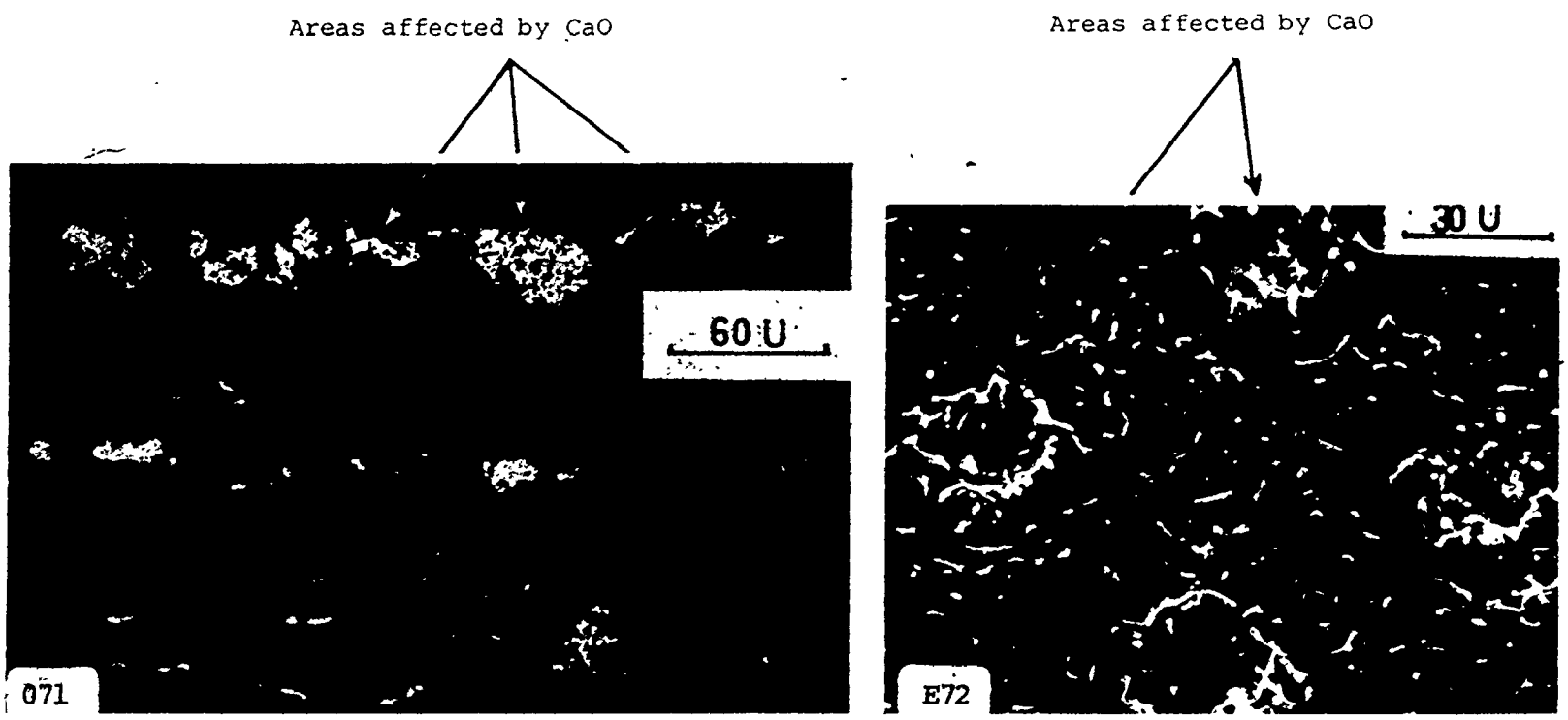

Figure 8.33 Morphology of reduced specimens in zone 3, with regularly spaced 30 x 30 µm CaO films; (a) cross section of the plate, (b) surface. Reduction temprature was 900°C.

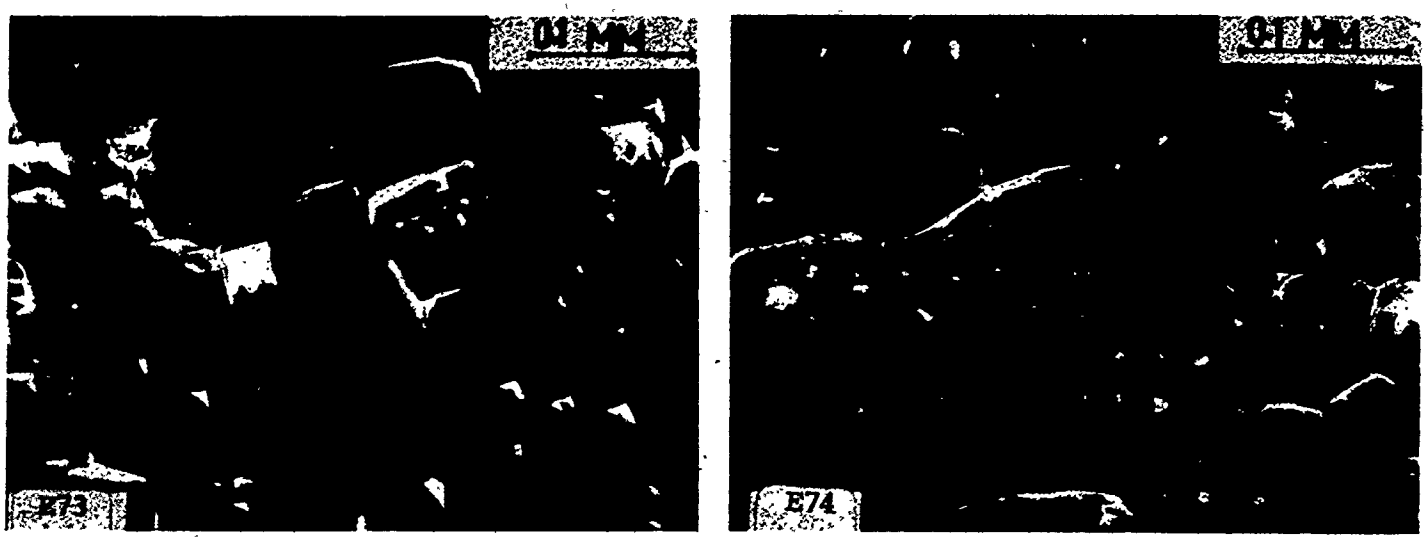

Before reduction

After reduction

Figure 8.34 Appearance of zone 3 with 12 μm dia. CaO films after reduction for 1 hour at 750°C.

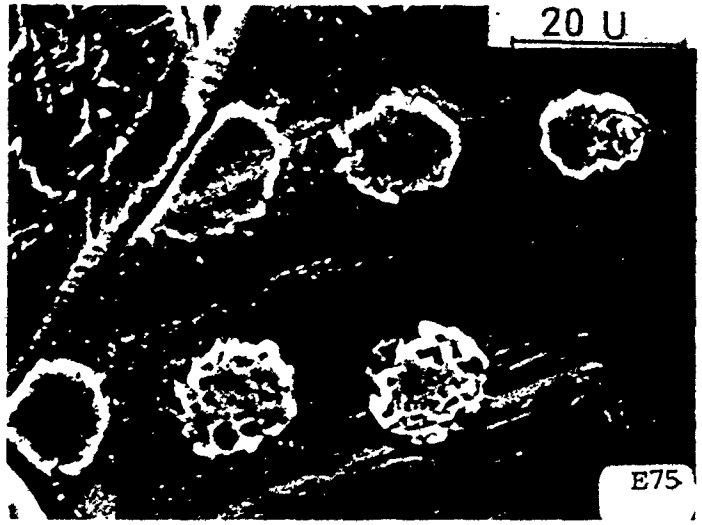

Plate was positioned horizontally under microscope

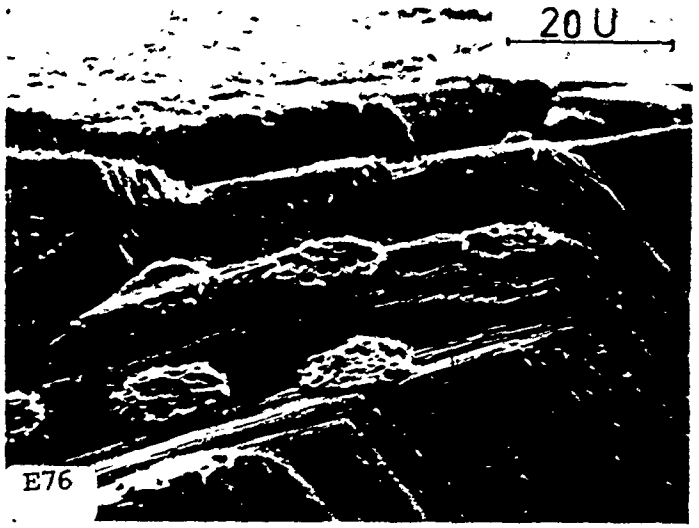

Plate was tilted by 30° under microscope

Figure 8.35 Enlarged views of zone 3 after reduction at 750°C.

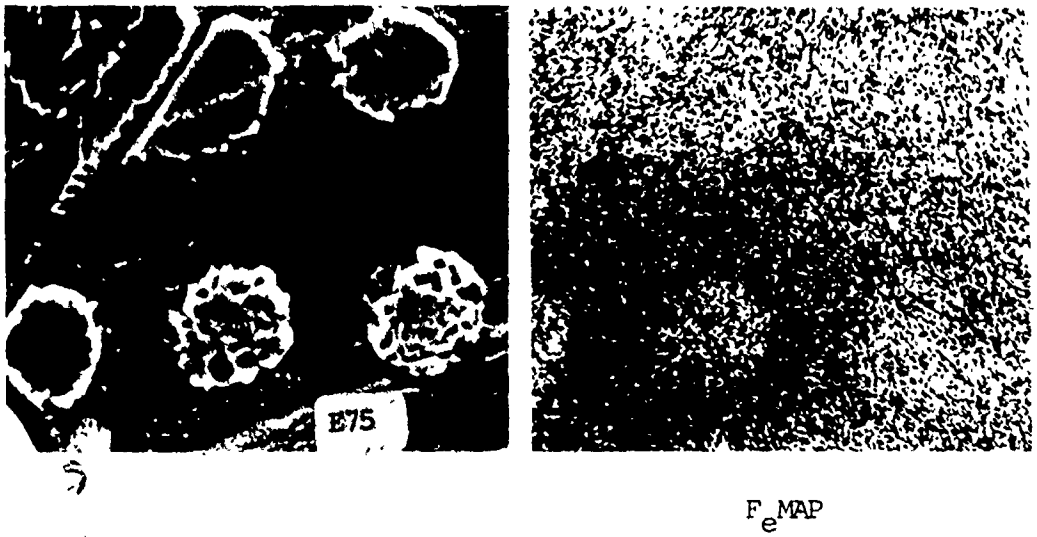

Figure 8.36 X-ray mapping of part of zone 3, after reduction at 750°C.

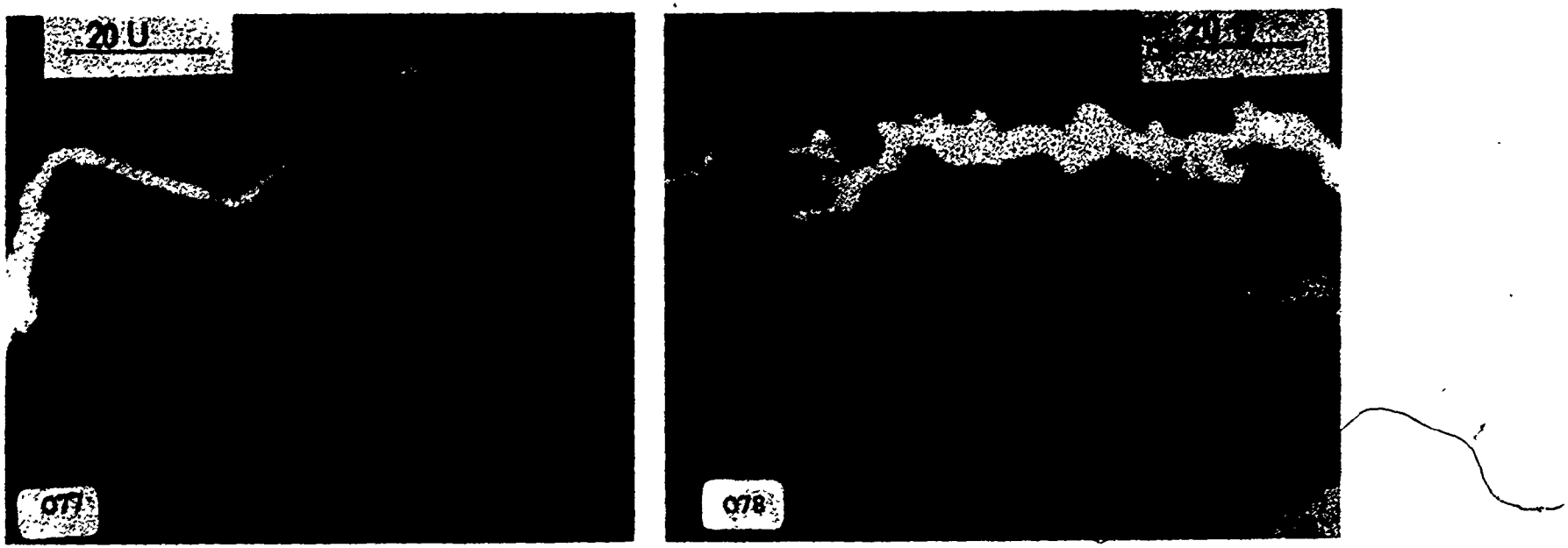

(a) Wustite plate without coating

(b) Wustite plate coated with MgO

Figure 8.37 The effect of MgO coating on specimen on the morphology of iron after reduction at 900°C for 2 hours with gas GRS.

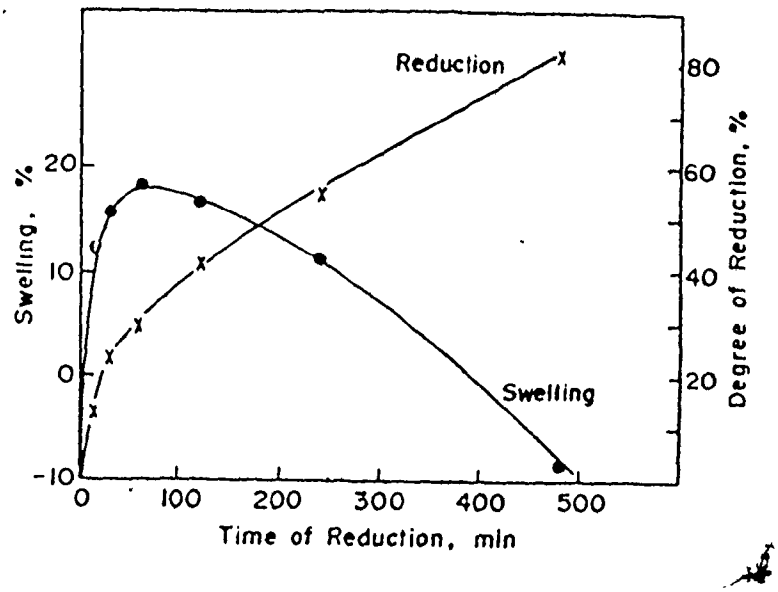

Figure 8.38 Reduction of commercial pellets as-received under standard conditions.

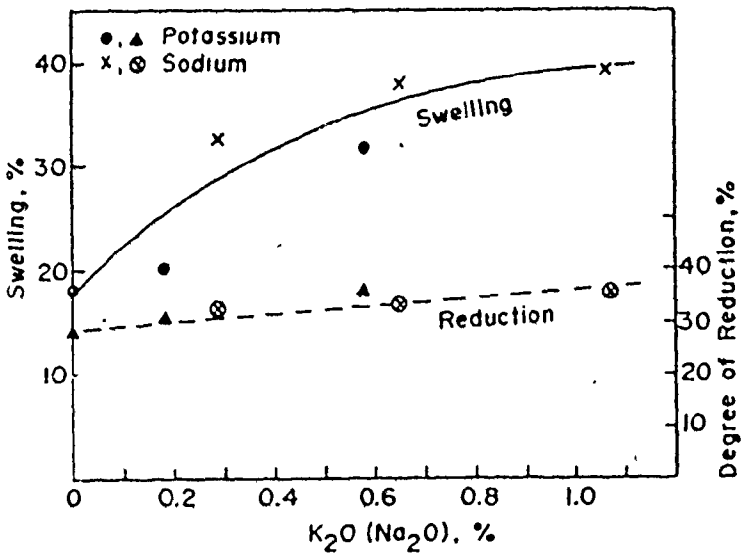

Figure 8.39 Commercial pellets impregnated in alkali carbonate solution and reduced under standard conditions.

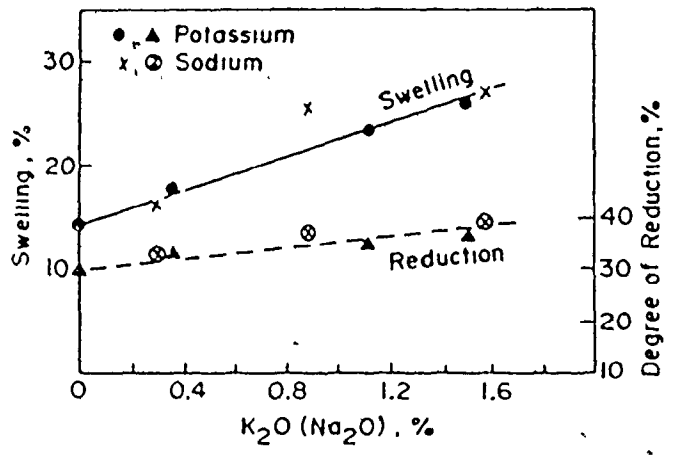

Figure 8.40 Commercial pellets impregnated in alkali carbonate solution and reduced at 700°C for two hours with standard reducing gas.

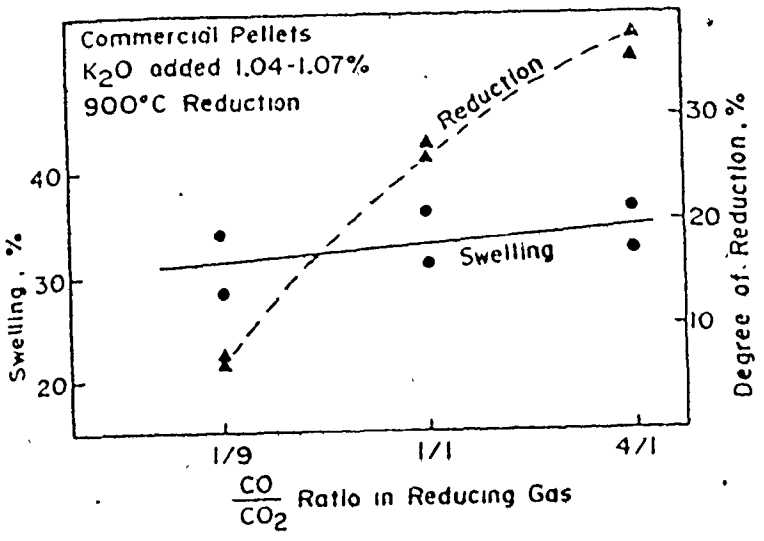

Figure 8.41 Impregnated commercial pellets reduced to magnetite, wustite, at 900°C and that under standard conditions.

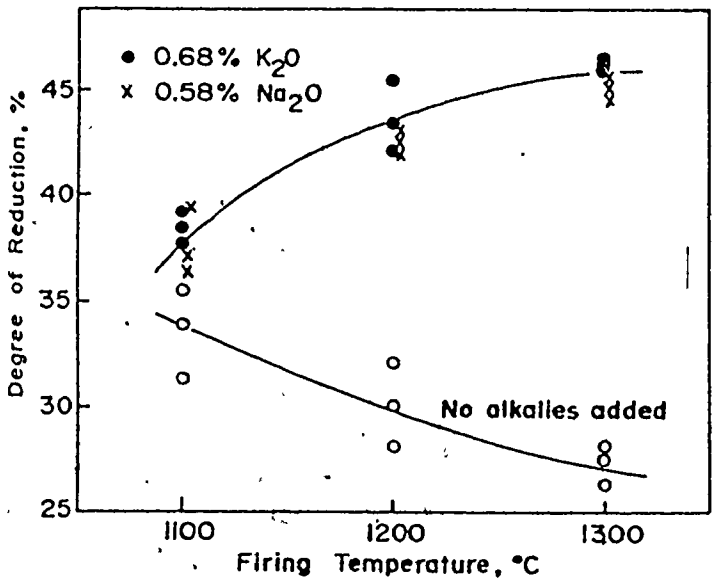

Figure 8.42 Laboratory pellets reduced under standard conditions.

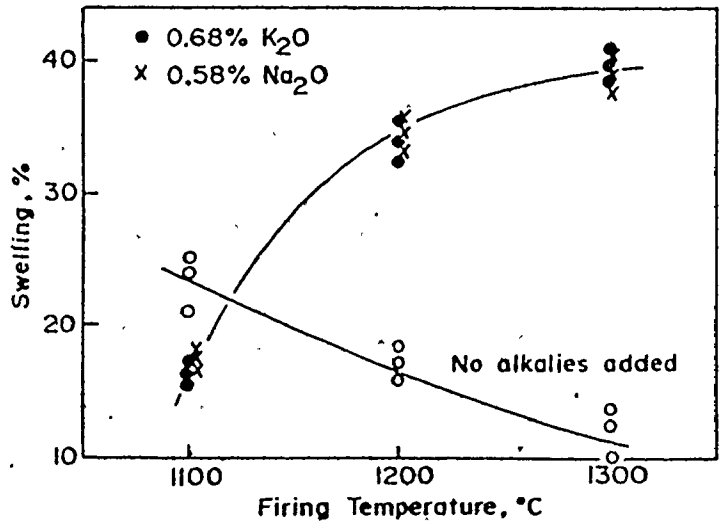

Figure 8.43 Laboratory pellets reduced under standard conditions.

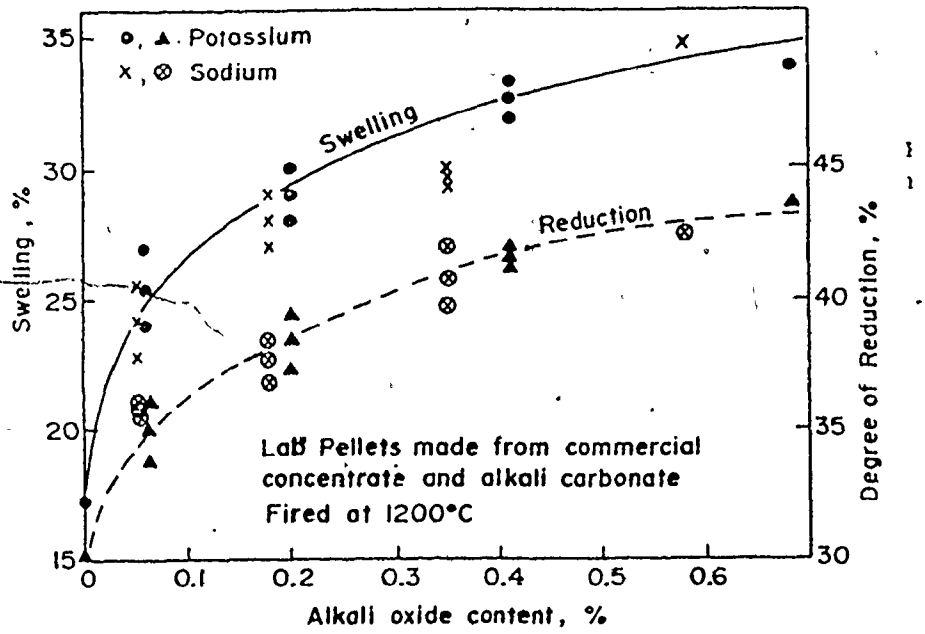

Figure 8.44 Laboratory pellets reduced under standard conditions.

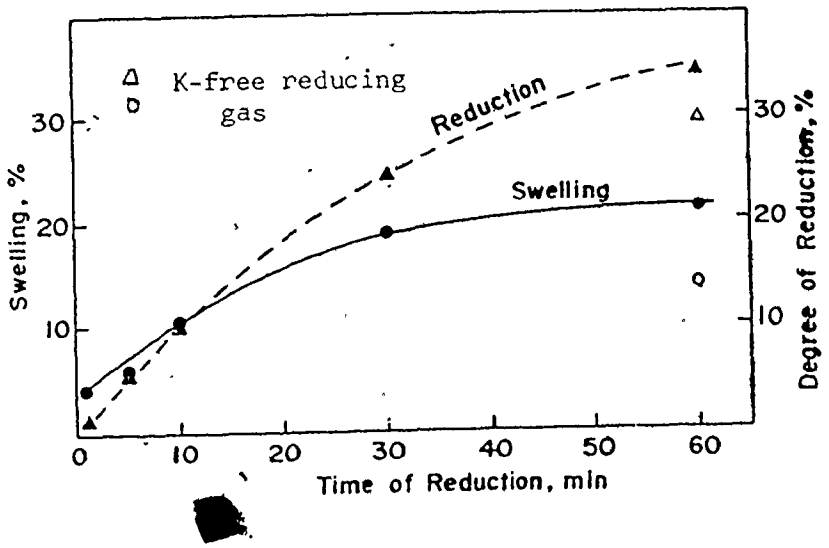

Figure 8.45 Commercial pellets reduced by potassium-containing $CO-N_2$ mixture at 900°C. Partial pressure of potassium vapor was about 10^{-3} atm.

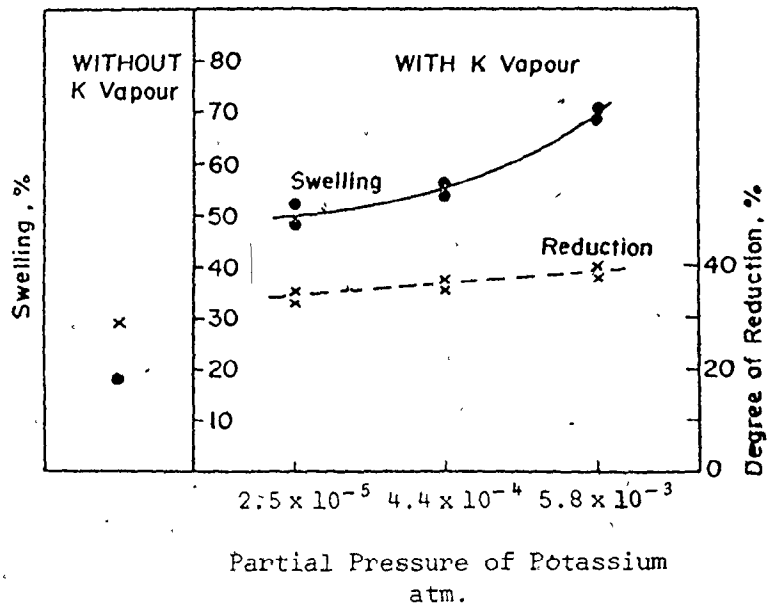

Figure 8.46 Commercial pellets reduced by standard reducing gas of various potassium contents at 900°C for one hour.

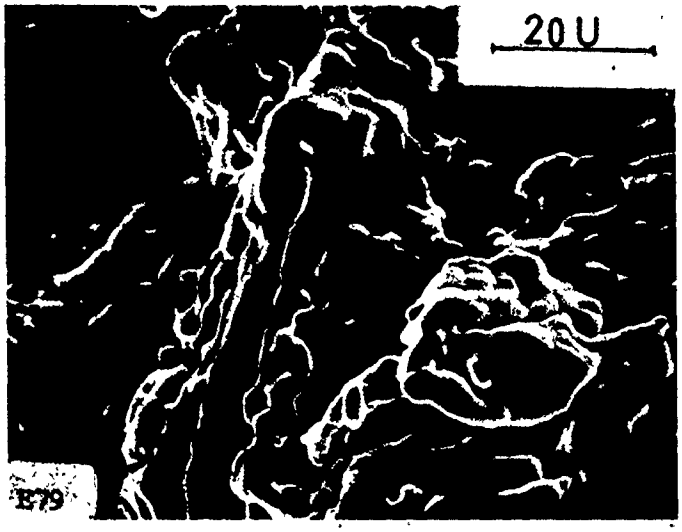

No Additives

0.68% K_2O

0.58% Na_2O

Figure 8.47 Appearance of silica free briquettes fired at 1200°C, after standard reduction.

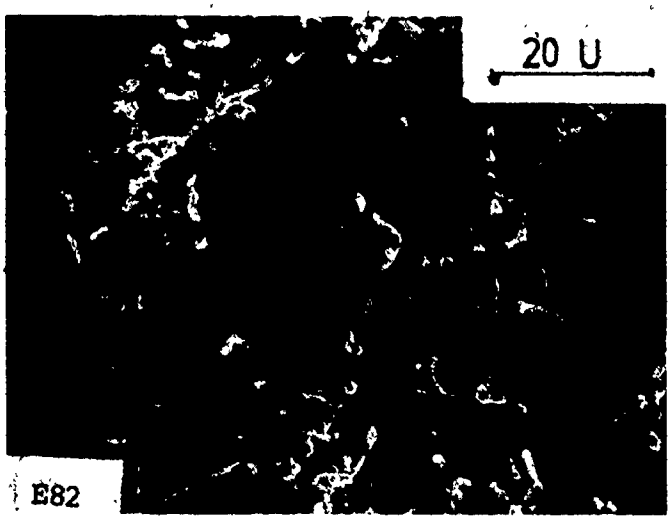

Silica free briquette
(0.68% K_2O)

Silica free briquette
(0.58% Na_2O)

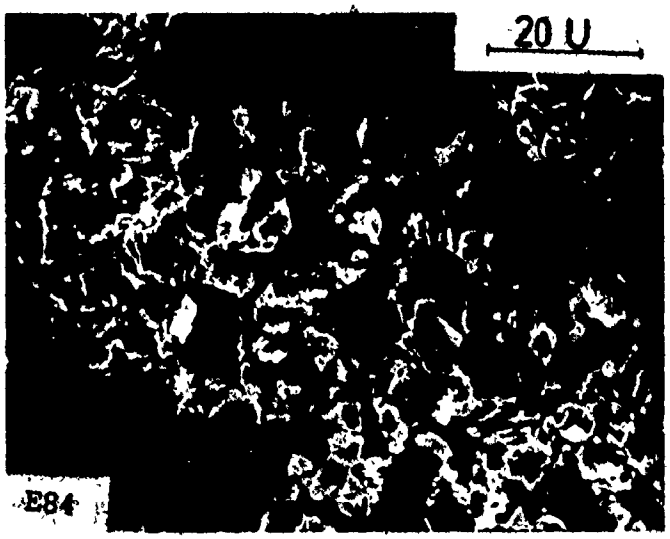

Laboratory pellet
(0.68% K_2O)
containing silica

Figure 8.48 Appearance of silica free briquettes and laboratory pellets, fired at 1300°C, after standard reduction.

As Received

Alkali Impregnated
2 - 3 wt% K_2O

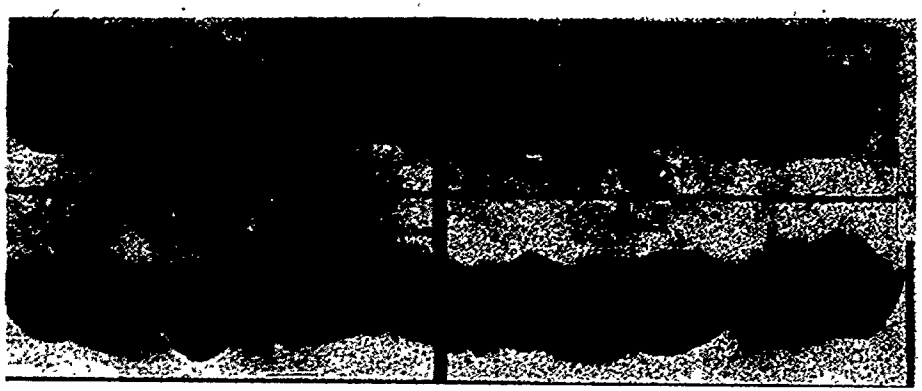

Ordinary Cooling Slow Cooling

Figure 8.49 Appearance of commercial pellets after standard reduction.

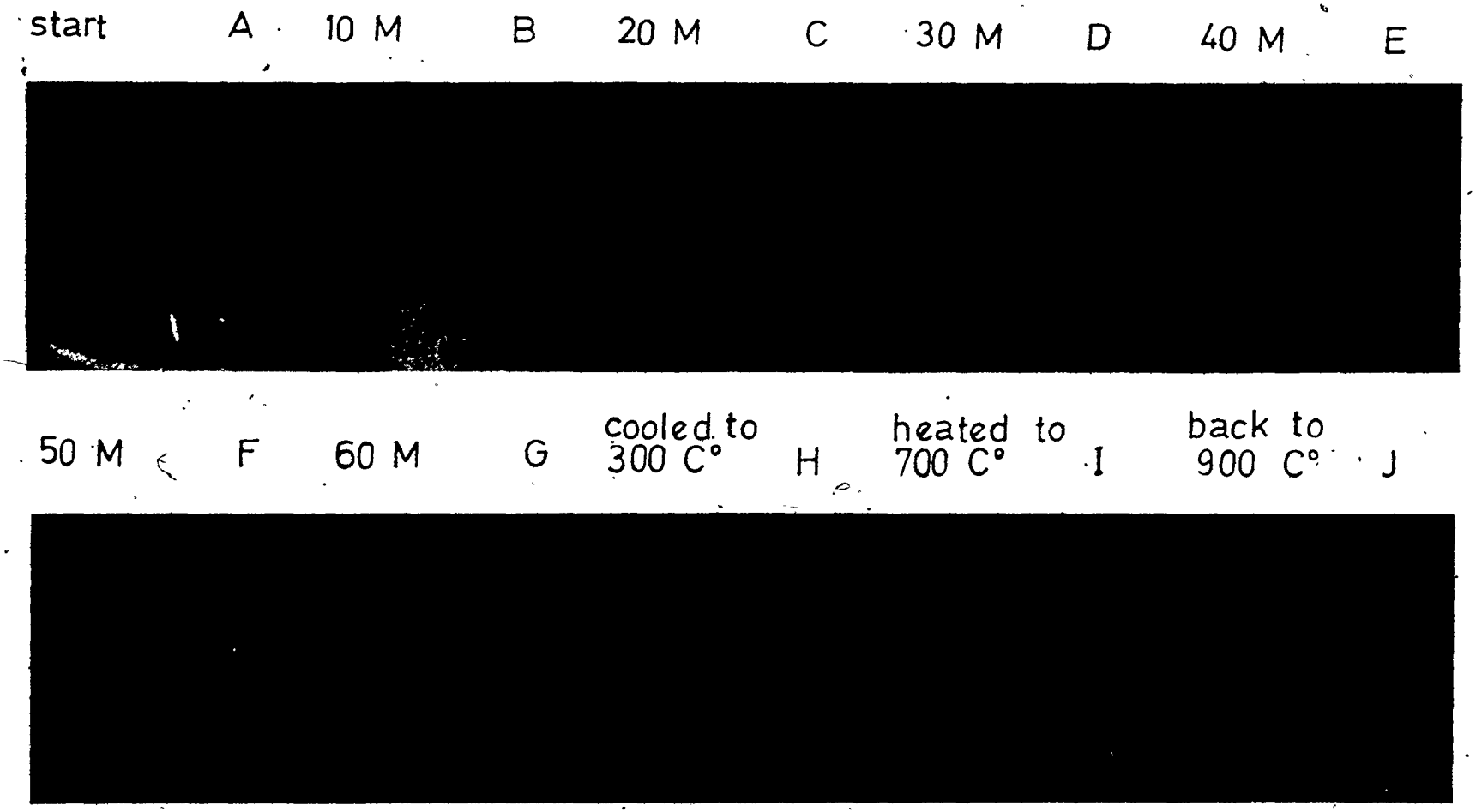

Figure 8.50 Reduction and cooling of impregnated commercial pellets.

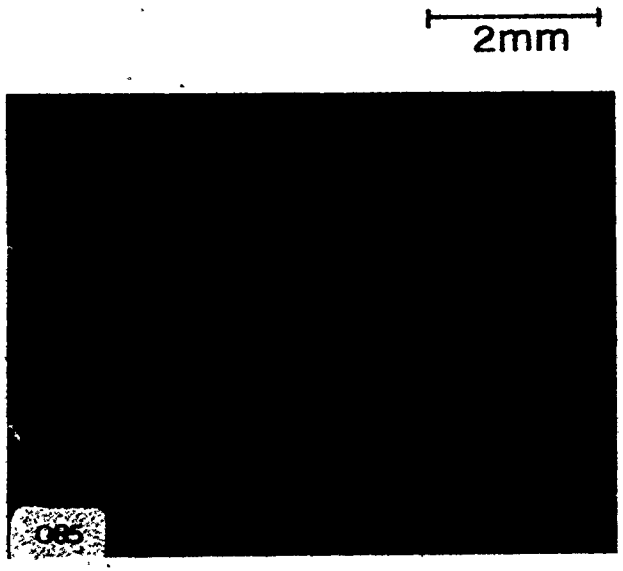

(a) Low magnification view

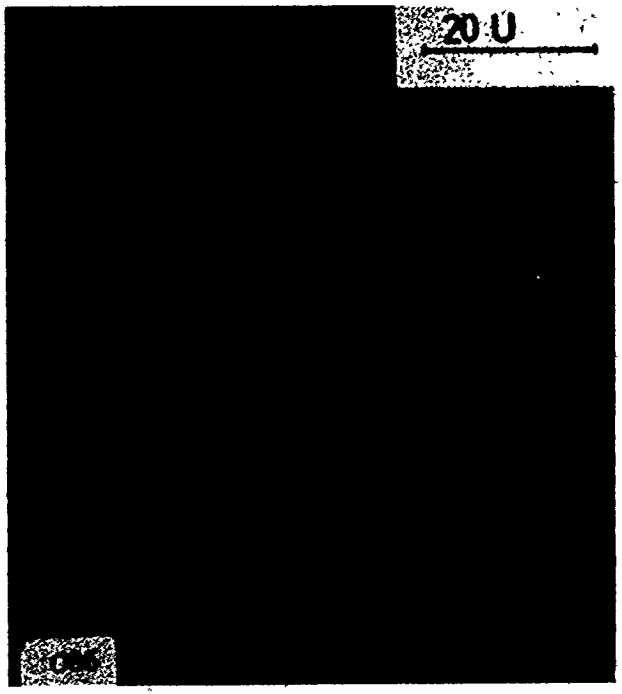

(b) High magnification view

Figure 8. 51 Sections of the commercial pellet after standard reduction: (a) non-topical reduction, (b) internal nucleation of iron. (The defects in the middle of photograph (a) are polishing defects.)

Low magnification view

Grains near the pellet's outer surface

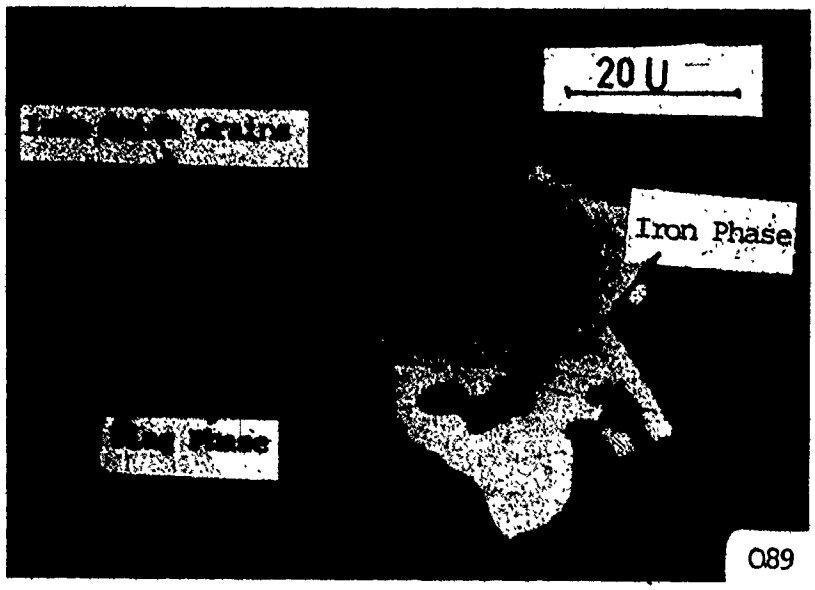

Grains inside the pellet, just outside the highly metallized zone

Figure 8.52 Section of partially reduced alkali impregnated pellet (1.32 wt% K_2O, before reduction).

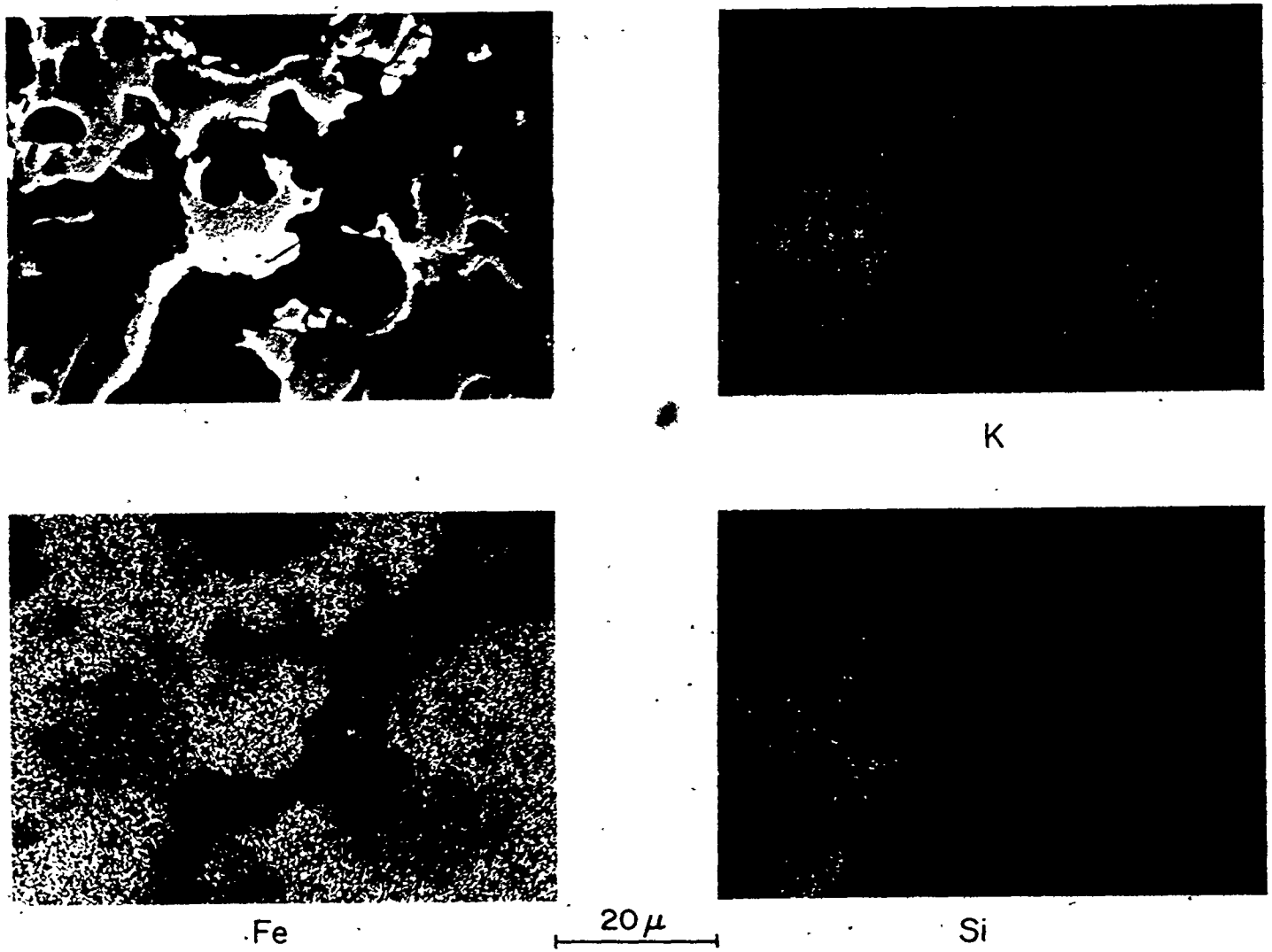

Figure 8.53 X-ray mapping for K, Si and Fe near pellet surface area A.

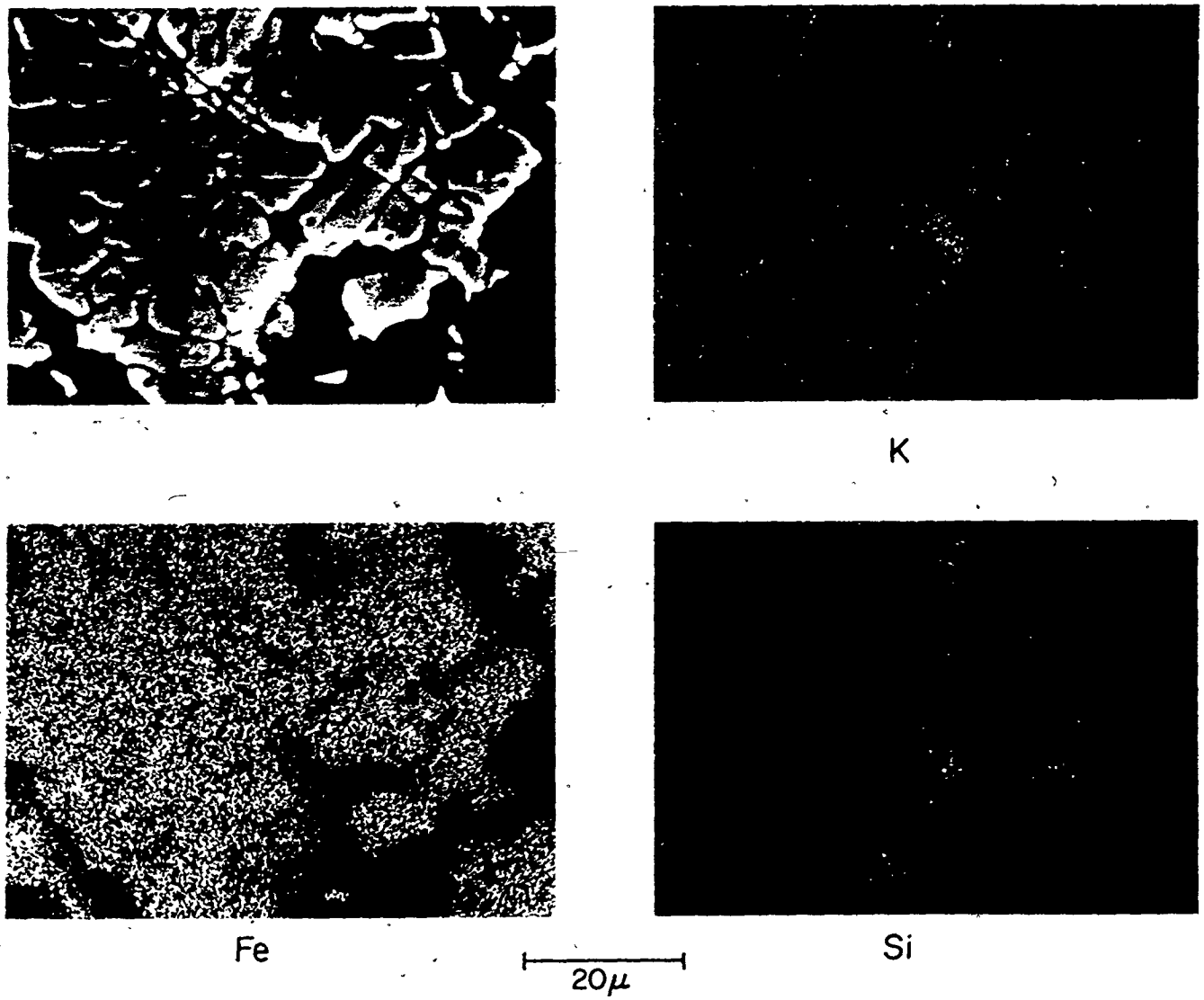

Figure 8.54 X-ray mapping for K, Si and Fe inside pellet area B.

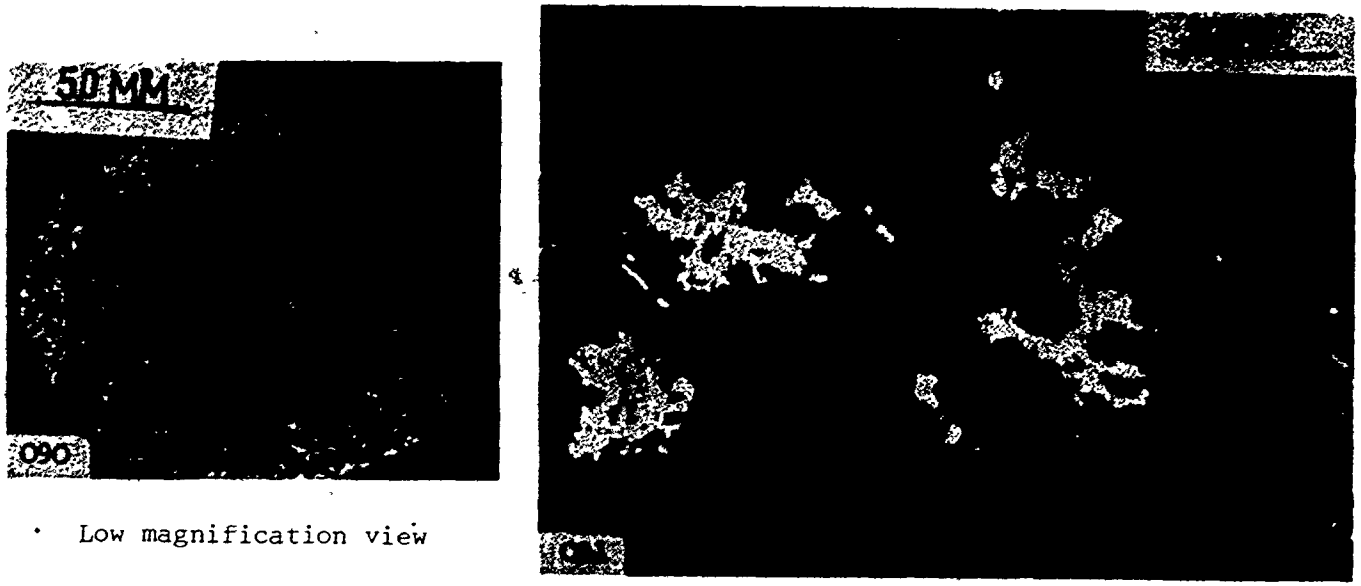

Low magnification view

High magnification view

Figure 8.55 Sections of commercial pellet after reduction with potassium containing reducing gas under otherwise standard conditions.

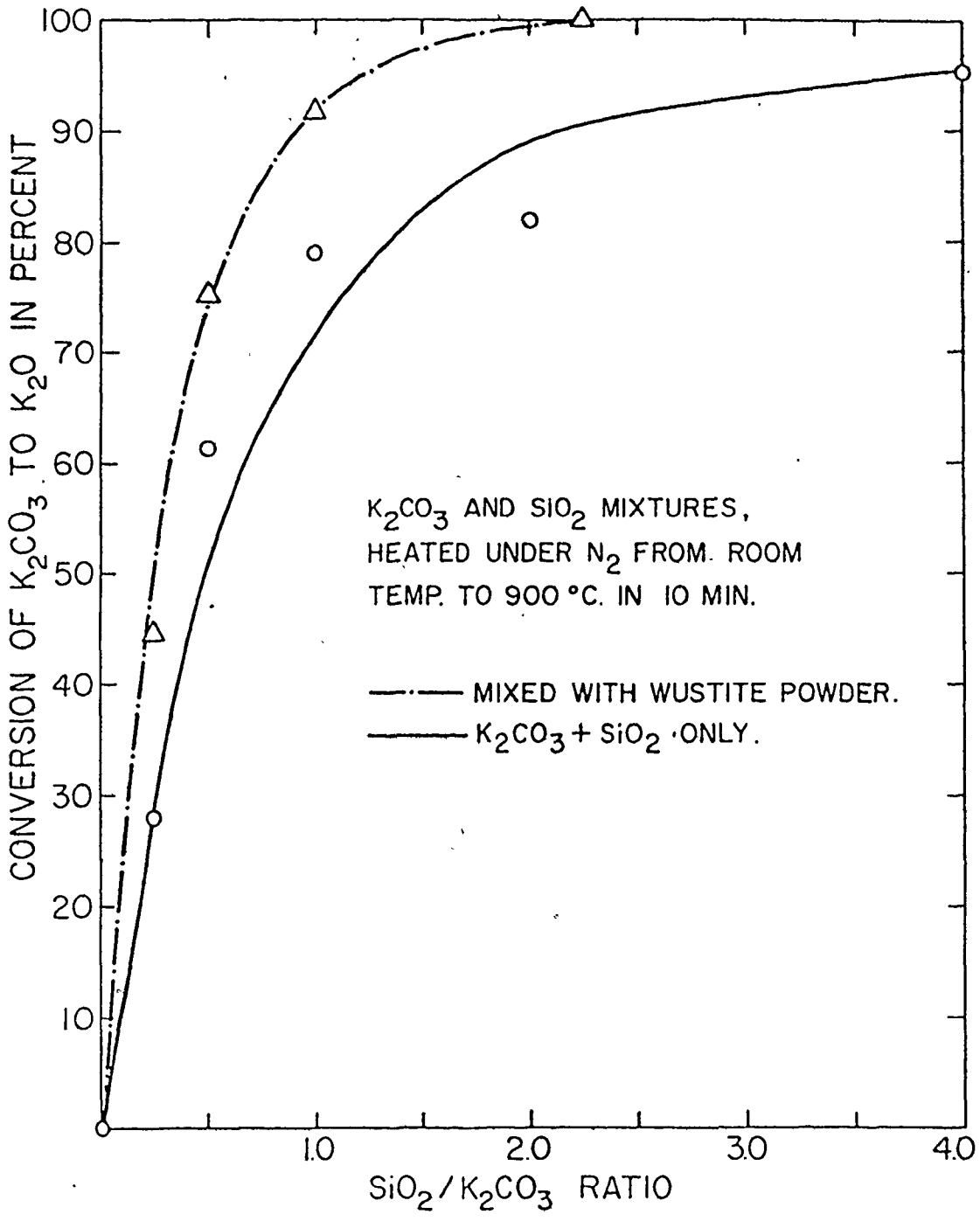

Figure 8.56 Calcination of potassium carbonate under flowing N_2 at 900°C.

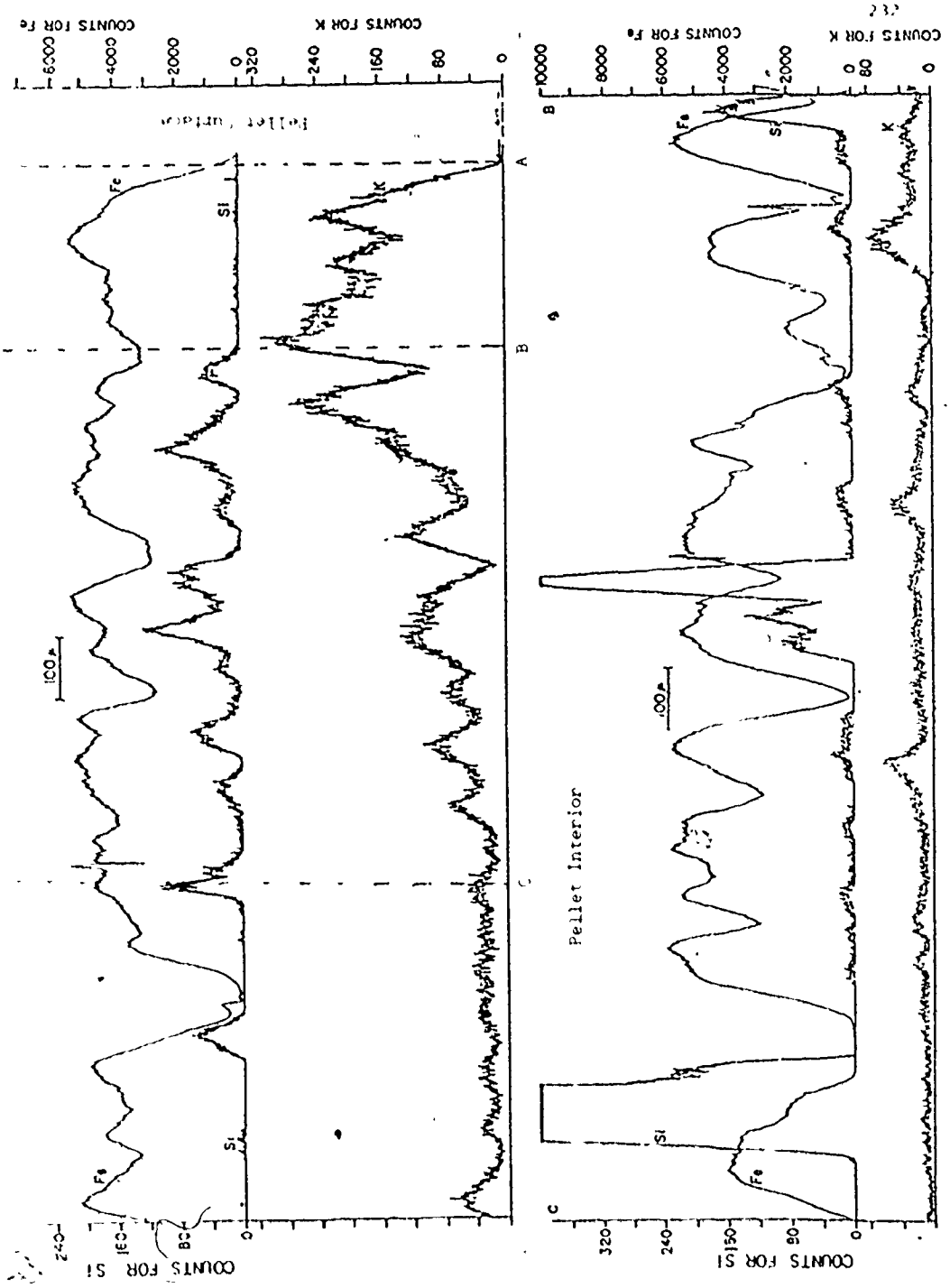

8.57

SMALL PRINT

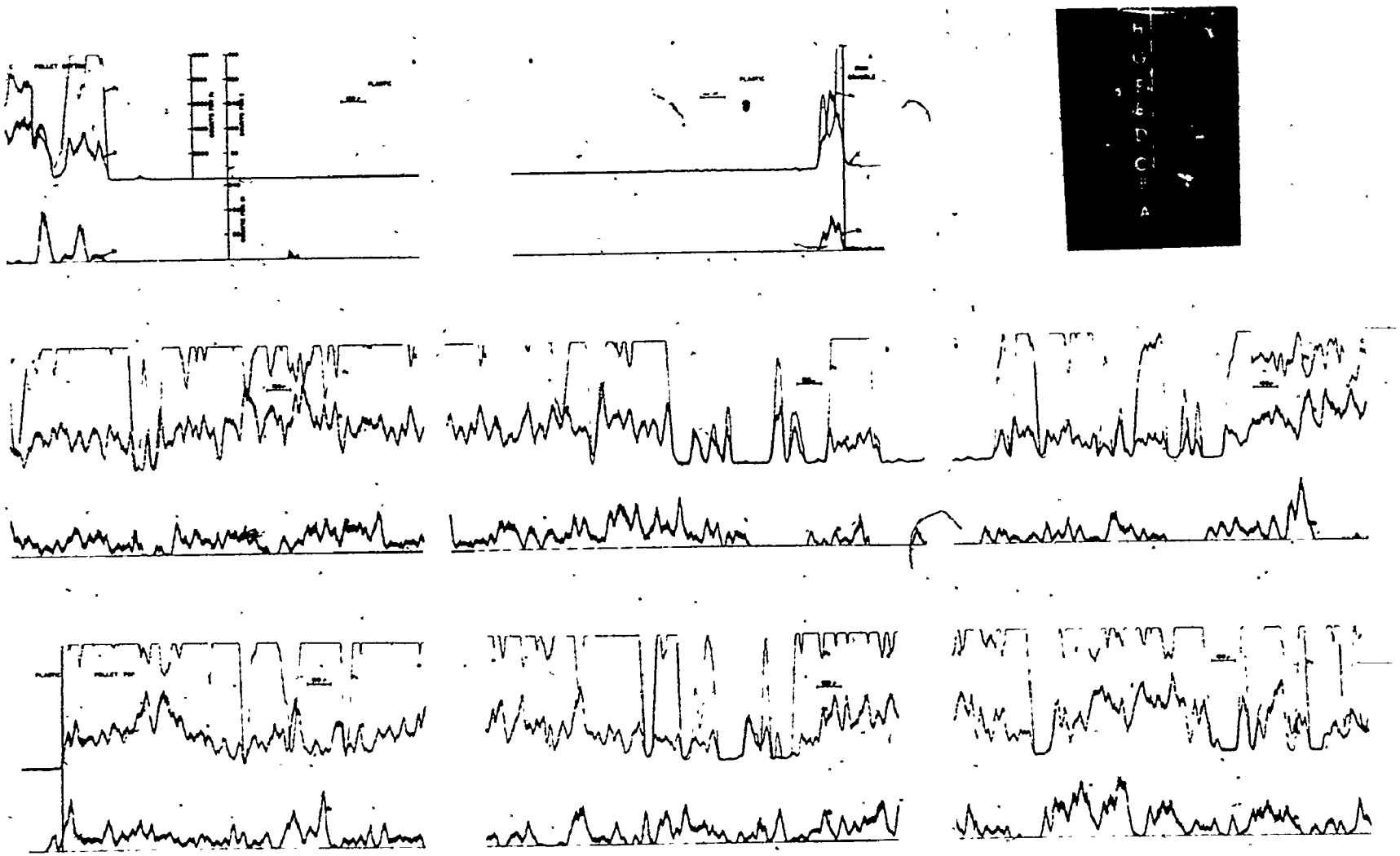

Figure 8.58 Distribution of K, Si and Fe across the center line, after reduction of commercial pellet specimens on top of K_2CO_3 under otherwise standard conditions.

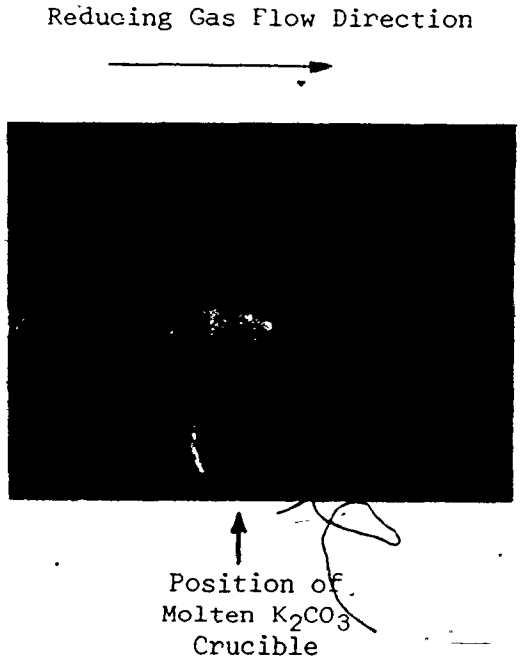

Figure 8.59 The attack of potassium vapor on the quartz tube.

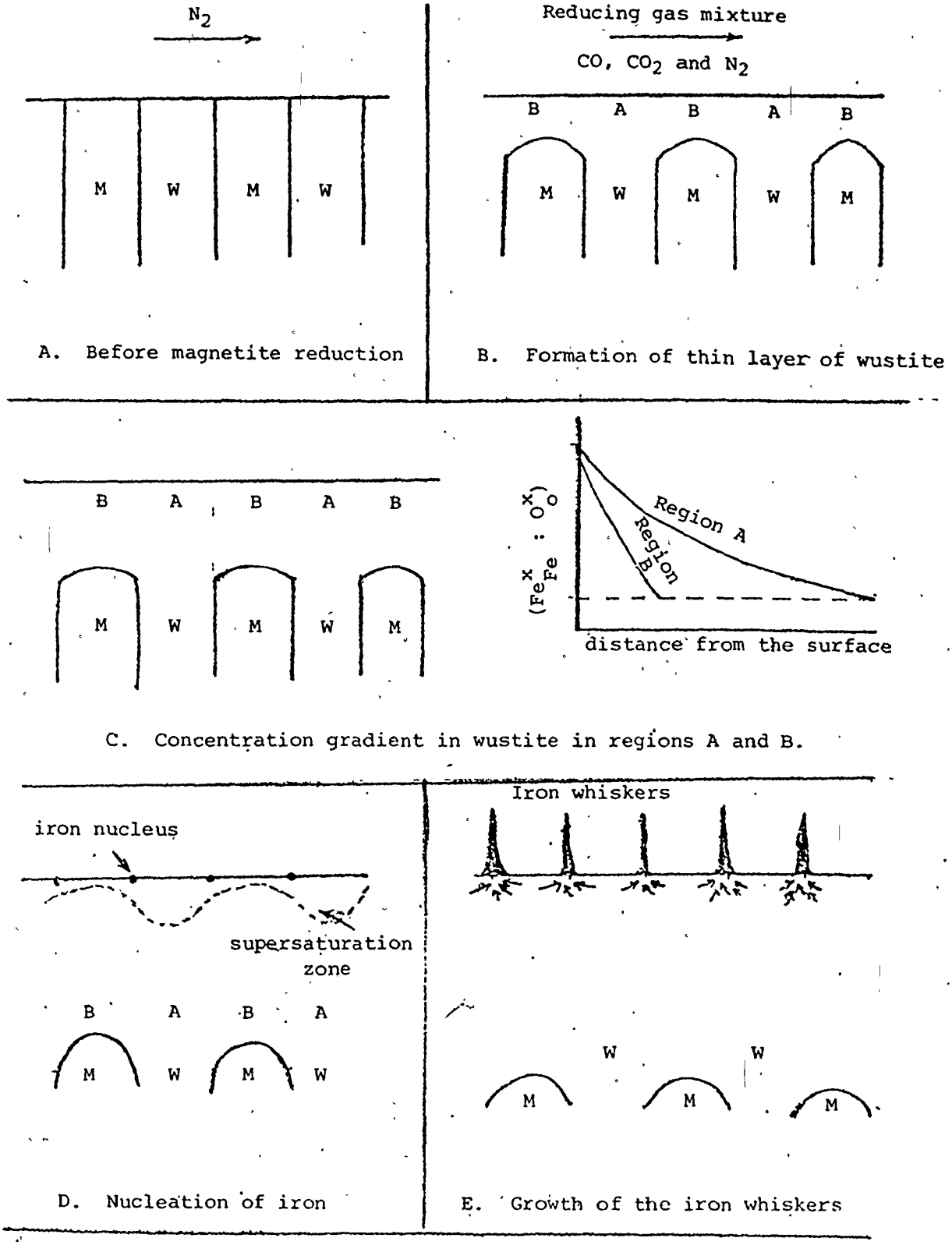

Figure 9.1 Schematic presentation of iron whisker growth, during reduction of heterogeneous wustite.